UNIVERSITÀ DEGLI STUDI DI MILANO

Dottorato di Ricerca in Scienze della Terra

Ciclo XXVIII

Lithofacies character and spatial distribution of travertine depositional systems in Central Italy: case studies from the Messinian Albegna and Pleistocene Acque Albule basins

Ph.D. Thesis

Andrea Croci
Matricola R10130

Tutor	**Academic Year**	*Coordinator*
Prof.ssa Giovanna Della Porta	**2015-2016**	**Prof. ssa Elisabetta Erba**

A Matilde

e alla mia famiglia

Contents

Abstract

The hydrocarbon reservoir discoveries in continental Lower Cretaceous carbonates in the South Atlantic Pre-Salt (offshore Brazil and Angola) have renewed the scientific interest in recent and ancient carbonates developed in lacustrine, hydrothermal and fluvial environments. Outcrop analogues provide key information to improve the understanding of the stratigraphic, sedimentological, diagenetic and petrophysical subsurface reservoir properties and lithofacies spatial distribution. To improve the knowledge about continental carbonates lithofacies types, stratigraphic architecture and diagenesis, this project focuses on two case studies: the Messinian mixed terrigenous-travertine succession of the Albegna Basin (Southern Tuscany, Central Italy) and the Pleistocene Acque Albule Lapis Tiburtinus (Tivoli, Central Italy). In the both studied areas, travertines include facies types precipitated from thermal water through abiotic and biologically influenced processes, ranging from clotted peloidal micrite boundstone, to crystalline dendrites and coated reeds.

The 70 m thick Messinian mixed terrigenous-travertine system, accumulated in the extensional continental Neogene Albegna Basin, was investigated in terms of lithofacies types, depositional environment and their spatial distribution, petrographic analysis, carbon and oxygen stable isotope geochemistry, diagenesis and porosity. The succession recorded three phases of evolution of the depositional system. 1) At the base, a 20 m thick northward prograding hydrothermal travertine terraced slope interfingered in the eastern part with an alluvial plain system prograding northward and westward (Phase I). 2) The continuous travertine succession was interrupted by the deposition of several metres thick alluvial fan breccias intercalated with 2-3 m thick travertine lenses (Phase II). 3) During Phase III, the basin evolved into an alluvial plain with ponds rich in coated reed travertines. Travertine stable isotope signatures during phase I and II confirm the geothermal origin of the precipitating water with $\delta^{13}C$ value averaging 1.46 ‰ V-PDB, while $\delta^{18}O$ is -7.50 ‰. Phase III travertines, enriched in coated plants, show lighter $\delta^{13}C$ values (mean $\delta^{13}C$ -0.36 ‰; $\delta^{18}O$ -7.22 ‰) indicative of influence of meteoric water with soil-derived CO_2. The paragenetic history of the studied succession shows that it was affected by hydrothermal, meteoric and burial diagenesis. The studied succession was firstly affected by a burial phase, afterwards followed by uplift and exhumation to meteoric diagenesis.

The 20 km^2 and 50 m thick Pleistocene travertine succession accumulated in the Acque Albule Basin close to Tivoli village was investigated in terms of lithofacies types, its geometry and architecture, through the analyses and the correlation of six drilled borehole cores. The travertine unit consists of a wedge shape geometry thinning southwards and it is subdivided in a proximal, intermediate and distal part from North to South. The succession recorded four principal units separated by four main unconformities that consist of centimetre to few metres thick intraclastic/extraclastic wackestone to floatstone/rudstone, indicative of periods of non deposition and erosion, due to the temporary interruption of the thermal water out of the springs. The southern part of the wedge is intercalated with conglomerate and sandstone representing palaeo-river channels.

This study shows the stratigraphic architecture and sedimentary evolution of these two decametre scale continental sedimentary successions in which hydrothermal activity and travertine precipitation were driven by the extensional and transtensive tectonic regimes, with faults acting as fluid paths for thermal water and creation of accommodation space for terrigenous and travertine deposition. Humid climate might have been instrumental for the aquifer recharge that fed the hydrothermal vents.

This study proposes two different geological models useful for further comparison with other continental basin successions and hydrothermal travertine systems in outcrops and subsurface. It provides useful information for the petrographic, spatial and reservoir characterization of subsurface travertine analogues.

Chapter I

Introduction

1.1 Aims of the project

The interest in continental carbonate deposits has increased after the hydrocarbon discoveries in the continental rift basin carbonates in the Lower Cretaceous subsurface of the South Atlantic, offshore Brazil and West Africa (Angola). These discoveries have led to a renewed attention for both the industry and the academia, to improve the knowledge about the characters, the spatial distribution and the mechanisms that permit the precipitation of carbonate rocks in continental rift settings. Moreover, worldwide accepted classification and terminology for the different variety of continental carbonates have still to be developed.

This project focuses on continental carbonates precipitated and accumulated in hydrothermal systems, labelled as travertines (cf. Pedley, 1990; Pentecost, 2005). In order to improve the understanding of the products, the depositional environments and the diagenetic features of travertines, a multi-scale study of the upper Messinian mixed travertine-terrigenous succession of the Albegna Basin (Southern Tuscany, Central Italy) and the Pleistocene travertine succession of the Acque Albule Basin (Tivoli area, Latium, Central Italy) are presented. This project has the objectives: 1) to identify the carbonate facies and the lithofacies associations of the two successions, on the base of the terminology of carbonates provided by Dunham (1962) and Embry and Klovan (1971); 2) to provide palaeoenvironmental reconstructions that describe the geometries, the spatial distributions of the travertines and the relationships with terrigenous deposits in continental rift basins; 3) to asses the paragenetic histories that affected the studied deposits; 4) to develop geological models useful to define the reservoir properties of travertines as possible analogues for the South Atlantic reservoirs.

The research is summarized in the following chapters. Chapter 1 concerns the summary about general concepts of travertine characteristics based on a detailed literature review. Chapter 2 gives information regarding the geological setting of the study areas, the Albegna Basin and the Acque Albule Basin. Chapter 3 describes the depositional architecture of the mixed terrigenous-travertine succession of the Albegna Basin. Chapter 4 provides a study on the stable isotope signature and the diagenetic features of the upper Messinian travertines of the Albegna Basin. Chapter 5 gives a description of the Tivoli travertines, providing a 2D stratigraphic reconstruction. Chapter 6 includes a discussion regarding the architecture and evolution of the two studied travertine systems. The final conclusions are summarized in Chapter 7.

1.2 Hydrothermal travertine literature review

This chapter describes some of the background published knowledge about travertines, the used terminology, geodynamic setting, fabric types, depositional environments, precipitation processes, diagenetic features and isotope signatures.

1.2.1 Terminology and classification

There is a lack of clarity regarding the terminology applied to describe continental carbonates and various terms have been proposed. According to Pentecost and Viles (1994) the CO_2 career is a parameter that allows the classification of these continental carbonate rocks: CO_2 can derive from two careers, defining two classes of travertines: the first is the soil-zone that feeds groundwater of soil and atmospheric carbon dioxide; travertines precipitated from this type of groundwater are labelled as meteogene (Pentecost and Viles, 1994). The second career is the Earth's crust, in which CO_2 is thermally generated and dissolved in high concentrations in groundwater (Pentecost, 2005). From this career travertines, labelled as thermogene, are precipitated (Pentecost and Viles, 1994). Thermogene travertines result to be more localised and associated with magmatic and extensional tectonic activity (Pentecost, 2005).

Other authors classify continental carbonates on the basis of the water temperature, defining as "tufa" the continental carbonates precipitated under cool, ambient temperature freshwater (< 20°C), typically containing micro- and macrophytes, invertebrates and bacteria (Pedley, 1990; Ford and Pedley, 1996). The term "travertine" addresses continental carbonates precipitated from thermal water with temperature over 20° C (or 30° C, Capezzuoli et al., 2014), lacking macrophyte and animal remains (Pedley, 1990; Ford and Pedley, 1996). Moreover, Capezzuoli et al. (2014) introduced the term "travitufa" for those carbonate deposits precipitated from cooled thermal water in distal area from the hydrothermal vents. However, according to Jones and Renaut (2010) these classifications based on the water temperature or water sources do not consider the diagenetic processes, resulting problematic on ancient deposits. In this study, due to the sedimentological and geochemical results, the terminology used is that proposed by Pentecost and Viles (1994) and Pentecost (2005).

1.2.2 Travertine and geodynamic settings

It has been known that hydrothermal vents are aligned along some active fault traces and there is a worldwide association of travertine deposits within tectonically active zones. Faults play a key role in the transport and upwelling of hydrothermal fluids (Sibson, 1996) in those area characterized by anomalous geothermal gradients (Bellani et al., 2004). For this reason the site of a hot-spring travertine deposit can be used as an indicator of the approximate location of the trace of an active fault, increasing the confidence of interpretation when several adjacent travertine deposits are aligned along a possible fault (Hancock et al., 1999). Travertine deposits are preferentially located along fracture traces, either above extensional fissures or in the hanging walls of normal faults (Hancock et al., 1999). Faulting and fracturing improve permeability and favour hydrothermal circulation. Hydrothermal fluids giving rise to travertine are generally saline-rich solutions with very high sealing capacity. Furthermore to reopen a fault or a fracture to a new fluid circulation, an earthquake is necessary. Thus, fluid flow and faulting are generally contemporaneous and travertine deposition becomes indicative for the age of the tectonic activity (Hancock et al., 1999; Brogi et al., 2010). According to Hancock et al. (1999) the rheology of the substrate below a travertine deposit influences the morphology of the travertine unit; thus, mounds, towers and pinnacles underlie unconsolidated sediments, whereas fissure-ridges develop where the substrate consists of lithified hard rocks.

1.2.3 Travertine mineralogies and fabric types

Almost all travertines consist of two polymorphs of calcium carbonate, aragonite and calcite. The principal factors that control the formation of these minerals are the chemical composition of the source water, the temperature, the pressure and rate of CO_2 evasion (Pentecost, 2005). Aragonite is less stable at room temperature, but it occurs widely in nature and is frequently found in hot spring travertines. In fact aragonite precipitates preferentially from hot water and limiting temperature lies between 30 and 60° C (Lippmann, 1973). At lower temperature aragonite is normally formed only in presence of high concentration of magnesium (Chafetz et al., 1991). Instead calcite precipitates in the range of temperature up to 40° C (Folk, 1993). Fouke et al. (2000) showed that calcite and aragonite precipitate together at water temperature between 30 and 43°C.

Magnesium concentration in water rarely exceeds 10 mmol L^{-1} and aragonitic travertines are infrequently encountered in cold water, except if it is concentrated by evaporation (Pentecost, 2005). Fischbeck and Müller (1971) showed that aragonite precipitation becomes significant when the Mg/Ca ratio attained ~2.9. Folk (1994) suggested that aragonite would precipitate from any water that has Mg/Ca ratio 2:1 and temperature more than 40°C.

Kitano (1963) reported that aragonite predominates where the rate of CO_2 evaporation was high. The rate of CO_2 degassing from spring water is controlled by: 1) the pCO_2 of the spring water when discharged at its vent (Chafetz and Lawrence, 1994), 2) the area and depth of water on the discharge apron (Dandurand et al., 1982), 3) the amount of water agitation and turbulence (Jacobson

and Usdowski, 1975), and 4) aeration and low pressure effects (Zhang et al., 2001). High turbulent flows and agitation that cause rapid degassing of CO_2 with high pCO_2, can produce waters strongly supersaturated with respect to $CaCO_3$; in this condition aragonite precipitation occurs (Kitano, 1962; Holland et al., 1964). According to Folk (1994) sites of rapid degassing of CO_2 would lead to aragonite precipitation even if the temperature and Mg/Ca ratio would favour calcite precipitation. However, studies conducted by Jones and Renaut (1995, 1996) demonstrate that calcite precipitation can occur also from water with temperature less than 90° C, concluding that mineralogy could be related to the high turbulence of the flow water that increases the degassing and the saturation level.

Travertine fabric types were described in several studies. The first travertine fabric classification was proposed by Chafetz and Folk (1984), focusing on origin and petrography of travertine deposits. Afterwards other authors such as Guo and Riding (1992; 1998) and Chafetz and Guidry (1999) regrouped travertine fabric types as follow (Fig. 1.1 A-H):

1. Crystalline crust
2. Shrub
3. Pisoid
4. Paper thin rafts
5. Coated bubble
6. Reed
7. Lithoclast-breccia

1) **Crystalline crusts** form dense, white, laminated deposits, made of elongate crystals orientated perpendicular to the depositional surface and crossed by thin micritic laminae formed by needle aggregates, giving to the rock a regularly laminated appearance (Guo and Riding, 1992). According to Folk et al. (1985) a lamina has been interpreted as diurnal. Crystalline crusts develop on steep slopes (30-90°), cliffs, rims and vertical walls of terrace pools and typically form thick, laterally extensive deposits (Guo and Riding, 1998; Özkul et al., 2002), reflecting fast rapid precipitation from fast flowing water (Guo and Riding, 1992), which leads the crystal orientation and limits microbial influence on carbonate precipitation (Özkul et al., 2002). The steep surface is often corrugated in microterraces with a relief of 5-20 mm, making a soft and powdery deposit below a harder surface (Guo and Riding, 1992), becoming whole hard and compact with time. The dendrite crystals have blade morphology (Guo and Riding, 1992) and, when they are well developed, give a “cedar-tree” appearance to the crystal aggregates (Folk et al., 1985). The layered crusts are from few to tens of centimetres in thickness (Guo and Riding, 1998). Petrographically, there is an alternation between micrite and sparite laminae (Özkul et al., 2002); micrite laminae are dark-coloured and millimetre-thick, instead the sparite laminae are centimetre to decimetre in thickness (Özkul et al., 2002). The dendrite crystals grow up radially on the micritic substrate or organized in bundles (Özkul et al., 2002). If the crystals are fractured they occur distributed randomly on the micritic floor (Özkul et al., 2002).

2) **Travertine shrubs** are short, squat, porous and dense crystalline masses of $CaCO_3$ (Guo and Riding, 1994), dominated by shrub-like growths (Chafetz and Folk, 1984). The dendritic morphology can be very irregular and can range from short and vertical to elongate and radiating

(Guo and Riding, 1994). Shrubs are a few millimetres to centimetres in size, pale grey to pale brown and they are arranged in multiple horizontal layers, separated by thin micritic laminae (Guo and Riding, 1998). Travertine shrubs typically occur in terrace pools, in depressions and flats where they are thicker and more laterally extensive (Guo and Riding, 1998). Guo and Riding (1998) recognised two main shrub types: a) micritic/rhomb shrubs, formed mainly under microbial influence, and b) needle crystal shrubs already described by Casanova (1986) and Pentecost (1990), formed by also an abiotic component driving precipitation. Based on morphology, Chafetz and Guidry (1999) classified shrubs in three main classes: a) bacterial shrubs have an irregular form; b) crystal shrubs and c) ray-crystal crusts display regular geometric patterns. Bacterial shrubs are the product of bacterially induced precipitation, have an irregular morphology similar to woody plants (Chafetz and Guidry, 1999). Ray-crystal crusts and crystal shrubs are dominated by abiotic precipitation and show distinct crystal habits; ray crystal shrubs are made of large fan-shaped features composed of subparallel, extremely coarse bladed crystals (Chafetz and Guidry, 1999). The common feature in the three fabric types is the occurrence of bacterial body fossils or bacterial moulds (Chafetz and Guidry, 1999). Under the microscope they are composed of a crystal association of sparite and micrite organized in different ways, without a real boundary between two types of crystal shapes (Özkul et al., 2002). Shrub crystals are euhedral to subhedral in shape, 5-10 μm in size, without having any internal architecture (Özkul et al., 2002); the spar crystals follow in the form of residue under the micritic clumps support (Özkul et al., 2002).

3) **Travertine pisoids** are pale yellow colour and range in shape from spherical, through irregularly rounded, to hemispherical, depending on water-energy and microbial activity (Folk and Chafetz, 1983). Folk and Chafetz (1983) distinguished two types of pisoids, based on microstructure: 1) concentrically laminated and 2) radial shrubs; Guo (1993) added the 3) stromatolitic mammillated pisoids. 1) According to Folk and Chafetz (1983) concentrically laminated are regarded as inorganic but may be partly influenced by biotic processes (Guo, 1993); normally concentric pisoids range from 3 to 10 mm in diameter. They form in turbulent water (Guo and Riding, 1998). These pisoids are roughly spherical and the overall shape corresponds with that of the nucleus (Folk and Chafetz, 1983). The conformal-concentric accretion growth indicates a constant rate on all sides of the pisoid and shows that the shapes are not due to later compaction of a soft body (Folk and Chafetz, 1983). The inner-pisoids material consists of bacterial clumps in sparry calcite cement (Folk and Chafetz, 1983). 2) Radial shrubs, called also bacterial pisoids by Folk and Chafetz (1983), according to Guo and Riding (1998) are influenced by a combination of microbial and abiotic processes; they present a crude lamination and are aggregated in layers 1-2 cm thick, parallel with the bedding and often interbedded with bacterial shrubs layers (Folk and Chafetz, 1983). Radial shrubs form in depositional environments with little agitation, rich in microbial activity (Folk and Chafetz, 1983), associated with diatoms (Guo and Riding, 1994). 3) Stomatolitic mammilated pisoids shows irregular nodular outgrowth, are often covered by cyanobacteria filaments, and develop in low energy environments.

4) **Paper thin rafts travertine** consists of thin, delicate, brittle crystalline layers precipitated at the water surface, and occurs widely as a few individual sheets representing water

films (Guo and Riding, 1998). These layers are composed of aragonite or calcite radiating needles, making a slightly undulatory flat fragment that represents at the water-air interface (Chafetz et al., 1991). Paper-thin raft develops in shallow stagnant pools, and almost always are linked with diatom frustules (Chafetz et al., 1991; Guo and Riding, 1998). These sheets are broken into irregular fragments by disturbance, whereas desiccation leaves them intact, causing an accumulation on pool floors (Guo and Riding, 1998).

5) **Coated bubbles** are a fabric type made by layers of lithified gas bubbles preserved by the rapid precipitation of $CaCO_3$ around them in the stagnant water column, such as in terrace pools and large ponds (Guo and Riding, 1998). They are generated near the sediment-water interface and worked their way upward (Chafetz and Folk, 1984). The main source of these gas bubbles is microbial activity in underlying sediment (Guo and Riding, 1998). They are, initially, composed of pure oxygen and devoid of CO_2 (Chafetz et al., 1991); this lack of CO_2 within the bubble brings the adjacent microenvironment around them, to lose CO_2 to equilibrate with the gas in the bubbles; this will drive the level of saturation of $CaCO_3$ to extremely high levels and precipitate (Chafetz et al., 1991). Often the bubbles occur as lenticular layers of foam rock, 2-10 cm thick, in which porosity can approach 80% (Chafetz and Folk, 1984). Bubbles can generate near-vertical tubes up to 3 mm in diameter, with slight constrictions like a sausage, and both top and bottom ends are hemispheres when more bubbles stack up in a vertical train of bubbles (Chafetz and Folk, 1984). Surface tension facilitates chain formation by creating sufficient time for incipient lithification (Guo and Riding, 1998).

6) According to Guo and Riding (1998), **reed travertine** consists of plant stems and roots coated by micrite. It forms when high densities of stems slow down the water flow and this material becomes encrusted by fine crystalline carbonate which often fills the space between them (Guo and Riding, 1998). The plant stems and roots create cylindrical moulds, whose interiors mostly remain empty or partly filled by sediment or spar crystals (Guo, 1993). These moulds are largely responsible for the large porosity of this fabric type (Guo and Riding, 1998). Accumulation of reeds are typical of marshy flat covered by very shallow still water or could develop reed mounds near the base of slopes (Guo and Riding, 1998).

7) **Lithoclast travertine** is made of detrital grains eroded from previously precipitated travertine and deposited in lower depressions, where pedogenetic processes occur, mixed with *in situ* precipitates (Guo and Riding, 1998). It is dominated by silt-sand grade detritus and also can contain reed fragments, ostracodes, gastropods and quartz silt matrix and extraclasts (Guo and Riding, 1998). Lithoclast travertine is often characterized by pedogenic fabrics and widespread fenestrae. Another lithoclastic deposit is formed by accumulation of breccia clasts derived by collapse of low wall, such as from travertine waterfalls (Guo and Riding, 1998). Pedley (1990) classified lithoclast travertine into four types: a) phytoclast, cemented crust formed around plants; b) oncoidal; c) intraclast, silt- to sand-sized particles carried downstream and redeposited as clastic grain-supported fabrics; d) microdetrital, consisting of micrite which is structureless.

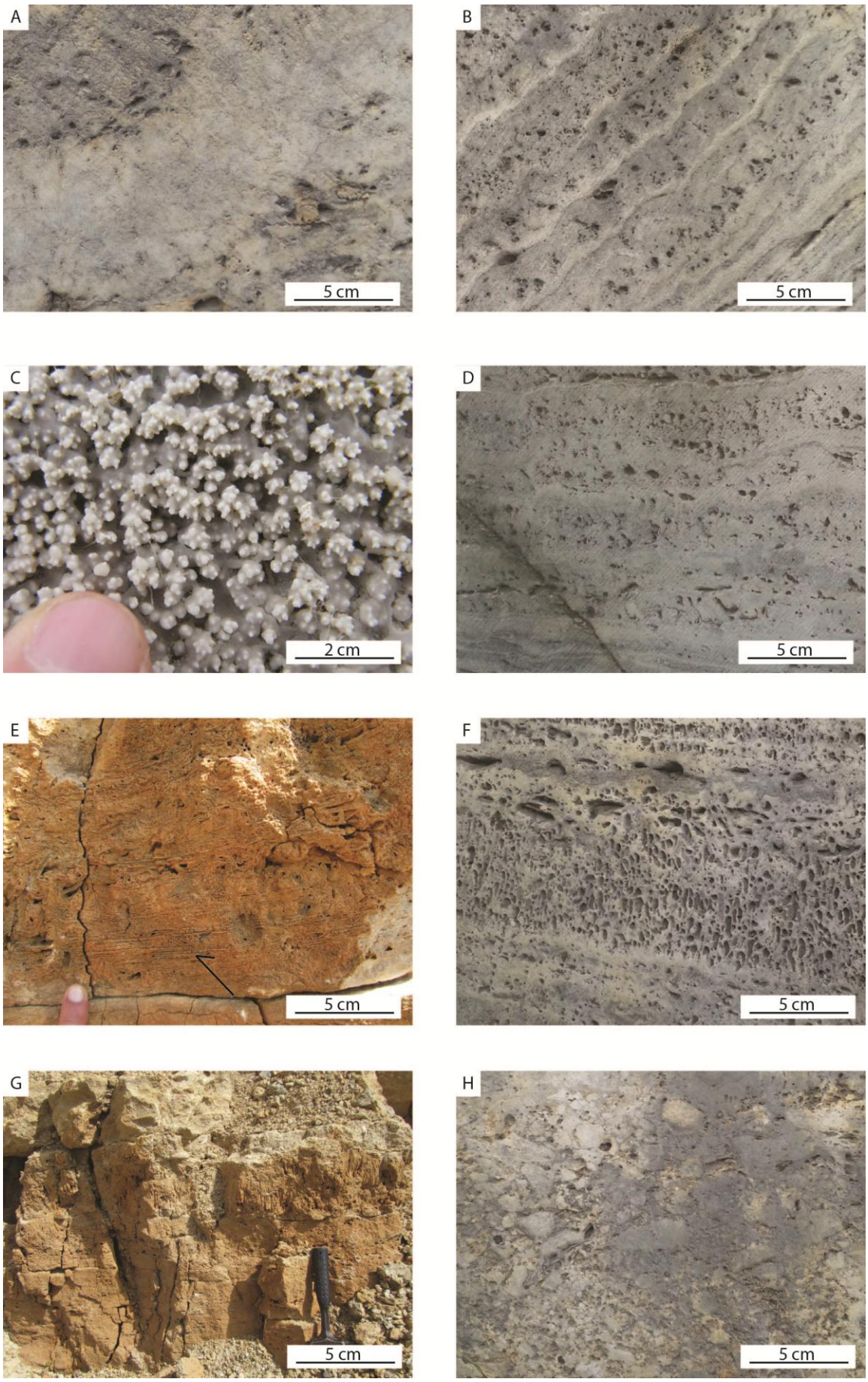
A
5 cm
B
5 cm
C
2 cm
D
5 cm
E
5 cm
F
5 cm
G
5 cm
H
5 cm

Figure 1-1. Crystalline crusts are dense white, layered fibrous crusts, typically of rapid flow on slopes. B-C. Travertine shrubs have a dendritic growth morphology, which may range from short to elongate and vertical or radiating, and arranged in horizontal layers, separated by micritic laminae. D. The shape of pisoids change depending of water energy and microbial activity, ranging from spherical to irregularly rounded and may have different internal arrangement, concentrically laminated, radial or stromatolitic mammilated. E. Paper thin rafts are sub-horizontal thin sheets precipitated on the surface of still water. F. Coated bubbles consist of chains of individual bubbles aligned vertically; each bubble has a central hollow around which fine micrite precipitates; adjacent chains are separated by micritic matrix. G. Reed travertines are moulds of reeds or coarse grasses, sometimes forming clump, around which limestone precipitated. H. Lithoclast travertines derive from erosion of slope deposits and are deposited in depression or at toe of slope.

1.2.4 Travertine depositional environments

The occurrence of thermal springs can produce different travertine unit morphologies; travertine morphologies are extremely varied and reflect accretionary rather than erosive processes (Pentecost and Viles, 1994). Pentecost and Viles (1994), Guo and Riding (1998) and Pentecost (2005) drew up different classifications about travertine morphologies, embodying descriptions from many papers and publications, plus their own observations. These morphologies are regrouped here in six categories (Fig 1.2 A-F).

a) **Spring mounds**, according to Pentecost and Viles (1994) spring mound consist of domes surrounding a spring orifice, and they can be up to 50 m in height. Mounds are the result of instantaneous precipitation from thermal spring water that issues from point sources within segments of active faults and flows down a slope to build a mound of travertine (Hancock et al., 1999).

b) **Fissure ridges** result from build-ups around spring orifices along fractures and range from 1 metre to 15 metres in height and may be up to 500 metres in length (Pentecost and Viles, 1994). Hancock et al. (1999) suggested that mounds occur where fissures underlie soft sediments, while fissure ridges where the fractures continue to the surface. Moreover Hancock et al. (1999) divided the morphology of fissure ridges depending on the velocity of the flow rate: if the flow rate from a fissure is high, water spreads out rapidly and a ridge with a low aspect ratio (0.1-0.2) develops; in contrast, where slow flow rate from a fissure occurs, the ridge formed is high but narrow. The outermost surface of the fissure ridges is abundantly ornamented with microterraces; these microterraces are considerably smaller than mound terraces (Chafetz and Folk, 1984).

c) **Slope** depositional system can be distinguished in two different morphologies: terraced slope and smooth slope (Guo and Riding, 1998).

The terraced slope consists of vertical to overhanging walls, sub-horizontal pools and rims. Walls range in height from several centimetres up to few metres. The main fabrics precipitated in this environment are the crystalline crusts (Guo and Riding, 1998).

Terrace pools are centimetre to decimetre in size. The energy flow is reduced in the pools and the typical facies precipitated in this element are shrub dendrite, coated gas bubble boundstone,

raft rudstone and coated rounded grains (Chafetz and Folk, 1984). The pools are surrounded by rims that are usually raised (Guo and Riding, 1998).

The smooth slope consists of a uniform profile, lacking terraces, and with an angle from 10° to 40°. This morphology develops under higher flow than the terraced slope (Guo and Riding, 1998). According to Folk et al. (1985) smooth slopes are composed of crystalline crusts precipitated under agitated flow.

d) **Shrub flat** facies precipitates as horizontal tabular travertine deposits dominated by thin-bedded shrub facies interlayered with pisoids, coated bubbles and lithoclasts (Guo and Riding, 1998). This travertine is light-coloured (Özkul et al., 2002). According to Özkul et al. (2002) this environment is subjected to long-term erosional periods and precipitation interruptions resulting in the development of palaeosols and desiccation features.

e) **Marsh pools** are characterized by horizontal, grey, brown-coloured and porous travertine that is rich in reeds and is populated by gastropods and ostracodes, showing a development far away from water source (Guo and Riding, 1998; Özkul et al., 2002). As shrub flat facies, also marsh pool facies are widespread subjected to pedogenesis and fenestrae are often abundant (Guo and Riding, 1998). Furthermore, marsh-pool facies are interlayered with clay flats and breccia layers (Guo and Riding, 1998). A difference from shrub flat is the reduced lateral extension of the layers (Guo and Riding, 1998).

f) **Reed mound** facies consists of a complex of wedge shape and lenticular units with convex surfaces that slope from 0 to 35°, characterized by asymmetric outlines with one side steeper than the other (Guo and Riding, 1998). Reed travertine is the dominant lithotype, associated with paper-thin raft and coated bubbles, with ostracodes and gastropods in the reed cavities (Guo and Riding, 1998). Mounds are frequently cut by exposure surfaces (Guo and Riding, 1998).

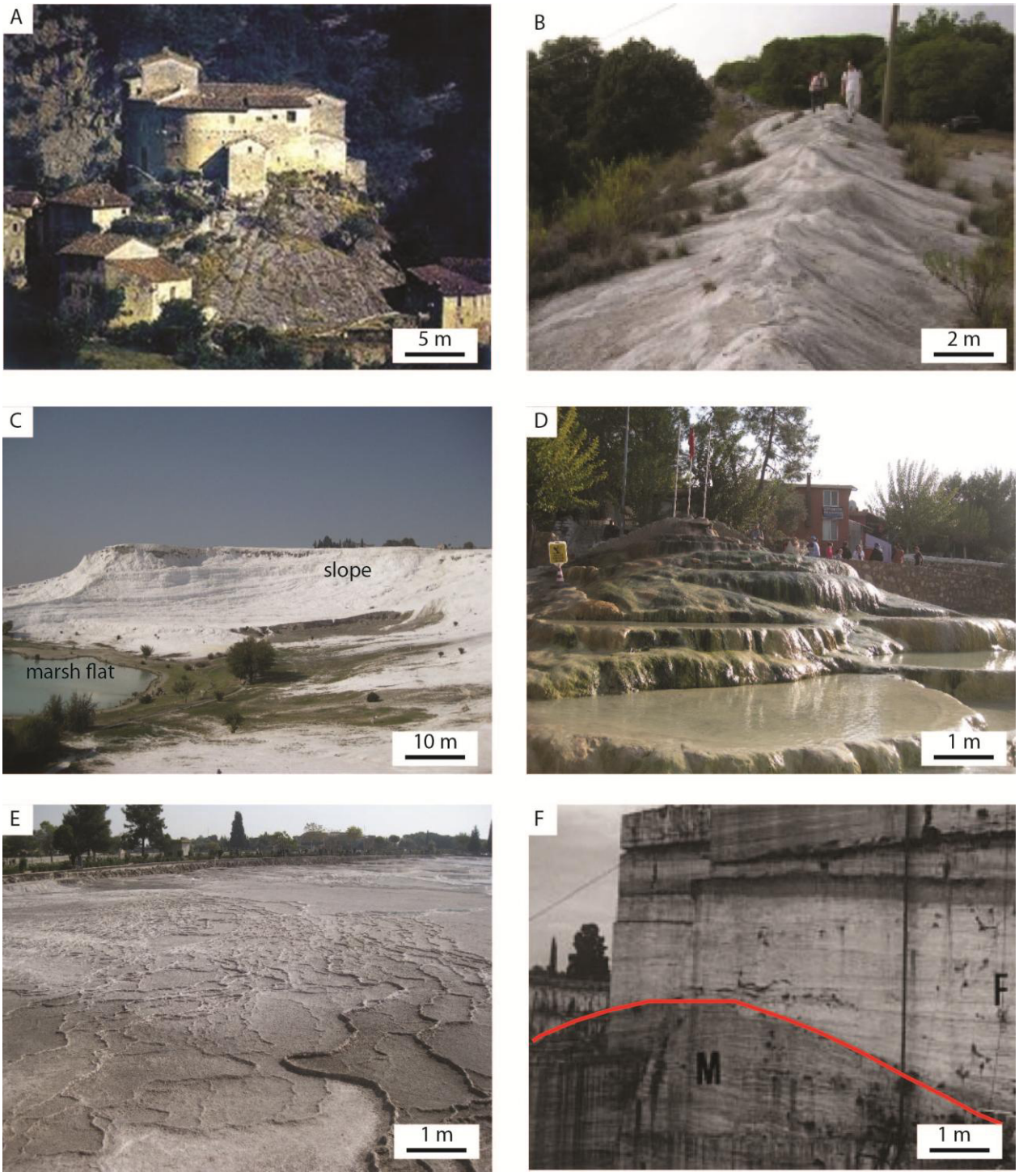

Figure 1-2. A "Castel di Luco" (Ascoli Piceno, Italy) is a castle built above a fossil subaerial hydrothermal spring mound, more than 20 m high, consisting of a dome surrounding a spring orifice (ascoli-ontheroad.blogspot.com). B. Fissure ridges result from build-ups around spring vents along fractures; their shapes depending on the velocity of the flow rate, building ridges high and narrow when the flow rate is low, on the contrary the ridges are small but wide. The flanks of fissure ridge at Rapolano Terme complex (Tuscany, Italy) are characterized by microterraces (www2.hull.ac.uk). C. Slope system of Pamukkale hydrothermal complex (Hierapolis, Turkey) consists of smooth inclined and terraced layers. This system passes toward valley to a marsh environment that consists of shallow pools enriched in plants and reeds. D Example of terraced slope system (Hierapolis, Turkey). E) Shrubs flat facies occurs in sub-horizontal undulated layers. F) Reed mound facies (M) overlain by shrub flat facies (F).

1.2.5 Travertine precipitation processes

The precipitation of continental carbonates takes place when dissolved carbon dioxide in a groundwater attacks and dissolves carbonate rocks to form a solution containing calcium and bicarbonate ions (Pentecost, 2005). The sources of carbon dioxide are the respired soil-zone CO_2 and thermally generated CO_2. When this groundwater comes into contact with the atmosphere, less rich in carbon dioxide, the environment recovers the balance bringing CO_2 from the water to the atmosphere with this reaction:

$$Ca^{2+} + 2(HCO_3)^- = CaCO_3 + CO_2 + H_2O$$

With the result of precipitation of calcium carbonate from CO_2 evasion. This process is common in spring and flowing water settings such as freshwater streams or hydrothermal travertines.

In agreement with O'Neil and Barnes (1971), groundwater from regions undergoing serpentinization or those in contact with natural or industrially produced calcium hydroxide, which acquire high pH, precipitates carbonate calcium, through this reaction:

$$Ca(OH)_2 + CO_2 = CaCO_3 + H_2O$$

Another process that allows the precipitation of calcium carbonate, happens when groundwater rich in calcium mixes with alkaline surface waters, mainly in saline lakes where the concentration of OH^- is elevated (Pentecost, 2005). Hydroxyl ions in the lake water react with bicarbonate (HCO_3^-) to form carbonate (CO_3^{2-}), followed by the precipitation of calcium carbonate (Pentecost, 2005).

$$Ca\,(HCO_3)_2 + OH^- = CaCO_3 + HCO_3^- + H_2O$$

Microbial mats are widely regarded as the Earth's earliest ecosystem (Tice and Lowe, 2004, 2006; Noffke et al., 2006) and have been present on Earth for over 3 billion years (Hofmann et al., 1999; Schopf, 2006). Microbial mats have been defined as laminated organo-sedimentary structures, where each mat layer contains different microorganisms with distinct metabolic activities (Krumbein et al., 1983; Van Gemerden, 1993). The presence of microbial mats, common in different environments as lacustrine and hydrothermal, influences the calcium carbonate precipitation. Microbial communities, formed by cyanobacteria, other phototrophic bacteria and heterotrophic bacteria, promote the precipitation of calcium carbonate as product of microbial metabolism (Des Marais, 1997), in water where there is a favourable saturation state of Ca^{2+} and bicarbonate. The precipitation is the key process of production, accumulation of calcified microbes and improving mat accretion and preservation (Riding, 2000). Carbonate precipitation is stimulated by alkalinity, which increases through various metabolic processes, such as photosynthetic uptake of CO_2 and HCO_3^- by cyanobacteria, ammonification, denitrification and sulphate reduction by heterotrophic bacteria (Riding, 2000). According to Dupraz and Visscher (2005), microbial metabolism consists of 6 simple

reduction-oxidation reaction, involving C, O, S and N and driven by 6 different bacteria groups (Fig. 1.3 A-B):

1. $2HCO_3^- + Ca^{2+} \leftrightarrow (CH_2O) + CaCO_3 + O_2$ (photosynthesis)

2. $(CH_2O) + CaCO_3 + O_2 \leftrightarrow 2HCO_3^- + Ca^{2+}$ (glycocen degradation)

3. $3HCO_3^- + Ca^{2+} + HS^- \leftrightarrow (CH_2O) + CaCO_3 + SO_4^{2-}$ (fermentation-denitrification)

4. $2(CH_2O) + SO_4^{2-} + OH^- + Ca^{2+} \leftrightarrow CaCO_3 + CO_2 + 2H_2O + HS^-$ (sulphate reduction)

5. $3HS^- + 4O_2 + CaCO_3 + HCO_3^- \leftrightarrow 2\ (CH_2O) + Ca^{2+} + 3SO_4^{2-}$ (fermentation-denitrification)

6. $3(CH_2O) + CaCo_3 + H_2O \leftrightarrow HCO_3^- + Ca^{2+} + C_2H_6O$ (fermentation)

Also Extracellular Polymeric Substances (EPS) are important suppliers of nucleation sites and facilitating sediment trapping (Riding, 2000), and also are important in the protection and stabilization of microbial microenvironments, where microbial metabolism takes place (Decho, 2000; Dupraz et al., 2004), from variable hydrodynamic regime and multiple environmental stress conditions (Decho, 2000). EPS consist of a variety of molecules such as polysaccharides and amino acids (Dupraz and Visscher, 2005). EPS biofilms allow rapid solute exchange, importing nutrient and removing waste products (Dupraz et al., 2004). Further EPS can facilitate carbonate precipitation forming heterogeneous microdomains, which support different types of microbial metabolism, and serving as an energy and carbon source for heterotrophic bacteria (Dupraz et al., 2004). According to Braissant et al. (2003), the EPS matrix plays a key role in organomineralization. Dupraz and Visscher (2005) proposed 3 types of EPS alteration leading to $CaCO_3$ precipitation (Fig. 2): a) microbially mediated decomposition of EPS, liberating HCO_3^- and Ca^{2+}, that will increase the saturation index of carbonate and calcium ions in the water; b) during organomineralization, the process of mineral formation mediated by organic matter (Trichet and Défarge, 1995), the reorganization of acid binding sites creates a template, which enables $CaCO_3$ to precipitate; and c) precipitation regulated by the balance of external cation concentration and binding capacity of EPS: when the available negatively charged groups are saturated with Ca^{2+}, precipitation can commence. However, EPS can inhibit carbonate precipitation, binding bivalent cations (Dupraz et al., 2004), such as Ca^{2+}, when the EPS Ca/bindimg capacity is not saturated (Dupraz et al., 2009). Microbial carbonate microfacies are heterogeneous, but the main component is dense clotted peloidal micrite resulting from the calcification of bacteria cells and biofilms (Riding, 2000). Microbial precipitation has been an important process for the formation of carbonate marine sediments since the Archean, but also contributes to hot-spring travertine, cold-

spring mound, calcrete, cave crust and coated grain deposits as well as influencing carbonate cementation, recrystallization and replacement (Riding, 2000).

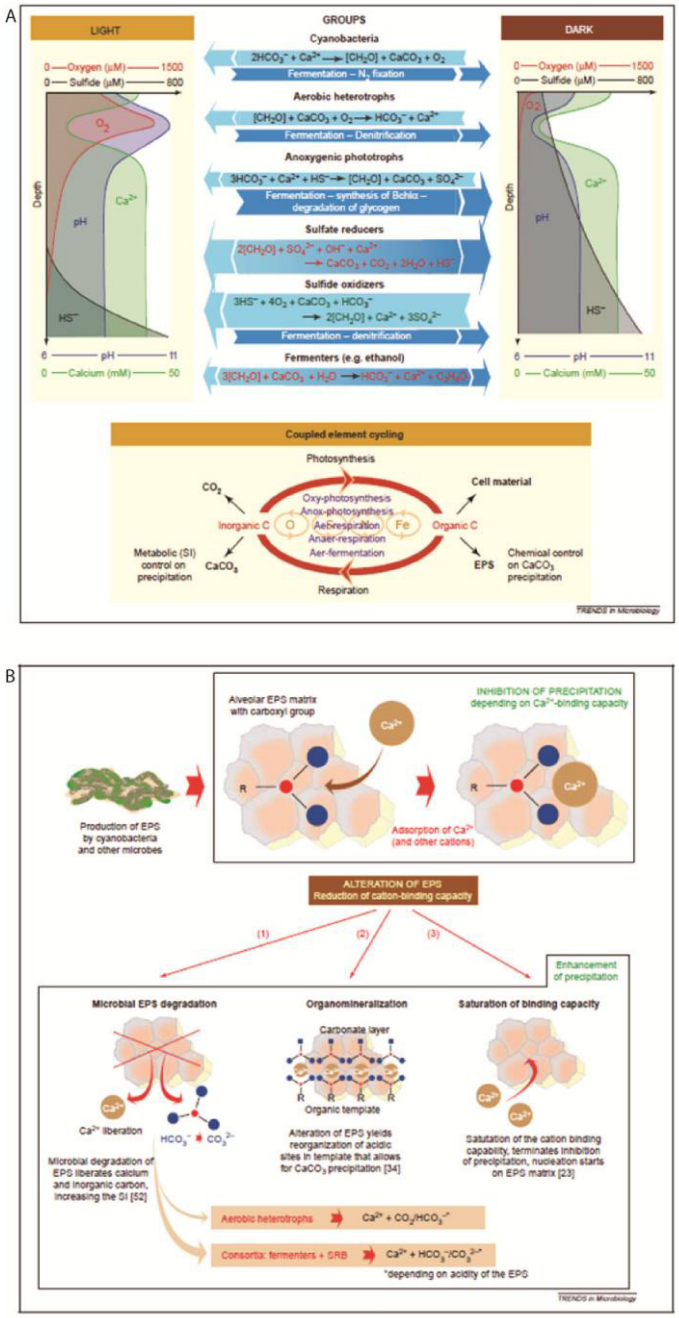

Figure 1.3. Metabolic pathways and geochemical gradients in a lithifying microbial mat. Six major groups of microbes composing the microbial mat community impact calcium carbonate precipitation and dissolution through metabolic activities. Note the daily fluctuations of oxygen, sulphide and pH caused by dependence of photosynthesis on light. Local differences in the saturation index (SI) are caused by the different metabolism among day and night, and different behaviour of the various metabolic reactions. The calcium profile shows a minimum in correspondence with the layer of maximum photosynthesis. Carbon cycling is coupled to element cycles of O, S and N (Dupraz and Visscher, 2005). 3B. The role of exopolymeric substances in calcium carbonate precipitation. Initially, EPS produced by various microbes, predominantly cyanobacteria, bind cations, including Ca^{2+}, which inhibit precipitation. Following this, microbial EPS degradation, organomineralization and saturation of binding capacity, allow to $CaCO_3$ to precipitate (Dupraz and Visscher, 2005).

1.2.6 Diagenesis and stable isotope signature

Diagenesis includes the alteration of a rock fabric after it has been deposited. Concerning travertines, diagenesis can be divided into processes that work during two different stages: meteoric diagenesis and late burial diagenesis (Pentecost, 2005). Tucker and Wright (1991) listed the effect of diagenesis on marine carbonates, such as dissolution, recrystallization, microbial micritisation, bioturbation, cementation, compaction, oxidation of organic matter and formation of authigenic minerals. In Recent travertines cementation is the most important process (Pentecost, 2005). Being most of the travertines originally made by low-Mg calcite, changes in crystal size and recrystallization (aggradational neomorphism) are often observed (Pentecost, 2005).

Meteoric diagenesis occurs in near-surface environments at ambient pressure and temperature. Percolating groundwater and rainwater result to be the principal causes of meteoric diagenesis. Depending upon the saturation state in Ca^{2+} and HCO_3^- of percolating waters, diagenesis can result in the dissolution or precipitation of carbonate (Pentecost, 2005). The porous framework of travertines promotes the flow of the water through the rock mass. In cases where a primary fabric is formed the porosity may be as low as 10 %, but the average porosity of Recent travertines is 50-60 % (Pentecost, (2005).

Meteoric diagenetic settings are distinguished in two parts: the vadose and the phreatic. In the vadose region cementation is characterized by two forms, meniscus and gravitational and both have been observed in travertine fabrics . Phreatic waters precipitate mosaic and scalenohedral fabrics, often developing isopachous layers (Pedley, 1987; Pentecost, 2005).

Where travertines are exposed to solutions undersaturated with respect to a carbonate mineral, surface dissolution occurs, evolving in karsification (Viles and Goudie, 1990) and the formation of soils. In addition to the development of large pores to caves, the dissolved products of travertines can re-precipitate lower in the sequence, forming stalactites and flowstones (Pentecost, 2005). Sparmicritization is a term devised by Kahle (1977) to describe the dissolution activities of microorganism on carbonate rocks. In travertines sparmicritization was described by Chafetz et al. (1994) from the Plitvice Lakes travertine and by Guo and Riding (1994) from shrub fabrics in Rapolano Terme, Central Italy. According to Kahle (1977) sparmicritization could be caused both by abiotic and organically mediated processes. These products of sparmicritization are the destruction of crystal outlines, developing of “spiky crystals” (Folk, 1985) and ultimately a micritic appearance of the fabric.

Recrystallization of calcite in travertines concerns principally the transformation of micrite into sparite. This process was termed by Love and Chafetz (1988) as aggradational neomorphism. The beginning of diagenesis involves algal bushes, which are partially encased in a spar crystal. This crystal becomes the starting point of aggradational neomorphism, acting as substratum for the growth of other crystals, resulting then in the formation of larger columnar crystals (Love and Chafetz, 1988).

Burial diagenesis is the result from increased lithostatic and hydrostatic pressure, heating, the ingress of mineral enriched solutions and the absence of dissolved oxygen. Compaction, porosity reduction due to further cementation, dissolution of original fabric with replacement by other minerals

are the main products of burial diagenesis. Also dolomitization was observed in a few studies such as Donovan (1973) from Devonian travertine-like deposits from Scotland.

Stable isotopic data of travertines are significantly distinguishable from other non-marine carbonates. In many studies (Chafetz and Lawrence, 1994; Guo and Riding, 1996; Fouke et al., 2000; Minissale et al., 2002a,b; Minissale, 2004; Pentecost, 2005; Gandin and Capezzuoli, 2008; Kele et al., 2008; Della Porta, 2015) stable isotopic data obtained from calcite precipitated from hot water show positive values of $\delta^{13}C$ and negative values of $\delta^{18}O$. Hydrothermal travertine oxygen stable isotope values reflect the groundwater isotopic composition and water temperature (Gonfiantini et al., 1968; Friedman, 1970; Guo et al., 1996), whereas carbon isotope values depend on the CO_2 sources, which can be magmatic mantle derived, metamorphic or organic. Pentecost (2005), to provide his classification of travertines, collected many studies and developed ranges for stable oxygen and stable carbon values to separate thermogene and meteogene travertines.

The signature of stable oxygen isotopes in meteogene travertines varies between -13‰ and 4‰ (V-PDB), with a median at -7.58‰ (V-PDB) (Pentecost, 2005). Stable carbon isotope values range between -12‰ and 8‰ (V-PDB) with a median at -8.48‰ (V-PDB) (Pentecost, 2005).

According to Pentecost (2005), in thermogene travertines, oxygen isotope values are distributed between -26‰ and -1‰ (V-PDB), having a median of -6.95‰ (V-PDB), similar to that of meteogene travertines. Carbon isotope distribution in thermogene travertines varies between -8‰ and 11‰ (V-PDB), with a median of 4.3‰ (V-PDB), significantly displaced towards positive values with respect to the meteogene travertine values (Pentecost, 2005).

The rates of CO_2 degassing influences the carbonate the carbon isotopes, consequently the $\delta^{13}C$ of the precipitated carbonates increases with increasing distance from the spring (Guo et al., 1996; Fouke et al., 2000; Kele et al., 2008).

Chapter II

Geological setting

2.1 Albegna Basin

The Neogene Albegna Basin (Fig. 2.1) developed on the Cenozoic Apennine fold-and-thrust belt from the Tortonian (Late Miocene) time, when the inner northern part of the Apennine orogen was subjected to extensional tectonics, which was time equivalent to the eastward migration of the thrust propagation (Patacca et al., 1990; Carmignani et al., 1994). Extensional structures were superimposed on the previous contractional structures (Pasquarè et al., 1983; Zanchi and Tozzi, 1987; Brogi et al., 2014). The Albegna Basin substrate includes the following pre-extension superimposed tectonic units (Kligfield, 1979 and references therein): 1) Ligurian and Sub-Ligurian Units, composed of remnants of the Jurassic oceanic crust and its Jurassic–Cretaceous sedimentary cover, as well as Cretaceous–Oligocene turbidites; 2) Tuscan Nappe, composed of non-metamorphic sedimentary succession including the Upper Triassic Anidrite di Burano/Calcare Cavernoso Formation and Cretaceous–Lower Miocene marine clastic deposits; and 3) the metamorphic Tuscan succession.

The Miocene extensional phase led to the development of hinterland basins separated by NW–SE-oriented transverse lineaments (Pascucci et al., 2007). During the Pliocene, structural depressions developed controlled by WSW–ENE-oriented tectonic lines (Zanchi and Tozzi, 1987; Pascucci et al., 2007; Cornamusini et al., 2011 and references therein), such as the Albegna Line (Fig. 2.1). These extensional basins were filled by upper Tortonian lacustrine clays and fluvial conglomerates (Unit T in Bossio et al., 2003–2004; cf. Fig. 2.2), overlain by brackish deposits that denoted an early Messinian marine transgression (Unit M1 in Bossio et al., 2003–2004). The following uplift of the Middle Tuscany Ridge during the late Messinian promoted the deposition of fluvio-lacustrine conglomerates and clays (M3 in Bossio et al., 2003–2004). In the study area, unit M3 is represented by the Poggio Capraio Formation, which unconformably overlies the Ligurian Unit (Fig. 2.3). The Albegna Basin was oriented SSW–NNE during the Pliocene when at least 200 m of marine claystone were deposited (Blue Clays; Unit-P1 in Bossio et al., 2003–2004; Figs. 2.1 and 2.2). The Late Pliocene to Holocene sedimentary history of the Albegna Basin was characterized by tectonic uplift as well as glacio-eustasy and climate, with the deposition of various continental lacustrine to brackish successions (Units P2, P3 and Q1–Q3; cf. Bossio et al. 2003–2004 and Fig. 2.2) unconformably overlying the Lower Pliocene marine Blue Clays.

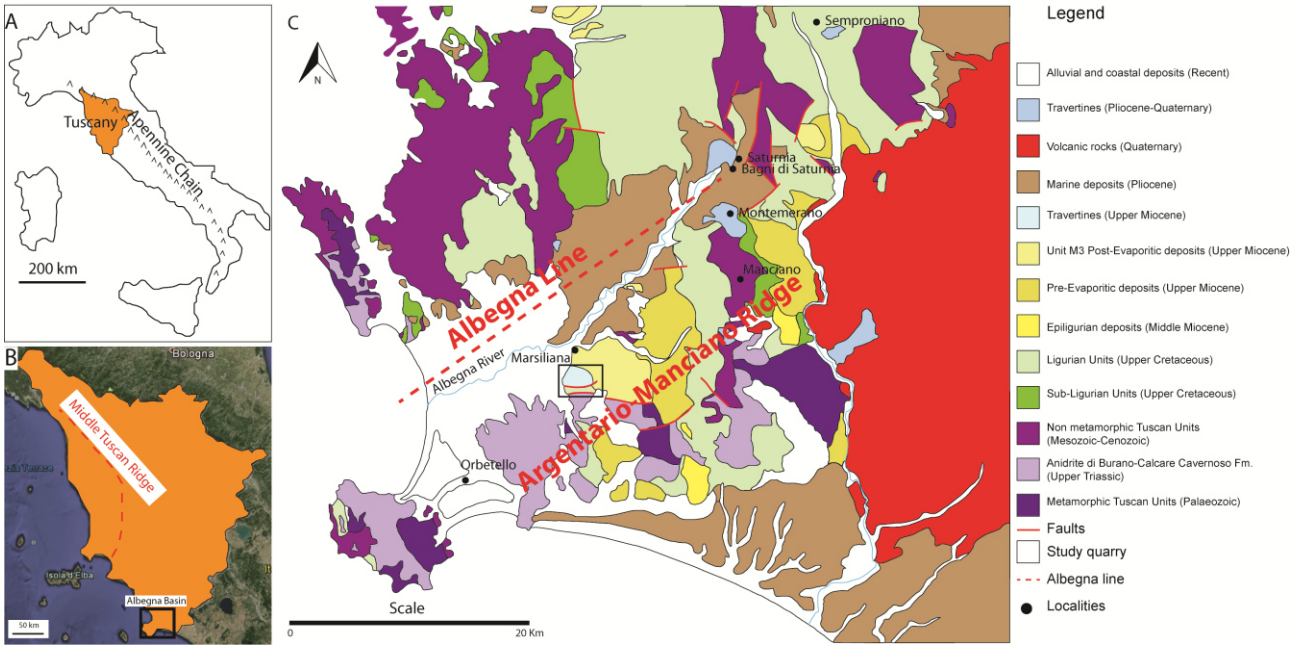

Figure 2.1. Regional geological setting of the study area. A) The studied area is located in the Northern Apennines, in the Tuscany region, highlighted in orange. B) From Google Earth, satellite image of Tuscany, Central Italy, highlighted in orange; the Albegna Basin is framed in a black square. C) Geological map of the Albegna Basin redrafted after Cornamusini et al. (2011). From the Pliocene, the Albegna Basin is controlled by tectonic lineaments oriented SSW–NNE, such as the Albegna Line. The studied area is delimited by the black square.

2.2. Distribution of travertine outcrops in the Albegna Basin

The Albegna Basin includes several Neogene to Holocene thermogene travertine units, which are distributed along faults and fractures, related to hydrothermal activity. Travertines occur close to the Manciano, Montemerano, Saturnia and Marsiliana localities (Fig. 2.1c; Zanchi and Tozzi 1987; Bosi et al., 1996; Barilaro et al., 2011, 2012). Bosi et al. (1996) distinguished five travertine units of different ages from the Messinian to the Holocene (Tr1–Tr5 in Fig. 2.2). Bosi et al. (1996) determined the relative ages of these travertine units based on their stratigraphic positions, sedimentary and tectonic features and, for the youngest units, their occurrence with respect to three orders of Quaternary fluvial terraces developed in the Albegna River valley, labelled as A1, A2 and A3 (Fig. 2.2). Tr1 represents the Holocene travertine deposits at Bagni di Saturnia (Fig. 2.1), which developed on the youngest and lowest (25–80 m above sea level a.s.l.) fluvial terrace A1 (Bosi et al., 1996). This active system is characterized by a water temperature of 37 °C and a pH of 6.3 (Minissale, 2004). Tr2 denotes the Middle–Upper Pleistocene travertines cropping out near the Montemerano and Manciano villages, which developed on the fluvial terrace A2, from 80 to 160 m a.s.l. (Bosi et al., 1996). The Middle Pleistocene Tr3 travertines developed adjacent to the A3 fluvial terrace (from 100 to 190 m a.s.l.), which then crop out at the village of Saturnia (Bosi et al., 1996). These three travertine units are untilted and characterized by sub-horizontal stratification. Tr4 refers to Pliocene travertine deposits close to the village of Semproniano, which developed above the Pliocene deposits (Bosi et al., 1996); this unit is also characterized by horizontal stratification, although the travertines show evidence of

tectonic deformation (Bosi et al., 1996). Tr5 represents the Messinian travertine deposits that crop out close to the Marsiliana village, which are the focus of this study (cf. Chapter 3 and 4). The Tr5 travertines overlie the Messinian deposits with a tilted appearance (dips 60–70°), and they are subjected to faults with a strike-slip component as the underlying Messinian strata (Bosi et al., 1996; Bossio et al., 2003–2004).

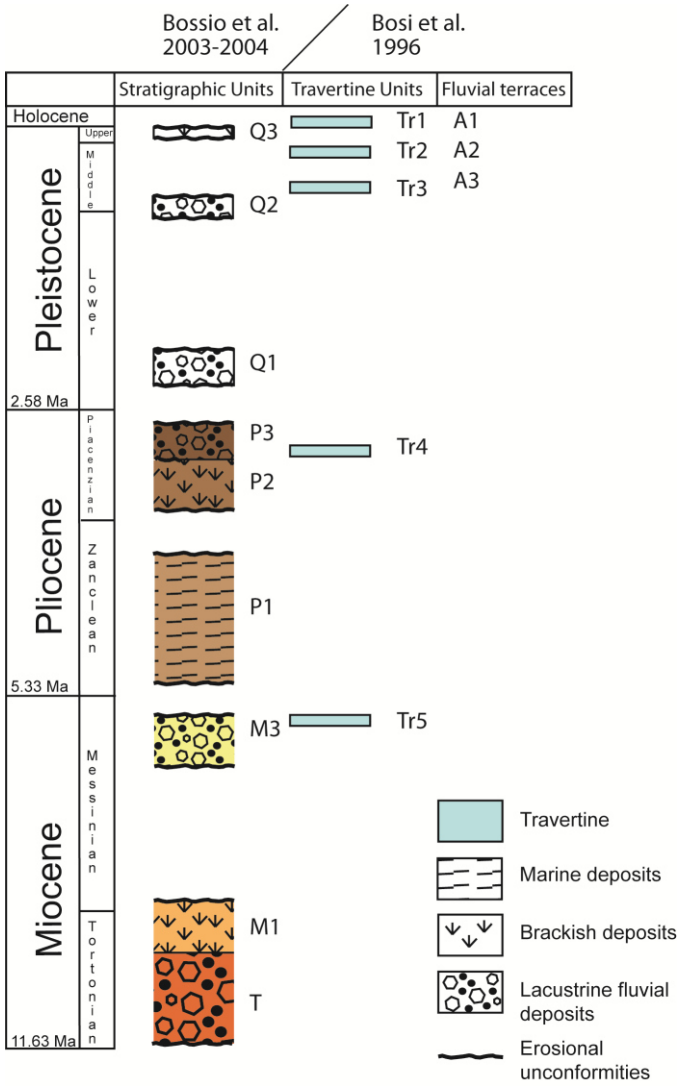

Figure 2.2. Stratigraphy of the Neogene to the Holocene succession cropping out in the Albegna Basin, redrafted after the studies by Bosi et al. (1996) and Bossio et al. (2003–2004).

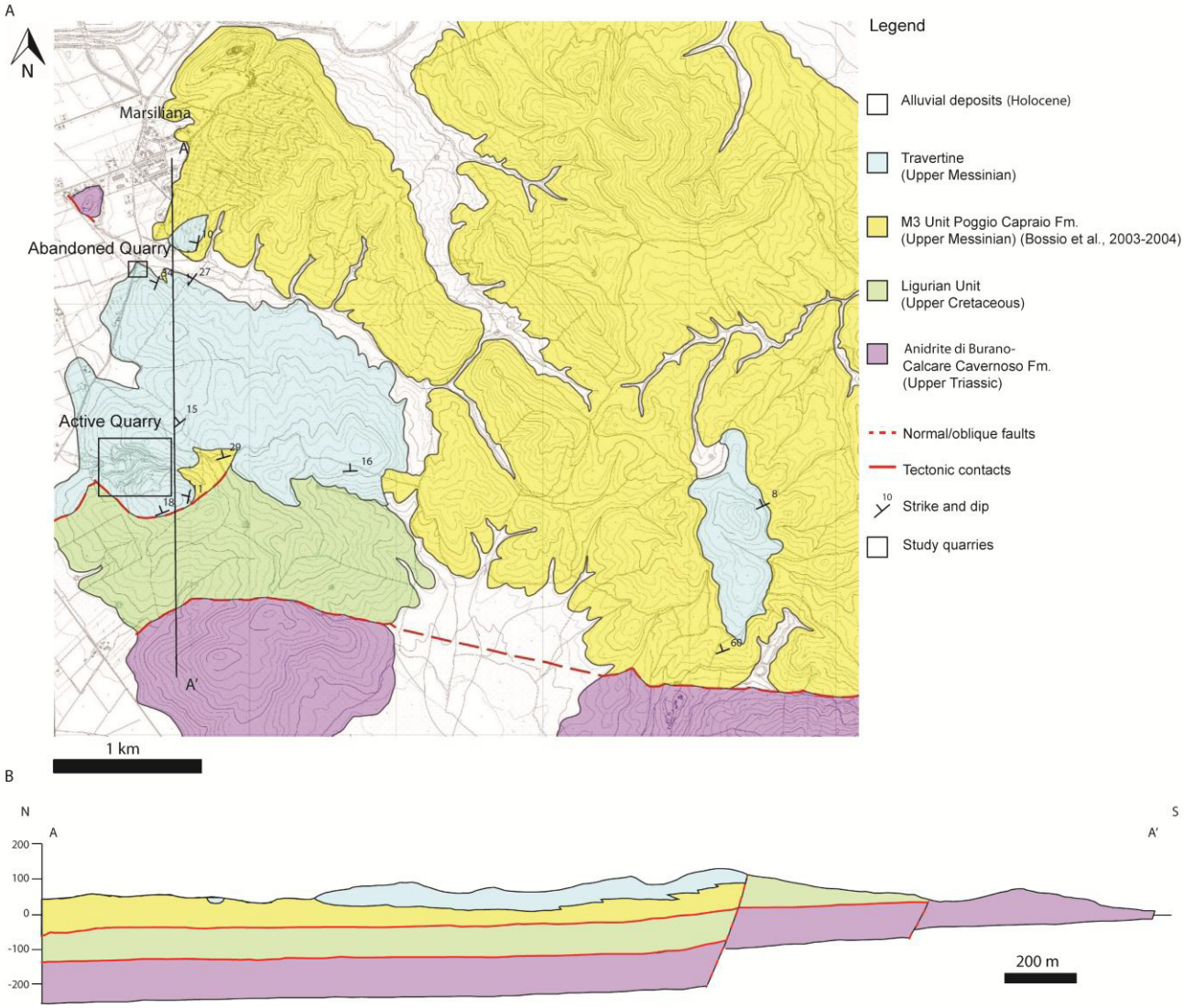

Figure 2.3. A) Geological map of the studied area redrafted after Pertusati et al. (2004). B) North–South geological cross section of the studied area showing the relationships of the Neogene M3 Unit Poggio Capraio Fm. with the deformed Mesozoic Anidrite di Burano/Calcare Cavernoso Formation and the Ligurian Unit.

2.3 The Neogene to Quaternary magmatic activity

The Neogene to Quaternary magmatic activity in the Tyrrhenian-Apennine region includes subduction-related calc-alkaline magmatism, intraplate alkaline magmatism and MORB-type basalts (Rosenbaum and Lister, 2004 and references therein). The magmatism is related to a west dipping subduction zone (Rosenbaum and Lister, 2004 and references therein). These magmas become younger from west to east, rather than according to a continuous migration of the site of the magmatism toward the east (Serri, 1997; Rosenbaum and Lister, 2004), interpreted as the response to rollback of the subduction hinge during the opening of the Tyrrhenian Sea (Rosenbaum and Lister 2004). According to Serri (1997) the magmatic activity in Northern Tyrrhenian developed in four phases (Fig. 2.4):

Phase I is documented only by one centre, the Sisco sill (Corsica). The age of this small lamproitic intrusion ranges from 13.5 and 15.0 Ma. The Sisco lamproitic sill represents the oldest activity related to the post collisional lithospheric extension.

Phase II includes Montecristo volcano, seamount Vercelli (central Tyrrhenian Sea) and Monte Capanne acid plutons (7.3-6.2 Ma) and most of the activity of the Capraia Island volcano (6.9-6.0 Ma).

Phase III took place between 5.1 and 2.2 Ma. It includes the Porto Azzurro, Giglio, Campiglia, Gavorrano, Castel di Pietra and Monteverdi acid plutons, the San Vincenzo rhyolites and the Orciatico and Montecatini Val di Cecina lamproites. The second period of activity of Capraia (4.7 to 3.5 Ma) took place entirely within the age limit of this phase. Also the Roccastrada rhyolites (2.5-2.2 Ma) and the volcanic products of the Tolfa district are considered to belong to this phase.

Phase IV started at 1.3 Ma and up to 0.8 Ma includes the Radicofani (1.3 Ma), Monti Cimini (1.3-0.9 Ma) and Torre Alfina (0.8 Ma) products. Most of the activity of this phase took place between 0.6 and 0.1 Ma and consists nearly entirely of potassic and ultrapotassic products of the undersaturated trend; the rocks of the saturated trend of Latera were erupted between 0.15 and 0.09 Ma. The Monte Amiata (0.30-0.28 Ma) is the sole volcanic centre of the Tuscan Province, which was active within the age range of the Roman Magmatic Province (0.63-0.08 Ma).

Magmatic activity accompanied extensional tectonics in southern Tuscany since late Miocene, with an overall eastward migration, following the extensional deformation front (Acocella and Rossetti, 2002 and references therein). The Tuscan Magmatic Province is made up of granites (7.0 Ma– present) and subordinate volcanic products (5.0–0.3 Ma; Acocella and Rossetti, 2002). Magmatic activity is responsible for a positive thermal anomaly in southern Tuscany from late Miocene to present, culminating in the active geothermal areas of Larderello and Mt. Amiata (Acocella and Rossetti, 2002).

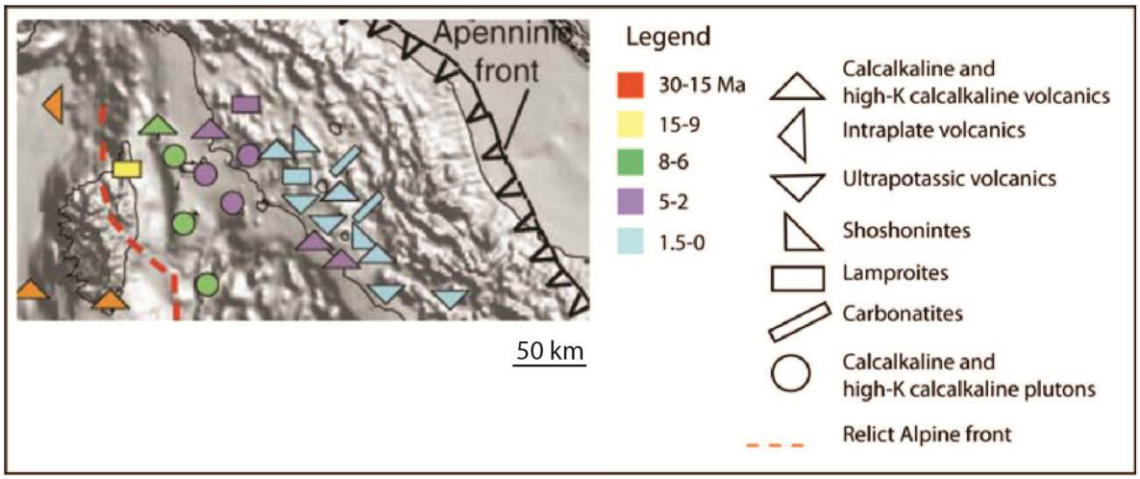

Figure 2.4. Magmatic and volcanic activities in the northern Tyrrhenian area from the Oligocene to the Present-day (after Serri, 1997).

2.4 Acque Albule Basin

The Acque Albule Basin (Fig. 2.5 A-B) is a morphological depression dipping toward the South (Faccenna et al., 2008), located to the west of Tivoli, a village 20 km East of Rome in Central Italy. The Acque Albule Basin is located in the inner sector of the Central Apennine fold-and-thrust belt and it extends over 30 km^2. Surface elevations across the plain range from 80 m a.s.l. to 40 m a.s.l. in the southwestern corner of the basin (Brunetti et al., 2013). This basin is bounded in the North by the Cornicolani Mountains, on the East by Lucretili-Tiburtini Mountains, on the West by gentle hills and on the South by the Aniene River (Brunetti et al., 2013).

The development of the Acque Albule basin started during the late Neogene, when the Tyrrhenian side of the Apennine belt was extended under a back-arc tectonic regime (Faccenna et al., 2008). Reduced thickness of the lithosphere, volcanism and high heat flow were the result of this extensional regime (Barchi et al., 1998; Jolivet et al., 1998; Chiodini et al., 2004; Acocella and Funiciello, 2006; Billi et al., 2006a). The Tyrrhenian side of the Central Apennines is also characterized by a system of NW-striking transfer faults and associated basins developed during the late Miocene-early Pleistocene (Acocella and Funiciello, 2006). During the Pleistocene and Holocene, a new tectonic phase was characterized by N-striking right-lateral and NE-striking transtensional to normal faults, which controlled the volcanism and the related hydrothermal activity (Faccenna et al., 2008).

From the Late Triassic to the Hettangian-Sinemurian time (Early Jurassic), the area was occupied by a large carbonate platform, called Laziale-Abruzzese platform, represented by the Upper Triassic dolomite (Dolomia Principale) and by the Lower Jurassic Calcare Massiccio Formation (Alberti et al., 1967; Bollati et al., 2011). The establishment of the extensional tectonic during the Early Jurassic, dismembered the carbonate platform and developed a submarine topography characterized by highs and lows, connected by escarpments with debris derived from the drowned and eroded carbonate platforms. Some sectors became deep basins, in which, during the Jurassic, pelagic successions accumulated (Bollati et al., 2011). Upon the structural highs, during the late Sinemurian to the early Pliensbachian, a mixed neritic/pelagic system established, with the accumulation of packstone and wackestone with calcareous algae, oncoids, sponge spicules, ammonites, radiolarians and calcareous nannoplanckton (Centamore et al., 1971). During the early Pliensbachian, these highs drowned and evolved into drowned platforms with condensed successions (cf. Pelagic Carbonate Platforms *sensu* Santantonio 1993; 1994). These platforms recorded reduced sedimentation rates of discontinuous succession characterized by condensed limestones rich in ammonites (Farinacci et al., 1981; Farinacci 1987; Cecca et al., 1991; Santantonio, 1993; 1994; Bartolini & Cecca, 1999; Galluzzo & Santantonio, 2002). Between the end of the Jurassic and the beginning of the Cretaceous period, the basin was filled by pelagic deposits, levelling the rift topography (Bollati et al., 2011). With the involvement of this sector in the orogenic system of the Apennines, during the Miocene the deposition of foredeep siliciclastic turbidite successions took place. Following the thrust progradation and uplift, extensional tectonics started from the late Miocene and there was the deposition of discordant Plio-Pleistocene marine clay sediments followed by Pleistocene-Holocene volcanic, lacustrine and fluvial-alluvial deposits (Bollati et al., 2011). In particular, during the mid-Pleistocene time, the Colli Albani

in the W-SW and the Colli Sabatini in the North were two large explosive volcanic districts in the Roman area, remaining active intermittently until recent times (De Rita et al., 1988, 1995).

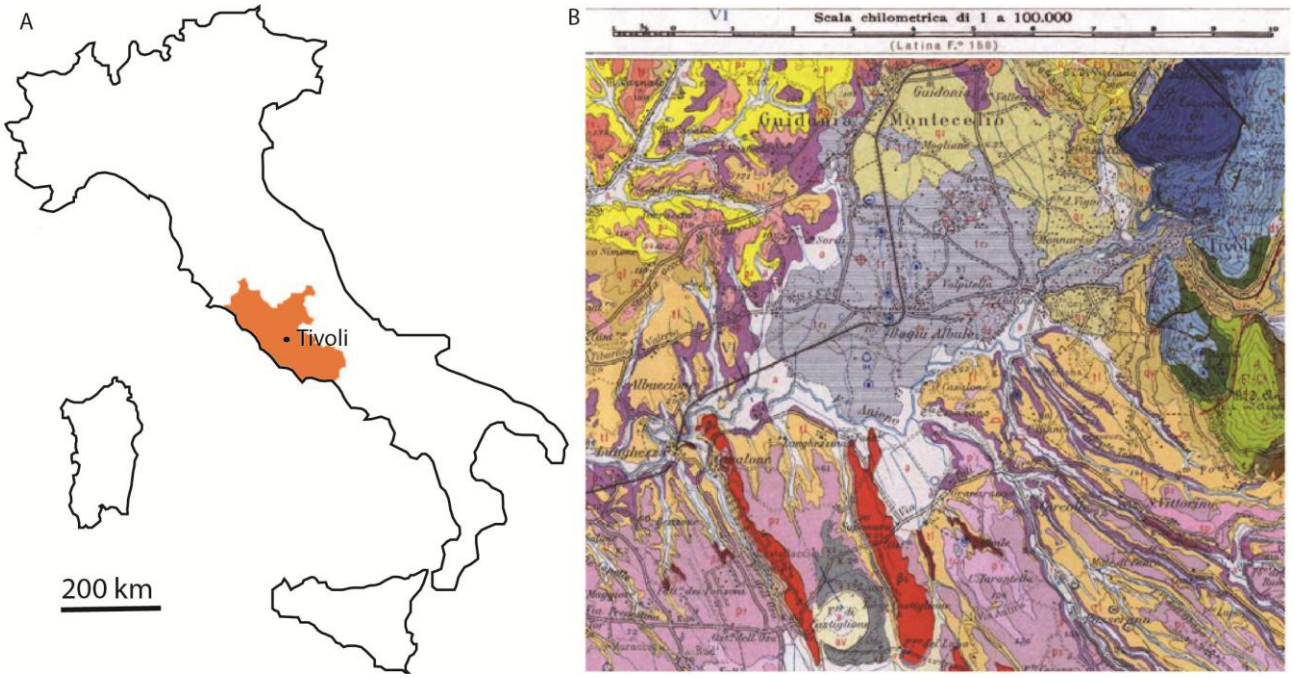

Figure. 2.5. Regional geological setting of the study area. A. The study area, in Tivoli, is located in the Apennines, in the Latium region, highlighted in orange. B. Detail of geological map 1:100,000 Roma sheet, surrounding the travertine deposit (tr), in grey. Travertines are surrounded and overlie the following units from bottom to top: Pliocene marine and coastal deposits (mainly yellow, p2, and p3), continental aeolian and fluvial deposits (PQ and qsb, brownish in colour) and volcanic deposits (ts1, p1, ts3, Tl, P2 and P'2), mainly coming from the south (after Alberti et al., 1967).

2.5 Structural and tectonic setting of the Acque Albule Basin

The Tivoli area is extended in the westernmost part of the fold and trusts belt of Central Apennines. The area comprises the Cornicolani, Lucretili, eastern Sabini, Tiburtini, Ruffi and Prenestini Mts. (Bollati et al., 2011; 2012). Within the Apennine orogenic belt, two main structural domains are recognized, separated by the Olevano-Antrodoco lineament: the Umbro-Sabino Domain, placed on the hangingwall of the lineament, and Laziale-Abruzzese Domain, placed on the footwall of the early Pliocene Olevano-Antrodoco lineament (Bollati et al., 2011). From a structural point of view the Sabina Domain is arranged into several thrust sheets verging towards to east, developed from middle-late Miocene to early Pliocene time (Cosentino and Parotto, 1986; Corrado et al., 1992). The Olevano-Antrodoco thrust marks the eastern tectonic boundary of this structural domain with the Laziale-Abruzzese Domain, bringing the sedimentary rocks of the Sabina Domain upon those of Laziale-Abruzzese Domain (Cipollario et al., 1992). During the same time, middle-late Miocene to early Pliocene, extensional tectonic, due to the opening of the Tyrrhenian Sea as a back-arc basin (Boccaletti and Manetti, 1978), down-threw the western border of this imbricated structure, enhancing the marine ingression along the peri-Tyrrhenian margin. The western border of the region was also reactivated by N-S right-lateral strike-slip fault, dissecting the earlier structures in the Pleistocene time (Alfonsi et al., 1991). This caused the formation of some pull-apart basins, including the Acque Albule basin (Kearey and Frederick, 1990).

Four tectonic units have been identified, separated by low-angle thrusts or by high-angle transpressive faults (Fig. 2.6):

- Unit 1 (Morra Mt.) made up of Upper Triassic to Lower Jurassic dolostones (Dolomia Principale) and Calcare Massiccio limestone (cyclic peritidal platform top successions), overthrust on Unit 2 (Bollati et al., 2012).
- Unit 2 (Cornicolani Mts., western Lucretili Mts.) made up of Dolomia Principale, Calcare Massiccio Detrital Corniola Formation (carbonate breccias and basinal calcimudstones) and Bugarone Group (carbonate and siliceous basinal deposits). This unit is characterized by long wavelength folds and by faults with high-angle cut-offs. Jurassic structural highs occur on the Cornicolani Mts., and on Castelvecchio Mt. (Bollati et al., 2012).
- Unit 3 (Elci Mt., eastern Lucretili Mts. and Tiburtini Mts.) is made up of most of the Sabina basin stratigraphic succession, from the Detrital Corniola Formation to the Guadagnolo Member (marly lithofacies); this unit is characterized by NW to NE verging overturned to recumbent folds (Bollati et al., 2012).
- Unit 4 (Prenestini Mts., Ruffi Mts. and eastern Sabini Mts.) made up of the upper portion of the basin succession between the Marne a Fucoidi (basinal marls) and Upper Miocene siliciclastic turbidites and the Rocca di Cave carbonate platform succession (Bollati et al., 2012). On the basis of the deformation style and stratigraphy, this unit is divided in two sub-units: the sub-unit 4A (Granaro Mt., Colle Serviano and Arzillo Mts. in the western Prenestini Mts.) is mainly characterized by east-verging packed asymmetrical folds with sub-vertical axial planes and N-S striking dextral-transpressive faults (Bollati et al., 2012). The sub-unit 4B (Castel Madama Area, eastern and central Prenestini Mts., Ruffi Mts. and eastern

Sabini Mts.) is characterized by a symmetrical anticline in the western portion, by folds with steep axial planes and N-S to NNW-striking dextral transpressional faults (Bollati et al., 2012).

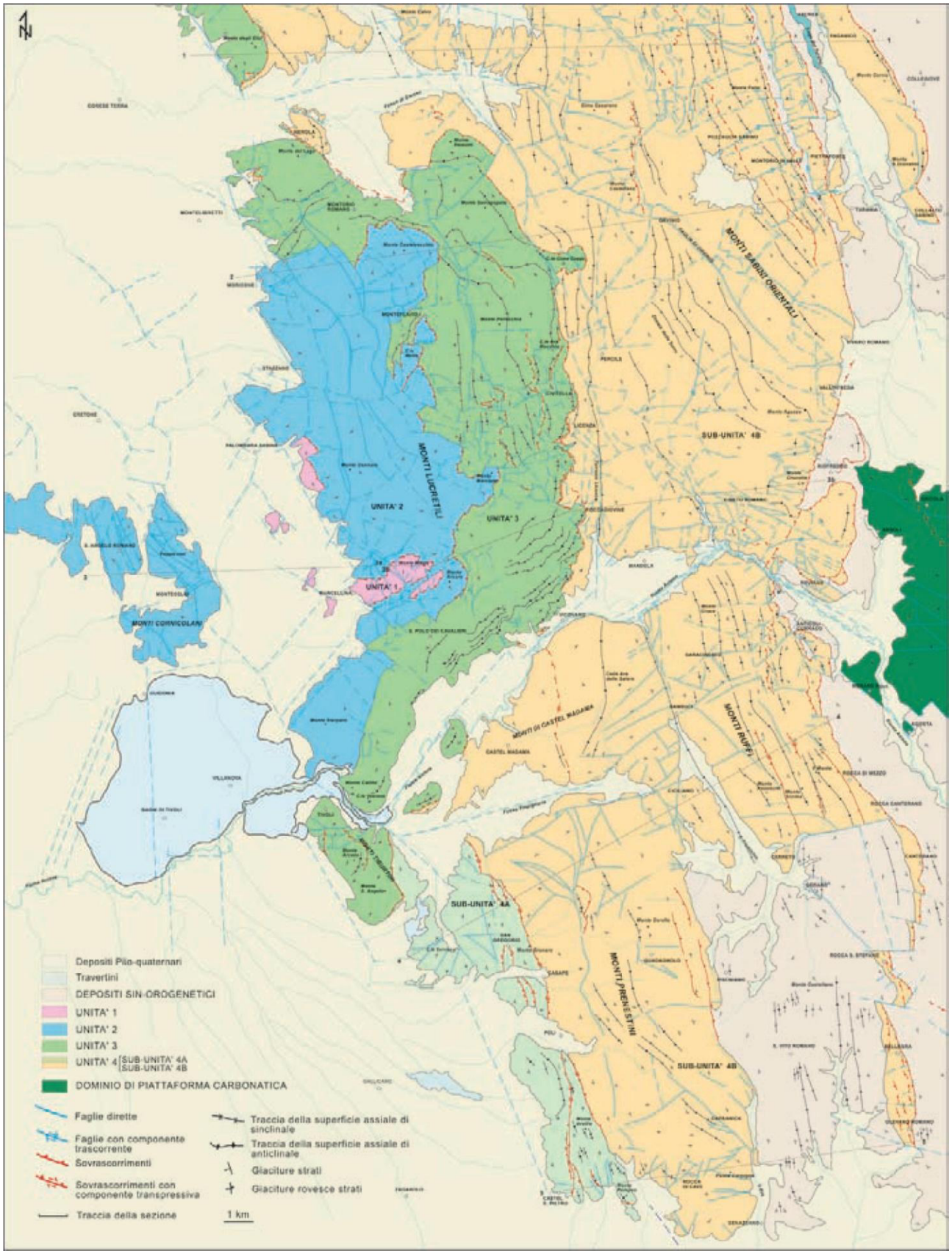

Figure. 2.6 Structural scheme of Palombara Sabina and Tivoli area: pink= unit 1; light blue= unit 2; light green= unit 3; yellow= unit 4; green= Triassic-Jurassic carbonate platform domain (after Bollati et al., 2011).

2.6 Volcanism and volcanic deposits

The origin of the Tyrrhenian volcanism is tied to the subduction of the Adria Plate beneath the Euro-Asiatic Plate. This subduction gave rise to the back-arc volcanic lineament (crossing the central Italian regions of Tuscany, Latium and Campania), which follows the NW-SE direction, the same of the Apennine chain. The area around the Tivoli village is characterized by the presence of volcanic deposits originated by the activity of the Colli Albani system (De Rita et al., 1992) (Fig. 2.6), which with the Vico volcanic system and Sabatini volcanic system, characterized the Roman area (Ventriglia, 2002). De Rita et al. (1995) defined the geologic evolution of the Colli Albani volcanic system, subdividing it in three phases: 1) Tuscolano-Artemisio; 2) Faete; and 3) late hydromagmatic phase. The Tuscolano-Artemisio phase covered a period from 600 kyrs to 350 kyrs (Marra et al., 2003), making the homonymous volcanic edifice. In this time period, four eruptive cycles are recognized: at their base there is a pyroclastic flow, followed by fall deposits covered by a lava flow. Each cycle is closed at the top by a paleosol (De Rita et al., 1995). The first of this pyroclastic flow is called Tor de' Cenci Formation (Palladino et al., 2001) or Tufi Antichi (Ventriglia, 2002). It covers a volume larger than 10 km^3. The second cycle of the Tuscolano-Artemisio time deposited 90 m thick volcanic units in fluvial paleovalleys for a volume of 34 km^3 (De Rita et al., 1988). The top of this ignimbrite body (Pozzolane Rosse Formation; Ventriglia, 2002) is dated at 480 kyrs. The third cycle covers a volume similar to the second one, but it is characterized by the lack of the lava cover, due to a strong erosional activity. The latter cycle, dated 360-350 kyrs, is characterized by a new ignimbrite emission, distinct in two flows, Tufo Lionato and Tufo di Villa Senni (Ventriglia, 2002), which covers a volume of 30 km^3 (Watkins et al., 2002). This eruption caused the collapse of the volcanic edifice, bringing to the formation of the Tuscolano-Artemisio caldera, with a diameter of 11 km. After a quiescent phase, the activity resumed with the second phase addressed as Faete. The products of this phase are reduced in volume with respect to the first phase: only 2 km^3 were issued in comparison to the 283 km^3 total of the first phase. The Faete volcanic phase covers a period from 277 kyrs to 250 kyrs (Watkins et al., 2002; Funiciello et al., 2003). De Rita et al. (1988) addressed the third phase of the volcanic activity as "final hydromagmatic phase", and later renamed as "phreatomagmatic phase" by Funiciello et al. (2003). This phase took place from 200 kyrs to 20 kyrs. During this period there was the development of some *maar*, hydromagmatic calderas, including Albano Nemi and Ariccia. The most significant event of this period is the deposition of the "Peperino di Albano", an ignimbrite dated at 25 kyrs, which covers a volume of 0.2-0.5 km^3 (Giordano et al., 2002). Also in the Holocene the hydromagmatic activity continued (Funiciello et al., 2002, 2003), always characterized by a phreatomagmatic activity and the deposition of lahar, dated around 5 kyrs (Funiciello et al., 2003).

2.7 Hydrogeology of the Acque Albule Basin

From a hydrologic point of view the Tivoli travertine plain represents the accumulation area of groundwaters of the Acque Albule Basin (La Vigna et al., 2013) (Fig. 2.7A). The plain is characterized by the presence of thermal springs, enriched in sulphurous water (Chafetz and Folk, 1984; La Vigna et al., 2013), mainly along the NNW-SSE shear zone (Faccenna et al., 2008). Two lakes, Lago delle Colonnelle and Lago Regina (Pentecost and Tortora, 1989), sink-holes and other karstic features (Pentecost and Tortora, 1989; Minissale et al., 2002; La Vigna et al., 2007) occur in the area. Three hydrostratigraphic units were recognized: the travertine body of the Acque Albule basin represents the shallow aquifer below a thin bed, consisting of an altered pyroclastic deposit and soils (with the exception of the quarried areas), which do not create an obstacle to the vertical recharge (Carucci et al., 2012; Di Salvo et al., 2013; La Vigna et al., 2013). The shallow travertine aquifer is separated from the deep confined aquifer by Pliocene clays, alluvial and volcanic low-permeability layers. This aquifer is contained within the Meso-Cenozoic limestones (Carucci et al., 2012; La Vigna et al., 2012; Di Salvo et al., 2013). The two aquifers are in hydraulic continuity through the sandstone layers of the Pleistocene deposits, erosion windows and tectonic discontinuity (Di Salvo et al., 2013; La Vigna et al., 2013).

The travertine aquifer is fed from three recharge areas: the carbonate ridge of the Lucretili-Tiburtini-Cornicolani Mountains (Capelli et al., 2005; Petitta et al., 2010), characterized by karst development; here the seepage is very high and Boni et al. (1986) estimated it as more than 800 mm y^{-1} with respect to rainfall of 1000-1200 mm y^{-1}. The second recharge system is fed by rainfall, which according to Di Salvo et al. (2013), can significantly vary the piezometric level in the shallow aquifer. The third recharge area is fed by the upwelling of deep groundwater, especially along the shear-zone of the Acque Albule plain (Carucci et al., 2012; Di Salvo et al., 2013; La Vigna et al., 2013). These buried fluids are generated from and interact with thermally-active volcanic bodies, linked to the magmatism of the Colli Albani (Billi et al., 2006b; Faccenna et al., 2008; Di Salvo et al., 2013) and cooling granitic intrusions (Minissale et al., 2002).

The results of the piezometric monitoring (Fig. 2.7B), conducted by La Vigna et al. (2013), concluded that the piezometric high is at the thermal springs of the Regina and Colonnelle lakes (65 m a.s.l.); instead there are pumping cones in correspondence of the quarried areas, where the water table falls to 30 m a.s.l.. Minissale et al. (2002), Carucci et al. (2012), La Vigna et al. (2013) and Di Salvo et al. (2013) measured the water temperature in the Acque Albule plain, confirming the previous data of Pentecost and Tortora (1989): the high values are in correspondence of the major springs (Sorgente Regina, Sorgente Colonnelle, Sorgente Bretella Autostradale) all along the NNW-SSE shear lineament, reaching temperature around 23°C. Instead the lowest temperatures, around 10°C, are in the Aniene river area, which is the final destination of the natural superficial drainage (La Vigna et al., 2013).

Carucci et al. (2012) associated the three different flow-paths mentioned before with three groundwater end-members based on water geochemistry (Fig. 2.7 C). The distinction of the facies is based on the results of water chemistry and isotope geochemistry approach (^{18}O and ^{2}H in water, ^{34}S and ^{18}O in SO_4, ^{13}C in DIC and $^{87}Sr/^{86}Sr$ ratios) (Fig. 2.8 A-D).

- Facies A, represents the infiltration and discharge from local springs of the carbonate ridge recharge area: it is characterized by Ca-HCO_3 composition and represents a flow system fed directly by meteoric water from carbonate ridge recharge areas; this flow can be distinguished in one that discharges directly into the travertine aquifer and in a deeper flow system feeding the buried carbonate bedrock.
- Facies B represents the flowpath within the travertine aquifer and consequently is characteristic of the quarry area; it has Ca-HCO_3-SO_4 chemical composition; it receives groundwater from the carbonate ridge recharge area and seepage from the deeper carbonate aquifer.
- Facies C represents the deep flowpath in buried Meso-Cenozoic carbonates, discharging into the travertine aquifer through tectonic pattern. It is characterized by Ca-Mg-HCO_3-SO_4 composition and has a contribution of high salinity fluids.

The depleted $\delta^{18}O$ (-4.5‰ to -8‰ SMOW) and $\delta^{2}H$ (-25‰ to -50‰) in all the springs of the recharging area, of the plain and in the springs fed directly by burial groundwater, show that there is a common recharge area for the shallow and the burial aquifer (Carucci et al., 2012). The large range of SO_4 concentration and the dissolved inorganic Carbon are the chemical fingerprints used to recognize the shallow and deep flow systems in the study area. Groundwater circulating in the deep aquifer is characterized by $\delta^{34}S$ = 15‰ with a concentration of SO_4 up to 1216 mg/l and $\delta^{13}C$ = 7‰, while the groundwater from the recharge area is represented by $\delta^{34}S$ = 8‰, with a SO_4 concentration that varies from 18 mg/l and 264 mg/l, and $\delta^{13}C$ = -11‰ (Carucci et al., 2012). The elevated concentration of SO_4 is probably caused by interaction of the circulating groundwater with the Triassic Ca-SO_4 evaporitic Anidrite di Burano Formation (Minissale et al., 2002) placed below the Calcare Massiccio Formation (Delfrati et al., 2001). The more depleted negative $\delta^{13}C$ values are attributed to an input of soil CO_2 during rainfall infiltration, whereas the heavier $\delta^{13}C$ values are associated with an input of ^{13}C enriched CO_2, characterized by a high concentration of HCO_3 associated with a deep contribution of hydrothermal fluids from the buried carbonate aquifer (Carucci et al., 2012).

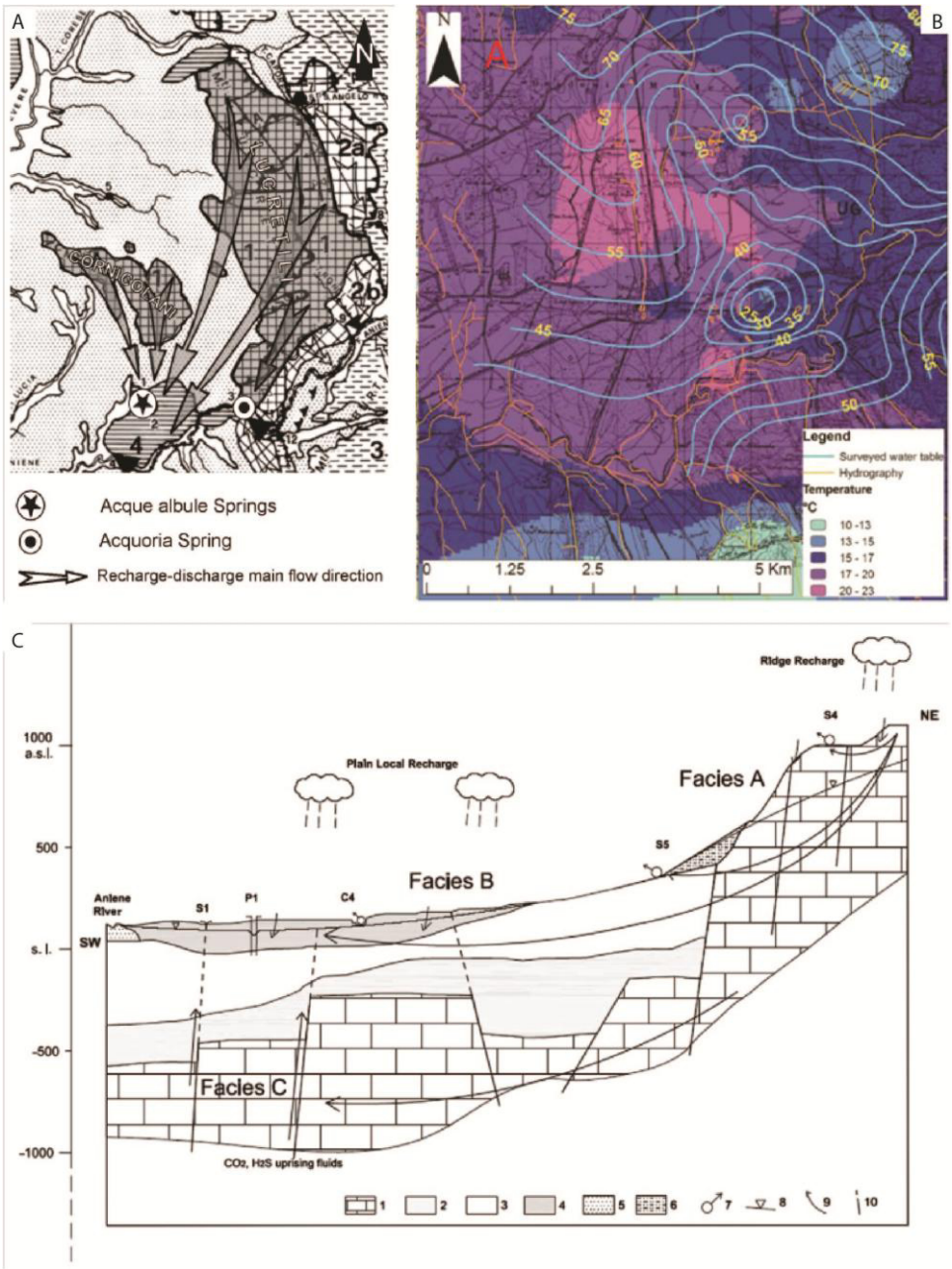

Figure. 2.1 A. Main recharge system of Acque Albule basin: the direct recharge on the Cornicolani and Lucretili Mountains outcrops recharges the Acque Albule travertine aquifer (Di Salvo et al., 2013). B. Temperature and water table depth (piezometry) of the superficial aquifer within the travertine (La Vigna et al., 2013). The piezometric minimum is in correspondence of the quarried area, where there water is artificially pumped and there is the development of a pumping cone. C. Conceptual hydrogeological and hydrogeochemical cross-section from hydrological, geochemical and isotope results. 1: Meso-Cenozoic carbonate aquifer; 2: Plio-Pleistocene aquitard, 3: Pleistocene volcanic and alluvial layers; 4: travertine aquifer; 5: Aniene river deposits; 6: colluvium; 7: spring; 8: water table; 9: groundwater flowpath; 10: main faults (Carucci et al., 2012).

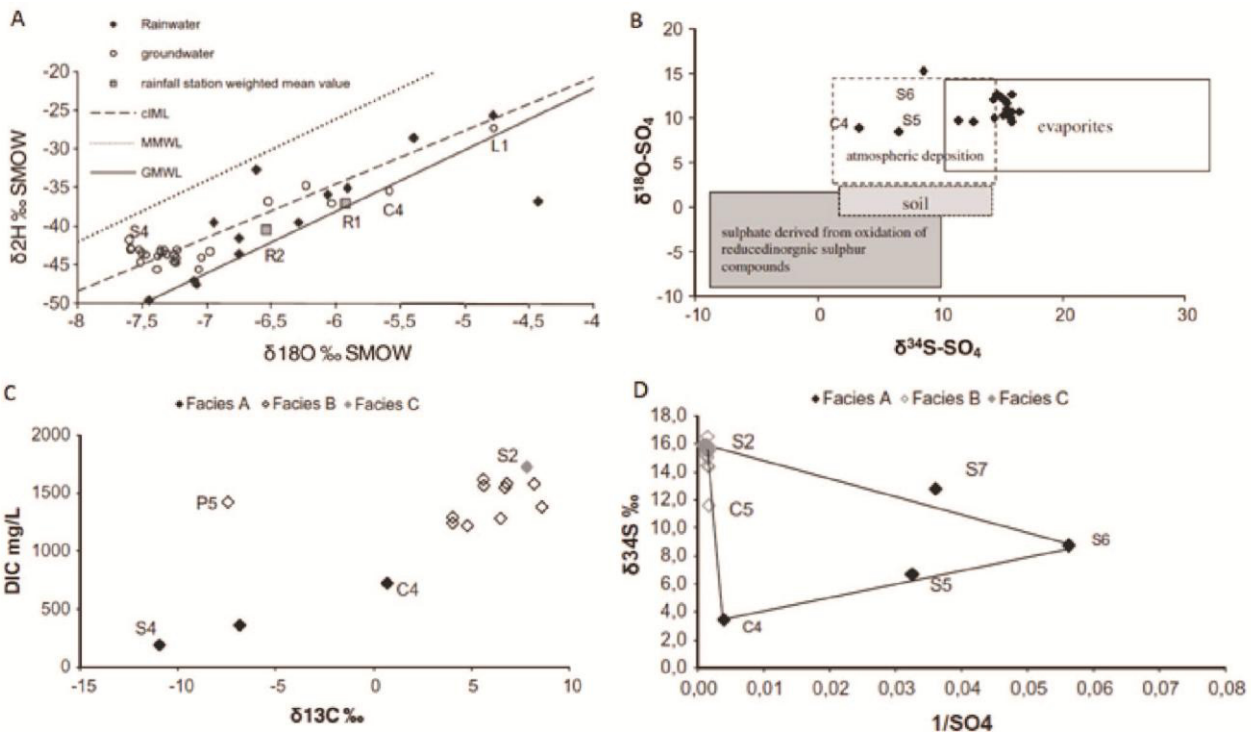

Figure. 2.8 From Carucci et al., (2013) A. ^{18}O – D correlation for groundwater and rainwater; B. $\delta^{34}S$ composition of different S compounds (from Clarck and Fritz, 1997, modified); C. δ13C DIC plot; D. $1/SO_4^{2-}$ vs $\delta^{34}S_{SO4}$ plot.

Chapter III

Depositional architecture of a mixed travertine–terrigenous system in a fault-controlled continental extensional basin (Messinian, Southern Tuscany, Central Italy)

ABSTRACT

The extensional Neogene Albegna Basin (Southern Tuscany, Italy) includes several thermogene travertine units dating from the Miocene to Holocene time. During the late Miocene (Messinian), a continental fault-controlled basin (of nearly 500-km^2 width) was filled by precipitated travertine and detrital terrigenous strata, characterized by a wedge-shaped geometry that thinned northward, with a maximum thickness of nearly 70 m. This mixed travertine–terrigenous succession was investigated in terms of lithofacies types, depositional environment and architecture and the variety of precipitated travertine fabrics.

Deposited as beds with thickness ranging from centimetres to a few decimetres, carbonates include nine travertine facies types: F1) clotted peloidal micrite and microsparite boundstone, F2) raft rudstone/floatstone, F3) sub-rounded radial coated grain grainstone, F4) coated gas bubble boundstone, F5) crystalline dendrite cementstone, F6) laminated boundstone, F7) coated reed boundstone and rudstone, F8) peloidal skeletal grainstone and F9) calci-mudstone and microsparstone. Beds of terrigenous deposits with thickness varying from a decimetre to >10 m include five lithofacies: F10) breccia, F11) conglomerate, F12) massive sandstone, F13) laminated sandstone and F14) claystone.

The succession recorded the following three phases of evolution of the depositional setting: 1) At the base, a northward-thinning thermogene travertine terraced slope (Phase I, travertine slope lithofacies association, F1–F6) developed close to the extensional fault system, placed southward with respect to the travertine deposition. 2) In Phase II, the accumulation of travertines was interrupted by the deposition of colluvial fan deposits with a thickness of several metres (colluvial fan lithofacies association, F10 and F12), which consisted of massive breccias, adjacent to the

alluvial plain lithofacies association (F11–F14) including massive claystone and sandstone and channelized conglomerates. Travertine lenses, of 2–3-m thickness, appeared intermittently alternating with the colluvial fan breccias. 3) In the third phase, the filled fault-controlled basin evolved into an alluvial plain with ponds rich in coated reed travertines, which record the influence of freshwater (travertine flat lithofacies association, F7–F9).

This study shows the stratigraphic architecture and sedimentary evolution of a continental succession, wherein the hydrothermal activity and consequent travertine precipitation were driven by the extensional tectonic regime, with faults acting as fluid paths for the thermal water. Fault activity created the accommodation space for travertine and colluvial fan accumulation. Erosion of the uplifted footwall blocks provided the source of sediments for the colluvial fan breccias, which alternated with the thermogene travertine precipitation. Climatic oscillations might have led to the recharge of the aquifer that fed the hydrothermal vents.

The studied continental succession in an extensional basin provides valuable information about the interplay between thermogene travertine and alluvial/colluvial deposition, which in turn might improve the understanding of similar fault-controlled continental depositional systems in outcrops and the subsurface.

This Chapter has been redrafted after a published manuscript: Croci, A., Della Porta, G., & Capezzuoli, E. (2016). Depositional architecture of a mixed travertine-terrigenous system in a fault-controlled continental extensional basin (Messinian, Southern Tuscany, Central Italy). *Sedimentary Geology*,*332*, 13-39, Elsevier

3.1. Introduction

Continental rift and strike-slip basins, such as the present-day examples of the East African Rift (McCall, 2010) and the Dead Sea Basin in the Middle East (Stein, 2001), present a variety of depositional environments and lithofacies including lacustrine carbonates, hydrothermal vent-related travertines as well as alluvial and fluvial deposits. In ancient cases of such fault-controlled basins, with deposition being influenced by varying rates of tectonic subsidence (Blair, 1987), mixed siliciclastic–carbonate successions occur alternately, as observed in the Jurassic–Lower Cretaceous of the Todos Santos Formation in Mexico (Blair, 1987), the Pliocene Ridge Basin in California (Link et al., 1978) and the Namibe Basin in southern Angola (Beglinger et al., 2012).

An important prerequisite for the development of travertine deposits is groundwater enriched in calcium and bicarbonate ions (Pentecost, 2005). Two classes of travertines are defined based on the two sources from which CO_2 can be derived: a) meteogene travertines are precipitated by groundwater enriched in meteoric carbon dioxide derived from soils and the atmosphere (Pentecost and Viles, 1994) and b) thermogene travertines are produced by thermally generated CO_2 (Pentecost, 2005). The signature of stable oxygen isotopes in meteogene travertines varies between −13‰ and 4‰ Vienna Pee Dee Belemnite (V-PDB), whereas the $\delta^{13}C$ values range from −12‰ to 4‰ V-PDB (Pentecost, 2005). In thermogene travertines, the oxygen isotope values range from −18‰ to −1‰ V-PDB, whereas carbon isotopes vary between −3‰ and 11‰ V-PDB (Pentecost, 2005). Some authors use the term ‘travertines’ exclusively to address continental carbonates precipitated by thermal water and the term ‘calcareous tufa’ to denote those carbonates associated

with groundwater of ambient temperature (Pedley, 1990; Ford and Pedley, 1996; Capezzuoli et al., 2014). However, according to Jones and Renaut (2010), classifications based on the water temperature or water sources do not consider the diagenetic processes, which is problematic in the case of ancient deposits. In this study, due to the sedimentological and geochemical results, the terminology proposed by Pentecost (2005) is used.

In the last decade, thermogene travertine deposits accumulated in rift basins have been increasingly studied as a valuable archive of information about Quaternary palaeoclimate, palaeohydrology and groundwater isotope geochemistry (Minissale et al., 2002a and b; Minissale, 2004; Faccenna et al., 2008; Kele et al., 2008, 2011; Özkul et al., 2014) and tectonics (Hancock et al., 1999; Altunel and Karabacak, 2005; Brogi et al., 2010). In addition, recent discoveries of Lower Cretaceous hydrocarbon reservoirs in the subsurface of the South Atlantic, offshore Brazil and West Africa, have led to more studies on travertines and lacustrine carbonates accumulated in continental rift basins (Abilio and Inkollu, 1989; Wright, 2012; Dorobek et al., 2012; Ronchi and Cruciani, 2015; Wright and Barnett, 2015). Despite extensive study, the present knowledge on continental carbonate facies, their precipitation processes and the extrinsic and intrinsic factors controlling their depositional architecture is still limited (cf. Wright, 2012; Della Porta, 2015). However, only few known fossil travertine deposits have been noted in the pre-Quaternary geological record. The Messinian mixed carbonate–terrigenous succession of the Albegna Basin (Southern Tuscany, Central Italy), of nearly 70-m thickness, has not been studied in detail, despite being a valuable example of the interaction between travertines and colluvial–alluvial terrigenous deposits in a kilometre-scale fault-controlled rift basin. This study assesses the lithofacies characteristics and architecture as well as the factors controlling the sedimentary evolution over time of a mixed travertine–terrigenous succession. Thus, interpretative geological models are provided, which could prove useful in comparable outcrop and subsurface rift systems.

3.2. Geological setting of Albegna Basin

A fossil travertine unit, cropping out in an active and in an abandoned quarry close to the Marsiliana village, south-westward area of the Neogene Albegna Basin (Fig. 2.1) (Southern Tuscany, Central Italy) is the object of the present study. A detailed description of the geological setting of the area under study is reported in Chapter 2. According to Bosi et al. (1996), the travertine deposit should have accumulated during the Late Messinian. This travertine unit is ca. 2 km long and ca. 1.5 km wide. The active quarry with a depth of excavation of 70 m allows the investigation of the travertines in terms of carbonate fabrics, geometry of the sedimentary units and lateral and vertical evolution.

3.3. Methods

The investigated Messinian travertine unit and the associated terrigenous deposits crop out close to the Marsiliana village, particularly within an active and an abandoned quarry (Fig. 2.3). Satellite images were examined to document the extensions of the quarry and relative deposits using the published geological maps of the area (Pertusati et al., 2004; Cornamusini et al., 2011). Field data were obtained through macro-scale observations, 14 detailed stratigraphic logs and lithofacies mapping. Stratigraphic sections, with thickness varying from 2.5 to 61.5 m, were logged to characterize the different lithofacies types. Hundreds of samples of travertines and terrigenous deposits were collected from the field, which were then prepared to produce polished slabs and thin sections. Petrographic analyses of 98 thin sections provided information on the microfabric types. The porosity of each distinguished lithofacies was determined by the qualitative visualization of the pore space percentage per area at the scale of both hand samples (areas of nearly 25–50 cm^2) and thin sections (areas of nearly 2–4 cm^2), using the image analyses software ImageJ.

With the use of Open Gis software (Q-GIS) and three-dimensional (3D) modelling software (Move Midland Valley, 2012), a detailed geological map and a 3D model of the spatial distribution of the distinguished lithofacies association could be obtained.

The mineralogical composition of two carbonate samples was determined using an X-ray powder diffractometer Philips X'Pert MPD with a high-temperature chamber. Stable carbon and oxygen isotopes were measured in 53 calcite samples, from different facies types, outcrops and stratigraphic levels. Carbonate powders were extracted with a dental microdrill without mixing the carbonate components. Stable isotope analyses were conducted using a MAT253 mass spectrometer with an automated carbonate preparation device (gas bench II) at the University of Bochum, Institute for Geology, Mineralogy and Geophysics stable isotope facility. Stable isotope results were calibrated to the V-PDB scale by the international standards CO-1 and CO-8. The analytical precision is better than 0.07‰ for $\delta^{13}C$ and 0.13‰ for $\delta^{18}O$.

3.4. Lithofacies character and spatial distribution

The studied Messinian travertine–terrigenous succession cropping out at the Marsiliana active quarry is nearly 70 m thick and 300 m wide (Figs. 2.3, 3.1, 3.2). The tectonically tilted sedimentary unit dips towards the NW, with inclinations varying from a few degrees (4°) up to 70°, in the westernmost part of the quarry. The identified inverse and normal faults have steeply inclined fault planes and limited displacement, hence resulting in negligible disturbance.

The logged stratigraphic succession (Fig. 3.2) includes travertine deposits, which dominate in the lower portion and are overlain by or interfinger with terrigenous detrital strata in the intermediate and upper portion of the succession. Nine travertine lithofacies (Table 3.2) were distinguished based on meso- to micro-scale fabric characteristic and stratal architecture. They were labelled according to the terminology proposed by Chafetz and Folk (1984), D'Argenio and Ferreri (1986), Guo and Riding (1998), Jones and Renaut (2010), Barilaro et al. (2012), Gandin and Capezzuoli (2014) and Della Porta (2015). In this study, the term 'boundstone' is used to denote travertine lithofacies formed by a rigid framework of precipitated clotted peloidal micrite, already lithified at the time of deposition (cf. Della Porta, 2015). The term 'cementstone' is used to represent crystalline sparitic textures (cf. Wright, 1992; Della Porta, 2015). Travertine lithofacies consisting of grainy deposits were classified using the terminology of Dunham (1962) and Embry and Klovan (1971) for carbonate depositional textures. Based on X-ray diffraction (XRD) analysis, the carbonate mineralogy was found to be calcite. The five terrigenous lithofacies distinguished include detrital breccias, siliciclastic sandstone and claystone, as summarized in Table 3.2.

Figure 3.1. Panoramic view of the exposed succession in the active quarry indicated in Fig. 3.3, which shows the location of the measured stratigraphic logs.

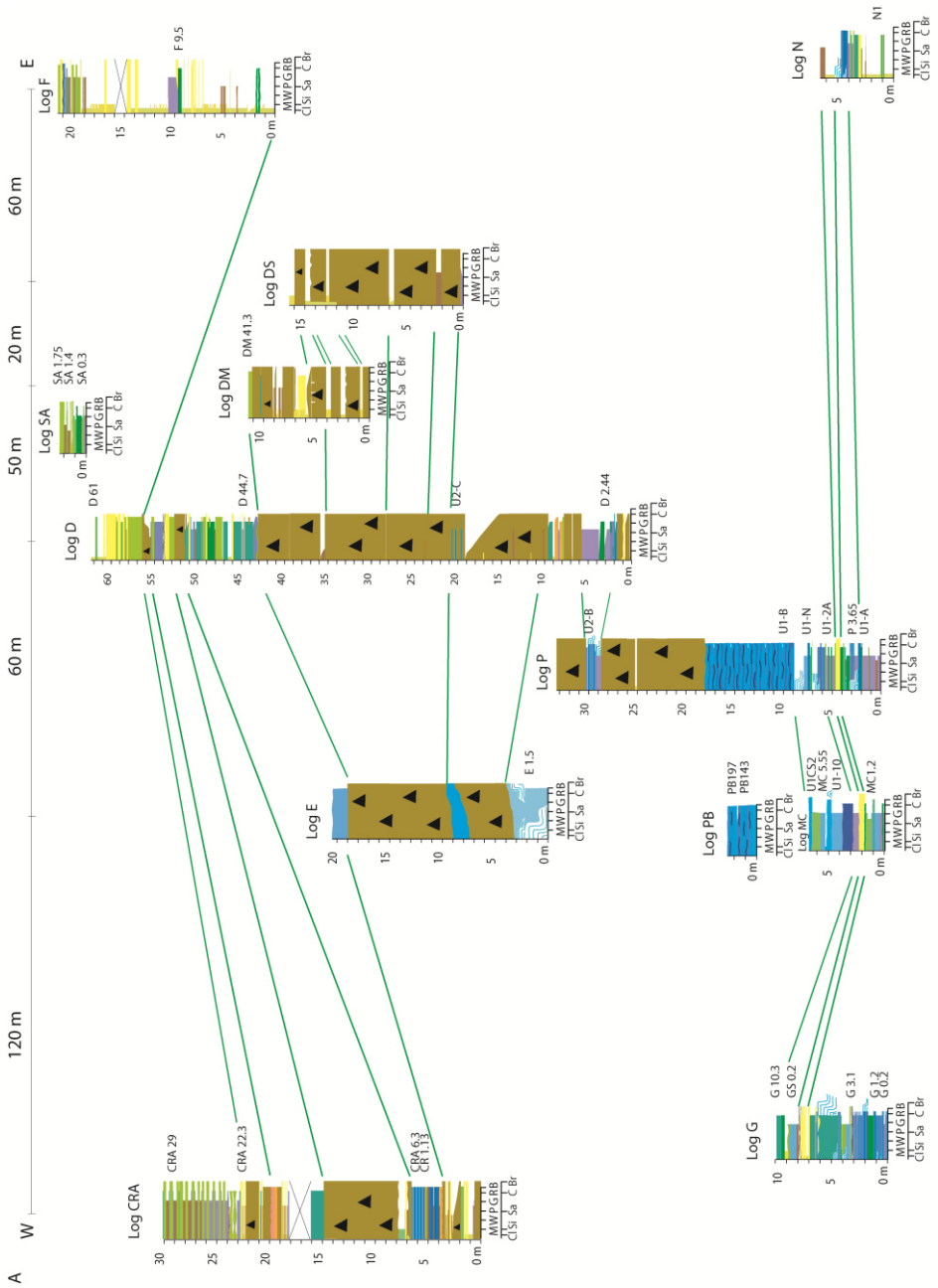

Figure 3.2. A) Correlation diagram of the measured stratigraphic logs. Green lines represent lithofacies correlation stratal surfaces tracked on the outcrop. Samples drilled for stable isotope analysis are reported on the right side of the stratigraphic logs (e.g., G02–G10.3 in log G). B) The legend of Fig. 3.2A shows the lithofacies grouped into lithofacies associations.

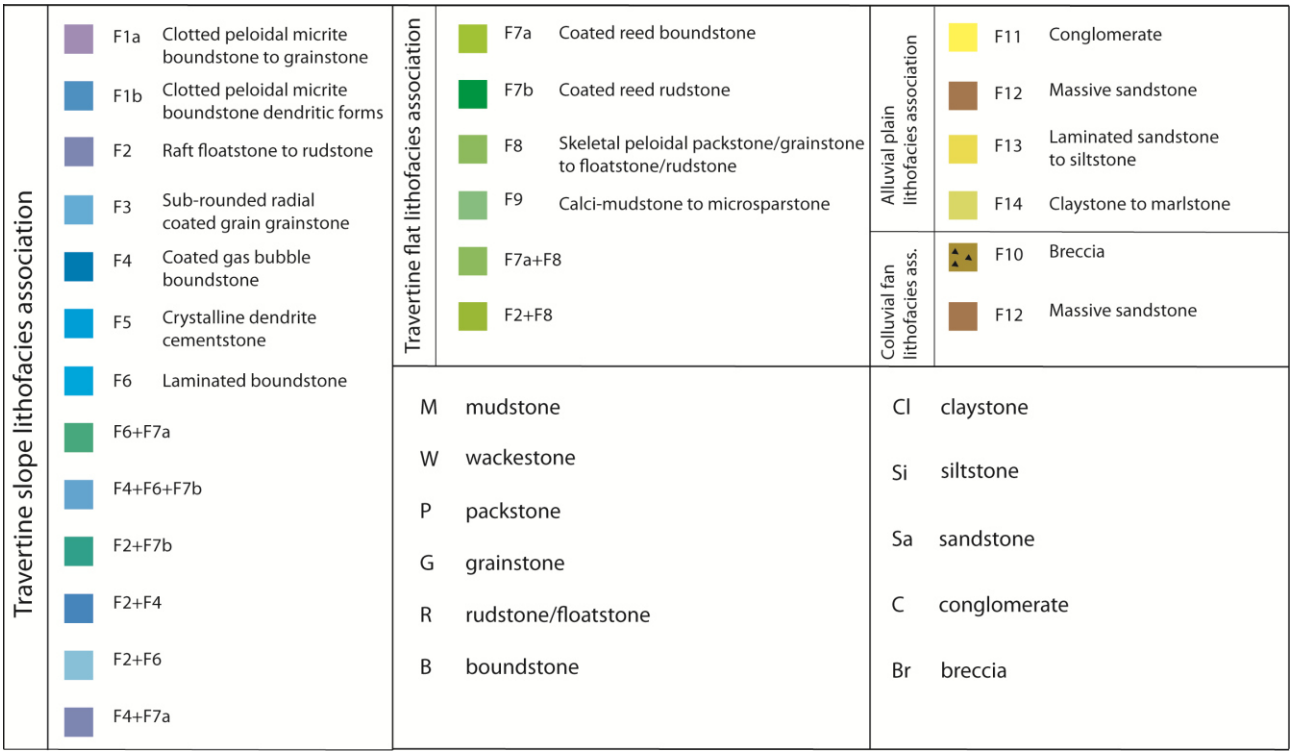

3.4.1. Clotted peloidal micrite and microsparite boundstone to grainstone (facies F1)

3.4.1.1. Description

Ranging from grainstone to boundstone, facies F1 is composed of irregular to sub-rounded grains of clotted peloidal micrite welded together to form an irregular framework (facies F1a) or dendritic shapes (facies F1b; Fig. 3.3A). The layers of facies 1 are centimetre thick, often undulated and locally associated with centimetre-scale erosional surfaces. Clotted peloidal micrite dendrites (facies F1b) develop perpendicular to the stratification, displaying a branching pattern with rounded terminations. Microscopically, the boundstone texture consists of clotted peloidal micrite and microsparite with either an irregular framework (Fig. 3.3B) or branching dendrites (Fig. 3.3C). The minor components of this facies are elongated moulds of reeds, gastropods and ostracodes, which are often surrounded by coatings of clotted peloidal micrite that are a few microns thick. Calcite cements, which are widespread, include the following components: 1) local growth of an irregular pendant cement at the bottom of the clots; 2) prismatic cement with scalenohedral terminations; and 3) pores subsequently filled with limpid equant cement, with a crystal size varying from a few microns up to 300 µm. The primary porosity consists of a sub-millimetre-scale framework, interparticle voids and irregular voids up to 1 cm in size, which are denoted as fenestrae. The secondary porosity consists of irregular vugs, 100–500 µm in size.

3.4.1.2. Interpretation

Several authors have attributed the precipitation of clotted peloidal micrite in both marine and non-marine environments to microbial mat mediated via various organomineralic pathways of biologically induced and influenced mineralization (Krumbein, 1979; Reitner, 1993; Reitner et al., 1995; Dupraz et al., 2009; Pedley et al., 2009; Pedley, 2014). In thermogene travertines, clotted peloidal micrite is deposited mainly in pond and flat low-energy depositional environments (Guo and Riding, 1998; Gandin and Capezzuoli, 2014; Della Porta, 2015 and references therein), which leads to dendrite morphologies, termed as 'bacterial shrubs' (Chafetz and Folk, 1984; Chafetz and Guidry, 1999). Chafetz and Folk (1984) suggested that the precipitation process is significantly influenced by microbial mats and that shrub growth is promoted by sulphide-oxidizing bacteria in H_2S-rich thermal water. Fouke et al. (2000) and Fouke (2011) largely documented the presence of various microbial communities thriving in thermogene travertine depositional systems. Gandin and Capezzuoli (2014) observed that shrub morphologies also develop on sub-vertical walls characterized by rapid evaporation of thin sheets of thermal water. In the studied Marsiliana system, dendritic shrub boundstone facies are not widespread, although they do occur occasionally on sub-horizontal to gently inclined surfaces, at places of inferred slow thermal water flow. Erosional surfaces are produced by subaerial exposure and meteoric weathering, suggesting that the thermal water flow must have been intermittent and/or have changed path over time, thus exposing the travertine deposits to meteoric alteration (cf. Chafetz and Folk, 1984; Guo and Riding, 1998; Özkul et al., 2002; Özkul et al., 2014). Rounded and fenestral porosities can be produced by the precipitation of carbonate around trapped gas bubbles, probably generated by microbial activity (Chafetz and Folk, 1984; Guo and Riding, 1998; Pentecost, 2005; Jones and Renaut, 2010). The primary porosity in the Marsiliana samples is filled by calcite cement including meteoric vadose pendant cement and prismatic scalenohedral to blocky cement precipitated by hydrothermal or meteoric phreatic groundwater (Török, 2003; Flügel, 2004; Palmer, 2007).

3.4.2. Raft floatstone/rudstone (facies F2)

3.4.2.1. Description

Rafts are elongated fragments (0.1–5 cm in width and hundreds of microns in thickness) of calcite blades, which form lenses of rudstone/floatstone (0.5–10 cm thick and tens of metres wide) deposited parallel to the depositional surfaces (Fig. 3.3D). Rafts often occur in association with skeletal grains (gastropods and ostracodes) or coated reed fragments, or isolated in clotted peloidal micrite grainstone (facies F1a). Microscopically, rafts consist of micritic and microsparitic films (Fig. 3.3E), which are coated by micrite envelopes followed by scalenohedral prismatic crystals.

The interparticle pores in rudstone textures are filled by a mosaic of equant calcite (Fig. 3.3F). The secondary porosity is characterized by the formation of vugs, 0.2–2 cm in size.

3.4.2.2. Interpretation

Rafts develop on the surface of stagnant pools (Guo and Riding, 1998), where surface water degassing of CO_2 and evaporation increase carbonate saturation, in turn leading to the precipitation of calcite or aragonite as thin films on the water surface (Folk et al., 1985). Various mechanisms may cause the formation of raft rudstones. According to Jones (1989) and Taylor et al. (2004), rafts can break when crystals, preferentially growing under the lower surface of the raft, increase in density, causing rafts to sink to the bottom of the pool. Other causes for raft breakage are water agitation due to wind, rain and current and the pressure exerted by gas bubbles under the raft surface (Folk et al., 1985; Guo and Riding, 1998; Gandin and Capezzuoli, 2014). In the Marsiliana travertine succession, rafts are interpreted as indicators of temporary stagnant water conditions in ponds. Prismatic and equant blocky calcite cements in facies F2 are formed in the saturated zone beneath pool floors and/or in the meteoric phreatic zone (cf. Clarke and Bourke, 2011).

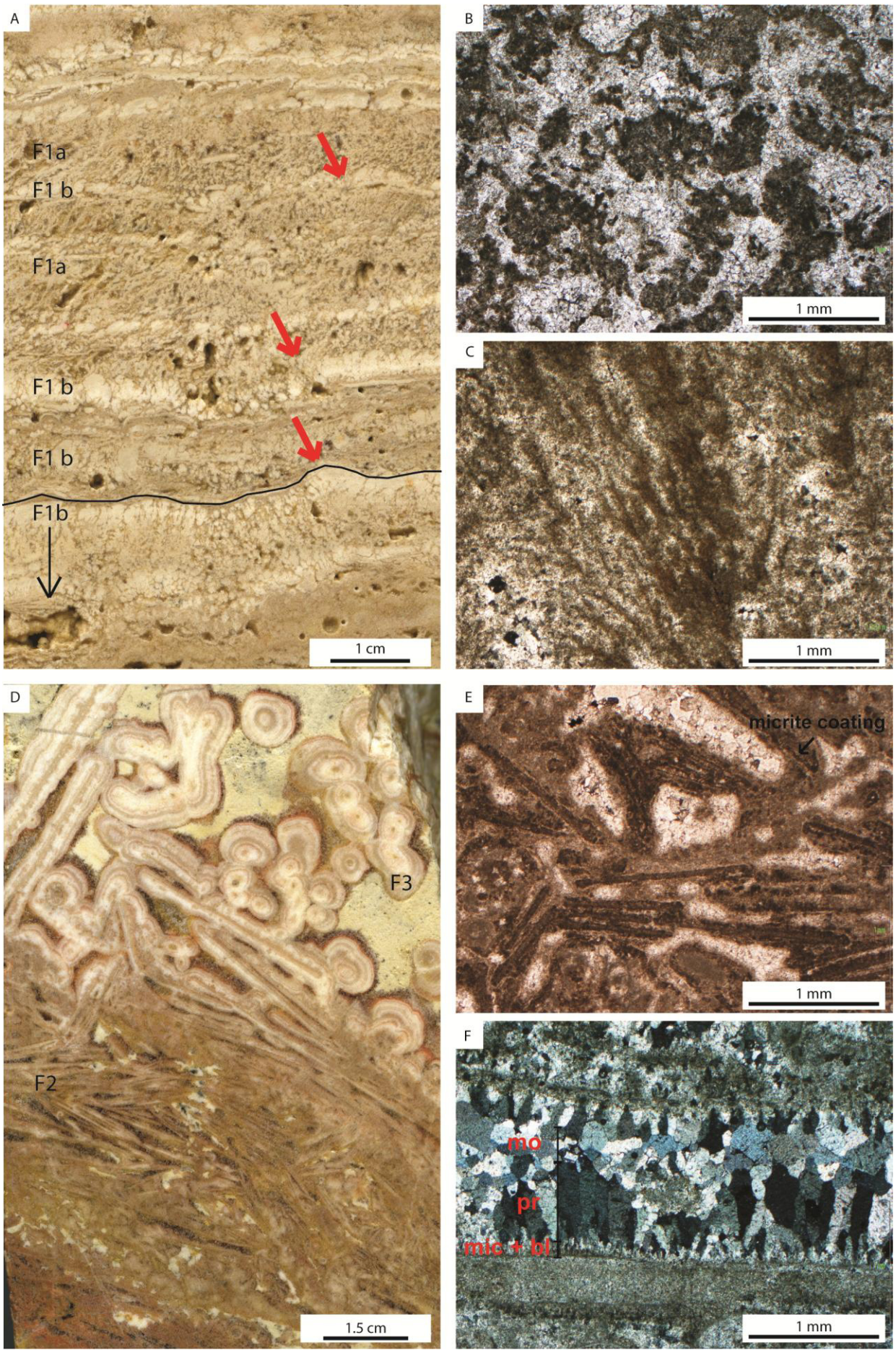
A
F1a
F1 b
F1a
F1 b
F1 b
F1b
1 cm
B
1 mm
C
1 mm
D
F3
F2
1.5 cm
E
micrite coating
1 mm
F
mo
pr
mic + bl
1 mm

Figure 3.3. Polished slabs and photomicrographs of facies F1 (A–C), F2 (D–F) and F3 (D). A) Alternation of layers of clotted peloidal micrite grainstone (facies F1a) with undulated shape and clotted peloidal micrite boundstone (facies F1b), composed of pale-white micritic dendrites of up to 2-cm thickness. Dendrites develop centimetre-scale micro-terraces (red arrows). B) Facies F1a grainstone to boundstone consists of irregular clots, 200–500 µm in size, composed of peloidal micrite with 10–20-µm peloids; equant microsparite is seen between the clots. C) Photomicrograph of micritic branching dendrites (facies 1b) built by aggregates of peloidal micrite, growing perpendicular to the substratum. D) Polished slab of raft floatstone/rudstone (facies F2) made of elongated calcite fragments surrounded by a white calcite coating. The primary interparticle porosity is widespread, but it is often filled by calcite cement. In the upper part of the slab, rafts are associated with sub-rounded radial coated grains, belonging to facies F3. E) Thin section showing rafts composed of recrystallized microsparite and enveloped by micrite coatings. F) Rafts are coated by different layers: from the base to top, the first layer consists of micrite followed by thin bladed cement (mic+bl), whereas the second layer consists of prismatic cement with scalenohedral termination up to 600 µm in thickness (pr), overlain by a mosaic of equant sparite (mo).

3.4.3. Sub-rounded radial coated grain grainstone/packstone (facies F3)

3.4.3.1. Description

This facies (Fig. 3.4A) forms horizontal lenses (15–20 cm in width and up to 6 cm in thickness), often being associated with clotted peloidal grainstone, raft rudstone and the skeletal remains of gastropods and ostracodes. The coated grains are composed of an irregular concentric radial coating around the peloidal nuclei (Fig. 3.4B), and are embedded in micrite, microsparite and sparite. In some cases, the radial coated grains are organized into fining-upward centimetre-thick beds, in turn separated by massive microsparite layers. The coated grain nuclei consist of peloids, gastropod or ostracode skeletal fragments (50–200 µm in size), surrounded by turbid lozenge-shaped or prismatic crystals of up to 700-µm length growing radially away from the nuclei (Fig. 3.4C–D). The interparticle porosity is usually occluded by scalenohedral and equant sparite. The secondary porosity is rare, characterized by irregular vugs up to 2 mm in size.

3.4.3.2. Interpretation

Similar sub-rounded radially arranged coated grains have been detected in various thermogene travertine depositional systems (Chafetz and Folk, 1984; Guo and Riding, 1998; Rainey and Jones, 2009; Della Porta, 2015). These grains, termed as ‘radial pisoids’ by Chafetz and Folk (1984), form in pools of terraced slopes and in horizontally bedded depressions with periodic turbulence (Chafetz and Folk, 1984; Guo and Riding, 1998). The growth of such sub-rounded coated grains is proposed to be influenced by both abiotic and biotic processes (Guo and Riding, 1994). Precipitation commences in low-energy conditions, followed by certain changes in environmental factors, such as the increase in water supply and energy, promoting the abiotic precipitation of calcium carbonate, for instance, when the grains are transported from one pool to another in terraced systems (Guo and Riding, 1998; Rainey and Jones, 2009). In the Marsiliana succession studied, this facies is localized in lenses, representing the accumulations of radial coated grains deposited in pools behind obstacles to the thermal water flow in a terraced slope system.

3.4.4. Coated gas bubble boundstone (facies F4)

3.4.4.1. Description

This facies consists of micrite that precipitates around rounded to elongated upward pore spaces, with sizes varying from several microns up to 4 cm (Fig. 3.4E). Layers of coated bubbles are associated with raft rudstone (facies F2), reed rudstone and boundstone (facies F7), which vertically alternate with laminated boundstone (facies F6). The micrite coatings (of 50–100-µm thickness) might be overlain by dendrites hundreds of microns in thickness or by irregular micrite crusts. These coatings are embedded in a framework of clotted peloidal micrite and microsparite, which provide a rigid boundstone texture (Fig. 3.4F). Scalenohedral prismatic calcite cement grows on both the inner and outer sides of the micritic hollows (Fig. 3.4G). In some cases, crystal terminations are draped by a thin (10-µm) red film of Fe and Mn oxides.

3.4.4.2. Interpretation

Gas bubbles can be preserved if they are trapped and coated by rapid precipitation of calcium carbonate (Chafetz and Folk, 1984; Guo and Riding, 1998; Jones and Renaut, 2010). Elongated bubble shapes are formed either by vertical gas escape or when more bubbles join in vertically stacked trains (Chafetz and Folk, 1984). Gas bubbles in hydrothermal vent settings may be produced by CO_2 degassing generated by turbulent water (Jones and Renaut, 2010), or they may be produced in low-energy pools by microbial activity through respiration and photosynthesis (Chafetz and Folk, 1984; Guo and Riding, 1998; Özkul et al., 2002; Pentecost, 2005; Jones and Renaut, 2010). Guido and Campbell (2011) described coated bubbles (termed as ‘foam texture’) in association with channelized geometries in a terraced system. In the Marsiliana system, coated gas bubbles form layers under the low-energy conditions of flat ponds and pools of terraced systems.

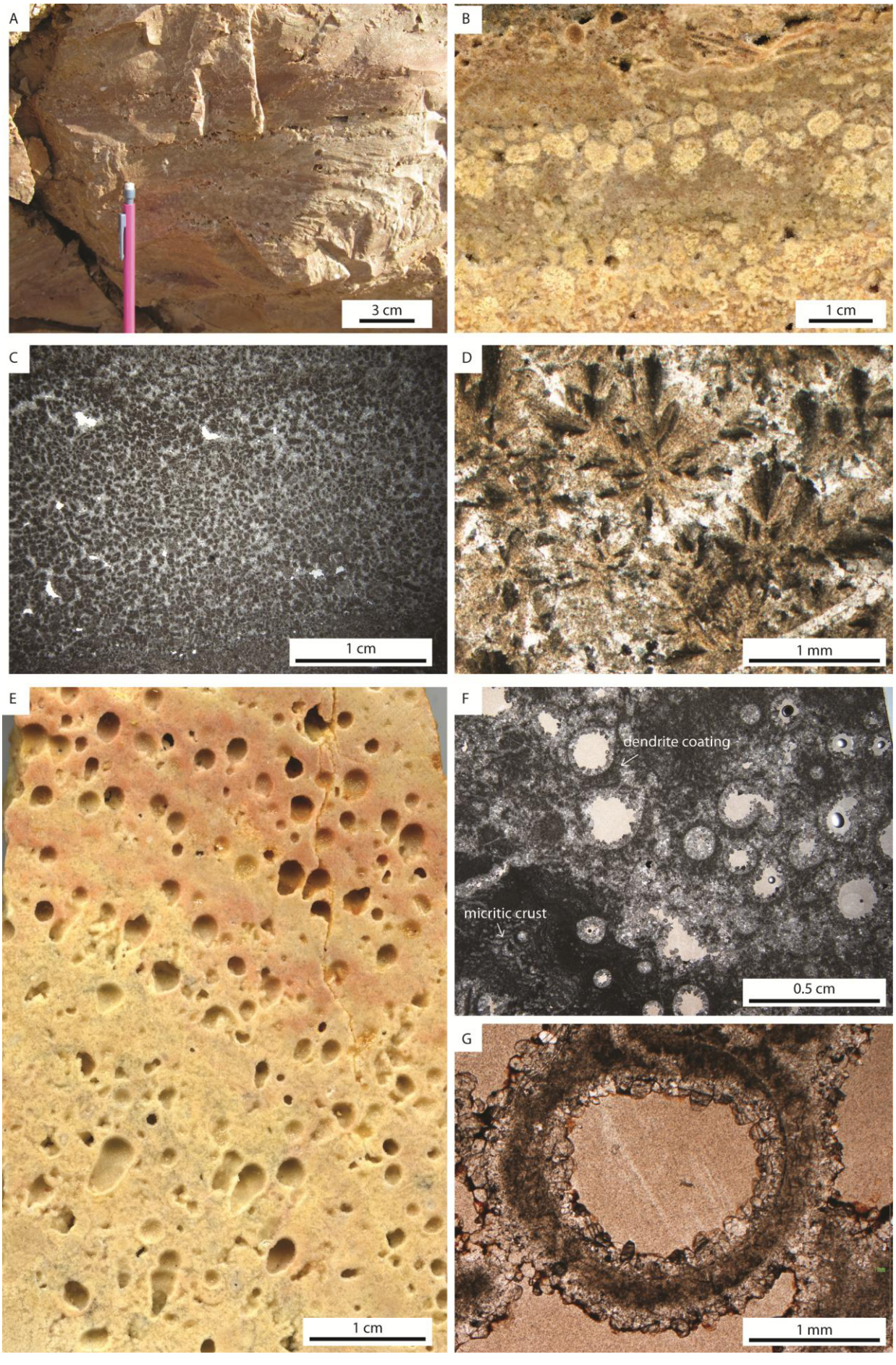
A
3 cm
B
1 cm
C
1 cm
D
1 mm
E
1 cm
F
dendrite coating
micritic crust
0.5 cm
G
1 mm

Figure 3.4. Outcrop photos, polished slabs and photomicrographs of facies F3 (A–D) and F4 (E–G). A) Sub-rounded radial coated grain grainstone (facies F3) deposited in sub-horizontal strata or concave lenses of 5-cm thickness, composed of white, millimetre-sized grains. B) Slab shows that coated grains have an irregular rounded shape, with a small dark core surrounded by white calcite coatings. The layers often occur in fining-upward sequences followed by massive microsparite-rich layers. C) The nuclei of sub-rounded radial coated grains can be composed of clots of micrite or microsparite and faecal pellets. The pores consist of irregular vugs of sizes up to 1–2 mm. D) The coating consists of radial lozenge calcite crystals with length up to 700 µm that grow adjacent to each other. Between the grains, calcite cement is composed of equant microsparite and sparite mosaics. E) Coated bubble boundstone (facies F4) consists of sub-rounded or vertically elongated hollows. The size of the hollows varies from a few millimetres up to 8 mm when the shape is vertically elongated. F) The thin section shows that the bubble coating is formed by micrite, constituting the substrate for the nucleation of micritic dendrites or undulated laminae that consist of peloidal micrite. G) Within the hollow, the growth of calcite cement is common, often comprising prismatic sparite with scalenohedral terminations.

3.4.5. Crystalline dendrite cementstone (facies F5)

3.4.5.1. Description

Crystalline dendrite cementstone consists of crusts (Fig. 3.5A) of vertically elongated branching calcite crystals that are adjacent to each other, varying in thickness from 2 up to 15 cm (Fig. 3.5B). Crystalline dendrite cementstone layers alternate with clotted peloidal micrite grainstone (facies F1a), laminated boundstone (facies F6) and coated gas bubble boundstone (facies F4).

Dendrites are composed of lozenge-shaped turbid crystals, of up to 100–200-µm length and 50–100-µm width, which run outward, often from a central elongate crystal acting as a stalk (Fig. 3.5C). Generally, the central stalk crystals are straight of 50–100-µm width, exhibiting uniform extinction under crossed polarizers. The dendrites are surrounded by cloudy microsparite and limpid equant microsparite to sparite. The horizontal laminae, which interrupt the vertical crystal growth, are composed of clotted peloidal micrite (Fig. 3.5D, E).

3.4.5.2. Interpretation

Thermogene travertine crystalline dendrites (Jones and Renaut, 1995) have also been termed as ‘feather crystals’ by Guo and Riding (1998) and Chafetz and Folk (1984) and as ‘crystal shrubs’ by Chafetz and Guidry (1999). The precipitation of crystalline dendrites is controlled by the concentration of Ca^{2+} ions in thermal water (Jones and Renaut, 1995; Rainey and Jones, 2009). This crystalline fabric is formed under the high-energy conditions of smooth slopes, terraced slopes, pool rims and cascades (Guo and Riding, 1998; Rainey and Jones, 2009; Özkul et al., 2014). The thickness of crystalline dendrites is proportional to precipitation rates and thermal water flow velocity (Guo and Riding, 1998), whereas the growth lamination is attributed to periodic changes in water flow (Pentecost, 2005). The crystalline dendrites of the Marsiliana travertines are interpreted as deposited under the turbulent conditions on slopes and pool rims during high discharge of thermal water and high rates of degassing and evaporation.

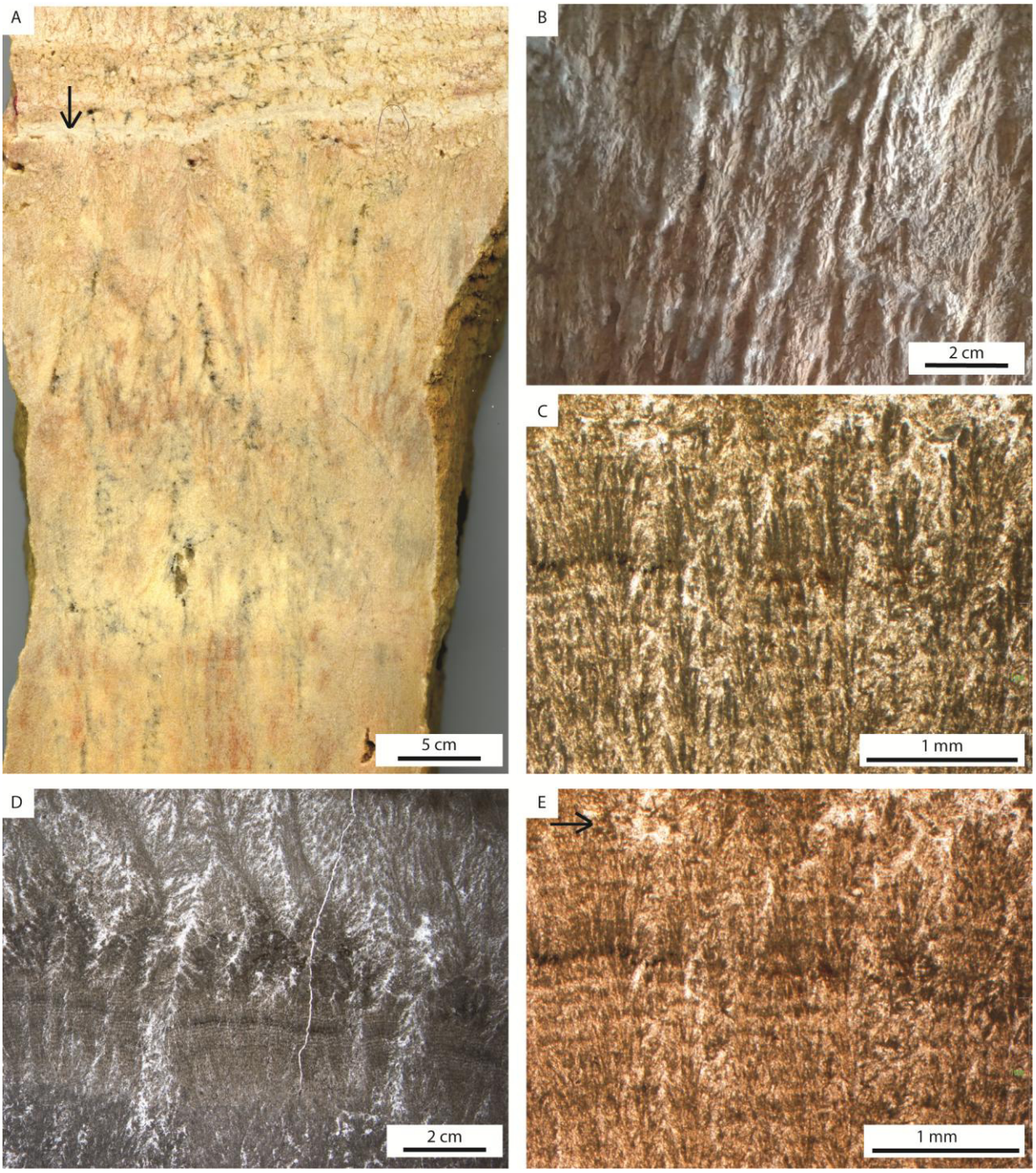

Figure 3.5. Outcrop photos, polished slabs and photomicrographs of facies F5. A) The colour of crystalline dendrites varies from white to pink and yellowish. The vertical growth is often interrupted by horizontal undulated laminae made of millimetre-thick dendrites and dense travertine calci-mudstone (black arrow). B) Outcrop photo of crystalline dendrites, size of centimetres (up to 5 cm), growing vertically, perpendicular to the substrate. C) Crystalline dendrites consist of millimetre- to centimetre-long, branching composite crystals composed of lozenge-shaped turbid crystals (up to 100–200 µm long and 50 µm wide) running outwards with axial divergences of 10–30°. D) The thin section shows that the sub-horizontal lamination consists of alternations between thin crystalline calcite and clotted peloidal micrite (black arrow). E) Close-up view of crystalline dendrites crossed by sub-parallel micritic growth laminae.

3.4.6. Laminated boundstone (facies F6)

3.4.6.1. Description

Laminated boundstone consists of dense calcite with wavy laminae (Fig. 3.6A), up to 2 mm in thickness and up to a few metres in width (2–3 m). These laminae are characterized by undulated patterns (Fig. 3.6B) that develop convex-upward morphologies. The pores between the laminae are lens shaped and horizontally elongated, but more frequently the laminae are amalgamated with no interlaminar porosity. This facies occur laterally adjacent to reed rudstone (facies F7) and alternate with crystalline dendrite cementstone (facies F5). The laminae consist of structureless micrite and clotted peloidal micrite, associated with microsparite (Fig. 3.6C). Scalenohedral and blocky sparite cements fill the primary porosity (Fig. 3.6C).

3.4.6.2. Interpretation

Laminated travertine fabrics have been interpreted as being precipitated by microbially mediated processes (cf. Rainey and Jones, 2009; Gandin and Capezzuoli, 2014). Generally, laminated boundstone forms under low-energy conditions, such as pools and ponds in terraced slope systems (Gandin and Capezzuoli, 2014). However, laminated boundstone can also precipitate on steeply inclined slopes under conditions of reduced volumes of flowing water from the hydrothermal vents (Rainey and Jones, 2009; Della Porta, 2015). In the Marsiliana travertines, the laminated boundstone facies occurs on inclined surfaces mostly alternating with centimetre-thick crystalline crust cementstone (facies F5). The replacement of crystalline dendrites by laminated boundstone on slopes suggests a change in the vent discharge rate, leading to a reduced output of thermal water.

3.4.7. Coated reed boundstone to rudstone/packstone (facies F7)

3.4.7.1. Description

Facies F7 is characterized by the presence of carbonate-encrusted plant stem moulds that appear as hollow tubes either vertically oriented perpendicular to the stratification or prostrated (Fig. 3.6D–E). Two types of facies F7 are identified. Reed boundstone (facies F7a) is composed of encrusted bushes of reeds that grew vertically and formed horizontal layers (5–20 cm thick), often

above terrigenous deposits, extending laterally for up to 10 m. Phytoclastic rudstone/packstone (facies F7b) consists of prostrated and fragmented carbonate-coated reed stems deposited as sub-horizontal layers, in association with rafts, coated bubbles, mollusc skeletal remains and peloidal grainstone. Facies F7 is either associated with the F1–F4 travertine facies or it overlies terrigenous deposits (facies F10 to F14). The stem coating consists of homogeneous micrite, clotted peloidal micrite and microsparite, developing thin (10–20-µm) films, similar to the layers around the gas bubbles; reed moulds are rarely coated by lozenge-shaped crystalline dendrites. The inner wall of the micrite coating serves as the substrate for the growth of scalenohedral prismatic cement and equant calcite crystals (Fig. 3.6G).

3.4.7.2. Interpretation

The coated reed boundstone F7a represents in situ reed bushes encrusted by precipitated carbonate in life position, whereas F7b packstone/rudstone represents the reworking of fragments of carbonate coated vegetation. The presence of coated reeds, peloids and skeletal remains of ostracodes and gastropods suggests the reduced influence of thermal water, either cooled down in distal settings farther away from the vent or mixed with freshwater of ambient temperature, in marsh depositional environments (Guo and Riding, 1998; Özkul et al., 2002, 2014; Guido and Campbell, 2011; Capezzuoli et al., 2014). In the Marsiliana travertines, the occurrence of facies F7 overlying terrigenous deposits (F10–F14) is interpreted as indicators of depositional settings distal form the hydrothermal vent. Field observations of the active hydrothermal system (Bagni di Saturnia Holocene thermogene travertine in Fig. 1) show that vegetation colonizes the travertine surface after subaerial exposure or grows in dry areas adjacent to the active thermal water (with a temperature up to 37 °C) being the water flow temporarily deviated in other directions. In these instances, the plant stems are encrusted by the precipitation of calcium carbonate when a renewed flux of thermal water floods the substrate on which they grow. Hence, in the Marsiliana travertines, when facies F7 occurs in association with facies F1–F4, reeds probably grew on the lateral edges of pools where water did not temporarily flow.

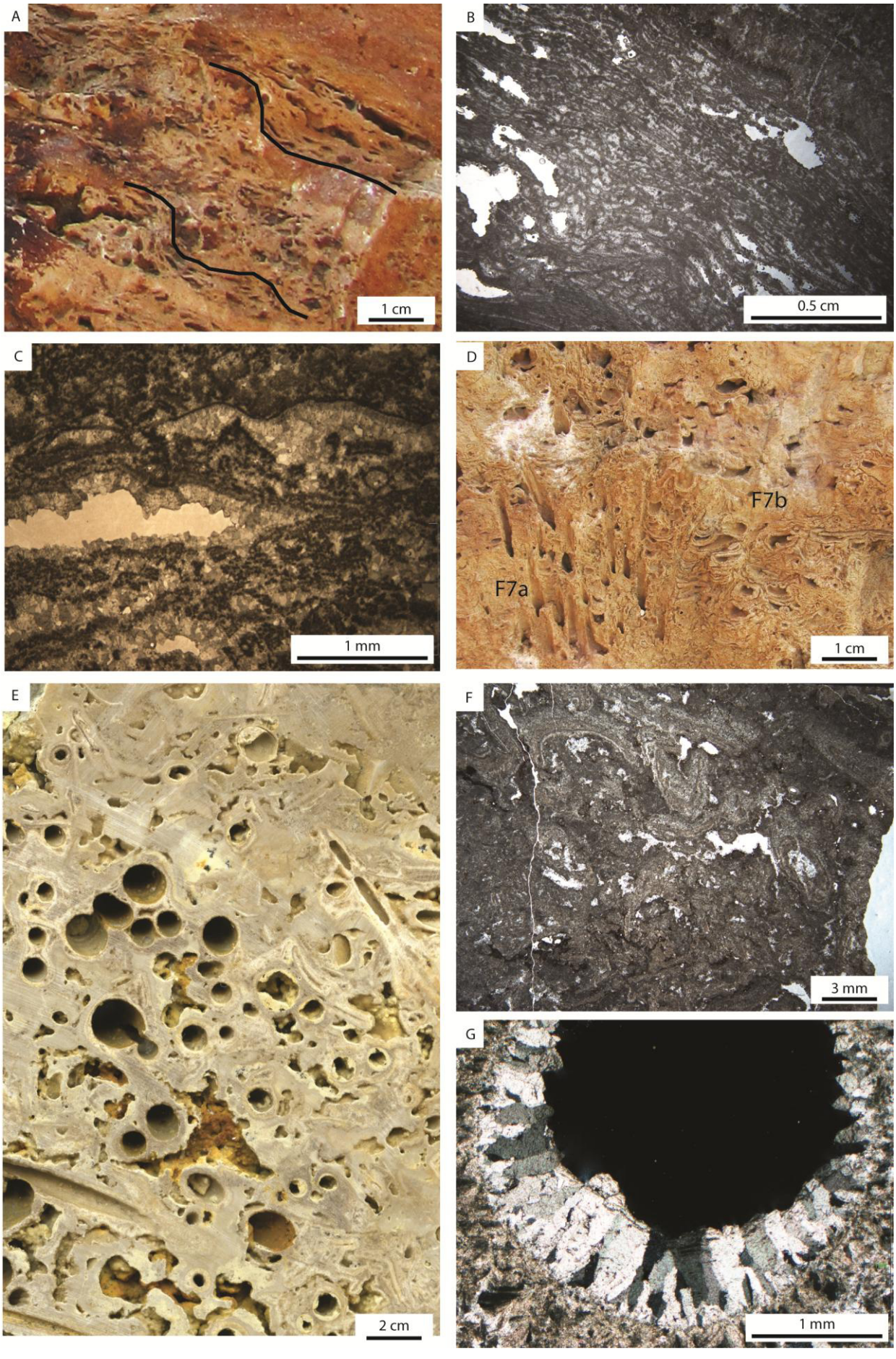
A
1 cm
B
0.5 cm
C
1 mm
D
F7b
F7a
1 cm
E
2 cm
F
3 mm
G
1 mm

Figure 3.6. Outcrop photos, polished slabs and photomicrographs of facies F6 and F7. A) Laminated boundstone consists of up to 5-cm-thick layers of wavy calcite laminae (2–5 mm thick), developing centimetre-thick terraces (black lines). B) Laminae consist of microsparite and clotted peloidal and structureless micrite. The cavities between the laminae are partially filled by equant sparite or are subjected to dissolution, thus developing irregular vugs up to 5 mm in size. C) Laminate boundstone composed of dense micrite laminae nearly 20 µm in thickness associated with clotted peloidal micrite. Primary interlaminar porosity is lined by scalenohedral cement. D) Example of vertical patches of reed moulds (facies F7a) >5 cm in height. On the right, prostrated and fragmented coated reed moulds (3–4 mm in diameter; facies F7b). E) Reed boundstone (facies F7a) consists of patches of sub-vertical or prostrate, centimetres-long carbonate-coated reed moulds. F) Photomicrograph of facies F7b phytoclastic packstone. G) Within the carbonate coating of reed moulds, the growth of prismatic sparite crystals with scalenohedral termination of up to 800-µm thickness is commonly observed.

3.4.8. Skeletal peloidal packstone/grainstone to floatstone/rudstone (facies F8)

3.4.8.1. Description

This lithotype consists of sub-horizontal nodular layers or concave-shaped lenses (5–60 cm thick) of skeletal peloidal packstone/grainstone to floatstone (Fig. 3.7A–B), with a grain size of 1–5 mm, rarely up to a few centimetres (Fig. 3.7C). Facies F8 is associated with clotted peloidal micrite grainstone (facies F1a) and reed facies (facies F7). Skeletal grains include gastropods, bivalves and ostracodes; they often appear as biomoulds coated by 1–2-mm-thick clotted peloidal micrite crusts and filled by clots of peloidal micrite of 20–30-µm size. The non-skeletal grains include faecal pellets (Fig. 3.7D), and aggregates of clotted peloidal micrite. Equant sparite cement fills the interparticle and intraparticle pores (Fig. 3.7E–F). In the upper part of the studied stratigraphic succession, pendant cement occurs in discontinuous crusts.

3.4.8.2. Interpretation

Lithotypes rich in clotted peloidal micrite, skeletal remains and faecal pellets typically occur in low-energy environments as ponds and pools. The occurrence of common molluscs and ostracodes is indicative of fresher and/or cooler waters than those precipitating travertine facies F1–F6. This lithotype is not generally associated with thermogene travertine facies, but it could develop at the edges of travertine systems. Guo and Riding (1998) and Guido and Campbell (2011) identified similar facies, which were rich in skeletal fragments and clotted peloidal micrite, in marsh environments developed at the distal end of travertine slopes. According to Freytet and Verrecchia (2002), some of the micritic and microsparitic coatings around grains might have developed in the vadose zone. Armenteros et al. (1997) described a similar nodular appearance, attributing it to palustrine environments, transitional between lacustrine and alluvial plain deposits. In the Marsiliana succession, facies F8 can be interpreted as being deposited in shallow marshs and low-energy freshwater environments with possible fluctuations of the water level.

3.4.9. Calci-mudstone to microsparstone (facies F9)

3.4.9.1. Description

This lithotype occurs as a dense homogeneous grey or red carbonate precipitate, deposited in sub-horizontal layers of thickness ranging from 2–3 to rarely 10 cm. Facies F9 does not show any sedimentary structure, and it alternates laterally and vertically with clotted peloidal grainstone (F1), raft (F2) and reed rudstone (F7) and coated gas bubble boundstone facies (F4). This calci-mudstone consists of aggregates of clotted peloidal micrite, structureless micrite and microsparite, gastropods, ostracodes and rafts (Fig. 3.7G–H). Blocky sparite cement has equant crystals sized 200–300 μm.

3.4.9.2. Interpretation

This massive facies is interpreted as accumulated in low-energy stagnant water pool settings, originating from sedimentation of carbonate mud derived from detrital, evaporative or biologically influenced processes. The microsparstone fabric may be derived from the diagenetic alteration of micrite or be primarily precipitated as micrite.

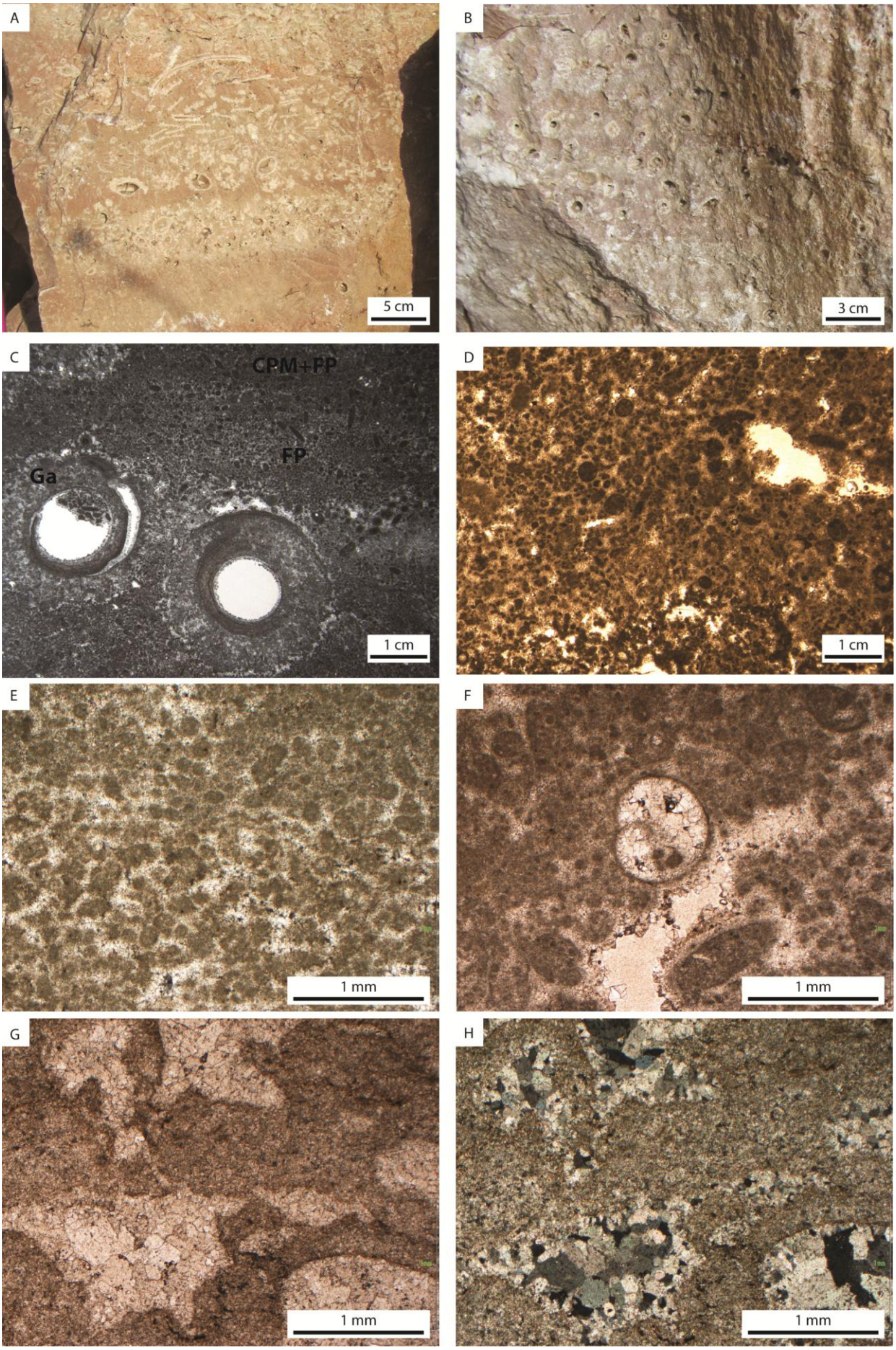
A
5 cm
B
3 cm
C
CPM+FP
FP
Ga
1 cm
D
1 cm
E
1 mm
F
1 mm
G
1 mm
H
1 mm

Figure 3.7. Outcrop photos, polished slabs and photomicrographs of facies F8 and F9. A) Facies F8, in 5–10-cm-thick layers, consists of skeletal and peloidal packstone/grainstone to floatstone/rudstone. The skeletal components include gastropods, bivalves and ostracodes. B) Gastropod packstone/rudstone (facies F8) in sub-horizontal layers. C) Gastropods (Ga), up to 1 cm in size, are associated with millimetre-size faecal pellets (FP) and aggregates of clotted peloidal micrite (CPM). D) Photomicrograph of peloidal grainstone/packstone with faecal pellets up to 500 µm in size. E) Facies F8 peloidal grainstone with equant sparite cement. F) Photomicrograph of gastropod peloidal grainstone with intraparticle porosity completely filled by sparite cement and clots of micrite. Around the large vug in the centre, scalenohedral calcite cement is observed. G). Facies F9 photomicrograph showing irregular aggregates of micrite and microsparite with vug porosity filled by equant calcite cement. H) The same image of panel 10G in crossed polarizers.

3.4.10. Breccia (facies F10)

3.4.10.1. Description

This facies consists of poorly sorted, matrix- to grain-supported breccias (Fig. 3.8A) with angular and subangular clasts (size ranging from several millimetres to 80 cm). The breccia layers (thickness varying from 1 m to >10 m; Fig. 5) are massive or crudely bedded in lobate or sheet-like geometry at a width of tens of metres, which decrease in thickness and pinch out towards the N–NW direction. Inverse and normal grading and erosional bases can be observed. The composition of the clasts includes >80% of dark-coloured, recrystallized calci-mudstone to microsparstone associated with fine-grained sandstone, siltstone, limestone, travertine reddened clasts and rare claystone lithic fragments. The interparticle space is filled by a detrital matrix consisting of structureless micrite and microsparite, as well as terrigenous silt and clays.

3.4.10.2. Interpretation

These breccia deposits are interpreted as gravity-flow fans, similar to those described by Leeder (2009), which developed along linear mountains front-fed by channels perpendicular to the axis of the main valley. Gravity flows are commonly observed in sedimentary basins bounded by thrust or normal faults, where periodic fault movements trigger slope instability and preserve the detrital fan deposits in the downthrown subsiding areas (cf. Leeder, 2009). Blikra and Nemec (1998) interpreted similar deposits in western Norway as high-viscosity debris flows in postglacial colluvial systems, which developed along the slopes of valley sides. In the studied succession, clast size, poor sorting and the uniform composition of the largely angular clasts suggest that the F10 breccias were deposited in a proximal colluvial fan system (cf. Blikra and Nemec, 1998). The main source of the carbonate clasts were the Ligurian and Tuscan Nappe Units (cf. paragraph 2.1 and Fig. 1), which crop out at the footwall of the fault system located south of the studied succession (Fig. 3). The micrite matrix among breccia clasts was likely to be derived from the abrasion and erosion of the carbonate clasts.

3.4.11. Conglomerate (facies F11)

3.4.11.1. Description

The facies F11 conglomerate consists of moderately sorted clasts, from subangular to rounded, mostly composed of dark-grey calci-mudstone (>80% of the clasts, ranging in size from a few millimetres to 20 cm; Fig. 3.8B). These conglomerates are often associated with sandstone facies (facies F12 and F13) in coarsening-upward sequences overlying the facies F14 claystone. They form lens-shaped, concave-upward layers (up to 50–60 cm in thickness) extending laterally from a few metres to hundreds of metres. The F11 conglomerate beds with erosional bases overlie claystone (facies F14) in the eastern area and travertines toward the western area of the active quarry (Figs. 3, 4 and 5). Some conglomerate beds display clast imbrications, and inverse or normal grading. The carbonate matrix consists of both structureless micrite and clotted peloidal micrite and microsparite.

3.4.11.2. Interpretation

Zembo (2010) interpreted similar lithofacies in the Val d'Agri Quaternary continental succession (Southern Italy) as deposits of sheet floods or channelized gravelly streams that entered a low-energy environment, such as a marginal shallow lake. This interpretation can be applied to the Marsiliana F11 conglomerate. The source of the calci-mudstone clasts is interpreted to be the erosion of the tilted rocks of the Tuscan Nappe and the Ligurian Units substrate, as for the F10 breccias. The filling of the interparticle space by clotted peloidal micrite and microsparite probably occurred under subaquatic low-energy conditions in shallow ponds of an alluvial plain.

3.4.12. Massive sandstone (facies F12)

3.4.12.1. Description

These sandstones form 5–20-cm-thick tabular beds and lenses that extend laterally for 5–10 m, without any internal sedimentary structures, except for a weak lamination (Fig. 3.8C). Various grains (medium to coarse sand of 0.5–2-mm size) are embedded in a carbonate mud matrix: dark-coloured limestone clasts, quartz grains and rare micas. This facies is mainly associated with facies

F10, and more rarely with facies F14 and F11 in fining- or coarsening-upward sequences up to 30 cm in thickness.

3.4.12.2. Interpretation

This massive sandstone lithofacies is interpreted as the finer portion of colluvial fan gravity-flow deposits, in association with the F10 breccia deposits. Miall (1996) described similar facies in sediment gravity-flow deposits, which they attributed to the progradation of colluvial fans when sandstones are overlain by breccias in coarsening-upward sequences (Blikra and Nemec, 1998). Massive F12 sandstones in coarsening-upward sequences between facies F14 at the base and the F11 conglomerate at the top are interpreted as accumulations under subaqueous low-energy conditions in shallow ponds of an alluvial plain, similar to the lithofacies interpreted by Zembo (2010).

3.4.13. Laminated sandstone to siltstone (facies F13)

3.4.13.1. Description

This facies is composed of fine sandstone to siltstone beds (5–20 cm thick, laterally extended for up to 30 m), yellow to grey in colour with normal gradation, and planar or undulate lamination (Fig. 3.8D). Sand grains are composed of lithic fragments of dark calci-mudstone and microsparstone, as well as siliciclastic siltstone, quartz and mica detrital grains. This facies is organized in both fining- and coarsening-upward trends when it overlies conglomerate (facies F11) and claystone beds (facies F14), respectively.

3.4.13.2. Interpretation

Laminated sandstone to siltstone facies are interpreted as deposits due to suspension and weak traction current in the overbank areas of an alluvial plain (Miall, 1996). When cross-laminated sandstones are interbedded with claystones, they can be interpreted as being deposited in the shoreline facies of lakes and ponds in an alluvial plain (cf. Link et al., 1978), or in fluvial lower-flow-regime conditions (Miall, 1996). In the Marsiliana succession, when facies F13 is associated with travertines of facies F7, it is interpreted as deposits on the margins of shallow water ponds; instead, when it is associated with conglomerates (facies F11), it is interpreted as being deposited by weak traction currents of streams and settling from suspension in an alluvial plain.

3.4.14. Claystone (facies F14)

3.4.14.1. Description

These deposits consist of claystones, grey in colour, massive, and nodular or finely laminated, displaying root moulds and carbonate nodules belonging to palaeosols (Fig. 3.8E–F). The thickness varies from a few centimetres up to 1.70 m (maximum thickness in the eastern area), laterally extending from a few centimetres to a width of 20–30 m.

3.4.14.2. Interpretation

Miall (1996) interpreted similar deposits as accumulations in standing pools, backswamps, overbanks or abandoned channels or as drape deposits in alluvial settings. Massive claystones are interpreted as being settled from suspension, following flood events in the mudflat areas of alluvial environments (Miall, 1996). Neves et al. (2005) interpreted similar facies associated with gravel deposits and developed in lenses, in relation to the formation of ponds with settlement of fine sediment. In the Marsiliana succession, in association with the F11 conglomerate and the F13 laminated sandstone, this facies F14 is interpreted as being deposited in an alluvial plain, with the development of shallow ponds or in overbank areas subjected to subaerial exposure and pedogenesis. In association with the F10 breccias, this claystone facies is interpreted as being deposited in standing water pools developed on the colluvial fan systems.

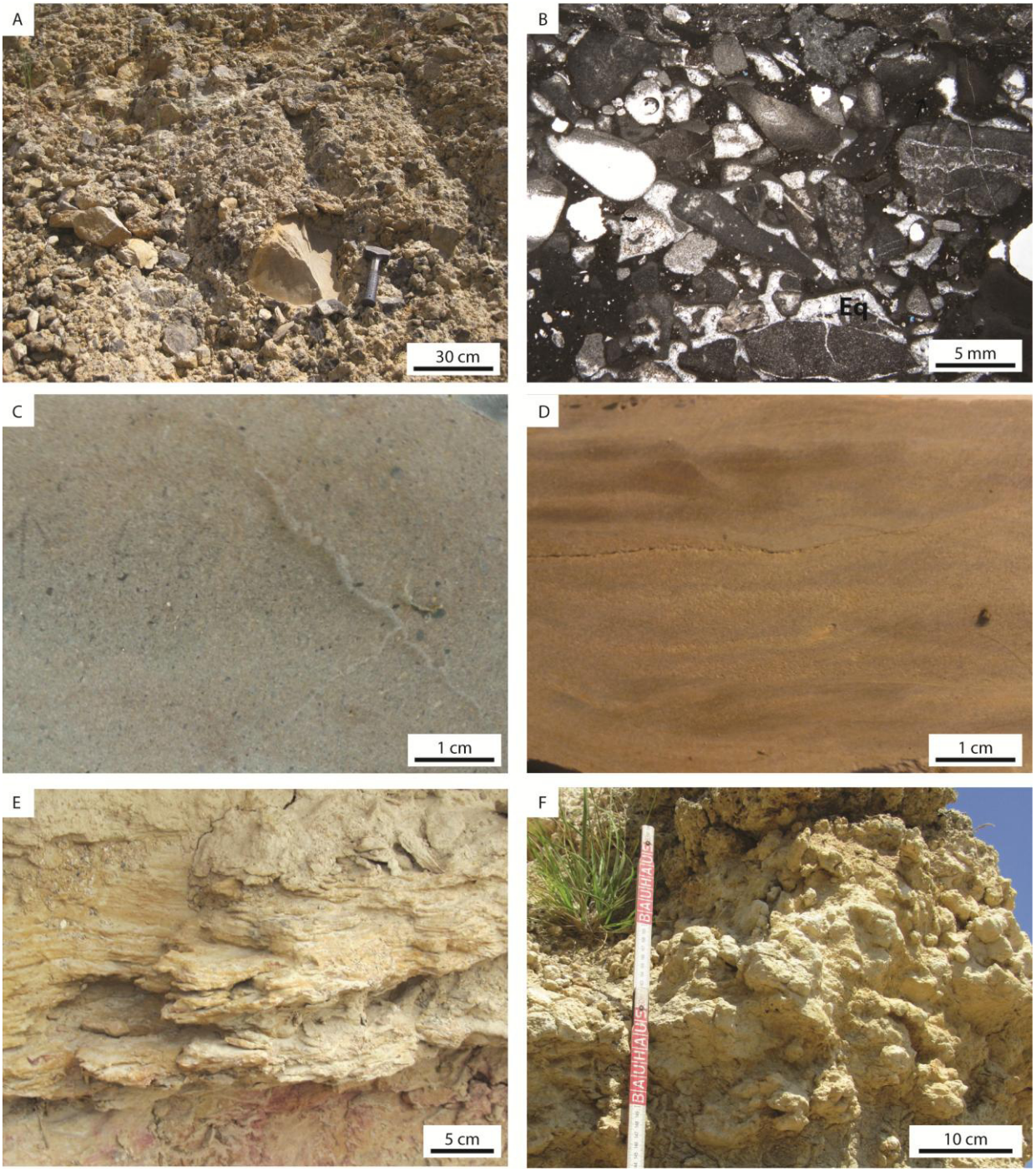

Figure 3.8. Outcrop photos and polished slabs of facies F10–F14. A) Breccias (facies F10) are made of dark-grey calci-mudstone to microsparstone clasts, from angular to subangular, with a micrite to microsparite matrix. Other components include clasts of cream sandstones, light-grey limestone and red travertine. B) Conglomerates (facies F11) consist of rounded to subangular clasts, with sizes ranging from sub-millimetres to centimetres, of recrystallized calci-mudstone and microsparstone; the interparticle spaces are filled by carbonate and terrigenous mud and mosaics of equant sparite (Eq). C) Massive sandstone (facies F12) consists of well-sorted, medium to coarse sand, with black calci-mudstone lithoclasts. D) Fine laminated sandstone to siltstone (facies F13) showing wavy lamination. E) Claystone (facies F14) is characterized by millimetre-thick lamination. F) Nodular claystone facies interpreted as pedogenetic features.

3.4.15. Oxygen and carbon stable isotope analyses

The Marsiliana travertines display $\delta^{18}O$ signatures varying from −10.5 to −6.1‰ V-PDB, and $\delta^{13}C$ values from −1.9 to 3.9‰ V-PDB (Fig. 3.9). The various types of travertine facies differ in their $\delta^{13}C$ values, which might reflect a different primary signature or the effect of meteoric diagenesis. Higher average $\delta^{13}C$ values are observed in F1 and F5 facies (1.7‰ and 1.9‰, respectively), whereas the lowest $\delta^{13}C$ average values are noted in facies F4 and F8 (−0.6‰ V-PDB and 0.3‰ V-PDB, respectively). The rest of the travertine facies can be subdivided into two classes based on the average of their $\delta^{13}C$ values, with F2 and F3 having a signature >1‰ and F7 and F9 <1‰. The average travertine $\delta^{18}O$ values vary between −8.1‰ (facies F7) and −7.1‰ (facies F5), which is of a narrower range than the $\delta^{13}C$ signatures. The $\delta^{18}O$ average values of facies F1, F8 and F9 are approximately −7.7‰. Instead, the F3 and F4 $\delta^{18}O$ values are −7.3‰ and −7.1‰, respectively. In the upper 20–25 m of the stratigraphic succession (Fig. 5), the $\delta^{13}C$ and $\delta^{18}O$ values of the travertines collected show decreasing trends from the bottom to the top (logs SA and F; Figs. 3.2 and 3.9) and from South to North.

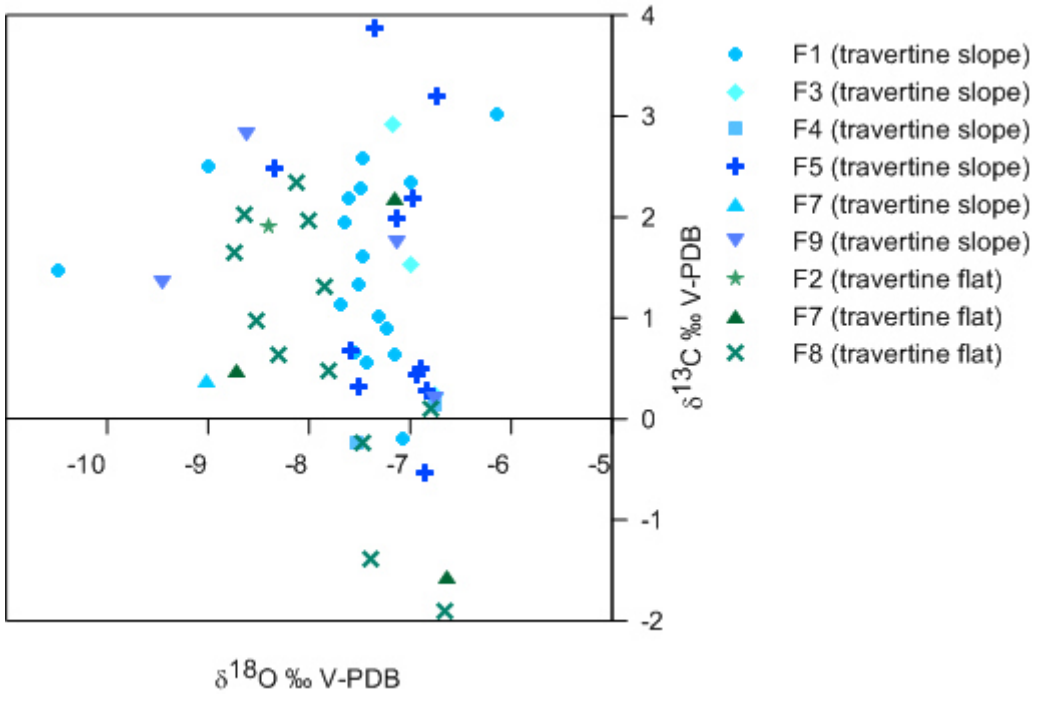

Figure 3.9. Stable isotope analyses of the Marsiliana studied succession with $\delta^{18}O$ and $\delta^{13}C$ values of the travertine samples distinguished based on lithofacies type and travertine lithofacies association, expressed in ‰ relative to the V-PDB scale: travertine slope lithofacies association is denoted in blue and travertine flat lithofacies association in green.

3.5. Depositional environments and sedimentary evolution over time

3.5.1. Lithofacies association

The vertical stacking and lateral spatial distribution of the distinguished lithofacies types is shown in the correlation diagram of the measured stratigraphic logs in Fig. 3.2, as well as in the lithofacies map and digital elevation model of Figs. 3.10 and 3.11. The lithofacies are assigned to four associations based on the interpretation of the depositional environment and their spatial distribution. The identified lithofacies associations are as follows: a) travertine slope (facies F1–F6), b) travertine flat (facies F1–F3 and F7–F9), c) alluvial plain (facies F11–14) and d) colluvial fan (facies F10, F12).

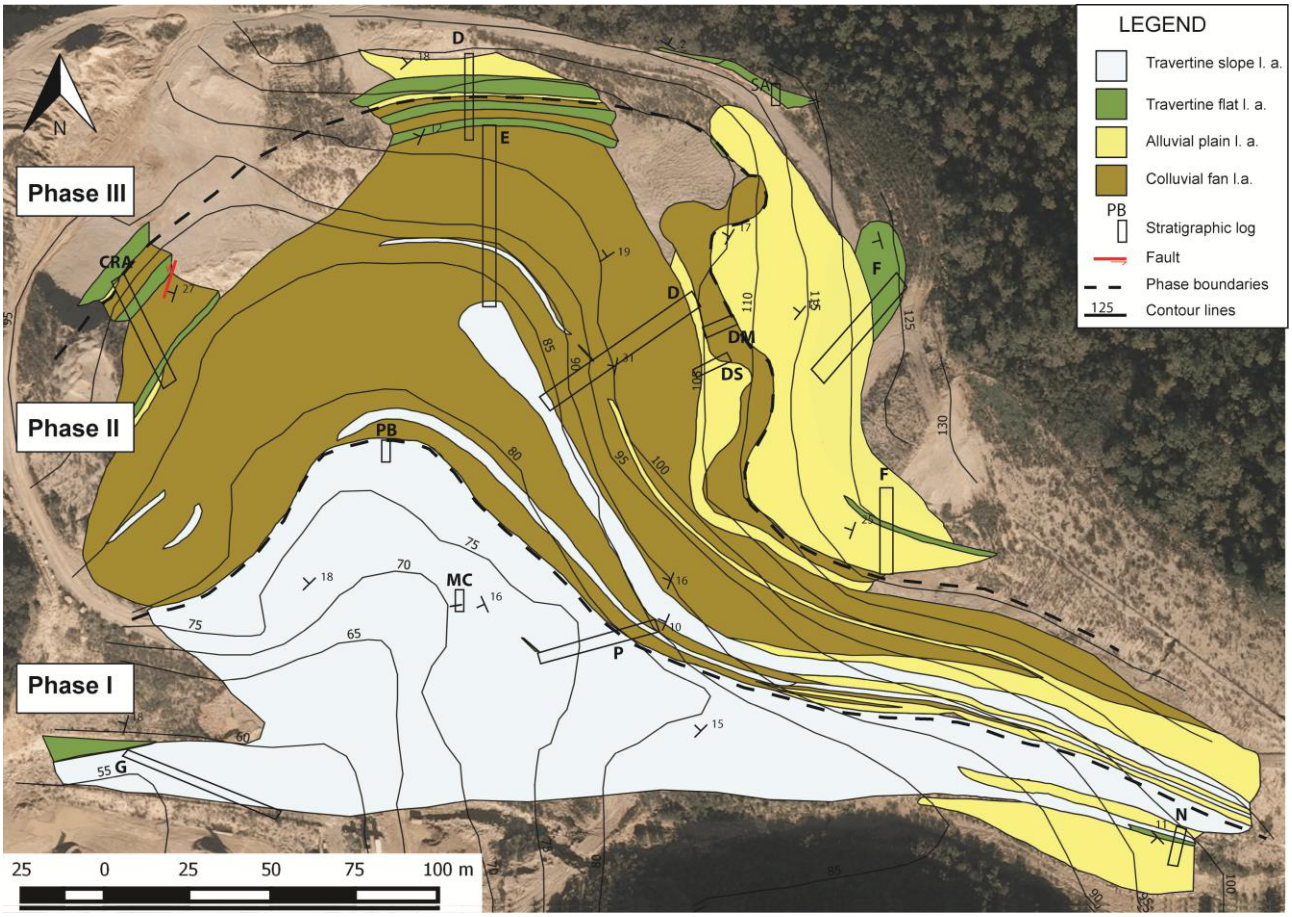

Figure 3.10. Map of the studied quarry showing the distribution of the four distinguished lithofacies associations, the three distinguished stratigraphic phases and the location of the stratigraphic logs.

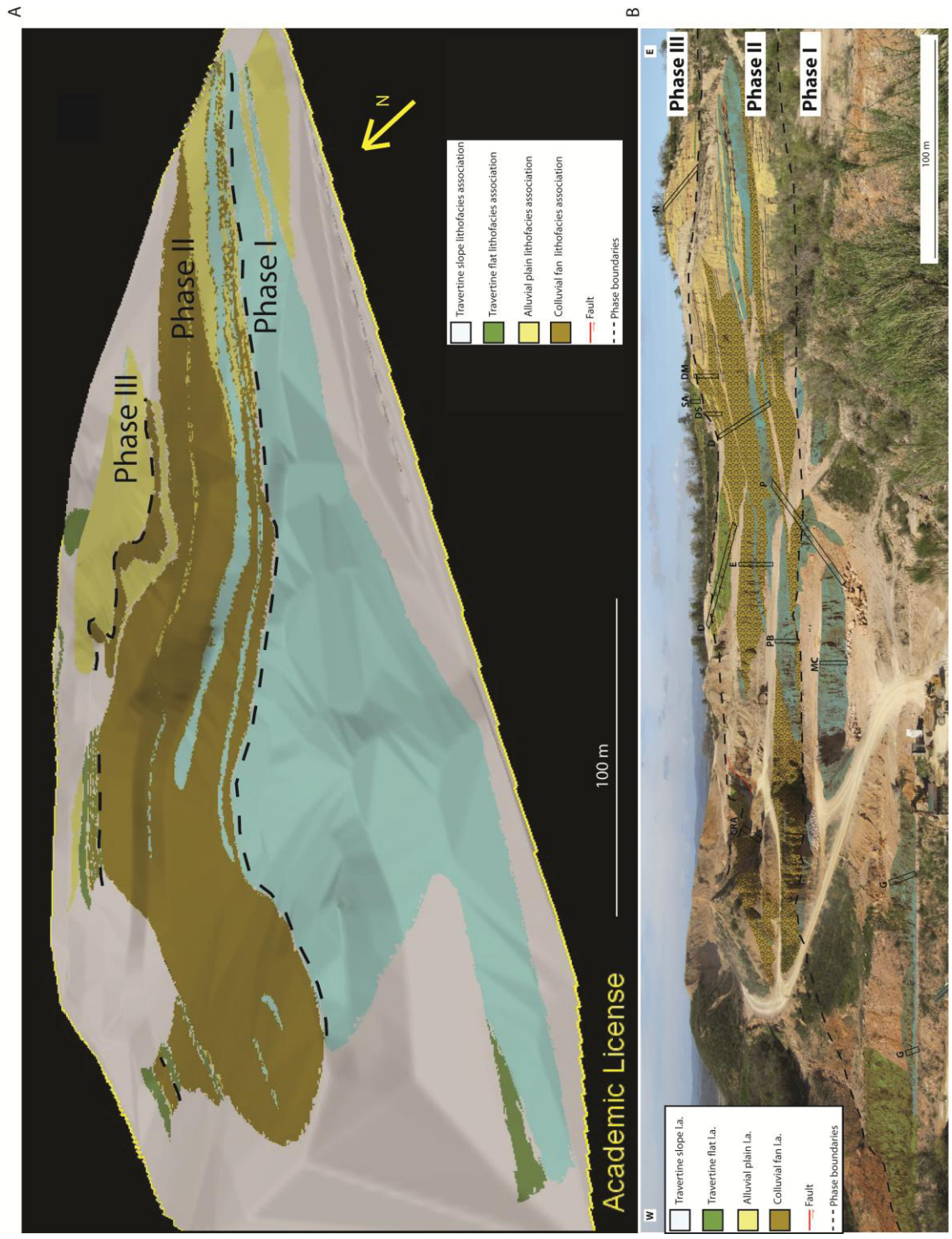

Figure 3.11. A) 3D representation of the distribution of the lithofacies association draped on the digital elevation model of the studied area developed with the software Move Midland Valley. B) Panoramic view of the Marsiliana quarry superimposing the lithofacies association distribution and the location of the stratigraphic logs within the active quarry.

3.5.1.1. Travertine slope lithofacies association

The travertine slope lithofacies association comprises facies F1–F6, accumulated in terraced and smooth slope depositional settings that alternate laterally and vertically, just as Özkul et al. (2002) and Claes et al. (2015) described the Pamukkale travertines. According to Guo and Riding (1999), slope terraces form when the water rapidly flows in laminar sheets on gently dipping topographic surfaces, and raised rims and walls begin to deposit due to turbulence, evaporation and obstacles to the flow.

This lithofacies association occupies the lower 20 m of the studied succession (logs G, PB, MC, P in Fig. 5), mainly in the central and western part (Figs. 3.10 and 3.11), further interfingering with claystone and conglomerate layers in the eastern part (facies 11 and 14 in log N of Fig. 5). Moreover, travertine lenses, intercalated within the breccia deposits (facies F10) in log E, belong to the slope lithofacies association. The travertine slope environment must have been affected by intermittent thermal water flow, as suggested by the periodic exposure to meteoric alteration (Fig. 3.12A) and alternation with terrigenous breccia deposits.

The Marsiliana terraced slope lithofacies association is characterized by a layered (0.5–5-cm-thick beds) down-stepping morphology with sub-horizontal metre-scale pools separated by rounded rims and sub-vertical walls (Fig. 3.12B–C). The walls of the terraces vary in height from a few millimetres (micro-terraces; Fig. 3.12D) up to 1 m; the inclined walls and rims consist of clotted peloidal micrite grainstone to boundstone (facies F1) and 2–4-cm-thick crystalline dendrite cementstone (facies F5) layers. Sub-horizontal layers form 3–4-m-wide pools, characterized by a concave-upward bottom of a depth of a few centimetres, and fronted by decimetre-thick rims on the downstream side, which is inferred to have been towards the NW direction based on the down-stepping topography (Fig. 3.12E–F). The pool lithofacies include raft rudstone (facies F2), radial coated grain grainstone (facies F3), coated gas bubble boundstone (facies F4) and reed rudstone to boundstone (facies F7). The pool travertines are characterized by a porous framework (Fig. 3.12E), due to the presence of intra-bubble and mouldic porosity. When the slope is smooth and inclined between 10° and 30° (logs P and PB in Fig. 5), it is composed of 10–15-cm-thick layers of crystalline dendrite cementstone (facies F5), alternating with 2–5-cm-thick layers of laminated boundstone (facies F6).

The geochemical signature of the travertine slope lithofacies association (average $\delta^{13}C$ 1.43 ‰ with a maximum of 3.88 ‰; average $\delta^{18}O$ of −7.50 ‰) confirms that the precipitating water was fed by geothermally generated CO_2, as reported in various studies on thermogene travertines (Pentecost, 2005; Capezzuoli and Gandin, 2008; Della Porta, 2015).

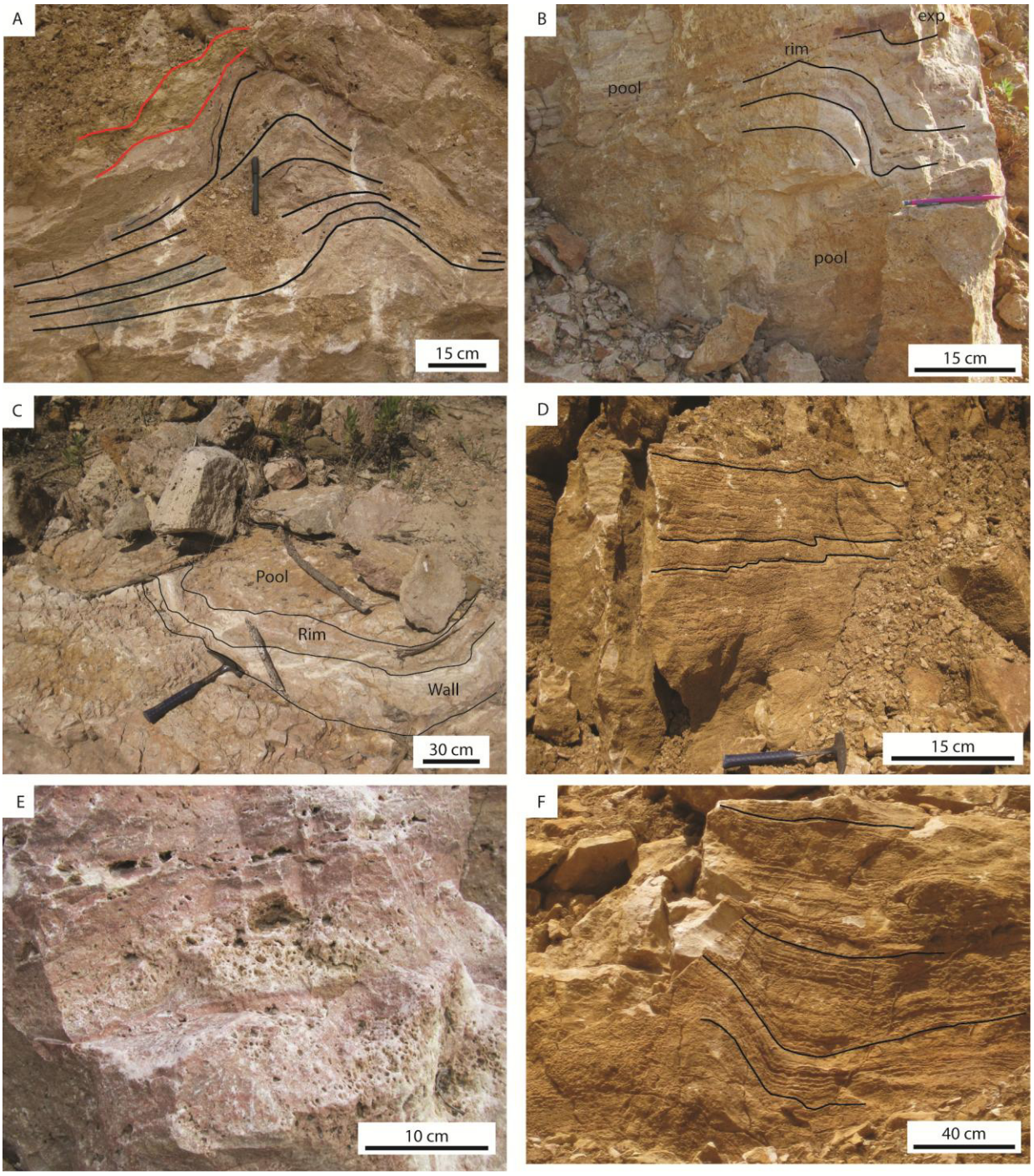

Figure 3.12. Outcrop photos of travertine slope lithofacies association. A) Convex-upward pool rim of nearly 45-cm thickness indicated by the black lines, covered by centimetre-thick yellow claystone, highlighted by the red lines. B) Terraced slope pool rim adjacent to sub-horizontal pools. The travertine is dark brown in colour due to exposure to meteoric weathering (exp). C) Terraces show a semicircular shape in plain view; the rim and wall lithofacies are white in colour, whereas the pool deposits are darker in colour, due to the concentrations of terrigenous detrital sediment. D) Centimetre-size micro-terraces that grow above a sub-horizontal surface. E) Detail of porous coated gas bubble boundstone decimetre-thick layers accumulated in a pool of the terraced slope. F) At the toe of the wall, the pool layers are characterized by a concave geometry, which becomes sub-horizontal when the pool is filled by carbonate precipitates.

3.5.1.2. Travertine flat lithofacies association

This lithofacies association is characterized by tabular sub-horizontal beds varying in thickness from a few centimetres to 1–2 dm (Fig. 3.13A–B). It is dominated by reed rudstone to boundstone (facies F7), skeletal peloidal packstone/grainstone to floatstone/rudstone (facies F8) and calci-mudstone/microsparstone (facies F9) with rare clotted peloidal micrite boundstone to grainstone (facies F1), raft rudstone (facies F2) and radial coated grain grainstone (facies F3). The travertine flat lithofacies association is interpreted as shallow pond deposits under conditions of stagnant or slow-flowing thermal water that was likely to be mixed with meteoric water, according to the low $\delta^{13}C$ values. These conditions can occur either in distal areas with respect to the vent or in proximal areas, but only after events of subaerial exposures identified by the underlying terrigenous deposits and the development of erosional surfaces and pedogenesis, or during terminal phases of the hydrothermal activity and thermogene travertine formation.

Travertine flat lithofacies types occur in stratigraphic logs G and CRA in the western part of the studied quarry (Figs. 3.2, 3.10 and 3.11), in the upper part of log D, in the entire expanse of log SA, in log MC and P in the central part of the quarry, at the top of logs F and in log N in the eastern part. In stratigraphic logs G, MC, P and N, the travertine flat lithofacies association is identified at the bottom of the studied succession, where it overlies the alluvial plain lithofacies association and is overlain by the travertine slope lithofacies association. By contrast, in the upper part of the studied area (stratigraphic logs CRA, D, SA and F in Fig. 3.2), the travertine flat did not evolve into the slope lithofacies association. The travertine flat lithofacies association characterizes the northern part of the studied area (Fig. 2.3), and it is noted in the stratigraphic log CE and MA as well (Fig. 3.13C–D), where it is 20 m thick (in 10–80-cm thick sub-horizontal beds) and extend laterally for a width of 50 m.

The average $\delta^{13}C$ value of the travertine flat is 0.46‰, varying from a minimum value of −1.9 ‰ to a maximum of 2.18 ‰. The lower (negative) $\delta^{13}C$ values (Fig. 3.9) were measured in samples from logs CRA, SA and F in the upper part of the succession, which show an inverse covariance with increasing $\delta^{18}O$ and decreasing $\delta^{13}C$ values. This trend of $\delta^{18}O$ is suggested to be indicative of soil-derived CO_2 and cooling of the travertine precipitating water likely due to mixing with meteoric water (Deocampo, 2010). According to Guo and Riding (1998) and Guido and Campbell (2011), distal travertine flat lithofacies should record the significant influence of meteoric freshwater. The highest (positive) values of $\delta^{13}C$ were recorded in samples from the travertine flat lithofacies cropping out in the northern abandoned quarry (Fig. 2.3), farther away from the southern faults and the supposed location of the vent. This increase in $\delta^{13}C$ might be attributed to the progressive degassing of CO_2 at increasing distances from the vent (Fouke et al., 2000; Kele et al., 2008; Faccenna et al., 2008; Della Porta, 2015).

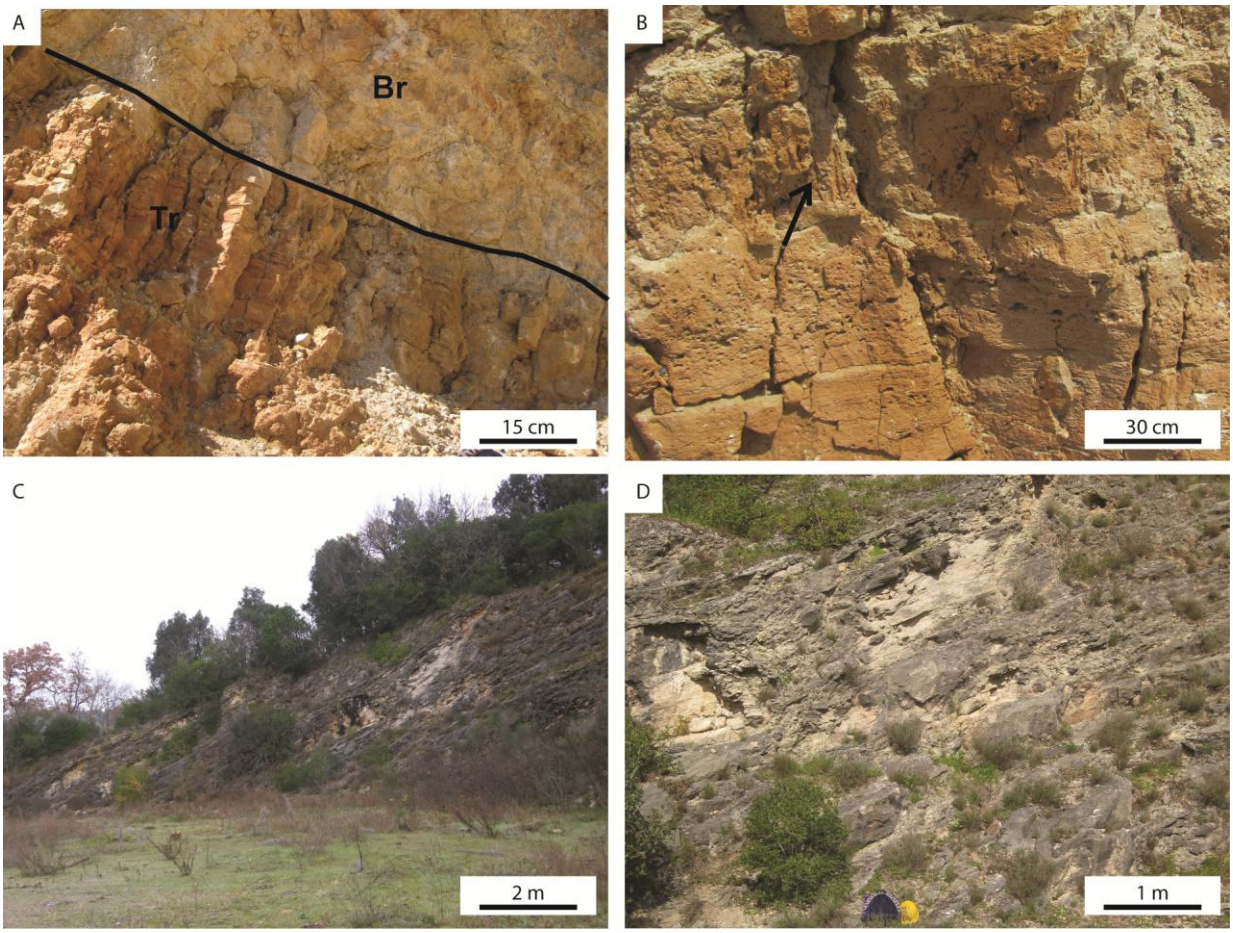

Figure 3.13. Outcrop photos of travertine flat lithofacies association. A) Centimetre- to decimetre-thick beds of travertine flat lithofacies association (TR) overlain by breccia (Br; facies F10) in the lower part of log CRA. B) Travertine flat lithofacies association at the top of stratigraphic log F characterized by vertical coated reeds (arrow) and mouldic and fenestral millimetre-size porosity. C) Panoramic view of the northern part of the studied area, with travertine strata from the flat environment dipping towards the NW direction due to tectonic tilting. D) Outcrop photo of stratigraphic log CE, with travertine flat sub-parallel layers white and grey in colour.

3.5.1.3. Alluvial plain lithofacies association

This lithofacies association represents the lateral and vertical transitions of the terrigenous facies F11, F12, F13 and F14 (Fig. 3.14A) and the occurrence of travertines enriched in phytoclasts (facies F7) and skeletal fragments (facies F8), in the form of lenses of 1–2-dm thickness and 5–6-m width (Fig. 3.14B–C). These travertines are often associated with thick (80–120 cm) deposits of massive and laminated (facies F14) claystone (Fig. 3.14D, E). This lithofacies association is interpreted as being indicative of an alluvial plain (facies F14) with channelized streams (lenticular beds of facies F11–13), shallow marshes and palustrine ponds (facies F7, F8), cropping out mostly in the eastern and upper parts of the study area. The alluvial plain lithofacies are well developed in the following regions: a) in the eastern stratigraphic logs F and N; b) in the uppermost part of log D; c) in logs DM and DS, where they are interbedded with the breccia deposits (facies F10); and d) in logs P, MC and G (Fig. 3.14F), in the lower part of the studied quarry, where alluvial plain lithofacies occur between the travertine slope and the travertine flat lithofacies association.

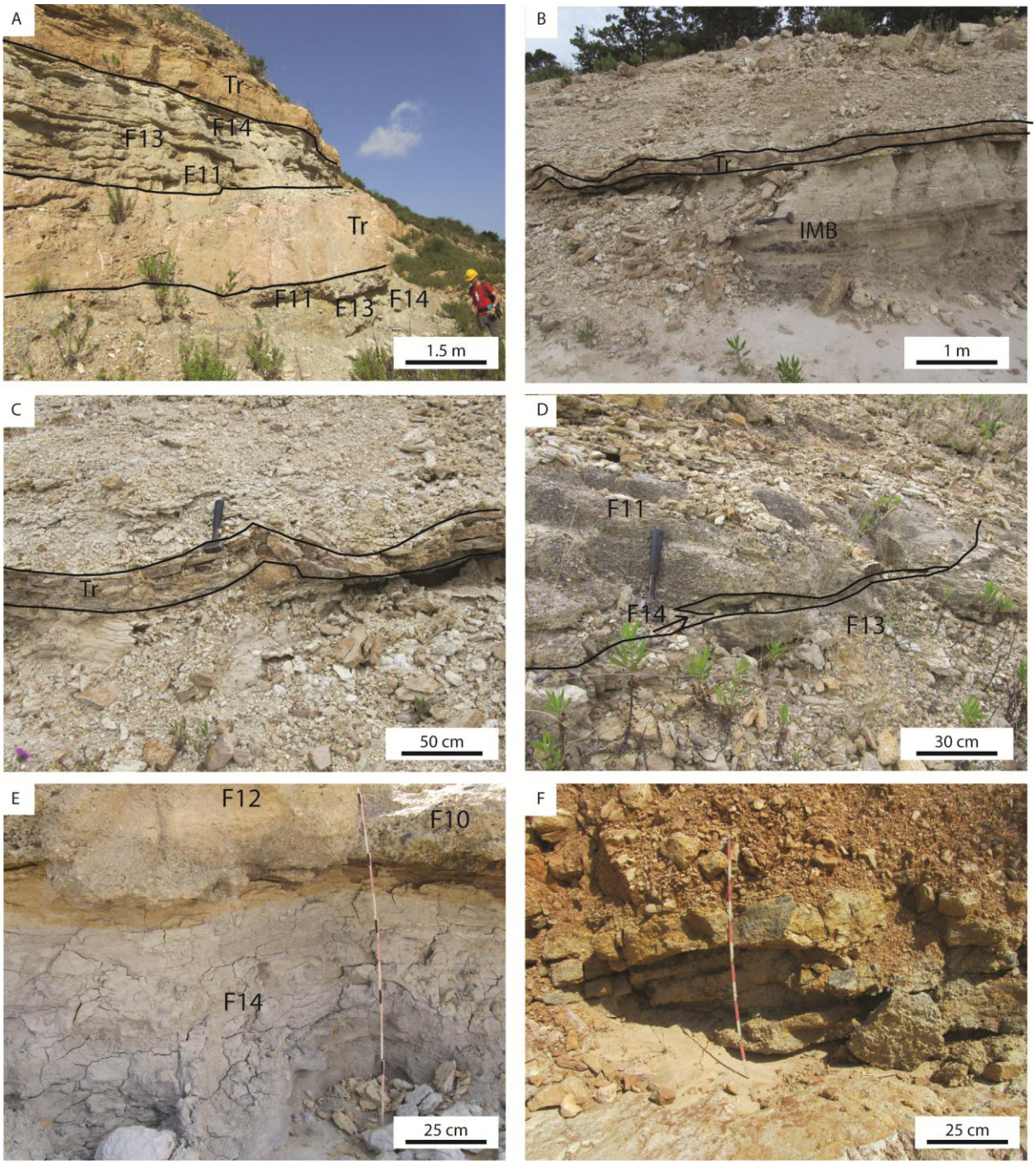

Figure 3.14. Outcrop photos of alluvial plain lithofacies association. A) Alluvial plain lithofacies association in the lower eastern part of the studied area consisting of facies F11, F13 and F14, deposited in layers of thickness varying from centimetres to 1 m, alternating with travertines slope facies association (Tr). B) Travertine lenses (Tr) that are brown to slightly reddish in colour are intercalated in decimetre-thick claystone deposits. The occurrence of imbricate pebbles (IMB) confirms the deposition of F11 conglomerates in flowing water with traction. C) Close-up view of travertine layered phytoclastic- and skeletal-rich deposits (Tr; facies F7 and F8) that develop 20-cm-thick undulated lenses. D) Lens of claystone (facies F14) deposited between laminated sandstone (facies F13) and the conglomerate (facies F11). E) Claystone layer of 6-cm thickness (facies F14) interpreted as overbank deposit in the alluvial plain, overlain by 10–20-cm-thick breccia (facies F10) and 10-cm-thick massive sandstone (facies F12) of the colluvial fan lithofacies association. F) Alluvial plain lithofacies in stratigraphic log G including conglomerate facies (F11) with clasts of up to 1-dm size.

3.5.1.4. Colluvial fan lithofacies association

This lithofacies association consists of 10–20-m-thick deposits of amalgamated breccia beds (facies F10) with erosional bases (Fig. 3.15A–D), alternating with decimetre-thick massive sandstone beds (facies F12) and rare, massive claystone of <1-m thickness (facies F14). Laterally, this lithofacies association extends for 100–200 m, with the breccia beds decreasing in thickness and pinching out northwards. This lithofacies association represents proximal debris flow-dominated colluvial fans (cf. Blikra and Nemec, 1998). Nemec and Kazanci (1999) described a similar lithofacies association in the Taurus Mountains, west-central Anatolia (Turkey), concluding that the development of such thick colluvial fans is characteristic of a semi-arid climate, where occasional rainstorms trigger debris flows. This interpretation may also be applied to the facies F10 breccias. In addition, because the uplifted substrate sedimentary rocks may have been the source of the debris-flow clasts, a tectonic trigger for the generation of debris flow cannot be excluded in the Albegna extensional basin, as in other continental rift basins (cf. Heward, 1978).

The colluvial fan lithofacies association is recorded in stratigraphic logs CRA, E, P, D, DM and DS (Figs. 3.2, 3.10 and 3.11). In the eastern, lower part of the studied succession, the colluvial fan debris-flow deposits alternate with the alluvial plain lithofacies association (Fig. 13.15E). In the intermediate and upper portions (stratigraphic logs E and P), the colluvial fan deposits alternate with the travertine slope lithofacies association with seven alluvial fan units separated by six travertine lenses, forming layers of thickness ranging from a few centimetres up to 2–3 m (Fig. 13.15F). This shows that the thermal water flow was still active, promoting the rapid re-establishment of terraced travertine morphologies after the emplacement of the colluvial fans. In the upper part, colluvial fans interfinger with the alluvial plain lithofacies association (the top of stratigraphic log D; Fig. 3.2).

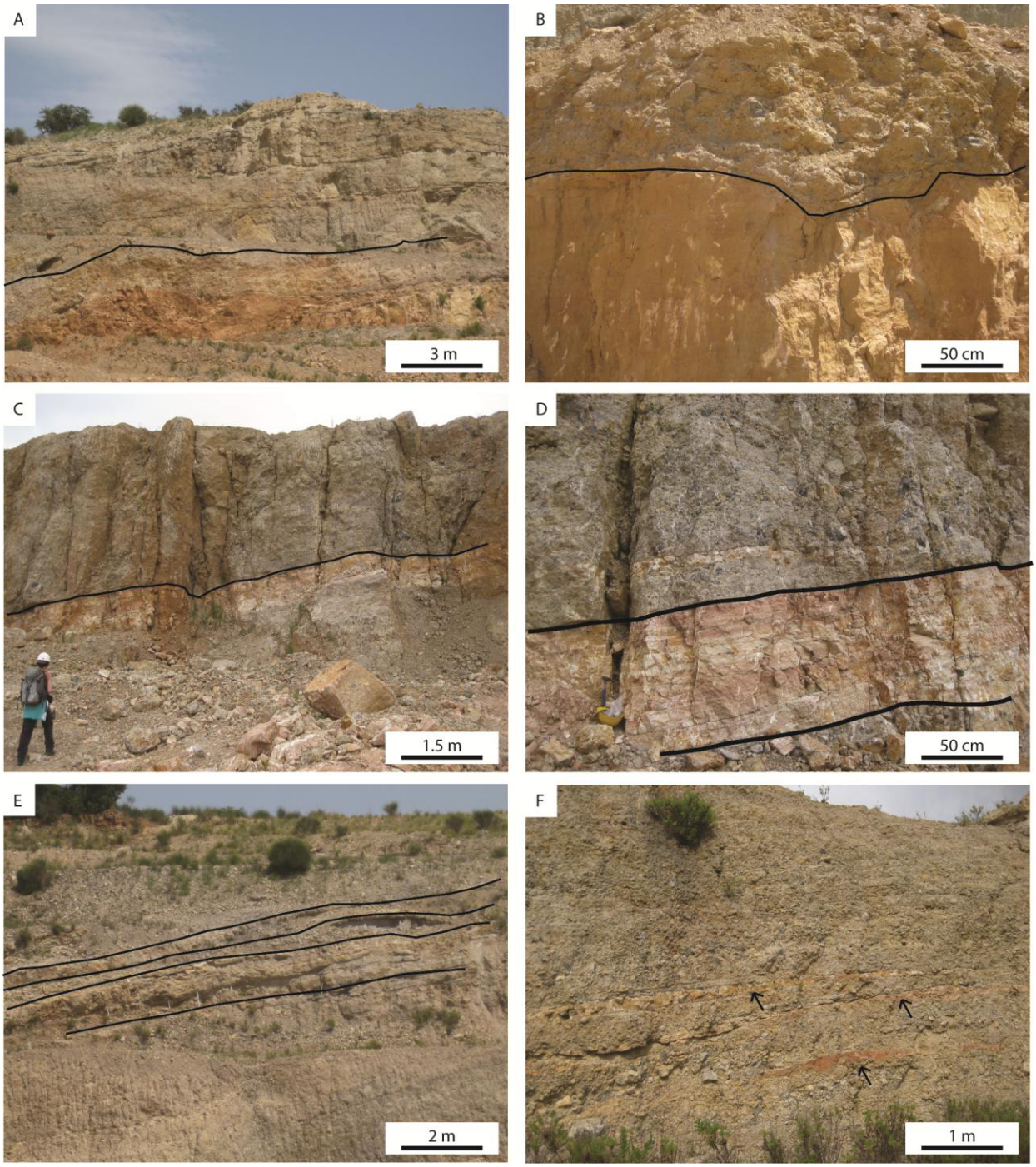

Figure 3.15. Outcrop photos of colluvial fan debris flow and alluvial plain lithofacies associations. A) Colluvial fan debris-flow lithofacies association occurs in 10–20-m-thick breccia deposits with an erosional base (black line). B) Detail of breccia erosional base overlying travertine strata (black line). C) Colluvial fan debris-flow breccia overlying in sharp contact the travertine slope lithofacies. D) Detail of the sharp contact between the travertine slope comprising crystalline crusts (facies F5) and the overlying breccia bed. E) Colluvial fan breccia (F10) with intercalations of sandstone and siltstone (F12 and F13; black lines). F) Thermogene travertine lenses belonging to facies F1 (black arrows), thickness ranging from centimetres to metres and width from metres to decametres, in-between the colluvial fan breccias.

3.5.2. Stratigraphic architecture and evolution of the depositional system

Based on the lithofacies characteristics and association, spatial distribution, geometry and vertical and lateral lithofacies transitions, the studied sedimentary succession can be divided into three parts representing three different progressive phases, from older to younger, of evolution of the deposition in a tectonically controlled sedimentary basin (Figs. 3.10, 3.11, 3.16 and 3.17).

3.5.2.1. Phase I

Phase I is characterized by the deposition of nearly 20 m of thermogene travertines in the form of terraced and smooth slope aprons at the base of the studied succession (Figs. 3.11, 3.16 and 3.17A). Travertine slopes dip and thin towards the N and NW direction, indicating that the hydrothermal vents might have been located close to the faults reported in the geological map at the southern border of the study area (Fig. 2.3). Hydrothermal vents are often linked to fault systems, as described by Sant'Anna et al. (2004) in the Itaboraí Basin (Brazil), and by Guido and Campbell (2011) in the Deseado Massif (Argentina), in the Rapolano Terme fissure ridge (Brogi and Capezzuoli, 2009) and in Della Porta (2015) in rift lakes from Western USA. An alluvial plain environment extended from the East towards the West and North adjacent to the growth of the travertine slope system (Fig. 3.17A). Similarly, Szulc et al. (2006) described alluvial deposits in association with travertines in the Upper Triassic of Southern Poland, as did Zentmyer et al. (2008) along the Holocene South Tibetan (China) fault system.

The accumulation of the travertine slope must have become an active component of the evolving landscape, thus obstructing the deposition of the alluvial plain environment, changing the direction of the superficial stream flow and promoting the formation of shallow ponds around the travertine deposits.

3.5.2.2. Phase II

Phase II (of nearly 30-m thickness) is marked by the onset and accumulation of tens of metres of colluvial fan breccias that buried the travertine slope system of Phase I. Colluvial fans thinned northwards and westwards (Fig. 3.17B), whereas this lithofacies association interfingered with the persistent alluvial plain environment in the eastern part of the studied succession. The occurrence of alluvial plain deposits in the western part of the quarry (Figs. 3.10 and 3.11) suggests that the alluvial plain environment surrounded the colluvial fans.

In the literature, Hernandez-Diaz and Hernandez-Enrile (2001) have already reported the precipitation of travertines related to colluvial debris-flow lobes. These authors described the accumulation of Pleistocene to Holocene travertine deposits in a pull-apart basin in the Betic

Cordillera (Spain). Ten Veen et al. (2004) reported a similar lithofacies succession in the Eşen Çay Basin in SW Turkey, as did Zentmyer et al. (2008) near Nyalam in Tibet. Jones and Arzani (2005) described the superposition of debris-flow breccias and travertine lenses in the Plio-Pleistocene succession of the Khrud Mountain belt in Central Iran.

The deposition of the colluvial fans might have been triggered by fault displacements related to the Neogene extensional tectonics in Southern Tuscany (see paragraph 5.1.4). During Phase II, the hydrothermal system was active but travertines could accumulate only during periods of quiescence of debris-flow deposition. During these periods, the alluvial plain environment extended towards the West and the North.

3.5.2.3. Phase III

Phase III (20–25 m in thickness) includes the interfingering of travertine flat and alluvial plain lithofacies associations representing adjacent and time-equivalent depositional environments (Fig. 3.17C). Phase III does not present a record of the travertine slope and colluvial fan lithofacies association. These two lithofacies associations may be absent due to removal by erosion or more likely due to non-deposition, because the sedimentary basin evolved into a flat plain with alluvial terrigenous deposits, channelized streams, marshes with vegetation (alluvial plain lithofacies association) and travertine deposits that reflect the terminal phases of hydrothermal activity (travertine flat lithofacies association). The travertine flat lithofacies were deposited in shallow ponds fed by thermal water mixed with groundwater charged with meteoric carrier. This is supported by the low negative $\delta^{13}C$ stable isotope data of the flat travertine lithofacies association at the top of the studied succession.

This evolution of the sedimentary succession might indicate a phase of tectonic quiescence and reduced displacement of extensional faults, which resulted in reduced hydrothermal activity and lack of travertine slope development, reduced creation of accommodation space, and filling of the basin with alluvial plain deposits. The lack of a colluvial fan lithofacies association in Phase III might be attributed to the reduced fault-controlled creation of structural highs, which acted as sources of coarse detrital sediment.

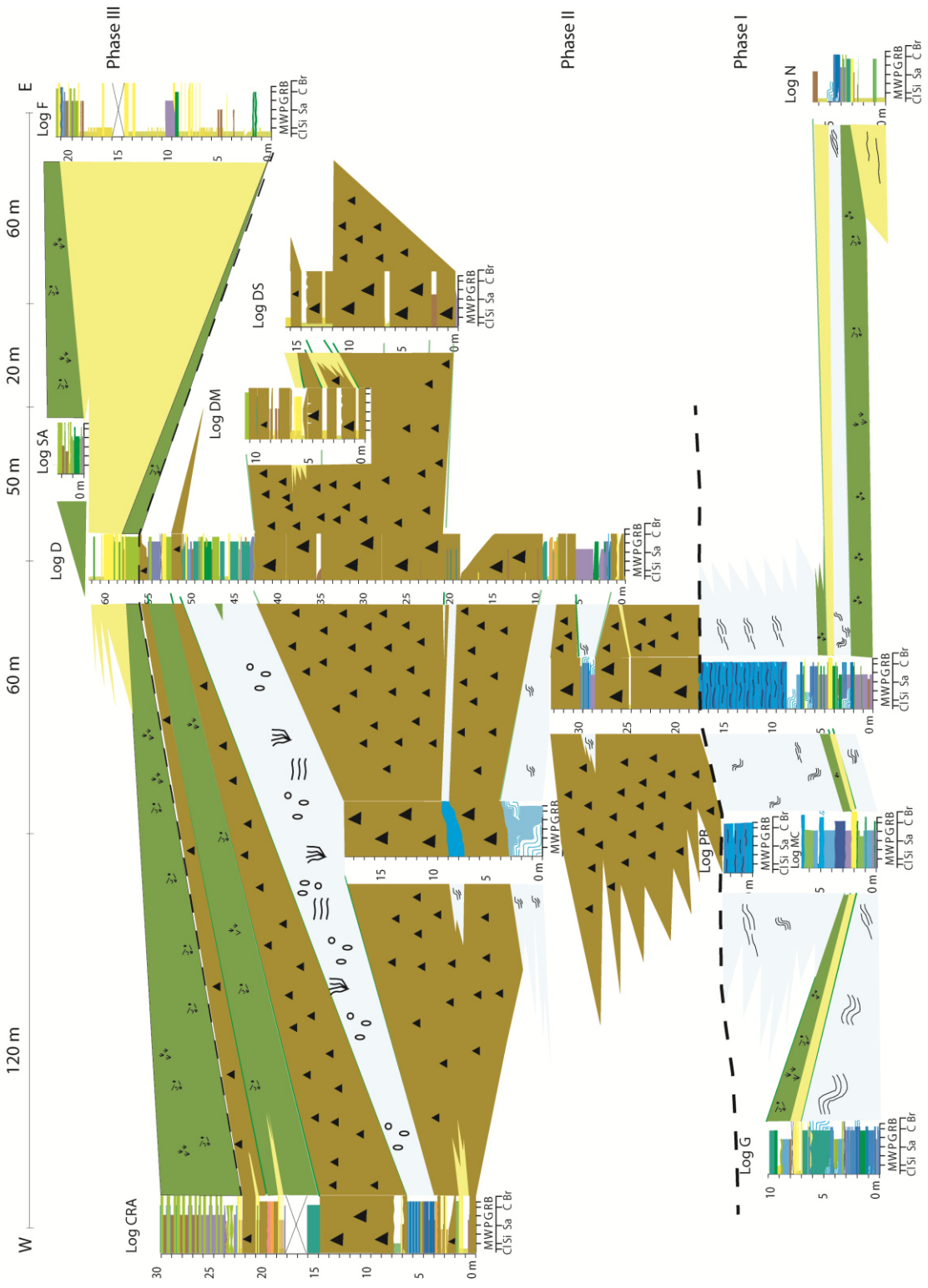

Figure 3.16. Correlation diagram of the measured stratigraphic logs showing the vertical and lateral distribution of the four distinguished lithofacies associations during the three phases of stratigraphic evolution. Legend in Fig. 3.17.

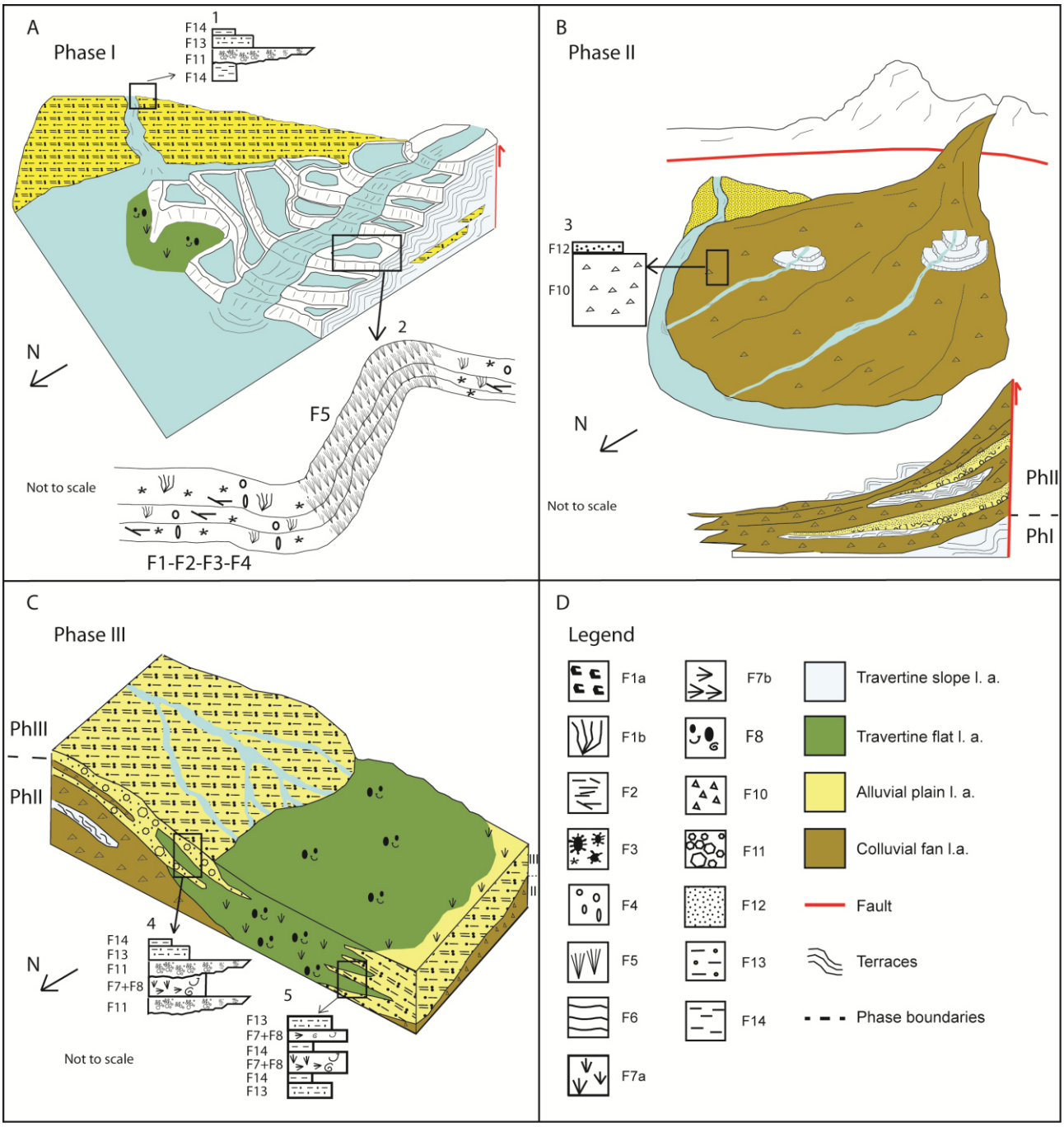

Figure 3.17. A) A possible paleoenvironmental reconstruction of Phase I, representing a travertine slope system evolving distally into a travertine flat, ultimately obstructing the deposition of the adjacent alluvial plain environment. 1) Alluvial plain consists of 1–2-m-thick strata of claystone (facies F14) with decimetre-thick channelized conglomerate (facies F11) and sandstone (facies F13). 2) Travertine terraces consist of sub-horizontal pools (facies F1–F4), pool rims and walls (facies F5). B) Interpretative model of Phase II with colluvial fan debris flow-dominated facies association overlain by travertine slope wedges. Laterally, towards the East, the alluvial plain environment overlies the travertine and colluvial fan lithofacies 3) Breccia (facies F10) with a thickness of several metres and massive sandstone deposits (facies F12) with thickness ranging from centimetres to decimetres form the colluvial fan. C) A possible paleoenvironmental reconstruction of Phase III in which the travertine system evolved into a travertine flat characterized by freshwater marshy environments. 4) In the eastern part, Phase III consists of claystone terrigenous deposits, lenses of conglomerates (facies F11) and travertine marshes. Towards the NW, the travertine flat deposits interfinger with alluvial plain laminated sandstones to siltstones and claystones (facies F13 and F14). D) Legend for Fig. 3.17 and 3.18 facies and lithofacies association

3.6. Discussion: Factors controlling the Messinian mixed travertine–terrigenous succession

The evolution of a sedimentary basin depends on extrinsic and intrinsic controlling factors that determine the deposition of different lithofacies types and their stratigraphic architecture. The studied Messinian fault-controlled basin contains vertical superposition and lateral transition between thermogene travertines and terrigenous deposits influenced by hydrothermal activity, tectonics and climate.

The lateral distribution of travertine facies in a thermogene system depends on the rates of water discharge out of the vent and the distance from the hydrothermal vent, due to the decrease in water temperature and the mixing with meteoric water away from the vent (Pentecost, 2005). This is reflected in travertine lithofacies associations that change from a proximal slope to a distal marsh flat, as described by Guo and Riding (1998) and Guido and Campbell (2011). In the Marsiliana succession, thermogene travertines are localized in the southern and older (lower) parts of the studied area, especially during Phase I when a travertine slope system evolved laterally into distal flat lithofacies. In the younger (upper) part, the influence of both thermal and meteoric water is recorded; during Phase III, travertines accumulated in the form of flat lithofacies association.

The deposition of travertines and geothermal systems are a common feature in Southern Tuscany during the Neogene–Holocene due to magmatism (Serri, 1997) and extensional tectonics (Patacca et al., 1990) that facilitated thermal activity and the influx of mantle CO_2 since the Tortonian Age (Minissale, 1991). As reported by Minissale (2004), a geothermal field in Central Italy led to the hydrolysis of carbonates and further generation of CO_2 via metamorphic decarbonation reactions of the buried Mesozoic marine limestone successions. CO_2 must have dissolved the evaporite and carbonate rocks of the Anidrite di Burano/Calcare Cavernoso Formation, producing Ca_2^+ and HCO_3^- ions that saturated the groundwater under the Albegna Basin. According to Forti et al. (1990), Doveri and Mussi (2014) and Guastaldi et al. (2014), the Mesozoic carbonate formations constitute an important regional aquifer in Southern Tuscany that feeds the active hydrothermal springs in present day (Minissale et al., 2002b). In addition to the Marsiliana travertines, other Miocene thermogene deposits have been identified in the adjacent Ombrone Basin (Bossio et al., 2003–2004) and in the Volterra Basin, close to Pignano (Gandin et al., 2002; Capezzuoli et al., 2004, 2009).

Active tectonics is another important factor that controls sedimentation in continental settings, creating accommodation space for sediment accumulation through fault-controlled subsidence. The association between travertines and active tectonics is evident in rift and pull-apart basins, as documented in several studies, for instance, by Altunel and Hancock (1993), Hernandez-Diaz and Hernandez-Enrile (2001), Özkul et al. (2002), Sant'Anna et al. (2004), Zentmyer et al. (2008), Guido and Campbell (2011), Nishikawa et al. (2012) and Henchiri (2014). The presence of normal and oblique faults provides paths for groundwater flow, rock fracturing and permeability increase (Sibson, 1996). In association with a geothermal field and a carbonate aquifer, these features permit the generation of thermogene travertine systems that can aggrade or prograde based on the interplay between travertine precipitation rates (function of thermal water discharge) and fault-induced

subsidence. Bettelli et al. (1992) and Pertusati et al. (2004) recognized normal faults, running in the E–W direction, located to the south of the Marsiliana travertine deposits (Fig. 2.3). The orientation of the faults (Fig. 2.3) and of the travertine slope environment of phases I and II that pinch out northwards (Figs. 3.10, 3.11 and 3.17a,b) indicates that the hydrothermal vents must have been located to the south of the studied quarry, close to the faults. These faults must have linked the surface with the aquifer that accommodated the hydrothermal groundwater. In addition, tectonic activity and fault-block uplift might have favoured the formation of gravity-flow fans, as reported in several studies (Heward, 1978; Blair, 1987; Neves et al., 2005; Leeder, 2009).

Climate is a fundamental controlling factor of basin hydrology with a consequent effect on spring-related travertines. Travertines precipitate in almost all climatic belts, but mostly in humid and warm climates, where high atmospheric precipitation rates recharge the groundwater circulation (Viles and Pentecost, 2007), although intensive rainfalls induce water dilution of calcium carbonate ions (Pentecost, 2005; Jones and Renaut, 2010). In arid climates, despite the reduced recharge of the aquifers, travertine precipitation may be favoured by higher evaporation rates and warmer waters (Guodie et al., 1993; Ford and Pedley, 1996; Evans, 1999; Jones and Renaut, 2010). At temperate latitudes such as Central Italy, alternating phases of thermogene travertine accretion/erosion have been linked to Pleistocene palaeoclimatic oscillations (Faccenna et al., 2008; De Filippis et al., 2013). Palynological data collected on Messinian deposits in the Piedmont and Emilia-Romagna regions (Bertini, 2006; Bertini and Martinetto, 2011) and in the Po valley (Fauquette et al., 2006) in Northern Italy reveal that palaeoclimatic conditions were warm and humid in these zones during the late Messinian, with precipitation ranging from 400 up to 1600 mm/year (Fauquette et al., 2006). Moreover, Fauquette et al. (2014) confirmed that vegetation in the Northern Apennines during the late Neogene and the early Pleistocene was similar to that observed in present-day subtropical South-East China, with travertine deposits of Tengchong occurring in the Yunnan province (Jones and Peng, 2012). This suggests that a hypothetical humid climate might have favoured the development of the late Messinian Marsiliana hydrothermal system and travertine deposition.

The three distinguished phases in the Marsiliana succession mark the evolution of a mixed travertine–terrigenous system controlled by tectonic activity and climate. The tectonics created accommodation space; linked the groundwater pathways with a geothermal heating source through faults; and triggered fault-block uplift, erosion and deposition of the colluvial fans. The climate controlled the basin hydrology, groundwater recharge and possibly the rates of travertine deposition.

3.7. Conclusions

The mixed Messinian terrigenous–carbonate succession, well exposed within an active quarry near the village of Marsiliana (Albegna Basin, Southern Tuscany, Central Italy), exhibits a wedge-shaped geometry thinning in the N–NW direction, which accumulated in an extensional basin controlled by faults located to the South. The stratigraphic evolution of the basin consists of three phases, distinguished based on the spatial and temporal distribution and depositional architecture of four lithofacies associations. Nine thermogene travertine lithofacies (F1–F9) compose the 1) terraced and smooth slopes and 2) travertine flat lithofacies associations. The terrigenous lithofacies associations consist of five lithofacies (F10–F14) and include the 3) alluvial plain and 4) colluvial fans depositional environments.

Phase I was characterized by the interplay between the travertine slope (facies F1–F7) thinning in the N–NW direction and the alluvial plain environment extending from the East towards the North and West. During Phase II, the accommodation space was filled by colluvial fans formed by stacked debris-flow breccias, reaching a thickness of nearly 30 m (facies F10 and F12), separated by events of metre-scale travertine precipitation. Phase III recorded a change in deposition with the accumulation of alluvial plain lithofacies including claystone, siltstone, sandstone and conglomerates (F11–14). During Phase III, the travertine lithofacies were indicative of shallow ponds and marsh environments with carbonate-coated reeds (F7–F9), with thermal water possibly mixing with meteoric groundwater, as confirmed by the decrease in carbon stable isotope data.

The evolution of the studied succession was influenced by external factors such as tectonics and climate. Active faulting controlled the creation of accommodation space for travertine and terrigenous sediment accumulation as well as the pathways of groundwater hydrothermal circulation to superficial vents; through fault-block uplift, it also promoted the sources of detrital sediment that fed the colluvial fan breccias. Climate might have played a role in the recharge of the aquifer, thermal water discharge at the vents and consequently the precipitation rate of the travertine.

The continental mixed carbonate–terrigenous depositional system of Marsiliana represents a succession in an extensional basin at scale of tens of metres, providing valuable information about the interplay between thermogene travertine and alluvial/colluvial depositional environments and the controlling factors of lithofacies architecture through space and time. The depositional interpretations presented in detail might provide further insight into similar fault-controlled continental depositional systems.

Table 1. Description and interpretation of travertine facies recognized in the studied succession.

Facies name and texture	Components	Bedding Thickness and Geometry	Diagenetic Features	Porosity type and %	Associated Facies	Depositional Environment	Distribution
F1a,b Clotted peloidal micrite and microsparite boundstone to grainstone	clotted peloidal micrite/10–20 µm/sub-rounded; aggregates of clotted peloidal micrite/200–300 µm/irregular; micritic dendrites up to 3 cm thick; microsparite crystals/ equant/10–20 µm; ostracodes, gastropods	undulated sub-horizontal convex shaped 0.5–10 cm	dissolution; cements: pendant (10 µm); scalenohedral (1 mm); equant (300 µm)	interparticle (100–500 µm) vuggy (100–500 µm) fenestral (0.5–1 cm) 2-5%	F1a: F2, F3, F4, F7a,b,c, F8, F9. F1b. F2, F3, F4, F7a,b	terraces and shallow pools of terraced slope system; ponds	Phase I: common Phase II: common Phase III: common
F2 Raft floatstone/rudstone	raft fragments (clotted peloidal micrite and microsparite)/200 µm thick, from mm to 5 cm in length reed moulds, gastropods, ostracodes, faecal pellets	undulated sub-horizontal 0.5–2 cm concave lenses 5–6 cm wide 2–6 cm thick	dissolution; cements: scalenohedral(600 µm); equant (300 µm)	interparticle elongated (mm up to 1 cm wide); vuggy (0.2–2 cm) 5-15%	F1a, b, F3, F4, F7b	pools of terraced slope system	Phase I: common Phase II: sparse Phase III: rare
F3 Sub-rounded radial coated grain grainstone/packstone	coated grains consist of: 1) nucleus = micrite and microsparite, faecal pellets, skeletal fragments/50–200 µm 2) radial coating = turbid calcite crystals/200–700 µm/lozenge forming spherulites microsparite/10–30 µm/equant, raft fragments	concave lenses 15–20 cm wide and 5–6 cm thick undulated sub-horizontal 1 cm	dissolution; cements: scalenohedral (200–250 µm); equant (20–30 µm)	interparticle (100–200 µm) vuggy (2 mm) 0-5%	F1a,b, F2, F4, F7b	pools of terraced slope system	Phase I: sparse Phase II: very rare Phase III: very rare
F4 Coated gas bubble boundstone	micrite/structureless aggregates of clotted peloidal micrite/50–100 µm/sub-rounded, dendrites, undulated films raft fragments	undulated sub-horizontal 3–20 cm	cements: scalenohedral (500–600 µm)	intra-bubble (from 100 µm up to 2 cm in diameter; 4 cm in length when elongated; vuggy (0.5–2 mm), 15–25 %	F2, F6, F7b	pools of terraced slope system channels	Phase I: common Phase II: common Phase III: no
F5 Crystalline dendrite cementstone	turbid calcite crystals/100–200 µm/elongate lozenge; aggregate of calcite crystals/500 µm–-5 cm/fan with axial divergences of 10–30°; microsparite/10–-20 µm	undulated inclined convex shaped geometries 2–15 cm	cements: microsparite/10–20 µm; replacive equant sparite	vuggy (up to 2 mm) 0–5%	F1a, F4, F6	smooth slope terraces (rim, wall)	Phase I: common Phase II: sparse Phase III: no
F6 Laminated boundstone	laminae (clotted peloidal micrite and microsparite)/50–200 µm thick/loosely to densely packed	undulated sub-horizontal horizontally wavy laminated 2–10 cm	cements: scalenohedral (300–500 µm); equant (300 µm)	inter-laminae (up to 5 cm) 0–2 % densely packed; 5–10 % loosely packed	F5, F7a,b	terraced slope system pools	Phase I: sparse Phase II: rare Phase III: no
F7a Coated reed boundstone F7b Phytoclastic rudstone/packstone	reed moulds/from mm to cm/from rounded to elongate; phytoclastic remains/30–50 µm thick, mm long/blade undulated faecal pellets, ostracodes, gastropods	undulated sub-horizontal 5–20 cm	dissolution cements: scalenohedral prismatic (200–800 µm); equant calcite (300 µm)	mouldic (up to 1 cm diameter; up to 15 cm in length); fenestral (5–7 cm) 10–20%	F7a: F1a,b, F7b, F8, F9, F10, F7b: F1a,b, F2, F3, F4	edge pools of terrace systems edge of ponds	Phase I: sparse Phase II: common Phase III: common
F8 Skeletal peloidal packstone/grainstone to floatstone/rudstone	faecal pellets/100-500 µm/rounded aggregates of clotted peloidal micrite/200–300 µm ostracodes/200 µm, gastropods/200µm–2cm phytoclastic remains, raft fragments.	undulated sub-horizontal 5–10 cm	dissolution cements: scalenohedral prismatic (300 µm) pendant (10–20 µm);	interparticle (200–500 µm); fenestral (up to 4 cm); intraparticle(0.5–1 mm)	F1a, F7a, b, F9	ponds	Phase I: very rare Phase II: very rare Phase III: common

			equant (100–250 µm)	5-10%			
F9 Calci-mudstone to microsparstone	clotted peloidal micrite/10–20 µm/sub-rounded ; aggregates of clotted peloidal micrite/200–300 µm/irregular to dendrite; microsparite crystals/rhombic/10–20 µm; micrite/structureless	sub-horizontal 2–10 cm	dissolution cements: equant calcite (300 µm)	vuggy, channel (0.5–2 mm) 0-2%	F1a, F2, F4, ponds F7a, b, F8		Phase I: very rare Phase II: sparse Phase III: sparse

Table 2. Description and interpretation of terrigenous facies recognized in the studied succession.

Facies name	**Bedding and structures**	**Facies thickness**	**Texture and Grain size**	**Composition**	**Sorting**	**Roundness sphericity**	**Porosity %**	**Depositional environment**	**Associated facies**
F10 Breccia	crudely bedded massive	min: 1 m max: 12 m	breccia matrix- to grain supported from mm to boulders (80 cm)	recrystallized calci-mudstone/microsparstone clasts 40–70% grey limestone clasts 10–20% fine-grained sandstone, siltstone and claystone lithic fragments 0–2% travertine intraclasts 0–2% micritic/microsparitic matrix 20–30%	very poor	angular/low sphericity	0%	colluvial fan debris flow	F12
F11 Conglomerate	horizontal bedding imbrication fining upward sequences	min: 5 cm max: 20 cm	conglomerate grain supported close framework granules and pebbles (mm to 20 cm)	recrystallized calci-mudstone/microsparstone clasts 30–70% grey limestone clasts 0–5% micritic microsparitic and clotted peloidal micrite matrix 10–20%	poor	sub-rounded/low sphericity	0–2%	channel bed lake delta	F13, F14
F12 Massive sandstone	massive weak lamination	min: 5 cm max: 20 cm	sandstone medium to coarse sand (0.25-1 mm)	detrital quartz 10–30% recrystallized calci-mudstone/microsparstone clasts 30–50% siltstone and claystone lithic fragments 10–-20% micas <2%	well	angular/low sphericity	0–2%	gravity flow sedimentary sheet flood lake delta	F10, F11, F13, F14
F13 Laminated sandstone to siltstone	cross-lamination	min: 5 cm max: 80 cm	sandstone/siltstone fine sand to siltstone (0.64-250 µm)	detrital quartz 10–30% recrystallized calci-mudstone/microsparstone clasts 30–50% siltstone and claystone lithic fragments 10–20% mica <2%	well	angular/low sphericity	0–2%	abandoned channel lower flow regime	F11, F14
F14 Claystone	massive horizontal laminated	min: 5 cm max: 170 cm	clay (< 0.64 µm)		well		0%	overbank of a flood plain drape deposits freshwater ponds	F11, F12, F13, F14

Chapter IV

Diagenesis and stable isotope signature of Messinian travertine deposits (Albegna Basin, Southern Tuscany, Central Italy).

Abstract

Travertine deposits cropping out near the village of Marsiliana, Albegna Basin (Central Italy) belong to a Messinian mixed siliciclastic-carbonate continental extensional basin, in which thermogene and meteogene travertine accumulation interplays with alluvial plain and alluvial debris flow deposits. On the basis of spatial distribution of lithofacies associations the stratigraphic succession was subdivided in three phases of sedimentary basin evolution. During Phase I travertines developed a terraced slope environment with an apron geometry prograding northward and interfingered with an alluvial plain environment towards the East. The travertine stable carbon isotope signature varies between -0.53 and 3.88 ‰ V-PDB (mean value 1.46 ‰) and indicates that groundwater was fed by geothermally generated CO_2. The influence of geothermal activity heating groundwater is confirmed by the light $\delta^{18}O$ that recorded a mean value of -7.50 ‰ V-PDB. Phase II is marked by the accumulation of tens of metres thick alluvial fan breccias that thinned northward and westward. Within these breccia deposits, 2-3 m thick travertine lenses are intercalated. Phase II travertines show the vertical transition from hydrothermal terraced slope environment to mixed freshwater facies of a travertine flat lithofacies association. Despite the vertical change of travertine lithofacies, the stable isotope signatures show that travertine precipitated from water similar to those of the Phase I, warm and with CO_2 generated at depth. $\delta^{13}C$ varies between 0.2 and 2.58 ‰, while $\delta^{18}O$ varies between -10.48 and -6.76 ‰. Phase III includes the alternation of travertine flat and alluvial plain lithofacies associations. This phase is characterized by lighter stable carbon isotope data with a mean value of -0.36 ‰ suggesting a meteoric CO_2 derived from soil. Instead $\delta^{18}O$ records values between -8.73 and -4.14 ‰ indicative of cooling of the travertine precipitating water due to mixing of thermal water with meteoric freshwater. The whole travertine deposits are characterized by the occurrence of microsparite and sparite crystals originate from recrystallization of precipitated micrite deposits. Prismatic and blocky cements formed during hidrothermal and phreatic diagenesis fill the primary porosity. Locally these cements show red and

orange luminescences. Often within the pores vadose sediment occurs, both before, after or interlayered with the calcite cements. These Messinian travertines were also affected by burial diagenesis that is recorded by the presence of stylolites, sutured contacts and rims of sparite that are luminescent. The Marsiliana travertine succession permits the identification of burial diagenetic features in this type of rocks, resulting useful for a comparison to buried analogues of petroleum systems.

4.1 Introduction

Diagenesis refers to any alteration of a rock after deposition. This may be broken into four possible stages: pre-burial, early-burial, late-burial, and uplift. In the case of travertines, which are typically geologically young deposits, meteoric diagenesis is a key component within the first two stages of alteration. This takes place near the surface at low pressures and temperatures, contrary to deeper burial diagenesis which occurs at higher pressures and temperatures. “The process does not result in significant compaction or dolomitization, but cementation, sparmicritization, neomorphism and dissolution have been widely documented” (Pentecost, 2005,). As discussed earlier in this thesis, meteoric water can either promote the generation of travertine or cause dissolution and erosion. As water percolates into a deposit, it may continue to add minerals to it and continue to generate travertine. This would alter the primary fabric as a secondary fabric develops, or it may dissolve the primary fabric and leave pore space. Post-depositional infestation by microbes may also play a role (Guo and Riding, 1994).

Sparmicritization is a process where biota etch sparry carbonate rocks and leave voids that fill with micrite. The micrite often remains as a stable residue after the original crystals are gone (Bathurst, 1975).

Dissolution occurs when the water surrounding a travertine deposit is undersaturated with respect to calcite and dissolves the carbonate. This process occurs frequently from exposure to direct rainfall. Dissolution can create ragged surfaces on initial spar crystal outlines (Guo and riding, 1994). Neomorphis is a process where unstable carbonate crystals go into solution and precipitate in more stable forms. Aragonite, which is an unstable mineral at normal surface pressures and temperature, will go into solution and the reactants can precipitate as calcite.

4.2 Geological setting of Messinian travertines in the Albegna Basin

This study focuses on upper Messinian travertine deposits (cf. Bosi et al., 1996; Croci et al., 2016), cropping out in an active and in an abandoned quarry close to the Marsiliana village, south-westward area of the Neogene Albegna Basin (Fig. 2.1) (Southern Tuscany, Central Italy). A detailed description of the geological setting of the area under study is reported in Chapter 2. The detailed description of the travertine fabric types, geometry of the depositional system and lithofacies architecture are reported in Chapter 3.

4.3 Methods

A total of 98 thin sections were examined by plane-polarized and cross-polarized microscopy. Cathodoluminescence was performed on 20 thin-sections with a luminoscope CITL Cambridge Image Technology Limited, Cambridge, UK (model MK 5-2 operating system at 10–14 kV with a beam current between 300–600 mA, and vacuum gauge 50–70 mTorr) at the Earth Sciences Department, Milan University. Scanning electron microscope (SEM) analyses were performed on 8 polished slabs and freshly broken surfaces, gold coated, and 2 thin sections, graphite coated, with a Cambridge Stereoscan 360, operating at 20 kV with working distance of 15 mm at the Earth Sciences Department, Milan University. XRD analyses of 4 powdered mineral samples were carried out with an X-ray powder diffractometer (Philips X'Pert MPD) with a high temperature chamber at the Earth Science Department, Milan University. Chemical analyses of minerals were carried out using the JEOL JXA-8200 WD/ED combined microanalyzer, microprobe at the Earth Science Department, University of Milan.

Stable carbon and oxygen isotopes were measured in 60 calcite samples, from different facies types, outcrops, stratigraphic levels, paying attention to the colour that characterizes the travertines. Carbonate powder samples were measured for 49 travertine precipitated fabrics (Table 4.3) described in detail in Chapter 3 and Croci et al. (2016), and 11 cement samples (Table 4.4). The samples belonging to the stratigraphic log CE were collected in the abandoned quarry (Fig. 3.3), located to the North with respect to the active quarry where most of the samples were collected. Carbonate powders were extracted with a dental microdrill without mixing the carbonate components. Stable isotope analyses were conducted using a MAT253 mass spectrometer with an automated carbonate preparation device (gas bench II) at the University of Bochum, Institute for Geology, Mineralogy and Geophysics stable isotope facility. Stable isotope results were calibrated to the V-PDB scale by the international standards CO-1 and CO-8. The analytical precision is better than 0.07‰ for $\delta^{13}C$ and 0.13‰ for $\delta^{18}O$.

4.4 Results

4.4.1 Petrographic characterization of primary travertine precipitated fabrics

All of the carbonate precipitates analyzed in the course of this investigation is composed of low-magnesian calcite. The calcite displays a wide range of textures, from microporous micrite to laminated crusts of spar. The calcite comprising the travertines investigated can be divided into: 1) the original micrite to sparite hydrothermal precipitates, 2) micrite geopetal infill, 3) recrystallized microsparite to sparite, 4) millimetre thick laminated crust of bladed to columnar sparite, and 5) bladed and equant calcite cement precipitated in primary pore space sustained by the travertine precipitated fabrics (Table 4.1).

The most common original precipitated travertine lithofacies in the upper Messinian Albegna Basin travertines form as boundstone or grainstone of clotted peloidal micrite, micrite to microsparite and equant calcite (p1, Fig. 4.1 A-H). This calcite type precipitates on any substrate available to the flowing waters, such as phytoclastic remains gas bubbles or calcite raft, developing also a few microns thick coating around grains. The initial calcite is generally cloudy due to the presence of organic matter. Clotted peloidal micrite can form dendrites a few millimetres to centimetres thick. Micrite can be deposited also as faecal pellets, forming peloidal packstone to grainstone. Microsparite is grey in colour, fills the spaces between micrite, and reached dimension up to 20 µm in size. The microporosity that occurs is < 1µm in size. Clotted peloidal micrite occurs in clotted peloidal micrite and microsparite boundstone to grainstone (facies F1), raft floatstone/rudstone (Facies F2), coated gas bubble boundstone (facies F4), laminated boundstone (facies F6), coated reed boundstone and phytoclastic rudstone/packstone (facies F7) and in calci-mudstone to microspartstone (facies F9). Microsparite occurs in clotted peloidal micrite and microsparite boundstone to grainstone (facies F1), raft floatstone/rudstone (facies F2), in the nucleus of sub-rounded radial coated grains grainstone to packsone (facies F3), laminated boundstone (facies F6) and calci-mudstone to microsparstone (facies F9). Micrite occurs aggregated as faecal pellets in the skeletal peloidal pckstone/grainstone to floatstone/rudstone (facies F8).

Dendrite sparite crystals (ds, Fig. 4.2 A-H) are the other primary travertine product of the studied travertines. This sparite develops crystalline cemenstone crusts or coatings around nuclei of micrite and microsparite, or around skeletal remains. These crystals, in crystalline cementstone fabric (facies F5), form three-dimensional V-shaped fabrics with multiple levels of branching originated from a central point. Crystal branches form sheets that are imbricated over each other reaching millimetres size in length. Crystals have a trigonal transverse cross section with edges that are sharp or curved. The surface shows scattered sub-rounded to elongated pores with dimensions that range from <1 µm up to 5 µm. Dendrite sparite crystals characterize the coatings of sub-rounded radial coated grain grainstone packstone (facies F3) and the precipitates of crystalline dendrite cementstones (facies F5).

4.4.2 Petrographic characterization of secondary precipitates: cements, detrital micrite and speleothemes

Another common calcite precipitate includes all the microsparite to sparite that are products of the diagenesis. The fabrics of these calcites are bladed to equant, with dimension up to 1 mm.

Bladed calcite (b, Fig.4.3 A-B) includes non isopachous layers of fine bladed sparite, growing syntaxially with the same extinction patterns as the primarytravertine deposits, and oriented perpendicularly to the substrate upon which they have grown. The top of these calcite crystals can be eroded and covered by Fe-Mn hydroxides. This cement is rare and grows mostly in the travertines of the Phase 1, but it rarely occurs in the other phases too.

Microsparite to sparite (m1) includes those crystals that cement the initial precipitates, with crystal size between 5 and 30 µm. This calcite is limpid and non-luminescent.

Microsparite to sparite (m2, Fig. 4.3 C) includes white to cloudy crystals that replace the primary precipitates, such as dendritic crystals. The size of this calcite reaches 200 µm forming columnar crystals that can grow up to 1 mm in length. This calcite presents bright luminescence.

A geopetal sediment deposit (mi, Fig. 4.3 D) consists of a grey to brown detrital micrite to microsparite that is deposited at the base of skeletal or reed moulds and it is interpreted as internal sediment infill, resulting from the erosion of the primary travertine deposits.

Equant sparite (s, Fig. 4.3 D) is a quite common calcite cement of the studied travertines and it is found in all of the 3 phases, precipitating often as the first cement. This cement grows both in interparticles, intraparticle and mouldic pores. The colour of this calcite varies between white to grey, with crystals 50-70 µm in size. The geometry can vary showing a rombohedral eqaunt morpohology or elongated crystals forming blades with scalenohedral termination.

Speleothem (sp, Fig, 4.3 E-F) consists of 500 µm thick blade dendrite to columnar spar. This spar forms crusts composed of millimetre-thick laminated fan speleothem-like deposits very similar to the cave flowstone (Frisia et al., 2000). The lamination is due to the different composition of the precipitate, showing laminae of white sparite, brown microsparite and black cloudy micrite. This calcite is non-luminescent.

Scalenohedral calcite (sh, Fig. 4.3 G-H, Fig. 4.4 C-D) consists of white to grey pore fill cement, both in interparticle, intraparticle and mouldic pores. The deposits are most commonly composed of layers of medium to coarse crystalline blades that reach 800 µm in thickness. The individual crystals are oriented perpendicularly to the substrate on which this spar grows, developing inwards from the margin of the pores. The top of this spar shows gothic arc terminations that can be eroded and/or covered by Fe-Mn oxides and hydroxides, or clay. This cement can grow both as first cement or follow the equant sparite (s).

Blocky calcite (bl, Fig. 4.3 G-H, Fig. 4.4 A-B, E-F) is a clear sparite, commonly coarse with a size that can reach 1 mm forming a mosaic that occludes pores and fractures. This cement sometimes develops a drusy mosaic fabric. This cement can grow directly attached to the travertine deposit, resulting lateral to the scalenohedral cement (sh), or can follow the previous cements such as the sparite cement (s) or the scalenohedral.

Table 4.1. Petrographic characteristics of mineral phases from the Late Messinian Albegna Basin travertines of this study with an indication of the figure numbers.

Mineral phase	**Petrographic character**	**Crystal morphology**	**Crystal size**	**Cathodoluminescence**	**Figures**
Peloidal micrite + microsparite (p1)	Gray to black clotted fabrics of micritic polids and microsparite. This calcite is characterized by widespread micro-porosity.	anhedral	1-20 µm	Non-luminescent to dull luminescent	4.3
Dendritic sparite crystals (ds)	Dark dendritic calcite crystals originating from a central point and grow imbricated over each other. Wide micro-porosity occurs on the crystal surface.	Euhedral, bladed with a trigonal transverse cross section with sharp or rounded sides.	Up to 50 µm long	Non-luminescent	4.4
Bladed calcite (b)	White to gray coating, as growth cement in pores, growing syntaxially with same extinction patterns as the p1 peloidal micrite microsparite. The top of this cement could be corroded and covered by (Fe-Mn)OH and clay	Coarse to fine elongated euhedral crystals	20-70 µm	Non-luminescent	4.5 A-B 4.7 A-B
Microsparite to sparite (m1)	White crystalline	Rhombic crystals Subhedral, ehuedral	5-30 µm	Non-luminescent	
Microsparite to sparite (m2)	White to cloudy crystalline neomorphic aggregates of microsparite to sparite. Replacement of crystalline dendrites	Rhombic to coarse columnar crystals Subhedral, ehuedral	5-200 µm	Bright Luminescent	
Detrital micrite (mi)	Brown gray detrital micrite and microsparite as geopetal sediment	anhedral	1-15 µm	Non-lumincescent	CT 0.8

	filling				
Sparite (s)	White to gray granular, pore fill, growth as cement in pores.	Rhombic crystals to dog-tooth to blade Subhedral, ehuedral	50-70 µm	Non-luminescent with a yellow rim	
Speleothem (sp)	White, brown and gray crystals forming fan around a micrtic nucleus. The crystals are characterized by perpendicular undulated, 30µm to 100 µm thick bands. The colour of the bands varies according to the grains size: peloidal micrite (black), microsparite (brown), sparite (white)	Bladed to columnar	2 mm	Non-luminescent	MC 5.55 Cra 6.30?
Scalenohedral calcite (sh)	White to gray, pores fill cement, mainly intra mouldic pores where it develops isopacous fringes. The top of this cement could be corroded and covered by (Fe-Mn)OH, or clay	Prismatic crystals with sharp or curved gothic arc terminations	50-800 µm	2 types 1) Non-luminescent characterized by frequent dull luminescent yellow fringes (mc 2.25) (sh1), often followed by sh2 2) Yellow luminescent characterized by dull luminescent patches (pb 68) (sh2).	MC 2.68 MC 5.4
Blocky calcite (bl)	White clear. As cement filling fractures and pore cavities. Intra-mouldic cement. The top of this cement could be corroded and covered by (Fe-Mn)OH, or clay	Rhombic crystals. Euhedral. Sharp or curved edges, the mosaic equant fabric is very abundant, rarely it is drusy.	50 µm-1 mm	5 different types under cathodoluminescence. 1) Non-luminescent with 1-2 dull luminescent yellow fringes (bl1)(CS2), often followed by 2) Yellow luminescent characterized by dull to non-luminescent patches (bl2) (mc 1.5). Could be the first cement. 3) Non-luminescent (bl3) (mc 1.5). It follows (bl2). 4) Yellow luminescent	MC 2.0

				(bl4). It forms a thin rim enriched in Mn^{2+}. It follows bl3. 5) Non-luminescent with dull yellow luminescent patches or rims (bl5) (mc 1.5)	

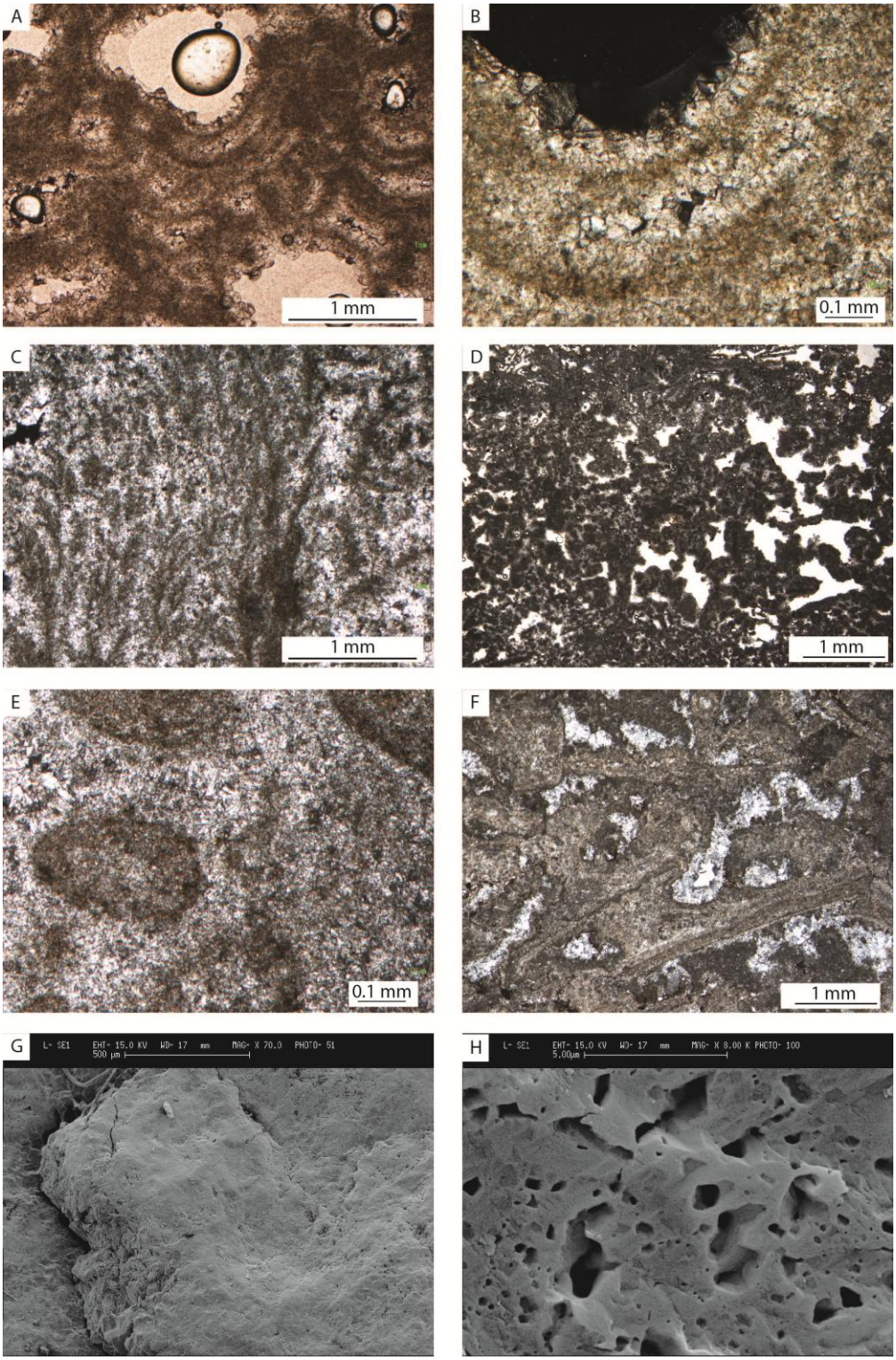

Figure 4.1. Photomicrographs and SEM images of clotted peloidal micrite to microsparite (p1). A) Clotted peloidal micrite to microsparite develops coatings around sub-rounded pores. B) Between micrite coatings equant sparite precipitates. Scalenohedral cement precipitates within the pore. C) Crossed polarized light image showing micritic dendrites embedded in microsparite and sparite. D) Boundstone of cloudy clotted peloidal micrite that develops clots up to 500 µm in size. E) Faecal pellets of micrite and microsparite embedded in a microsparite to sparite cement. F) Phytoclastic remains are coated by microsparite coatings. These coatings show micrite cloudy boundaries. Within secondary pores white clear sparite precipitate filling them. G) SEM image showing clotted peloidal micrite. F) The micrite is characterized by microporosity.

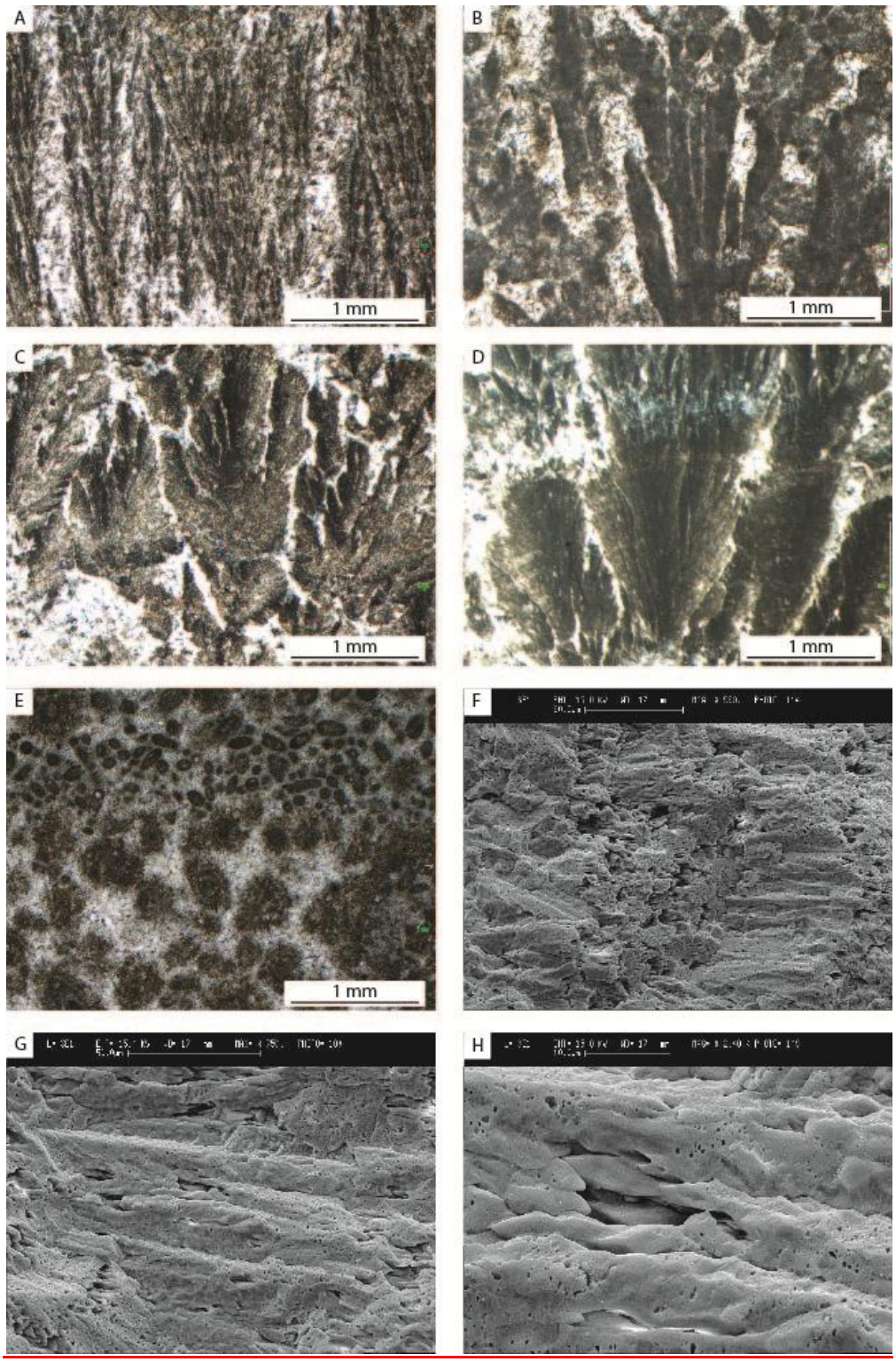

Figure 4.2. Photomicrographs and SEM images of crystalline dendrite (ds). A) Crossed polarized light image of dendrites showing the lozenge shaped turbid crystals and clear microsparite to sparite between them. B) Other type of crystalline dendrite spar characterized by wide cloudy crystals. C-D) Crystalline dendrites develop fans that can show different shape. Crystalline dendrites fans underwent dissolution that appears principally on the edge of the crystals. E) Crystalline dendrites can grow around faecal pellets developing coatings. F) SEM image showing the upper part of the dendrites characterized by a trigonal shape. G-H) Crystalline dendrites shows a wide microporosity

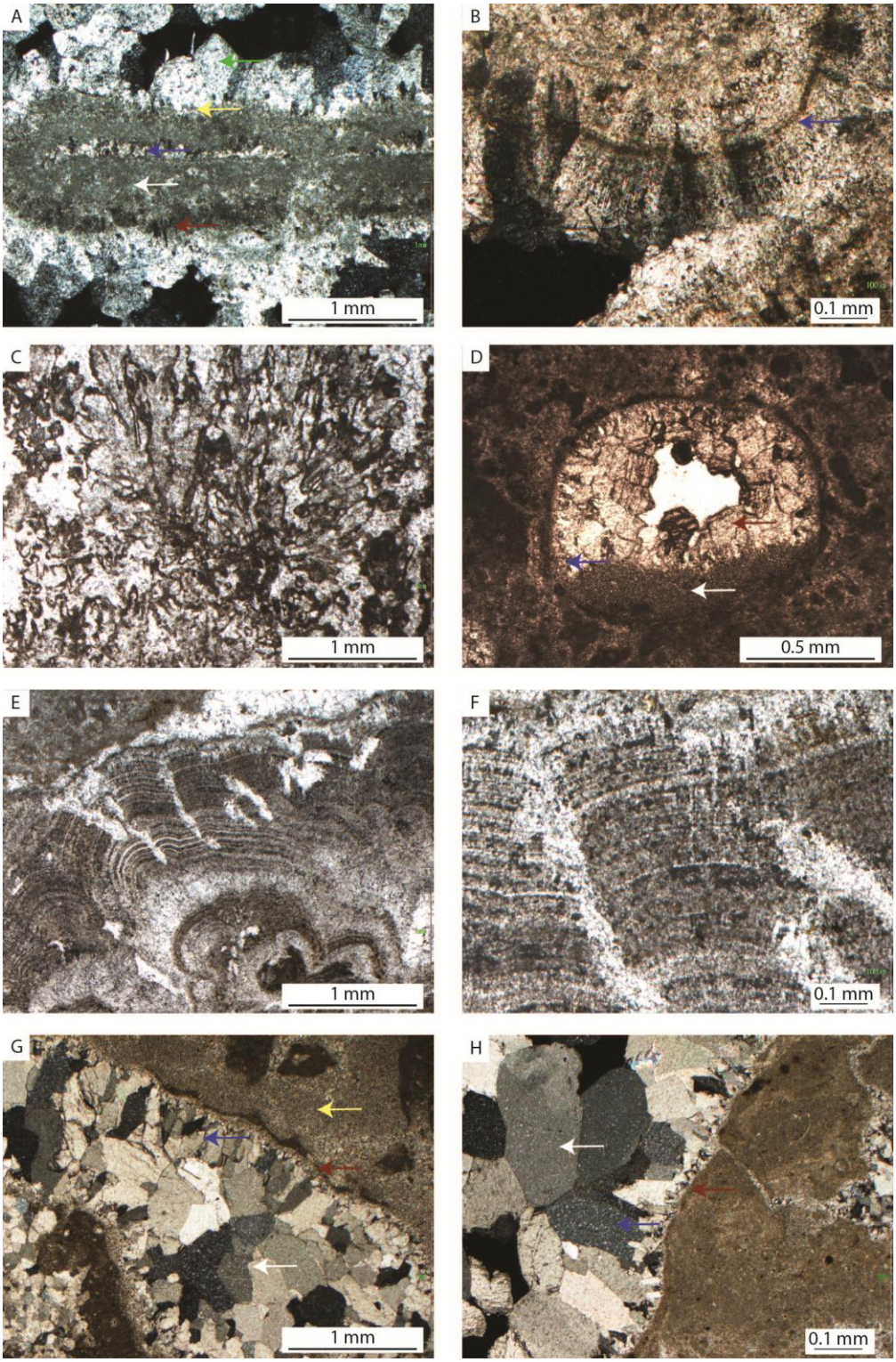

Figure 4.3. Photomicrographs of calcite cement types. A) White arrow indicates the primary micrite deposit (p1); blue arrow indicates microsparite and sparite (m2) that recrystallizes the initial micrite. Brown arrow indicates the blade calcite (b); yellow arrow indicates the sparite (s) followed by the scalenohedral sparite (green arrow). B) Crossed polarized light image shows that the blade calcite grows in optical continuity with respect to the initial precipitate. The blade calcite is preceded by a micrite coating (blue arrow). C) Recrystallized sparite (m2) substituted the original crystalline precipitate. The former dendrites are embedded in a micrite envelope. D) Gastropod had undergone organic matter dissolution and micritization of the skeleton. The mould was infilled by geopetal micrite infill (mi) (white arrow) followed by sparite (s) (blue arrow) and scalenohedral cement (sh) (brown arrow). E-F) Speleothem (sp) growth in vugs using primary travertine as substratum. Spelethem consists of blade elongated sparite crystals characterized by perpendicular lamination. G-H) Yellow arrow indicates microsparite and sparite (m1, m2). Brown arrow indicates sparite cement (s) followed by scalenohedral cement (blue arrow) and blocky equant sparite (bl) (white arrow) that fills the pores.

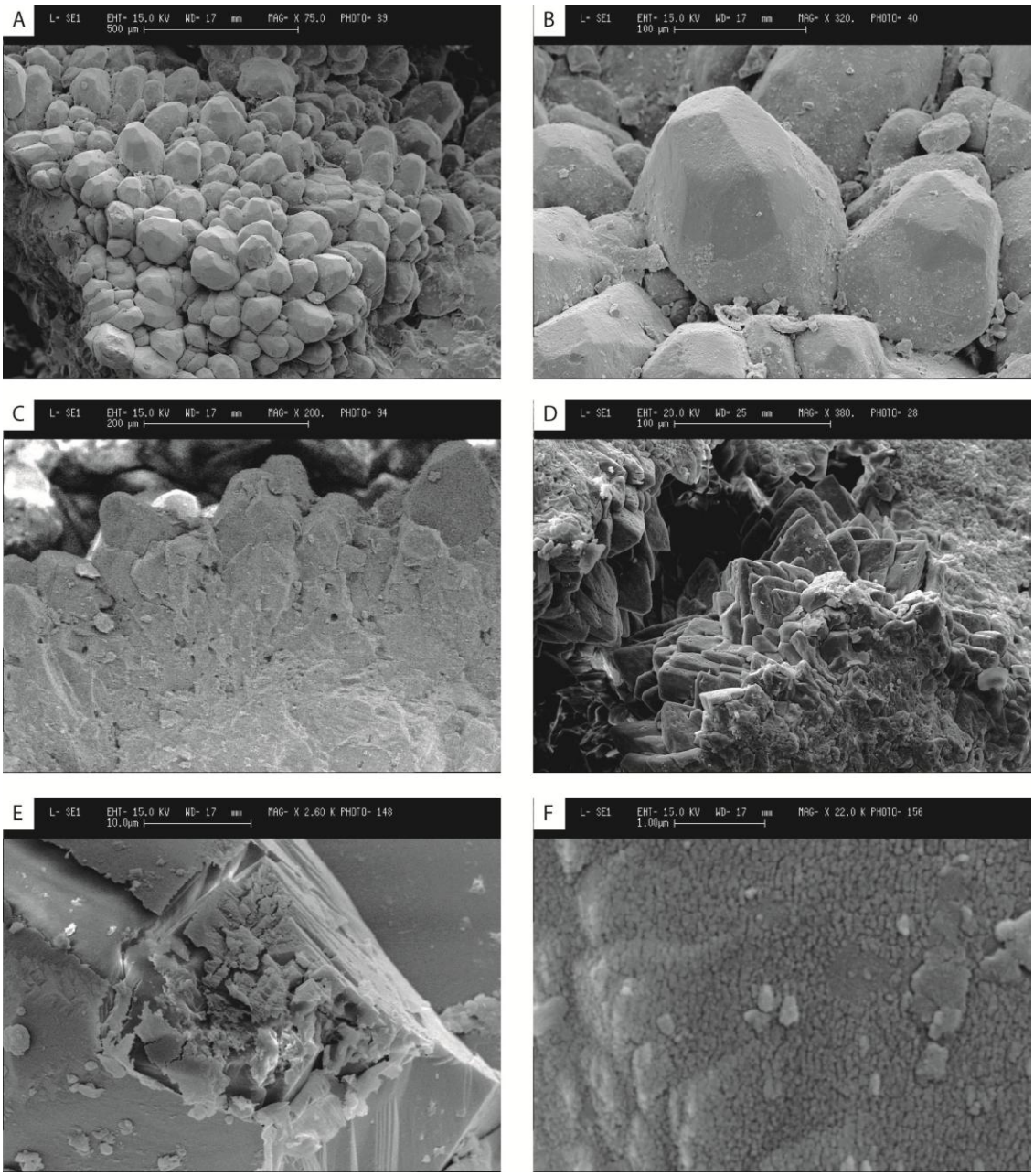

Figure 4.4. SEM images of calcite cements (. A-B) Rombohedral blocky equant calcite (bl) cement shows sharp to rounded edges. C-D) Scalenohedral cement (sh) with gothic arc termination. E-F) Cements are subjected to chemical and mechanical corrosion.

4.4.3 Cathodoluminescence and cement stratigraphy

The zoning and growth phases of the cement types distinguished in the upper Messinian Albegna Basin travertines are through cathodoluminescence analysis. The different sparite types are characterized by one or more variations in luminescence, which varies following different patterns (labelled as case 1 to 5) as shown in Figures 4.5 and 4.6.

Case 1. The initial travertine precipitates (p1) do not show any luminescence. In some cases the first cement that grows is the bladed calcite (b) (Fig. 4.5 A-B). This calcite is non luminescent. The bladed calcite (b) is followed by equant sparite (s). This sparite in cathodoluminescence presents growing zones that highlight gothic-arc geometries characterized by weak orange luminescence. The third generation of cement is the blocky calcite (bl) that occurs zoned in three different ways: blocky calcite (bl1 occurs with a luminescent pattern similar to the sparite luminescence (s) with a non-luminescence template zoned by yellow-luminescent rims. Blocky calcite (bl2) occurs yellow in luminescence characterized by non-luminescent or dull luminescent random patches. Bl2 is followed by blocky calcite (bl3) that is non-luminescent. Case 2. The cement that characterizes this case is the prismatic cement with scalenohedral terminations (sh). Scalenohedral cement occurs with 2 types of responses to cathodoluminescence. Sh1 occurs with a non-luminescent texture zoned by dull orange-luminescent rims. Sh2 consists of a luminescent texture with no-luminescent patches (Fig. 4.5 C-D). Case 3. In this case the non-luminescent travertines are not followed by the bladed calcite (b) but the first generation of cement consists in the equantsparite (s). A second generation of cement is represented by a scalenohedral cement (sh2). This cement fills also the fractures (Fig. 4.5 E-F). The sparite (s) could be preceded by the infill of detritalmicrite that results non-luminescent (mi, Fig. 4.6 A-B)

Case 4. In this case the first generation of cement that precipitates after the travertines is the blocky calcite (bl). This cement occurs initially with 2 patterns under cathodoluminescence: the first bl1 and the second bl2 (Fig. 4.6 C-D).

Case 5. This case shows the latest zones of cement growth that can characterize the blocky calcite (bl). After the precipitation of travertines the first generation of cement consists of the sparite (s). After this cement, laterally one to the other, there is the precipitation of the scalenohedral cement (sh2) and the blocky calcite cement (bl2). The fourth generation of precipitate is represented by a non-luminescent cement, that consists of blocky calcite (bl3). This zone is followed by a yellow luminescent rim that is characterized by a content of Mn^{2+} of 4300 ppm (as measured with microprobe? You did not write this even in the methods) that results much higher than the Mn^{2+} amount of the other orange-luminescent cements (see Table 4.2). This rim is labelled (bl4). The last phase consists in a non-luminescent blocky calcite (bl5) with yellow-luminescent rim or patches (Fig. 4.6 E-F).

The different cases show an ideal cement sequence that consists in 6 different principal phases:

1) Non-luminescent blade calcite (bl).
2) Sparite characterized by non-luminescent with orange luminescent rims (s, sh1, bl1).
3) Sparite characterized by yellow-luminescence and non-luminescent patches (sh2, bl2).
4) Non-luminescent sparite (bl4).

5) Yellow luminescent sparite rich in Mn^{2+} (bl4).
6) Non-luminescent sparite with yellow luminescent rims (bl5).

Table 4.2. Electron microprobe analyses. Mg, Ca, Mn and Fe ions values of different cement zonation expressed in ppm. See figure 4.6 E-F.

No.	Mg^{2+}	Ca^{2+}	Mn^{2+}	Fe^{2+}	Cement type
1	1363	551300	92	0	Primary travertine
2	0714	543800	0	3395	S
3	0778	547300	543	2955	Bl2 (non-luminescent)
4	0853	548300	360	212	Bl2 (luminescent)
5	2925	556600	0	215	Bl3
6	4223	543300	5676	471	Bl4
7	3701	549700	209	0	Bl5

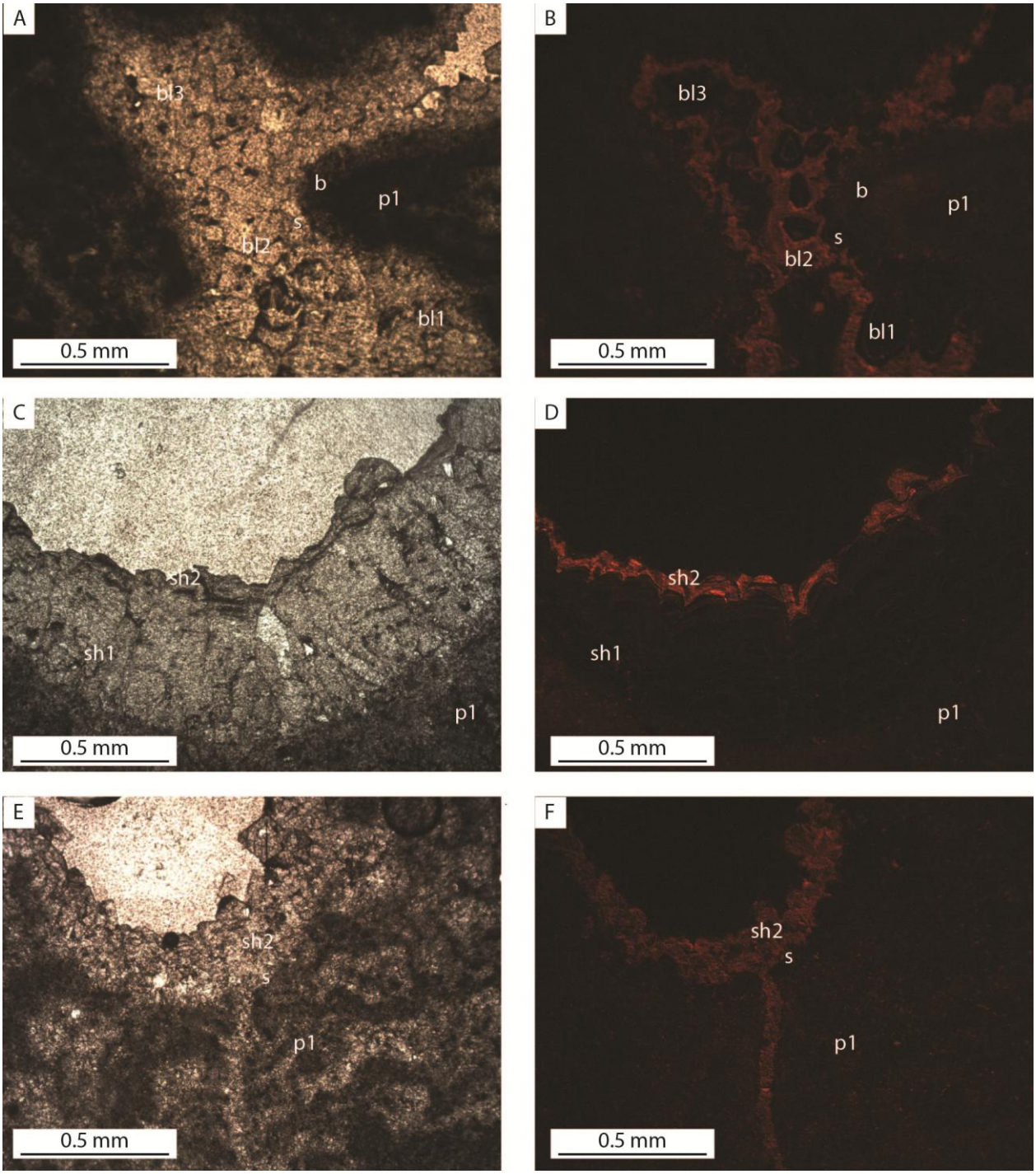

Figure 4.5. Photomicrographs and cathodoluminescence images. A-B) Example of Case 1. Interparticle vugs is filled by different cements that show different luminescence pattern: p1 (primary deposit) is non-luminescent to dull due probably to recrystallized crystals micrsoparite (m2) or due to decadence of organic matter. Blade calcite (b) is no luminescent followed by sparite (s) and blocky equant sparite (bl1). Blocky equant (bl2), yellow luminescent with non-luminescent patches, followed by non-luminescent blocky equant calcite (bl3) fills the pore. C-D) Example of case 2 in which a bubble pore is filled by scalenohedral calcite (sh1) non-luminescent with luminescent rims, with luminescent termination (sh2). E-F) Case 3. In this case yellow luminescent scalenohedral cement (sh2) is preceded by non-luminescent sparite (s). Sh2 fills the fracture.

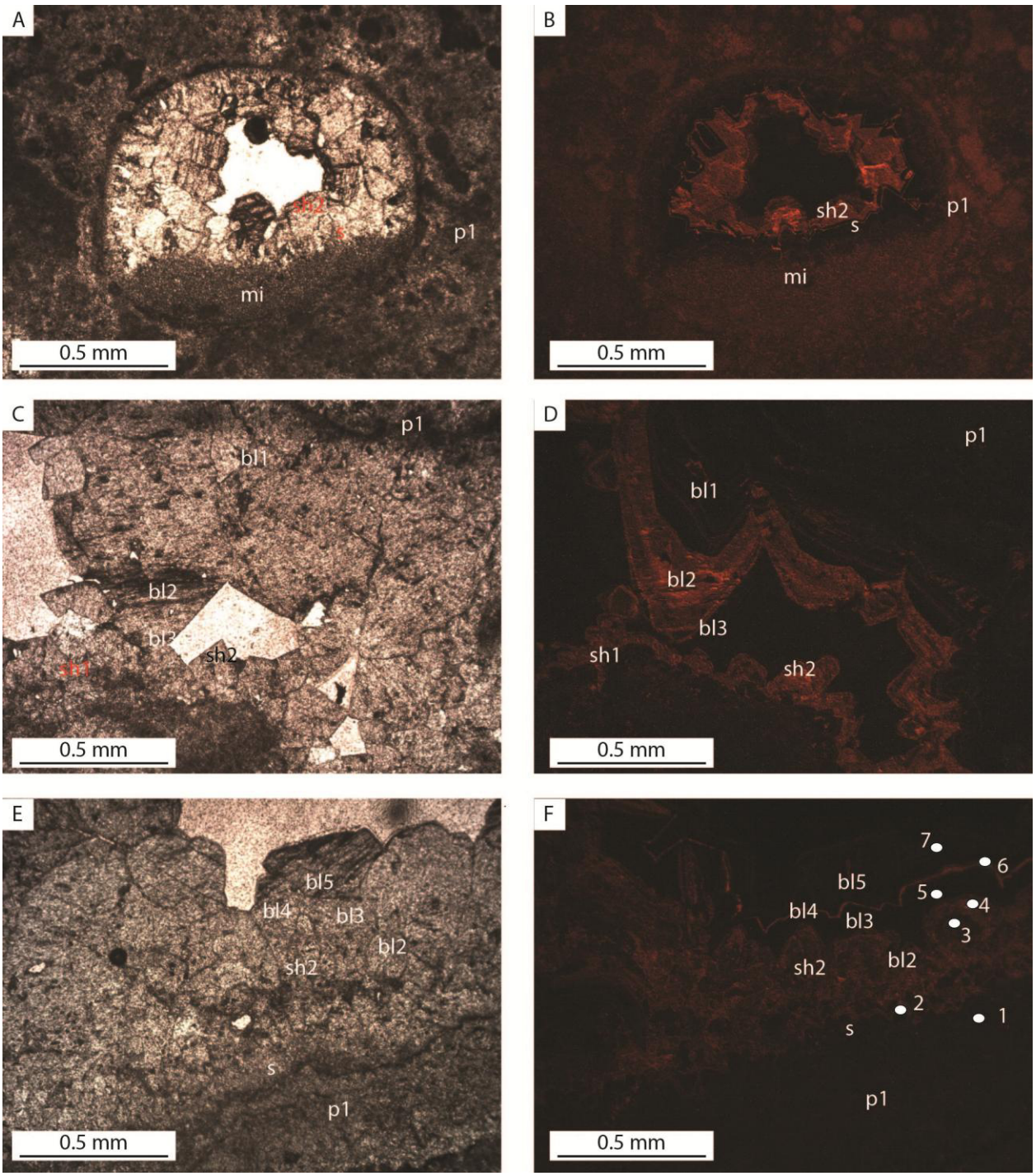

Figure 4.6. A-B) Other example of case 3 in which sparite (s) is preceded by dull red luminescent geopetal infill micrite (mi). C-D) The upper part of the pore shows the cement stratigraphic sequence of case for in which blocky equant calcite grows with 3 different patterns (bl1, bl2 and bl3), passing from non-luminescent with yellow-luminescent rim, to yellow luminescent with non-luminescent patches. In the bottom part of the hole the schalenohedral cement follow the same trend. E-F) Case 5 of cement stratigraphy where it is showed the almost complete sequence of cement in the studied travertines. From the second (s) to the fourth cement (bl3), interpreted as meteoric cement, the sequence continues with a yellow-luminescent rim (bl4) enriched in Mn^{2+} and interpreted as burial phase. The last phase consists of a non-luminescent rim of blocky equant calcite (bl5) interpreted as a renewed meteoric phase after the uplift of the studied succession. The numbers (1-7) indicate the points where electron probe analyses were made.

4.4.4 Other diagenetic features

In the studied travertines other numerous diagenetic features occur.
Exposure surfaces are characterized by undulating trend (Fig. 4.7A). These surfaces are often covered by red staining due to the precipitation of Fe-Mn(OH) or clay. Mineralogical composition determined by XRD and SEM analyses reveals that these precipitates are enriched in different elements such as Al, Ba, Co, K, Mn, Ti (Fig. 4.7 C-G). Mineral clay are made of aggregates of laminae, while Fe(OH) consist principally of structures that vary from fibrous to spherical aggregates. These precipitates may cover also the primary travertine precipitates or the cements. Rarely these red staining occur between different phases of cements. Associated to exposure surfaces rhyzocretions occur. These structures are made of laminae of micrite and characterized by interlaminae porosity (Fig. 4.7 H). Moreover exposure surfaces may be covered by detrital infill, grey or red in colour with grain size that varies between clay and sand (4.8 B-C).
Primary travertine precipitates may be characterized by the occurrence of edges, characterized by irregular black edges (Figure 4.8 A) and shows dissolution of travertines. Dissolution features characterize also the cements (Fig. 4.4 E-F) that present irregular surfaces.
The studied succession shows also rare compaction features such as stylolites (Fig. 4.8 D) that are parallel to the stratification and characterized by an extension of few millimeters. Sutured contacts rarely occur too in the studied succession, both in travertines and conglomerates (Facies F11).
In the studied succession fractures are recognized. Fractures occur vertically elongated and few µm wide. The space within the fractures may be filled by yellow luminescent cement (sh2, bl2, Fig. 4.5 E-F), or empty (Fig. 4.8 G).

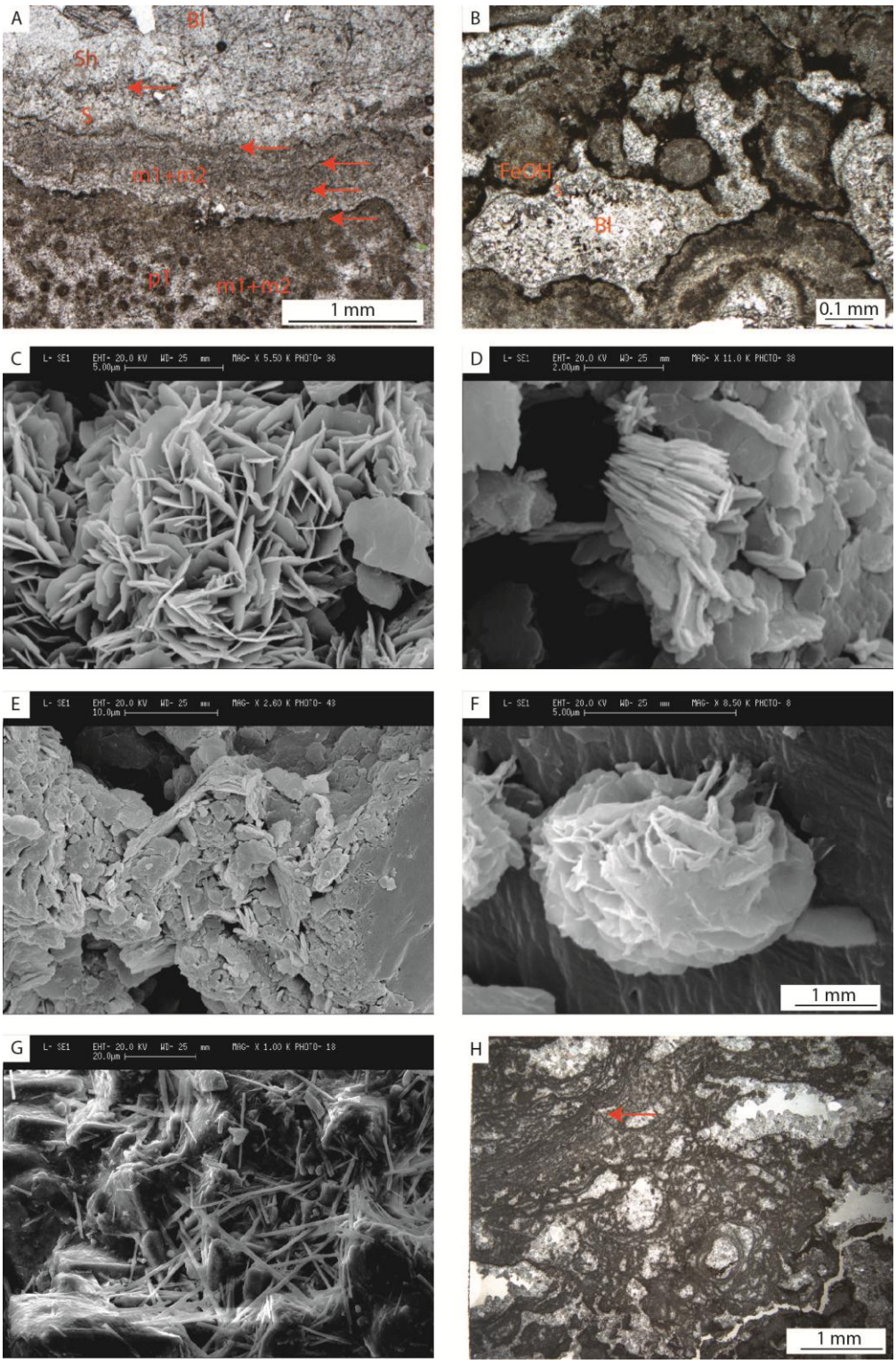

Figure 4.7. Photomicrographs and SEM images representing diagenetic features. A) Orange arrows indicate different exposure surfaces. M1 microsparite to sparite probably precipitates during renewed hydrothermal flowing. M2 substitutes m1 during the recrystallization. Other cement phases are recorded by sparite (s), scalenohedral cement (sh) and blocky equant calcite (bl). B) Fe-OH (Fe1, brown to red in colour) precipitates around the primary travertine deposits. The pores are filled by sparite (s) and scalenohedral calcite (sh). C) Example of laminated clay enriched in different elements in which there are Al, Ca, Fe, Al, Mg, K, Ti and Co. D) Micrometre thick sticks of Fe(OH) enriched in Ca, Al, K and Mn. E) Example of mineral clay with Ca and Al. F) Subrounded shape of a Fe(OH) enriched in Ca and Mn. G) 20 µm long sticks of claystone enriched in Ca, Fe and Al. H) Rhyzocretions displaying alveolar structure, probably a product of a paleosol.

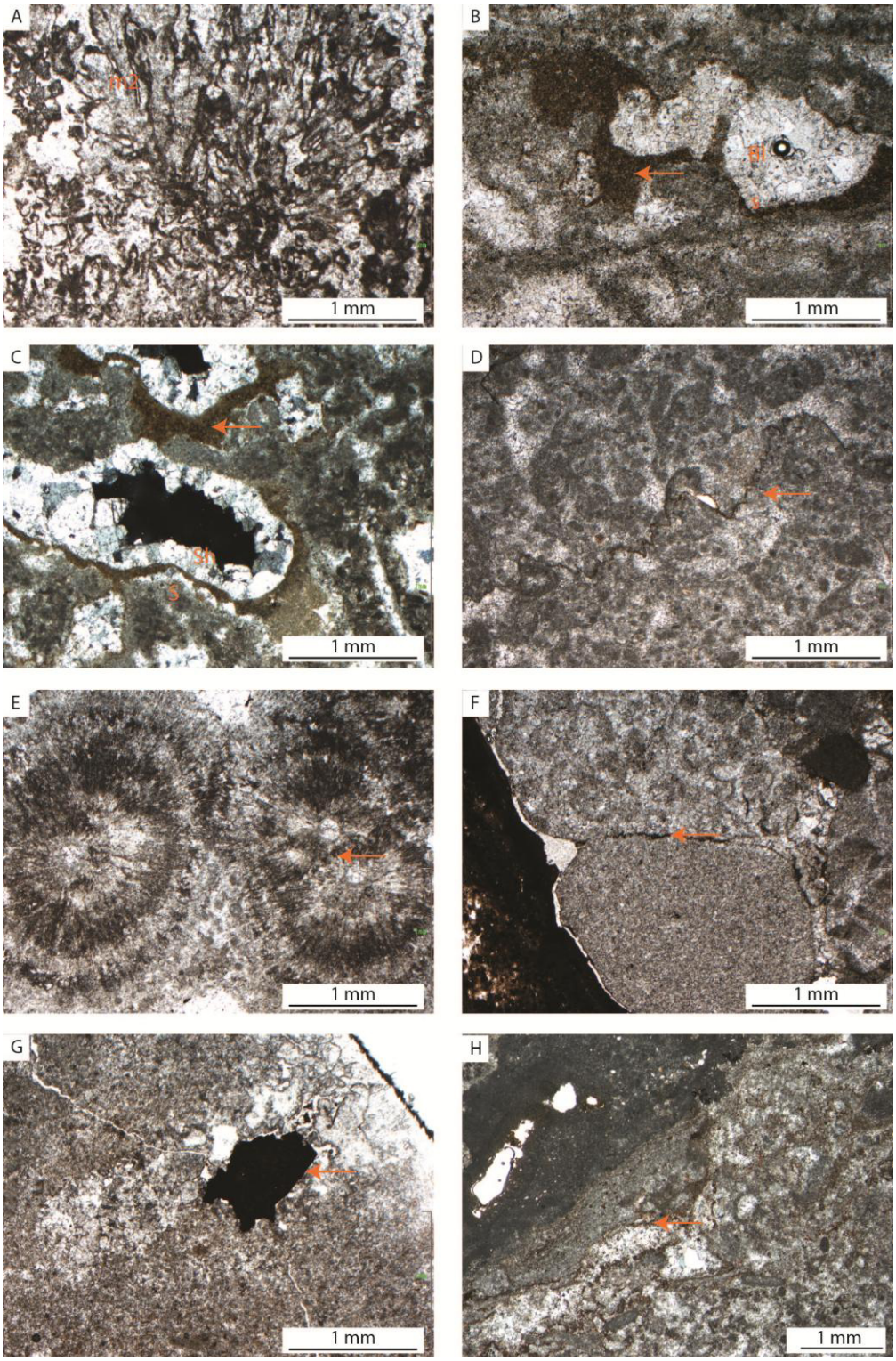

Figure 4.8. Photomicrographs representing diagenetic features. A) Crystalline dendrites are subjected to micritization of their edges and to recrystallization of the original sparite (ds) to a white sparite (m2). B) Secondary interparticle pores are filled by reddish silt (si1) that is followed by white sparite (s) and blocky equant calcite (bl). C) In this case the reddish silt (si1) precipitates after the sparite (s) and it is followed by the scalenohedral cement (sh). D) Example of a rare stylolites (st, orange arrow) that characterizes the studied travertines, indicating compaction due to a burial phase. E-F) Rare sutured contact (st, orange arrows) occur both in studied travertines and conglomerates. G) A late generation of fractures (f2) occurs and it is not filled by any cement. Fe(OH) (Fe2, orange arrow) precipitates after f2.

4.4.5 Geochemistry: travertines carbon and oxygen isotopes

The results of stable carbon and oxygen isotope analyses of the upper Messinian travertines (cf. Chapter 3; Croci et al., 2016) of the Albegna Basin are summarized in Tables 4.3 and 4.4 and plotted in Figures 4.1 and 4.2.

Stable ^{13}C data from the travertines of the 3 different phases of evolution of the depositional system generally overlap (Fig 4.9). However, the $\delta^{13}C$ values of travertine of the older Phase 1 and Phase 2 are generally higher than $\delta^{13}C$ of the younger Phase 3 travertines. The $\delta^{13}C$ values of Phase 1 travertines range between -0.53‰ and +3.19‰ with an average of 1.62‰; in Phase 2 the values range between +0.13‰ and +2.29‰ with an average of +1.38‰, while in Phase 3 the range is between -8.56‰ and +2.18‰, with an average of -0.48‰. The lowest carbon isotope values correspond to facies F7, coated reed boundstones (-8.56‰, -1.57‰), and Facies F8, skeletal peloidal packstones grainstones (-1.9‰, -1.39‰), of Phase 3. In contrast, $\delta^{13}C$ values of facies F5, crystalline dendrite cementstones, of Phase 1 show the highest values (+3.88‰, +3.02‰).

Oxygen isotopic values of travertines from the 3 different phases exhibit a single overlapping field and do not show significant differences between the three phases. The $\delta^{18}O$ values of Phase 1 travertines range between -8.99‰ and -6.14‰, with an average of -7.42‰. In Phase 2 the oxygen isotope values vary between -9.46‰ and -6.76‰, with an average of -7.72‰. The travertines of Phase 3 show a range between -8.73‰ and -4.14‰ and an average of -7.51‰. On average, the facies that shows the lowest oxygen values is facies F8 (-8.73‰ and -8.52‰ in Phase 3) while the highest values (in average) belong to facies F5 (-6.14‰ and -6.74‰ in Phase 1).

Within the same facies the carbon and oxygen isotopic values vary significantly and the isotope signal does not permit to identify differences between the different facies. For instance the carbon values of facies F1, clotted peloidal micrite and microsparite boundstones to grainstones range between +0.63‰ and +2.58‰; for facies F5 the range is between -0.53‰ and +3.88‰ and for facies F7 the range is between -1.9‰ and 2.34‰. The same overlap of values occurs for the $\delta^{18}O$.

Travertines of Phase 1 and Phase 2 of the studied are present different colours; they can be white, red or black. The black and red colours are due to the occurrence of impurities of Fe^{2+} and Mn^{2+} within the travertine precipitate that results white in absence of that impurities. Travertines of Phase 3 are steadily grey.

A correlation between the colour of the rock and the isotopic values of carbon occurs, mainly in Phase 1 and 2 where the travertines are better characterized by this difference in colour than in Phase 3 (Fig. 4.10). For instance white crystalline dendrite cementstone of facies F5 shows an average of 2.7‰, while when they are black or red the average is 0.81‰. The same trend occurs in all the facies and the results are summarized in Table 4.5. Regarding the white travertines the highest values of the carbon isotopes belong to the crystalline dendrite cementstone (facies F5), followed by the sub-rounded coated grains grainstone/packstone (facies F3). Both these facies are made of crystalline precipitates. Facies F1, characterized by the occurrence of micrite dendrites, presents intermediate values, while the lowest values belong to the skeletal peloidal packstone/grainstone (facies F8). On the contrary, concerning the red/black travertines, facies F8 results to show the highest values, while the coated gas bubbles boundstone (facies F4) is characterized by a negative value.

In Phase 3, where the travertine rocks are not characterized by different colours, the $\delta^{13}C$ values are higher in the samples collected in the log CE with respect to the samples collected in the active quarry. Instead the oxygen values are lighter in the sample belonging to the log CE than the samples collected in the active quarry. Concerning the isotopic values of cement samples (Table 4.4), $\delta^{13}C$ varies between -2.14‰ and +2.71‰ with an average of 0.35‰ similar to the carbon values of red or black travertines; the oxygen isotopes, in the cements, range between -8.31‰ and -5.45‰, with an average of -7.25‰, comparable to the oxygen isotope values of travertines in the different phases.

Table 4.3. Geochemical composition of studied travertines.

Sample	Log (cf. Fig. 3.?)	Phase (cf. Chapter 3)	Facies (cf. Chapter 3)	$\delta^{13}C$ (per mil V-PDB)	$\delta^{18}O$ (per mil V-PDB)	Outcrop or Petrographic evidence of meteoric diagenesis	Depositional environment
G 0.2A	G	1	Crystalline dendrite cementstone (F5)	3.02	-6.14	no	Terrace rim, wall
G 0.2B	G	1	Crystalline dendrite cementstone (F5)	0.55	-7.42	yes	Terrace rim, wall
G 1.2	G	1	Crystalline dendrite cementstone (F5)	3.19	-6.74	no	Terrace rim, wall
G 3.1B	G	1	Sub-rounded coated grains grainstone/packstone (F3)	2.35	-6.99	no	Terrace pool
Gs 0.2A	G	1	Skeletal peloidal packstone/grainstone (F8)	2.34	-8.13	no	
Gs 0.2B	G	1	Skeletal peloidal packstone/grainstone (F8)	1.96	-8.01	yes	
G 10.3A	G	1	Sub-rounded coated grains grainstone/packstone (F3)	0.2	-7.08	yes	Terrace pool
G 10.3B	G	1	Sub-rounded coated grains grainstone/packstone (F3)	2.92	-7.17	no	Terrace pool
MC 1.2B	MC	1	Skeletal peloidal packstone/grainstone (F8)	1.53	-7	no	
MC 5.55	MC	1	Coated reed rudstone to boundstone (F7)	2.01	-8.14	yes	
U1 CS2	MC	1	Clotted peloidal micrite and microsparite boundstone to grainstone (F1)	2.19	-7.16	no	Terrace pool
U1 10	MC	1	Clotted peloidal micrite and microsparite boundstone to grainstone (F1)	2.51	-8.99	no	Terrace pool
PB 143A	PB	1	Crystalline dendrite cementstone (F5)	0.28	-6.84	yes	Terrace rim, wall
PB 143B	PB	1	Crystalline dendrite cementstone (F5)	0.43	-6.94	yes	Terrace rim, wall
PB 197A	PB	1	Crystalline dendrite cementstone (F5)	0.31	-7.5	yes	Terrace rim, wall
PB 197B	PB	1	Crystalline dendrite cementstone (F5)	-0.53	-6.85	yes	Terrace rim, wall
U1 1A	P	1	Crystalline dendrite cementstone (F5)	1.61	-7.47	yes	Terrace rim, wall
U1 1B	P	1	Crystalline dendrite cementstone (F5)	1.99	-7.14	yes	Terrace rim, wall
U1 1AA	P	1	Clotted peloidal micrite and microsparite boundstone to grainstone (F1)	2.48	-8.35	no	Terrace pool
U1 1AB	P	1	Crystalline dendrite cementstone (F5)	2.82	-8.63	no	Terrace rim, wall

U1 1AC	P	1	Crystalline dendrite cementstone (F5)	3.88	-7.34	no	Terrace rim, wall
P 3.65	P	1	Coated reed rudstone to boundstone (F7)	1.22	-7.78	yes	Terrace pool
U1 2A	P	1	Coated gas bubble boundstone (F4)	-0.24	-7.53	yes	Terrace pool
U1 NC	P	1	Skeletal peloidal packstone/grainstone (F8)	1.75	-7.14	yes	Travertine flat
U1 ND	P	1	Skeletal peloidal packstone/grainstone (F8)	0.9	-7.23	yes	Travertine flat
U1 BB	P	1	Crystalline dendrite cementstone (F5)	1.99	-7.14	no	Terrace rim, wall
N 1	N	1	Coated reed rudstone to boundstone (F7)	0.29	-7.50	yes	Terrace pool
E 1.5	E	2	Crystalline dendrite cementstone (F5)	1.02	-7.31	yes	Terrace rim, wall
E 1.6	E	2	Clotted peloidal micrite and microsparite boundstone to grainstone (F1)	2.18	-7.5	no	Terrace pool
U2 B	P	2	Clotted peloidal micrite and microsparite boundstone to grainstone (F1)	1.94	-7.15	no	Terrace pool
D 2.44	D	2	Clotted peloidal micrite and microsparite boundstone to grainstone (F1)	2.58	-7.47	no	Terrace pool
D 37	D	2	Calci-mudstone to microsparstone (F9)	1.35	-9.46	yes	Terrace pool
DM 41.3A	DM	2	Coated reed rudstone to boundstone (F7)	0.37	-9.02	yes	Terrace pool
DM 41.3B	DM	2	Clotted peloidal micrite and microsparite boundstone to grainstone (F1)	2.29	-7.49	no	Terrace pool
CR 0.5	CRA	2	Coated gas bubble boundstone (F4)	0.13	-6.76	yes	Terrace pool
CR 1.13	CRA	2	Clotted peloidal micrite and microsparite boundstone to grainstone (F1)	0.65	-7.54	yes	Terrace pool
CRA 6.3	CRA	2	Crystalline dendrite cementstone (F5)	1.34	-7.51	no	Terrace rim, wall
D 61	D	3	Skeletal peloidal packstone/grainstone (F8)	-0.23	-7.47	yes	Travertine flat
CRA 22.3	CRA	3	Skeletal peloidal packstone/grainstone (F8)	0.09	-8.52	yes	Travertine flat
CRA 29	CRA	3	Coated reed rudstone to boundstone (F7)	2.18	-7.16	yes	Travertine flat
F 9.5	F	3	Coated reed rudstone to boundstone (F7)	-1.57	-6.64	yes	Travertine flat
FA	F	3	Coated reed rudstone to	-8.56	-4.14	yes	Travertine

			boundstone (F7)				flat
SA 0.3A	SA	3	Coated reed rudstone to boundstone (F7)	0.48	-8.71	no	Travertine flat
SA 0.3B	SA	3	Skeletal peloidal packstone/grainstone (F8)	-1.39	-7.39	no	Travertine flat
SA 1.4	SA	3	Skeletal peloidal packstone/grainstone (F8)	-1.9	-6.66	no	Travertine flat
SA 1.75	SA	3	Skeletal peloidal packstone/grainstone (F8)	0.47	-7.81	no	Travertine flat
CE 0.9	CE	3	Skeletal peloidal packstone/grainstone (F8)	0.98	-8.52	no	Travertine flat
CE 2.1A	CE	3	Raft floatstone/rudstone (F2)	1.9	-8.41	no	Travertine flat
CE 2.1B	CE	3	Skeletal peloidal packstone/grainstone (F8)	1.65	-8.73	no	Travertine flat

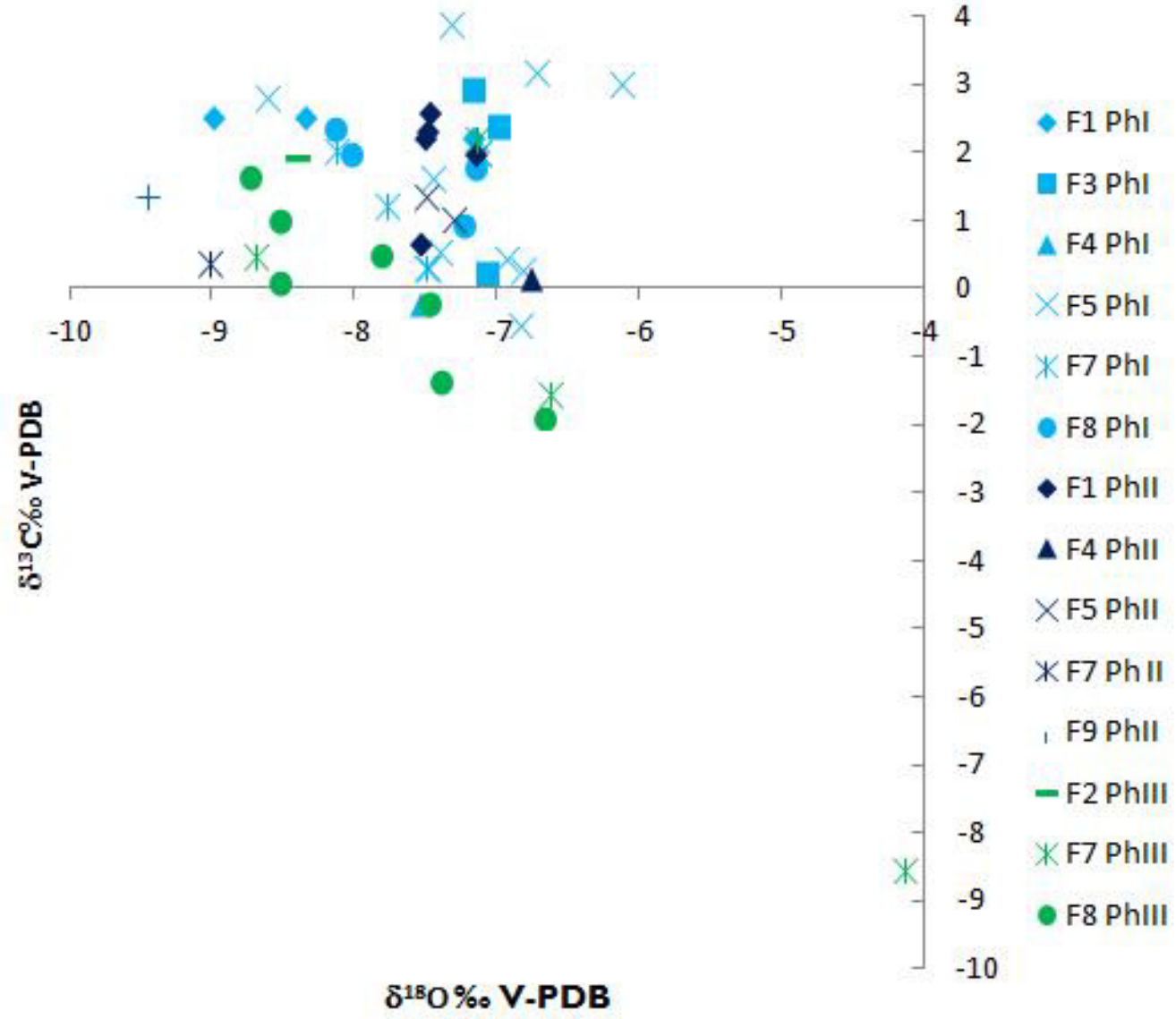

Figure 4.9. Plot of $\delta^{13}C$ and $\delta^{18}O$ of measured studied travertines subdivided per lithofacies type (F) and phases of sedimentary evolution (Ph).

Table 4.4. Geochemical composition of cements in studied travertines

Sample	**Log (cf. Fig. 3.?)**	**Phase (cf. Chapter 3)**	**Facies (cf. Chapter 3)**	**$\delta^{13}C$ (per mil V-PDB)**	**δ^{18}° (per mil V-PDB)**	**Petrographic characterization of cement type**
G 3.1A	G	1	Sub-rounded coated grains grainstone/packstone (F3)	2.71	-6.19	Equant sparite mosaic
MC 1.2A	MC	1	Sub-rounded coated grains grainstone/packstone (F3)	0.63	-8.31	Equant sparite mosaic
PB 143 A	PB	1	Crystalline dendrite cementstone (F5)	0.28	-6.84	Equant sparite mosaic
U1 2B	P	1	Coated gas bubble boundstone (F4)	-2.14	-7.25	Scalenohedral sparite
U1 NA	P	1	Clotted peloidal micrite and microsparite boundstone to grainstone (F1)	0.63	-7.15	Equant sparite mosaic
U1 NB	P	1	Sub-rounded coated grains grainstones/packstone (F3)	0.24	-6.76	Equant sparite mosaic
U2 CA	P	2	Clotted peloidal micrite and microsparite boundstone to grainstone (F1)	0.85	-8.26	Equant sparite mosaic
U2 CB	P	2	Clotted peloidal micrite and microsparite boundstone to grainstone (F1)	0.68	-7.59	Equant sparite mosaic
L 1B	P	2	Breccia (F10)	1.36	-8.8	Equant sparite mosaic
L 2A	P	2	Breccia (F10)	-0.86	-7.18	Equant sparite mosaic
U3S	S	3	Calci-mudstone to microsparstone (F9)	-0.51	-5.45	Equant sparite mosaic

Table 4.5. $\delta^{13}C$ average signatures of travertine lithofacies of phases 1 and 2 differentiated by colour of the rock.

Facies average	**Colour**	**$\delta^{13}C$ average (per mil V-PDB)**
F1	white	2.31
F1	red/black	0.65
F3	white	2.63
F3	red/black	0.20
F4	Red/black	-0.05
F5	white	2.70
F5	red/black	0.71
F7	red	0.97
F8	white	1.93
F8	red	1.54
F9	red	1.35

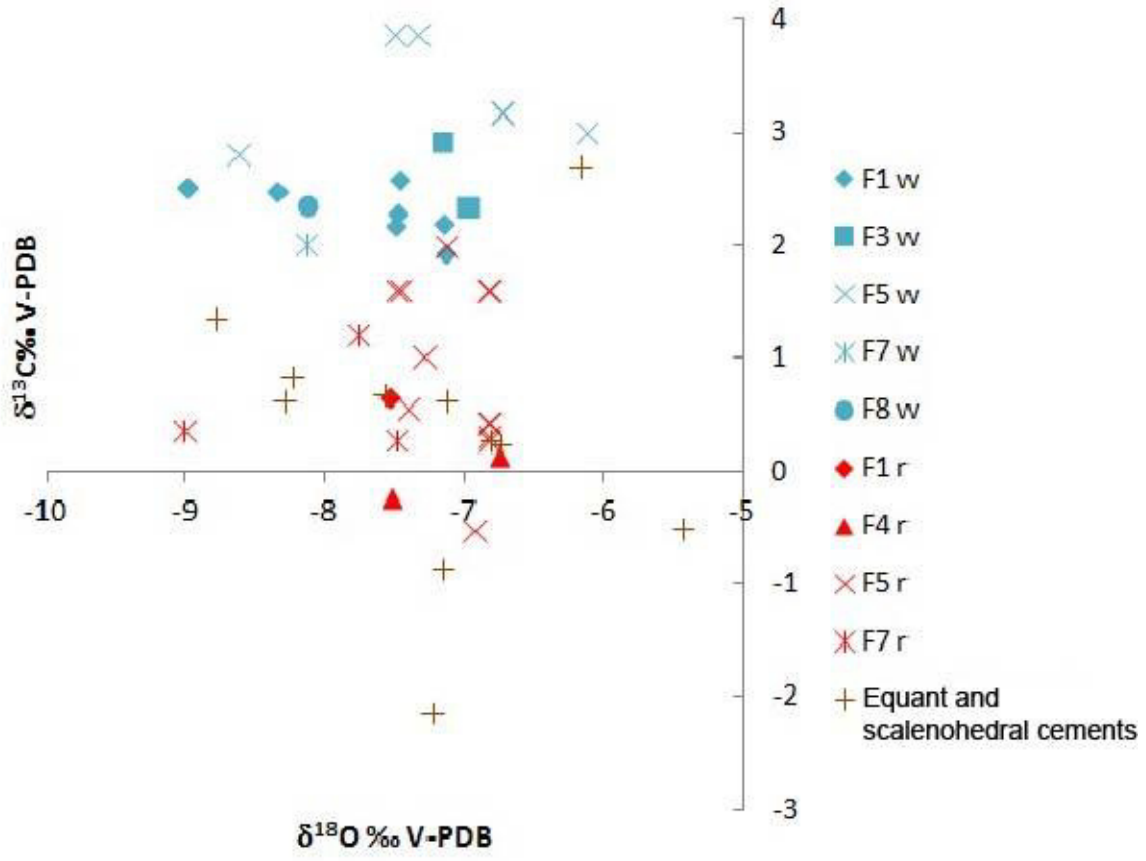

Figure 4.10. Plot of $\delta^{13}C$ and $\delta^{18}O$ of measured studied travertines grouped in facies and differentiated from the colour (w= white), r= red) of the rocks. Equant and scalenohedral cements are also represented.

4.5 Interpretation and discussion

4.5.1 Paragenetic sequence

Petrographic analysis of the three phases of the Late Messinian Albegna Basin travertines revealed the occurrence of a complex paragenetic sequence for these carbonates. The sequence includes 21 events corresponding to 7 major cement phases, 3 corrosion events, 2 fracturing events, 1 exposure event, 1 recrystallization event, 5 events of geopetal infill and clay to (Fe-Mn)OH and 1 compaction event. The proposed timing of the different diagenetic events is illustrated in Figure 4.11. The order of the paragenetic events has been established by combining the cement fabrics and their stratigraphy, the cross-cutting and overgrowth relationships and their spatial distribution. The most complete record of the paragenetic sequence was observed in the travertine of phase 1. Based on petrographic and geochemical analyses, the events of the paragenetic sequence have been grouped tentatively into diagenetic environments addressed as hydrothermal, meteoric, burial and telogenetic meteoric phase.

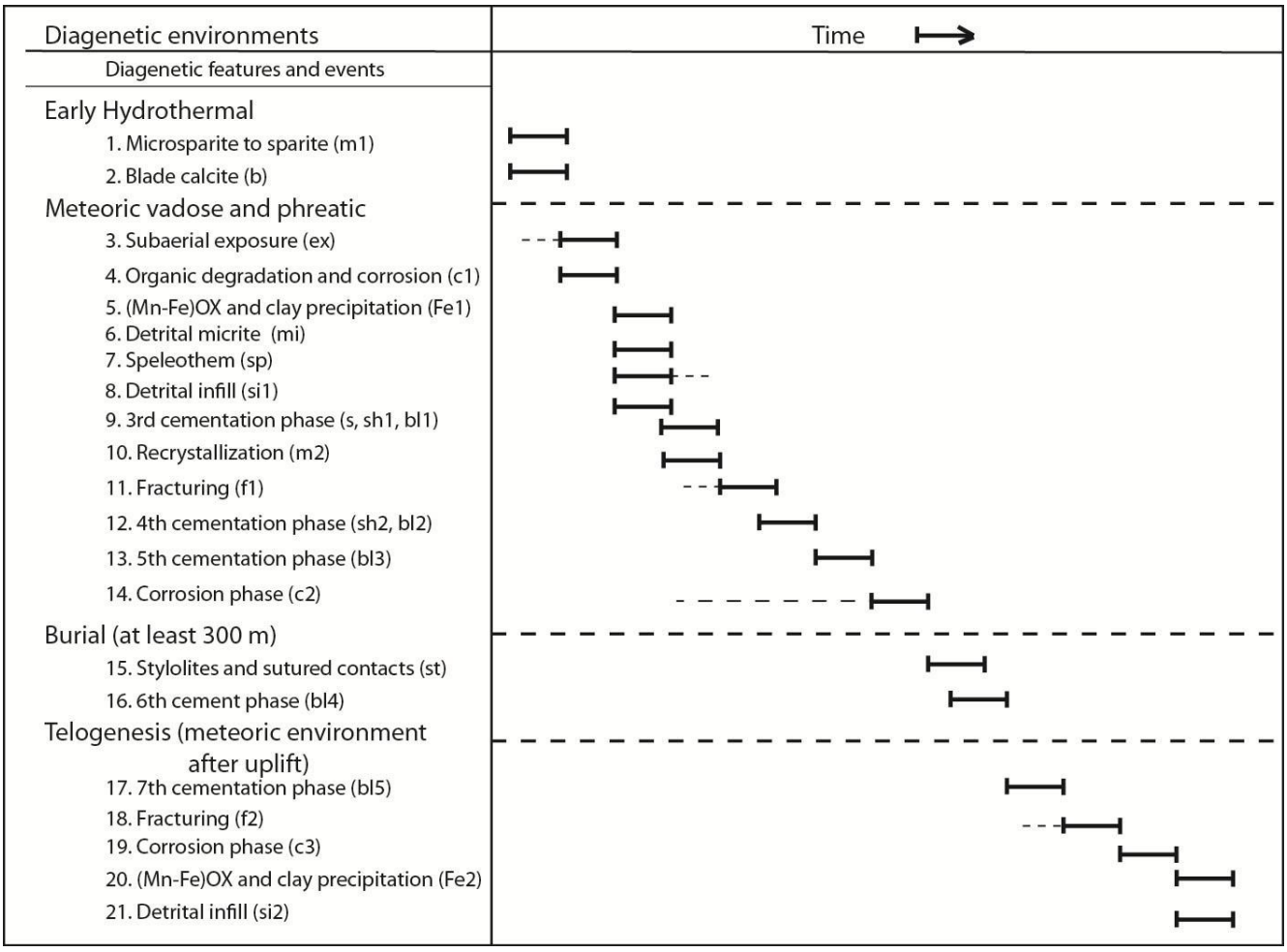

4.11. Relative timing distribution of the 21 paragenetic events recorded in the studied travertine succession. Thick lines indicate the relative duration of each event and thin lines indicate the probably maximum extent.

Hydrothermal diagenesis

The earliest paragenetic events (events 1,2 Fig.4.7 A-B) correspond to a cementation, due to the precipitation of sparite from hydrothermal waters. These events are recorded in each depositional phases. The cements precipitated fill the pores between the primary micrite and microsparite (m1) and coats the travertine precipitates through the bladed calcite (b), developing coating without a preferential growing direction, showing that probably the waters covered completely the travertines.

Meteoric diagenesis

The meteoric diagenesis corresponds to the events from the number 3 to the number 14. The occurrence of erosive surfaces (e.g., Fig. 4.7 A) sometimes covered by a reddish precipitates (Fe1). The exposure to the weathering and the percolation of water in the vadose zone caused the degradation (c1) of the organic matter of molluscs, ostracodes, reeds and of the peloidal precipitates, with the consequent development of secondary porosity, rhyzocretion features (Fig.4.7 H.) and micrite black coatings around clotted peloidal micrite and crystalline primary precipitates (Fig.4.8 A). During this diagenetic phase the pores are filled by different infills that consist of detritic micrite (Fig. 4.3 D) or detrital clay and silts, (Fig. 4.8 B). The detrital infill could be preceded by a first phase of meteoric sparite cement (s, Fig. 4.8 C), probably due to an oscillation of the phreatic water table. In the vadose zone the precipitation of speleothem-like crusts (sp) occurs (Fig. 4.3 E-F). After the deposition of the detrital clay and silts, the second phase of precipitation of different cements occur (s, sh1, bl1). These cements precipitate or directly in contact with the travertines or after the bladed cement (b). Contemporaneous to this cement phase probably the recrystallization of microsparite to sparite (m2) takes place. The third cement phase is cut-crossed by a first phase of fractures (f1, Fig. 4.7 E-F). This phase of fractures is filled by the third cement phase (sh2, bl2). The fourth cement phase (bl3) occurs in the blocky calcite, following both sh2 and bl2, characterized by a non-luminescent trend. The cements that develop the cement phases from 2 to 4 are characterized by irregular or rounded edges, well visible in cathodoluminescence that testify a corrosion event (c2). These cementation phases probably occurred in the phreatic zone.

Burial diagenesis

According to Bossio el al. (2003-2004) the Messinian Albegna Basin was filled and covered by at least 200 m of marine clay, due to the Pliocene marine transgression. The studied upper Messinian travertines recorded features that prove a burial phase that corresponds to the events 15-16 (fig.4.11). Stylolites and sutured grain contacts (st, Fig.4.8 D-F) occur in the each 3 travertine phases. Moreover stylolites cut-cross cements of the third phase of cement (sh2, bl2). Furthermore some pores are filled by drusy blocky spar that under cathodoluminescence show a yellow-luminescent rim, particularly enriched in Mn^{2+} (bl4) and probably precipitated from different and deeper fluids with respect to those that characterize the phreatic zone.

Telogenesis

After the burial phase the Albegna Basin was uplifted from the Late Pliocene to the Holocene (Bossio et al., 2003-2004). Consequently the studied travertines recorded this phase, which corresponds to the events from 17 to 21 (Fig. 4.11). This phase is characterized by the precipitation of the non-

luminescent blocky calcite (bl5) (Fig. 4.8 E-F) that shows corroded and rounded edges proving a late corrosion phase (c3). Moreover this phase recorded a late infill of detrital geopetal sediments (si2) and the precipitation of clay and (Fe-Mn)OH (Fe2) that covers the previous cements and are not cut by the first fracture phase (f1, Fig.4.8 G-H).

4.5.2 Travertines carbon and oxygen isotopes

The classification scheme of Pentecost (2005) contains two main travertine types, meteogene and thermogene, on the basis of the different career of CO_2, respectively from soils or originated from more deeply seated thermal processes. On the basis of geochemistry results obtained, the upper Messinian Albegna Basin travertines of this study can be labelled as thermogene. The travertine deposits of the Marsiliana area show textural and geochemical characteristic that can be used in the interpretation of geochemical data of fossil travertines, trying to find a relationship between the geochemical data and the depositional facies and depositional environments, and if it is possible, to find an association between controlling factors, such as water degassing and water evaporation, and isotope values. Stable isotope analysis provides a useful tool for the determination of depositional facies. Considering the carbon isotope, the stratigraphic stages of the evolution of the depositional system identified as phases 1 and 2 (cf. Chapter 3) present higher Carbon isotopic values than the phase 3 travertines, which are characterized by negative values. Moreover this difference is evident also in the lithofacies associations that in phases 1 and 2 are characterized by the occurrence of clotted peloidal micrite boundstone (Facies F1), sub-rounded coated grains grainstone (Facies F3), coated gas bubble boundstone (Facies F4) and crystalline dendrites cementstone (Facies F5), developing a slope environment, while Phase 3 is characterized by the occurrence of coated reeds boundstone (Facies F7) associated with skeletal peloidal packstone/grainstone (Facies F8) in a flat/marsh travertine environment with the expansion of the alluvial plain environment. This difference in lithofacies association can be explained by different sources of CO_2. According to Minissale et al. (2002) and Minissale (2004), the CO_2 in Central Italy that feeds the groundwaters to the hydrothermal springs, derived from deep decarbonatation of Mesozoic limestones that in Southern Tuscany are hosted in the Anidrite di Burano-Calcare Cavernoso Formation. Instead the drop of the carbon isotope values in phase 3 could be explained by a major mixing through the deep groundwaters, the shallow groundwaters and the freshwater. This increase of freshwater could derive from the expansion in this phase of the alluvial plain environment, due to a wetter climate; moreover another cause of the decrease of carbon isotope could be the shift of the thermal water circulation to East, where subsequently, in Albegna Basin, travertine deposits are hosted (Barilaro et al., 2012; Ronchi and Cruciani, 2015. Else the thermal waters were more deeply circulating in Phase 3 than during the Phase 1 and the Phase 2.

Concerning the individual travertine facies, the isotope values result to be significantly different in the same facies, but there is not evident differences between the various facies. The travertine systems are characterized by intermittent flow of the hydrothermal water that can also change rapidly its paths towards areas with more accommodation space, leaving the already precipitated carbonates subjected to the weathering. In the studied travertines it caused the development of a marked red and black

colour due to the oxidation of Fe. Instead white travertines probably were rapidly covered by other precipitated carbonates and less subjected to the weathering than the others. This is reflected also on the carbon signature that in the red to black travertines results to be similar to the $\delta^{13}C$ values of the meteoric cements.

Focusing only on white travertines of phase 1 and 2, the carbon signatures of the different facies can be grouped in different clusters. According to Fouke et al. (2000), Pentecost (2005) and Kele et al. (2008) the causes of the shift of $\delta^{13}C$ can be found in partial CO_2 removal during degassing, that has the major effect on the carbon isotope composition, due to the preferential loss of ^{12}C, leaving the thermal water dissolved carbon enriched in ^{13}C. In the upper Messinian travertines of the Albegna Basin crystalline dendrite cementstone (Facies F5) show the highest carbon values. According to Guo and Riding (1998), Rainey and Jones (2010?) and Özkul et al. (2014) this facies precipitates under high energy flow on terraces walls, characterized by high CO_2 degassing that promotes the precipitation of calcite dendrite crystals. Similar conclusion could be given for facies F3, which is often characterized by a crystalline coating. On the other hand the lowest carbon values occur for facies F8 that is made of skeletal remains and faecal pellets, and they are interpreted as deposited under low energy conditions in distal pools, where the degassing is less with respect to the terraces walls.

According to Fouke et al. (2000), Pentecost (2005) and Kele et al. (2008) the carbon values have a positive trend that reflects the distance from the vent of the deposits and the impoverishment of the waters in ^{12}C. This trend in the upper Messinian Albegna Basin travertines is shown only in phase 3, where the samples of log CE that belong to the distal area of the travertine system, are characterized by higher values of $\delta^{13}C$ than the samples in the active quarry, considered closer to the hydrothermal vents (cf. Fig.2.3).

The causes of positive shift of $\delta^{18}O$ might be due to the removal of H_2O during evaporation, resulting to be the dominant oxygen isotope controlling factor over degassing and disequilibrium precipitation (Chafetz and Lawrence, 1994; Fouke et al., 2000; Pentecost, 2005; Kele et al., 2008; Deocampo, 2010). CO_2 degassing would not cause an appreciable change in $\delta^{18}O$ composition of the dissolved carbon precipitates. H_2O evaporation removes a significant amount of oxygen from the system enriched in ^{16}O under both kinetic and equilibrium conditions (Kitano, 1963; Gonfiantini et al., 1968; Friedman, 1970; Pentecost, 2005; Sharp, 2007).

In the studied travertines $\delta^{18}O$ values do not depend from the colour of the rock linked to a possible weathering. Moreover it is difficult to distinguish different clusters linked to the depositional fabrics. The average of oxygen isotope in phase 1 results to be the highest of the 3 phases, even if minor values are expected correlated with higher water temperatures. Also in phase 3 the samples of log CE, in the distal area with respect to the supposed hydrothermal vents, show lighter oxygen values than the samples of the active quarry, developing an atypical inverse covariance with the carbon values from the proximal to the distal environment. It can explained due to a mixing of hydrothermal water with meteoric freshwater, major in the distal area, that enriched the water of ^{16}O.

4.6Conclusions

1) Petrographic analysis of the upper Messinian Albegna Basin travertines indicates that a wide variety of calcite precipitates occurs. The primary travertine deposits consist of a mixture of clotted peloidal micrite, microsparite and sparite (p1) that arrange in boundstones or grainstones characterized by an irregular framework, or they develop coatings around different clasts, or precipitate as faecal pellets developing peloidal grainstones.
   These travertines consist also of crystalline dendrite spar (ds) that develop crystalline dendrite cemenstones or make crystalline coatings around different clasts.
2) The other type of calcite precipitates derived from diagenetic events. Detrital micrite (mi) is the product of dissolution of the primary travertines and precipitate as geopetal infill. Series of cements include different morphologies of microsparite and sparite. Bladed calcite (b) and microsparite to sparite (m1), speleothem (sp), microsparite to sparite (m2), sparite (s) scalenohedral calcite (sh) and blocky equant calcite (bl). The burial diagenetic environment is characterized by the growth of the blocky calcite that is characterized by drusy morphology.
3) Cathodoluminescence and electron probe analyses on calcite cements and the content of Mn^{2+} and Fe^{2+} highlighted 6 different type of cement generations, distinguishing between the luminescent cements precipitated in the meteoric environments from those precipitated in the burial environments.
4) Combining the different analyses, this study permitted to develop a paragenetic sequence made of 21 events that consist of dissolution and corrosion, precipitation of the described types of calcite, fracturing, precipitation of Fe-Mn(OH) and clay minerals, geopetal infill and compaction, concluding that the Late Messinian Albegna travertines were subjected to a burial history passing through 3 diagenetic environments: hydrothermal, meteoric and burial, reaching a deep of least 300 m proved by the occurrence of stylolites and a luminescent calcite particularly enriched in Mn^{2+}. Then the succession was uplifted returning to a meteoric environment, exposed to the weathering as it is in the present-day outcrops.
5) Carbonate isotope value range in the studied travertines seems to depend on the CO_2 degassing and shows that $\delta^{13}C$ is a useful tool to distinguish the thermogene travertine lithofacies. Lithofacies that precipitate under high-energy conditions with high rate of CO_2 degassing such as crystalline dendrite cementstone are characterized by higher values of $\delta^{13}C$ than lithofacies enriched in skeletal or phytoclastic remains (facies F7 and F8). Decrease of $\delta^{13}C$ values are due to the mixing of hydrothermal waters with freshwater, or due to the presence of a meteoric freshwater input in the system, or due for the flow of diagenetic meteoric fluids.
   Mixing of meteoric freshwater enriched in ^{16}O with hydrothermal water, could take and justify unexpected variations of $\delta^{18}O$ in a travertine system, where $\delta^{18}O$ depends principally on water temperature and H_2O evaporation, as happened in phase 3 of the studied travertines where the $\delta^{18}O$ values decreased from the vent area to the distally parts.

Chapter V

The hydrothermal travertines of the Acque Albule Basin (Tivoli, Central Italy): facies character and architecture

Abstract

The sedimentary succession of the extensional Acque Albule Basin (Tivoli, Central Italy) includes Pleistocene fluvial lacustrine deposits intercalated with volcanic deposits, which are overlain by tens of metres thick hydrothermal travertines. In the literature, travertine deposition is related to hydrothermal circulations hosted in the Mesozoic-Cenozoic carbonate bedrock, favoured by extensional tectonics and relatively high geothermal gradients linked to the Colli Albani volcanism. To investigate the Acque Albule travertines, six boreholes were drilled and cored along a 3 km long N-S transect. The travertine unit is wedge-shaped (20-45 m thick) and gently dips towards the South, conformably to the topographic gradient. In the southernmost part, travertines are intercalated with fluvio-lacustrine siltstone and sandstone and overlay fluvial conglomerates of the Aniene river. Stratigraphic relationship between the travertine unit and the underlying succession suggests that the onset of hydrothermal carbonate precipitation followed the deposition of organic matter-rich mudstones of marsh environment over the studied area. The travertine succession is characterized by the occurrence of numerous centimetre- to a few metres thick intraclastic/extraclastic wackestone to floatstone/rudstone indicative of periods of non deposition and erosion, due to temporary interruption of the flow of thermal water out of the vents. Four major unconformities, 0.5-8 m thick, are recorded across the whole 3 km transect allowing lateral correlations. The travertine unit can be divided in three zones (proximal, intermediate and distal) with respect to facies composition and depositional environments. In the northern proximal area, close to the hydrothermal vents, travertines are characterized by facies types indicative of shallow ponds and pools of terraced slopes, such as clotted peloidal micrite dendrites boundstone, radial pisoid grainstone, coated reeds, clotted peloidal micrite grainstone to boundstone. The low-angle terraced system deposition alternates with a few metres thick, lens shaped units, rich in coated vegetation and Charophytes boundstone to packstone. The intermediate depositional zone, nearly 1-2 km southward of the proximal area, is characterized by 10 m thick, smooth slope facies with crystalline dendrite cementstone, laminated boundstone and radial

pisoid grainstone with dips up to 45°. Slope beds are overlain by shallow pool facies following a several metres thick unconformity. The distal zone, in the southernmost part of the studied transect, consists of travertine ponds dominated by coated vegetation and Charophytes due to cooled-down thermal water or to freshwater input, intercalated with siltstone and sandstone. Intervals of shallow lacustrine/palustrine facies with abundances of carbonate coated vegetation and Charophytes characterize most of the distal pond succession in the southern end of the analysed transect, and are, only locally, comprised within the proximal and intermediate zones. This occurrence of facies comparable to the distal pond zone also in proximal areas might be related to the general low temperature of the Acque Albule thermal water at the vent (present-day 23°C) and/or to events, related to the Pleistocene climate or local hydrology, during which thermal water mixed with freshwater to allow the growth of plants and Charophytes also in proximity of the hydrothermal vents.

5.1 Previous study about Tivoli Travertine (*Lapis Tiburtinus*)

For the geological setting of the Acque Albule Basin refer to Chapter 2 from the paragraph 2.4 to 2.7.

The ancient name of travertines was altered from the Latin name *Lapis Tiburtinus* that means stone of Tibur, now Tivoli. This stone was used from the 3rd century B.C. by the ancient Romans to the construction of buildings, due to the simplicity of mining, transport and processing. Moreover travertines are resistant in the time making it better than other stones such as the tuff, abundant in the Roman area and also used in the Roman architecture.Chafetz and Folk (1984) interpreted the deposits between Bagni di Tivoli, Tivoli and Guidonia area, as lake-fill deposits, made of thick, horizontally stratified and laterally extensive travertine accumulations. These deposits are primarily composed of laterally continuous and vertically stacked thin layers of shrubs, which represent summer accumulation, intercalated with fine laminated muddy layers and thicker crudely laminated mud, interpreted as winter deposits. These layers are laterally interrupted by zones composed of calcite crystal rays, intraclasts, and inorganic pisoids that represent spring deposits at the bottom of the lake. The lake-fill deposits are interrupted vertically by paleokarst zones due to the periodic drainage of the lakes.

Faccenna et al. (2008) reconstructed in a 3D model the shape of the *Lapis Tiburtinus* sedimentary unit (Fig. 5.1), interpreting it as a plateau made of travertine subhorizontal benches, separated by erosional surfaces, with a progradational trend toward the South. This alternating stages of deposition and erosion were controlled by fluctuations of the water table level in the Acque Albule Basin. Paleoclimate cycles possibly contributed to modulate the water table in the Acque Albule Basin and therefore the travertine depositional-erosional cycles. However, paleoclimate oscillations alone are not sufficient to fully explain the observed travertine cycles and travertine deposition onset and termination. Additional influencing factors, such as fault-related deformation and volcanic activity at the nearby Roman volcanic district (cf. Chapter 2, paragraph 2.6), could contribute to the control of the travertine deposition.

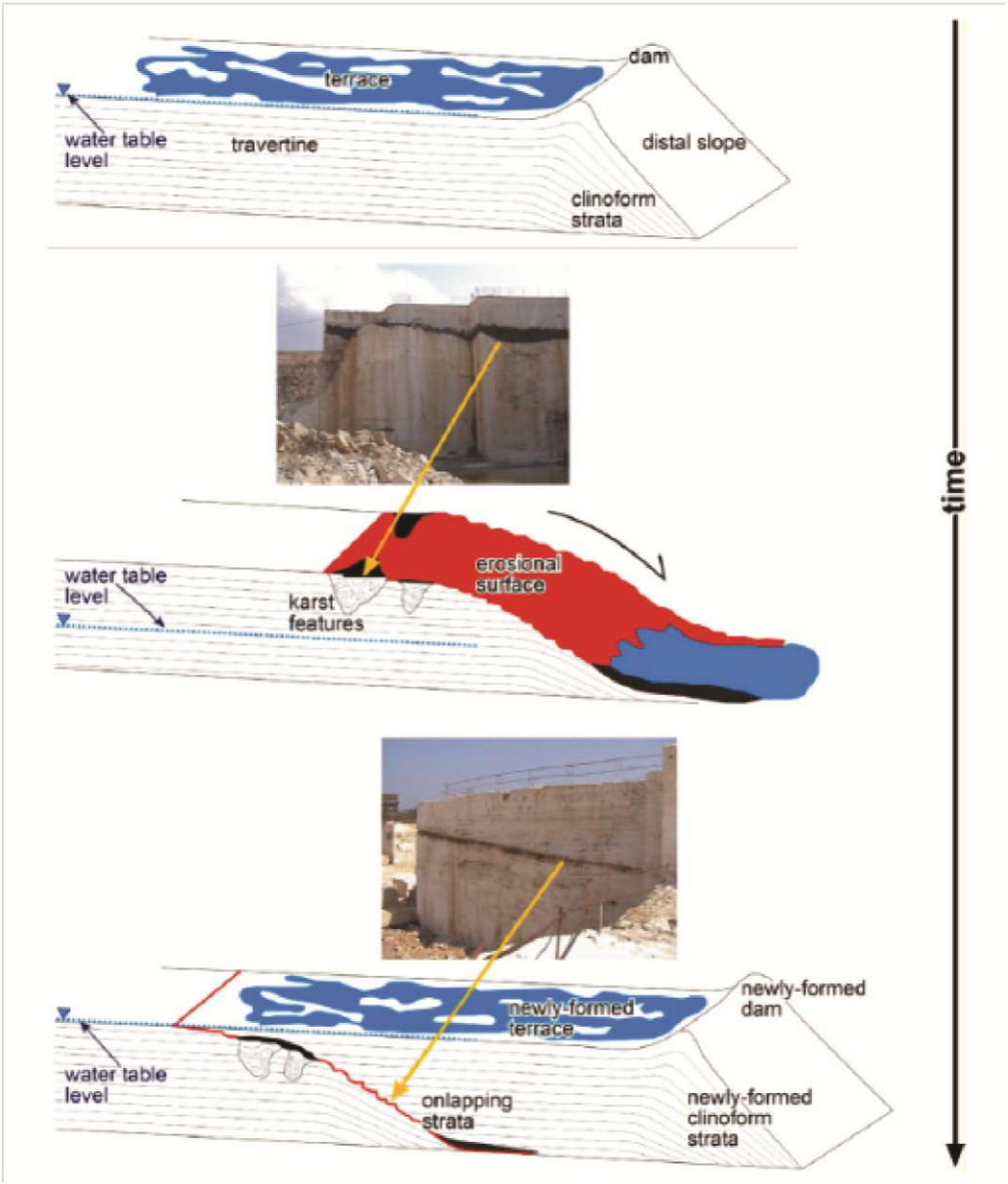

Figure 5.1. Conceptual model showing the relationship between cycles of travertine deposition, erosion and fluctuation of the water table in the basin (Faccenna et al., 2008).

5.2 Size shape and age of travertine deposit

The *Lapis Tiburtinus* travertines built a plateau with tabular shape, which covered an area of 20 km^2 with an average thickness of 40-50 m thick, for a total volume of 1 km^3 (De Filippis et al., 2013) (Fig. 5.2 A-B). The maximum thickness is over 85 -90 m. The depocentre coincides with the underlying N-striking fault and with the associated emergences of thermal waters and sinkholes toward its western side (Faccenna et al., 2008). To the west of the fault the travertine thickness rapidly decreases, instead toward the east, the north and the south sides of the plateau, the thickness gently decreases (Faccenna et al., 2008). The travertine deposit has a typical progradational pattern with an upward steepening of strata toward the south (De Filippis et al., 2013). The travertine body is composed of a sequence of four benches separated by erosional surfaces (called by Faccenna et al., 2008: S1, S2, S3 S4 and S5, from the younger to the older), with a thickness of benches that varies up to a maximum of about 8-10 m (Faccenna et al., 2008; De Filippis et al., 2013). The benches grow in a sub-horizontal to southward aggradational way, with the bottom of each travertine bench onlapping the underlying erosional surfaces (Facenna et al., 2008; De Filippis et al., 2013) (Fig. 5.3). Also the five erosional surfaces dip gently southward and usually are marked by thin (less than about 1 m) soil deposits associated with conglomerates and karstic features (Faccenna et al., 2008; De Filippis et al., 2013). The erosional surfaces are subparallel to the depositional benches, but often are oblique, cutting through the benches and also the older erosional surfaces (Facenna et al., 2008; De Filippis et al., 2013). The age of the travertine deposits ranges from 115 and 30 ka (Faccenna et al., 2008). The ages of the each erosional surfaces were calculated by Faccenna et al. (2008): S5 = 99 ± 5 ka, S4 = 82 ± 9 ka, S3 = 56.5 ± 8 ka, S2 = 44 ± 4 ka and S1 = 34 ± 5ka. Considering the average thickness of the Tivoli plateau, a deposition rate of 0.4 mm/yr is obtained (Faccenna et al., 2008); this rate should correspond with the average vertical subsidence rate of the Acque Albule Basin (De Filippis et al., 2013). The travertine deposition terminated beneath the surface S1: the upper and youngest surface separates the travertine body from the above “testina” layer, 3-4 m thick in average, consisting of a poorly compact limestone capping most part of Tivoli plateau and dated 29 ± 4 ka (Faccenna et al., 2008).

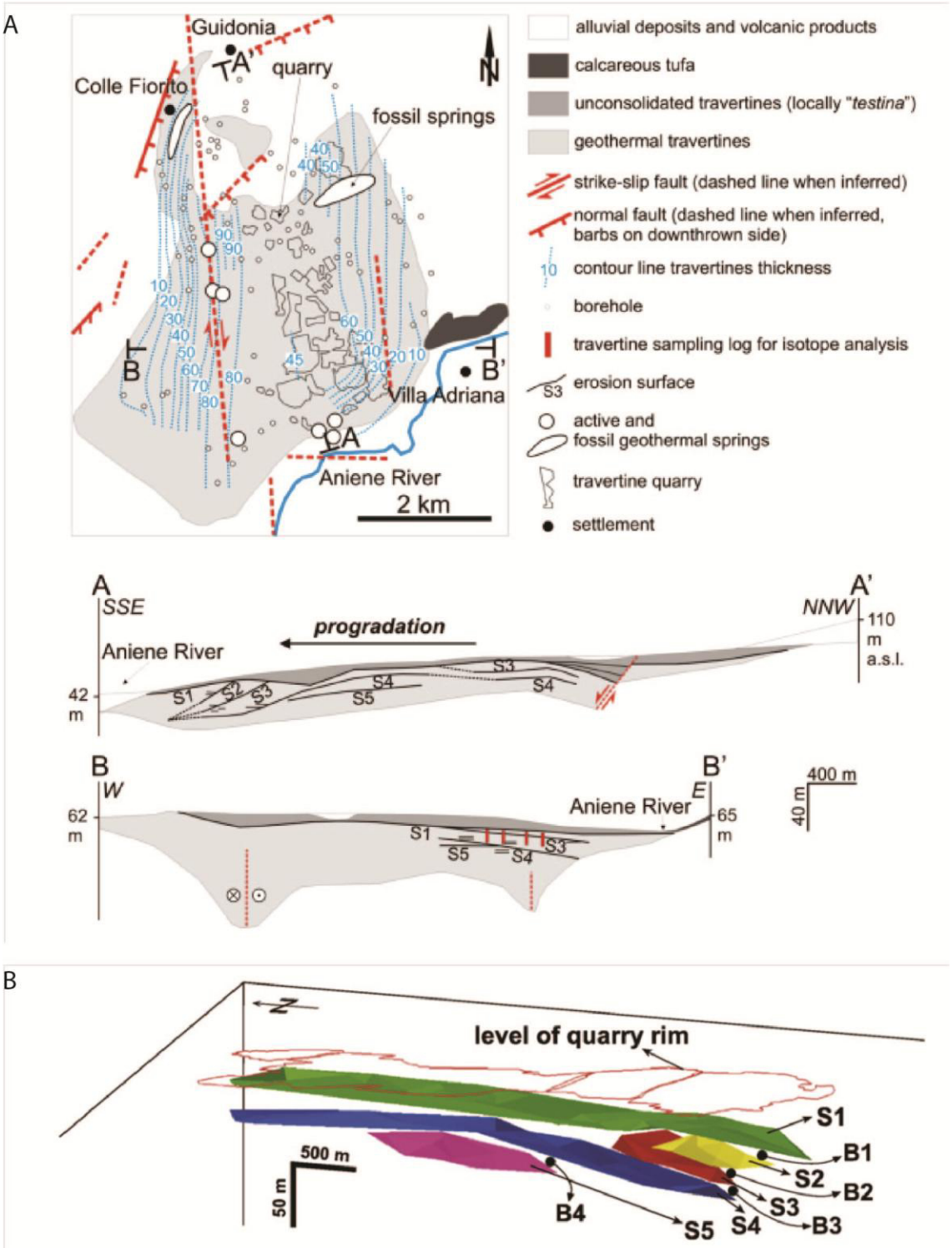

Figure 5.2. A. Geological map of Tivoli plateau and related cross-sections (De Filippis et al., 2013, modified from Faccenna et al., 2008). In the A-A' cross-section is highlighted the southward progradational pattern of the travertine strata (De Filippis et al., 2013). B. Lateral view of the three-dimensional model showing the spatial relationship between the S1, S2 , S3, S4 and S5 erosional surfaces across the travertine deposit (Faccenna et al., 2008).

5.3 Material and methods

Across the nearly 3100 m long transect in the active quarry area of the Acque Albule travertines located west of the town of Tivoli (Fig. 5.3), seven bore holes (labelled from S1 to S7) were drilled recovering nearly 200 m of travertines (with exception of S5 that had very limited recover) and underlying volcanic and sedimentary deposits. The seven borehole cores were analysed and described at the millimetre scale through mesoscale core description with a hand-lens, photographs and petrographic analysis of thin sections. Eleven travertine carbonate facies were distinguished on the basis of texture, fabric and components. An additional deposit that represents post/travertine precipitation sediment filling was also identified. These carbonate facies are described in detail in Table 5.1. The terrigenous deposits underlying the main travertine unit were distinguished in ten facies on the basis of composition (siliciclastic, carbonate, volcanic or volcaniclastic), grain size and degree of lithification and described in detail in Table 5.2.

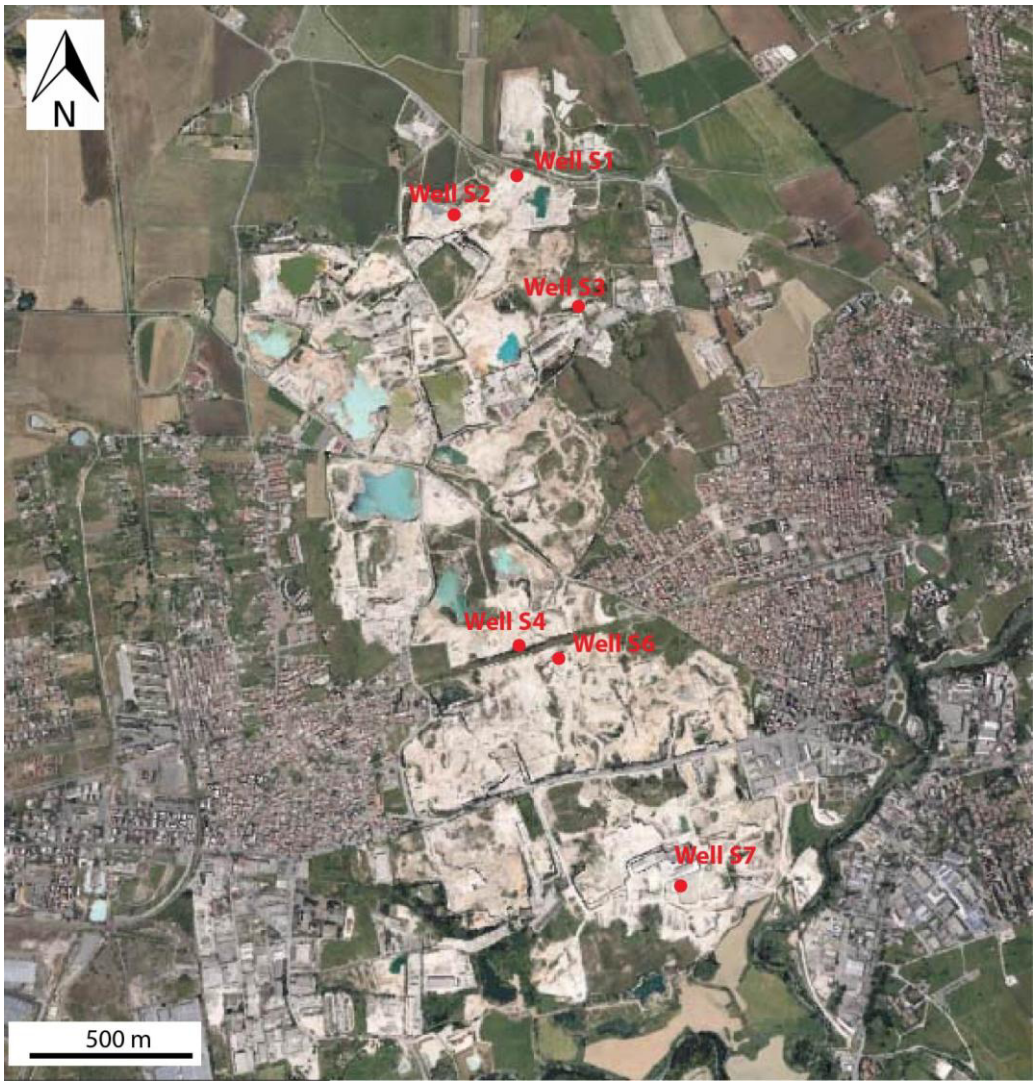

Figure 5.3. Satellite image from Google Earth shows the studied travertine area. Red points indicate the locations of the 6 wells.

5.4 Facies description and interpretation

Facies T1: Clotted peloidal micrite grainstone to boundstone with charophytes and ostracodes

Description

Macroscopically this facies consists of layers of cream coloured to light grey carbonate precipitate with a homogeneous texture, apparently resembling calci-mudstone/wackestone, made of irregular clots of carbonate mud with sparse porosity (Fig. 5.4A). Core observations show fragments and entire tubular structures with millimetre- to sub-millimetre diameters belonging to plant and algae stems, locally associated with raft fragments.

Porosity varies from sub-millimetre size round pores to centimetre-size fenestrae-like pores with sub-horizontal orientation and irregular vugs (likely associated with meteoric dissolution) or porosity consists of interparticle pores between irregular micrite clots. Pores associated with coated gas bubbles are eventually present (Figure 5.4B).

The layer thickness of facies T1 varies between 5 mm and 15 cm, reaching a bed thickness of up to 70 cm in S3 well, where between 4 m and 10 m T1 is the dominant lithofacies alternating with intraclastic wackestone/rudstone and grainstone (facies U). T1 facies is often associated with facies T2, T6 and mainly with T8, with which develops many alternations.

Microscopically the texture varies from grainstone, rarely packstone, to boundstone made of clotted peloidal micrite and microsparite forming an irregular framework (boundstone) or leiolitic peloids and irregular micrite clots (grainstone/packstone) consisting of irregular to sub-rounded aggregates of clotted peloidal micrite ranging in size from 1 mm to 100 µm, mostly 200-300 µm (Fig. 5.4C). The micrite clots/irregular peloids are made of leiolitic micrite, microsparite and peloidal micrite with peloids 10-20 µm in diameter. Facies T1 is characterized by the occurrence of charophyte stems, both in vertical life position and fragmented, with stem length of up to 0.5 mm, associated with ostracodes and gastropods (Fig. 5.4D).

Calcite cement types vary according to the sample location and depth of in the well: 1) a typical cement is equant limpid calcite producing an irregular rim around peloids and clotted peloidal micrite clots ranging from microsparite to sparite (20-100 µm) (Fig. 5.4 E, F); 2) in samples deeper than 18-20 m the previous equant microsparite/sparite is followed by prismatic cement with scalenohedral terminations (from 200-250 µm to nearly 1 mm long); 3) these two cement types are locally preceded by an irregular pendant cement. Evidences of dissolution of the micrite and equant microsparite are present in some samples.

Interpretation

The presence of clotted peloidal micrite indicates water rich in $CaCO_3$ that promotes microbial precipitation of carbonates in the photic zone (Gierlowski-Kordesch, 2010). This facies is interpreted as deposited in shallow little agitated fresh water that allows the presence of charophytes, small aquatic plants that are related to the green algae family (Johnson, 1961; Williamson and Picard, 1974). Also

the presence of ostracodes is clearly an environmental indicator of fresh water and a little agitated pond (Jaillard et al., 1993; Martin-Closas et al., 2008). Charophytes grow up to 2 m depth mainly, but can grow down to 10 m deep (Apolinarska et al., 2011), as far as they remain within the photic zone, (Gierlowski-Kordesch, 2010). According to Pentecost et al. (2006) charophytes grow in temperature water around 20° C. Moreover charophytes are indicators of high alkalinity (Pentecost et al., 2006; Apolinarska et al., 2011) The presence as well of charophyte stems and the absence of oogoniums means that they are probably dispersed by the slow flowing water and by the wind, confirming the accumulation of these deposits few metres under the water level (Murru et al., 2007). The association of these elements indicates a shallowl environment, as a large pool or a lake, characterized by richness in $CaCO_3$, alkaline Ph, temperature around 20° C and characterized by slow flowing water.

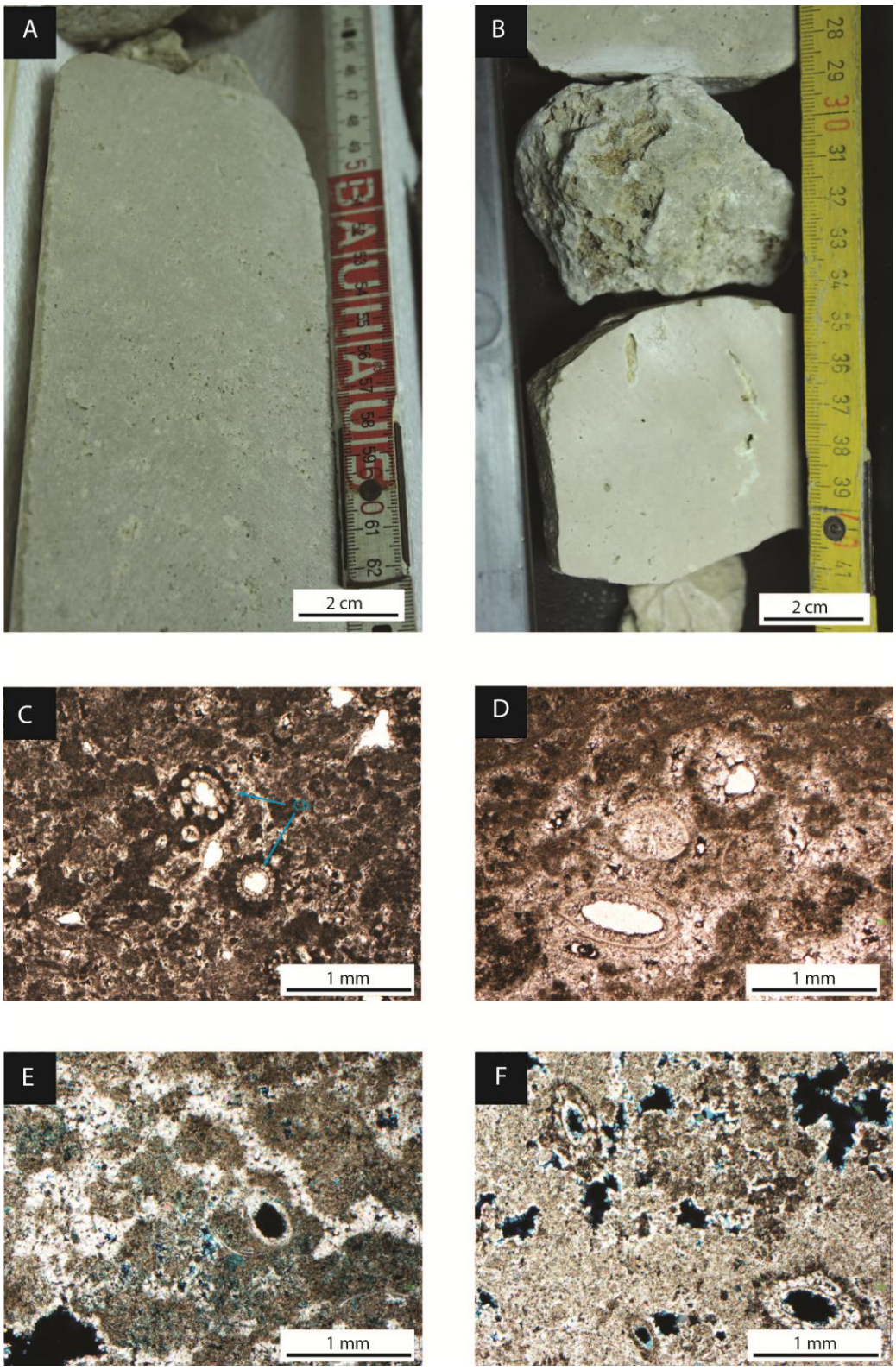

Figure 5.4. A) Macroscopically facies T1 consists of layers of cream coloured to light grey carbonate precipitate with an apparently resembling carbonate mudstone/wackestone texture, made of clots of carbonate mud and characterized by the presence of plant and algae remains. B) Porosity varies from sub-millimetre round or elongated mouldic pores to millimetre vugs. Rarely pores associated with coated gas bubble occur. C) Microscopically the texture varies from grainstone to boundstone; grainstone is made of leiolitic peloids and irregular micrite clots. Facies T1 is characterized by the presence of charophyte stems (ch). D) Other skeletal components are ostracod and gastropod shells. E) The equant sparite/microsparite is the typical cement that fills the interparticle porosity, ranging from 20-100 µm in size. In samples deeper than 18-20 m the

equant spirite is followed by prismatic cement with scalenohedral terminations. F) The cementation can fills the intraparticle porosity of charophyte stems and plant remains.

Facies T2: Clotted peloidal micrite dendrite boundstone

Description

Macroscopically facies T2 consists of white to light cream millimetre to centimetre-size dendritic branching structures (from 2 mm to 5 cm thick), vertically oriented and adjacent to each other so that to make layers of boundstone (Fig. 5.5A). These layers are often sub-horizontal or undulated and slightly inclined. Millimetre-centimetre thick layers of dendritic structures next to each other occur vertically stacked, separated by millimetre-thick micrite layers or crystalline crusts (facies T12). Facies T2 layers make intervals up to 10 cm in thickness rarely 20 cm (as at the top of S2 well). Sometimes clotted peloidal micrite dendrite boundstone forms centimetre to decimetre-size convex-upward structures forming either pool rims or bioherms (Fig. 5.5B). The macroscopic porosity is due to gas bubbles trapped in between the dendritic structures, which could be sub-millimetre in size up to 0.5 mm in diameter. Most of the porosity consists of inter-branching up to a few millimetre-size pore spaces in between laterally adjacent dendrites. Vertical porosity from one to the overlying layer seems limited by the millimetre-thick laminae separating the stacked boundstone layers. Facies T2 is associated with facies T4, T6 and T12.

Microscopically the clotted peloidal dendrites are built by irregular sub-rounded peloids (10-20 µm in diameter, rarely up to 50 µm; Fig. 5.5C) embedded in micrite and cloudy microsparite (10-20 µm equant crystals) (Fig. 5.4D) forming branches a few hundred microns to a few millimetre long departing from a central point or elongated stem and diverging outward. These clotted peloidal micrite dendrites have been addressed as shrubs and bacterial shrubs by Chafetz and Folk (1984) and Chafetz and Guidry (1999), respectively. Shrubs range from densely packed to loosely packed laterally: in the first case the framework is more chaotic and the shrub shape is hardly recognizable, constituted by small lumps of peloids (100 µm). The peloids are immersed in microsparite (30-50 µm), which is more turbid within the peloid lumps. Some dendrites have individual branches with a geometric rhombic shape with sharp boundaries made of dense micrite. Other rare components in the T2 facies are ostracodes, gastropods and bivalves millimetre-size. Ostracodes can also occur within the large pores overlain by micritic sediment and scalenohedral cement as they had colonized the internal cavities of the shrub boundstone.

The first cement phase in between the clotted peloidal micrite and microsparite branches is an equant calcite microsparite to sparite (20-80 µm in size). In several millimetre-large pore space equant cement is followed by prismatic crystals with scalenohedral terminations (a few 100 microns to nearly 1 mm), which can develop curved gothic arch terminations (Fig. 5.5E,F). In some cases, as in other facies the equant and scalenohedral cements are preceded by irregular pendant and microstalactitic cement. Some clotted peloidal shrubs shown and irregular patchy calcite sparite substituting the original micrite forming the branches.

Interpretation

The causes of precipitation of clotted peloidal micrite fabrics, mainly the shrub morphologies, in hydrothermal waters, have been debated in several studies. Krumbein (1979a) demonstrated that the precipitation of the clotted micrite is due to the microbial activity and Chafetz and Folk (1984) concluded that the dominant precipitation process, even within the hydrothermal water, is due to the microbial activity; moreover formation of shrubs requires a harsh environment, conditions satisfied in lakes fed by H_2S (Chafetz and Folk, 1984). Guo et al. (1996) concluded on the basis of the $\delta^{13}C$ values of this type of precipitates, that the shrub formation is microbially influenced. Instead Pentecost (1990) proposed that the abiotic precipitation for the peloidal shrubs, based on the lack of microbial remains in travertine deposits of Yellowstone, but Fouke (2011) and Fouke et al. (2000) demonstrated that the presence of these communities in the same travertines. This deposit grows up in pools of terrace systems, or depression systems or sub-horizontal layers (Guo and Riding, 1998) and in other several environments as reported by Gandin and Capezzuoli (2014), as sub-vertical walls of semi-dried channels, on the fringe of very shallow slow flowing water or within macroterraces and microterraces too. Gandin and Capezzuoli (2014) observed that the growth of shrub clusters in environments characterized by rapid evaporation of very thin sheets of water. The clotted peloidal micrite boundstone of Tivoli are rich in clotted micrite and shrub forms, thus this facies is interpreted as deposited in low-energy zones as pools of terraces in slope systems and in sub-horizontal ponds.

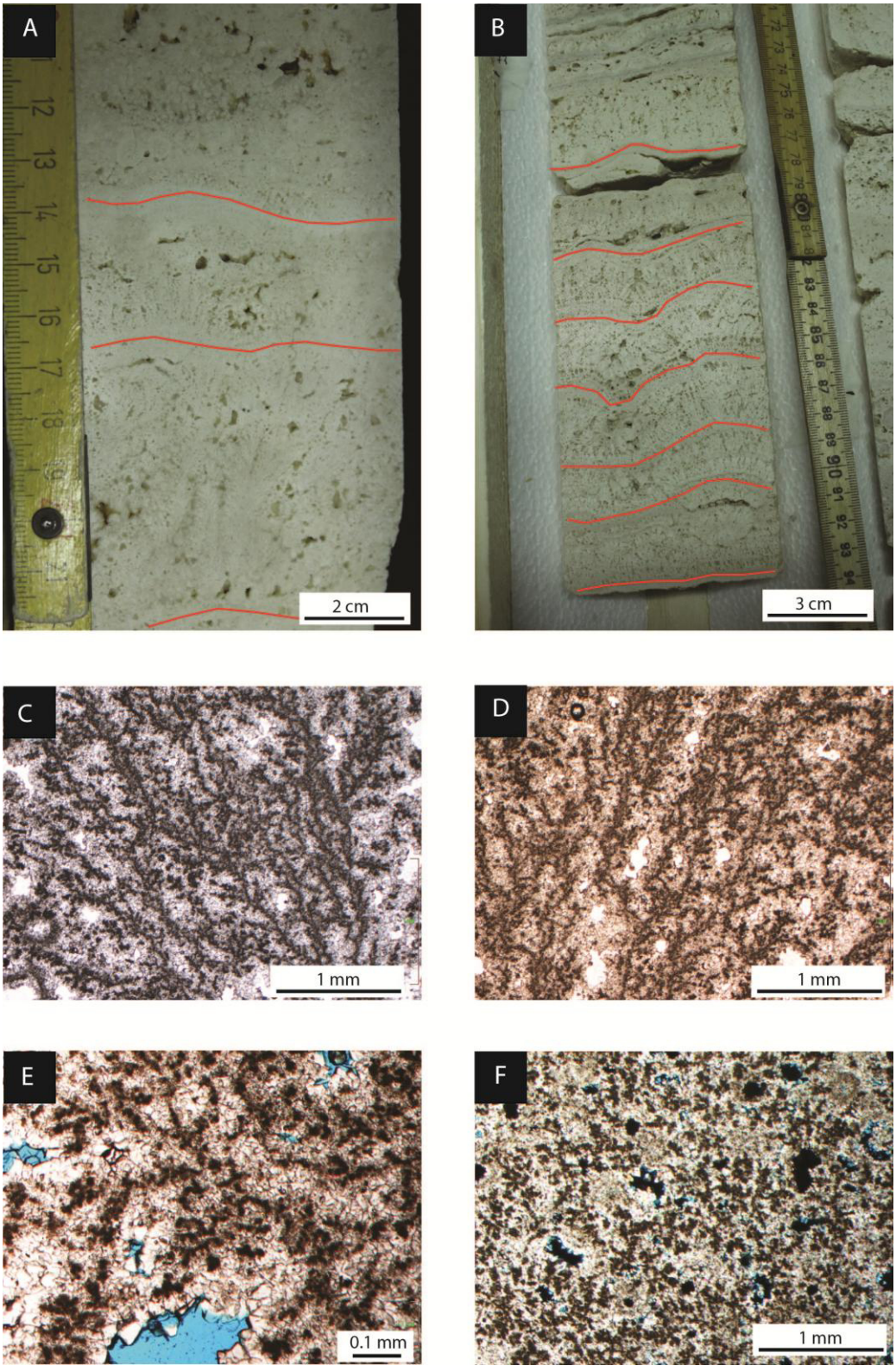

Figure 5.5. A) Macroscopically facies T2 consists of white or light cream millimetre to centimetre-size dendritic structures vertically oriented and laterally adjacent to each other making boundstone texture. B) Layers of facies T2 are often undulated and form centimetre to decimetre-size convex upward structures forming pool rims or bioherms. C) Microscopically the clotted peloidal dendrites are made by sub-rounded peloids forming branches departing from a central stem. D) The branches are embedded in micrite and microsparite. E and F) There are two main cement phases recognised by the occurrence of equant micrite and microsparite (20-80 µm in size), followed by prismatic crystals with scalenohedral terminations in millimetre-size pores.

Facies T3: Crystalline dendrite cementstone

Description

Macroscopically crystalline dendrite cementstone develops opaque white and dense crusts made of elongated branching dendritic calcite crystals one adjacent to each other, which in the more developed structures, present horizontal growth laminae and are vertically stacked in more layers (Fig. 5.6A). This precipitated fabric forms layers about 5 mm up to nearly 20 cm (in S6) in thickness, but mainly around 2-5 cm. Very often this facies makes convex-upward rim structures of different size, from a few millimetres to decimetres (Fig. 5.6B). Facies T3 is often laterally associated with facies T6 or T2 and it is vertically associated with facies T5 and T12.

Layers of crystalline dendrite cementstone are often tight or with minor porosity in between inter-branching areas between adjacent crystals.

Microscopically crystalline dendrite cementstone consists of centimetre-thick branching crystals (Fig. 5.6C) made of lozenge-shaped turbid inclusion-rich crystals 100-600 µm long (40-60 µm wide) (Fig. 5.6D, E) departing outward, often from a central elongate crystal acting as a stalk. The dentrites develop vertically. The central stalk crystal, when present, extinguishes as a unique crystal under crossed polarizers. In some cases, the central stalk crystal is absent and pairs of lozenge crystal branches form "v" vertically stacked on top of each other. The central stalk and laterally branching crystals have uniform extinction but they are so turbid as they consisted of an aggregate of micrite acquiring euhedral rational crystal faces.

The dendrites are surrounded by sparse cloudy microsparite (10-20 µm), limpid equant microsparite to sparite (20-100 µm) followed eventually by prismatic scalenohedral cement (Fig. 5.6F). Some dendrite turbid crystals are partly replaced by limpid calcite spar, which in crossed polarizers has the same extinction as the surrounding cement sparite. In some cases, the distinction between clotted peloidal micrite dendrite and crystalline dendrites is not apparent because there are some transitional forms of dendrites made mostly of micrite and lacking crystal extinction in crossed polarizers but with shapes of the branches resembling the crystal dendrite cementstone.

Interpretation

The abiotic (Rainey and Jones, 2009) precipitation of crystalline dendrite is controlled by the supersaturation of the hydrothermal water in Ca^{2+} ions (Jones and Renaut, 1995). These fabrics are associated with high-energy environments in smooth and steep slopes, terraced slopes, rims and dams (Guo and Riding, 1998; Rainey and Jones, 2009; Özkul et al., 2014), directly from very thin sheet of water (Guo and Riding, 1998, 1999; Gandin and Capezzuoli 2008). The feather aggregates can be observed disposed normal to the substrate and parallel to the water flux, progressively shaping the microterraces (Gandin and Capezzuoli, 2014). Then the crystalline dendrite of Tivoli travertines are interpreted are as deposited in terraced slope, developing rims, in condition of high water supply and high evaporation rates, with supersaturation of them in Ca^{2+}.

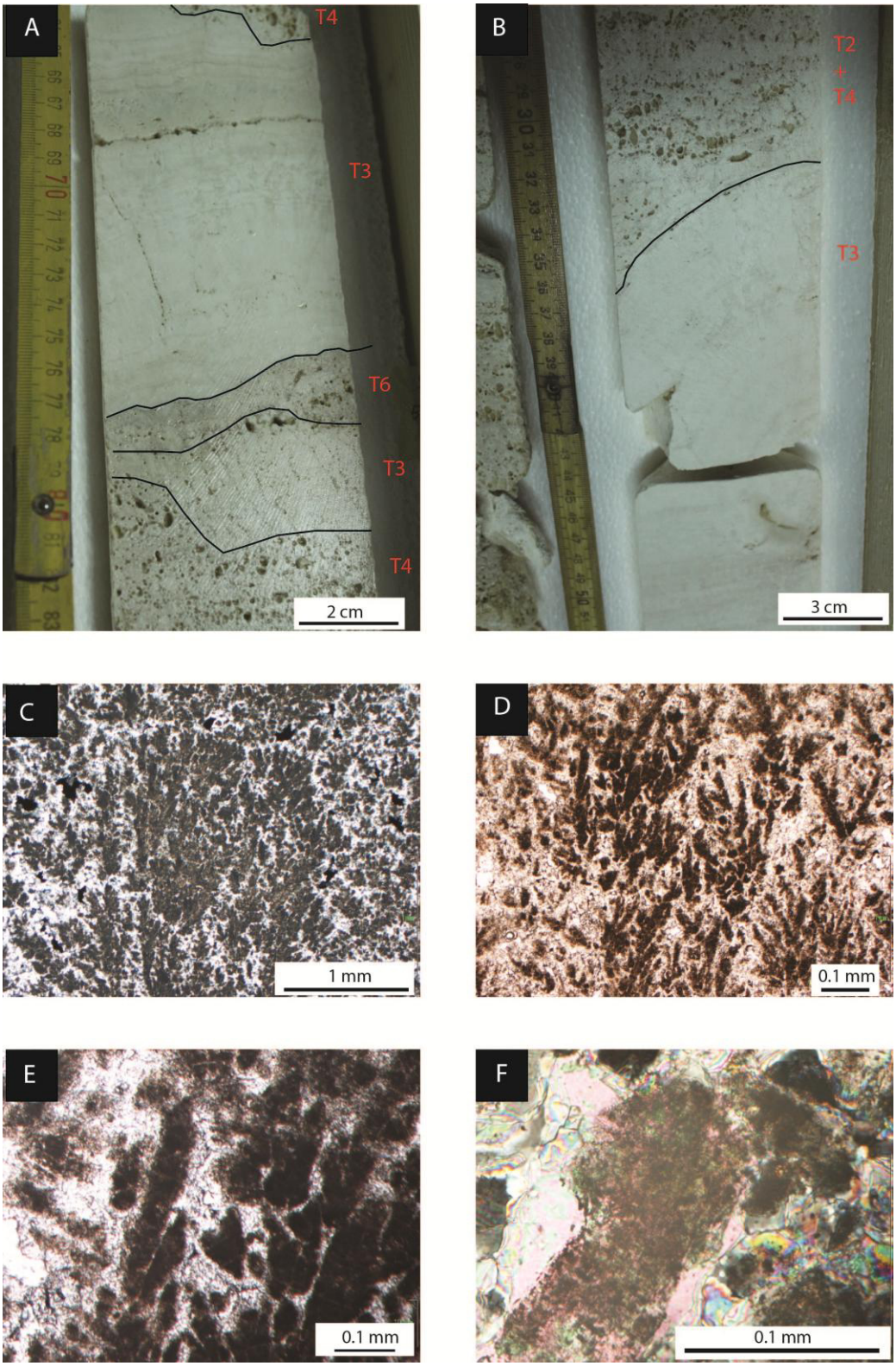

Figure 5.6. A) Crystalline dentrite cementstone develops opaque and dense crusts made by elongated branches of calcite crystals one adjacent to each other. B) These structures build convex-upward rim structures up to decimetre-size, and often laterally is associated with facies T6. C) Crystalline dendrite cemenstone consists of centimetre thick branching crystals departing outward from a central elongate crystal acting as a stalk. D) The branching crystals are rhombic in shape, 100-600 µm length and 40-60 µm wide. E) This crystals are turbid due to the occurrence of fluid inclusions. F) The dendrites are surrounded by cloudy microsparite, limpid equant micrite to microsparite and within the pores these cements can be followed by prismatic scalenohedral cement.

Facies T4: Coated gas bubble boundstone

Description

Macroscopically the coated bubble boundstone consists of light cream (rarely light grey) micrite precipitates around rounded hollow pore spaces (Fig. 5.7A) with spherical to elongated vertical shape, varying in size from sub-millimetre (0.5 mm) to 5 mm of diameter (Fig. 5.7B); sometimes a few bubbles are vertically stacked and welded together forming trains 2-3 cm long. In other cases the micrite coatings around the gas bubbles form a framework. Facies T4 develops mainly layers from 5 mm to 5 cm in thickness, but which can reach 20 cm (in S1). The coated gas bubble boundstone is often associated with facies T2, but it can occur associated with facies T6, T8, T3 and T5; moreover sparse coated gas bubbles develop in patches in facies T1. It is common to observe the coated bubble boundstone overlying the unconformity facies together with T8 facies. Porosity can reach several millimetre size but it appears isolated associated with individual unconnected bubbles.

Microscopically the thin layers (5-100 µm) of carbonate precipitates, coating the hollow structure, consist of micrite and microsparite forming a concentric layer around what was a gas bubble (Fig. 5.7C). On the outer surface of the bubble coating micron-size micritic dendritic structures can develop. Bubbles can be welded together forming a framework or be sparse in a peloidal grainstone with sparse clots of clotted micrite, bubble and other facies intraclasts, raft fragments and ostracodes (Fig. 5.7D).

Internally, the hollow structure coated by micrite is lined by cement: equant microsparite to sparite 20-200 µm and eventually prismatic cements (100-250 µm) (Fig. 5.7E and F).

Interpretation

The gas bubbles are easily broken and will be preserved only if they are trapped and coated by precipitated calcium carbonate (Chafetz and Folk, 1984; Guo and Riding, 1998; Jones and Renaut, 2010). The formation of this coating occurs only in low-energy environments such as pools (Chafetz and Folk, 1984; Guo and Riding, 1998; Özkul et al., 2002; Gandin and Capezzuoli, 2014), where there is sufficient time for incipient lithification of calcium carbonate around gas bubbles (Guo and Riding, 1998). The main source of gas bubbles is microbial activity (Chafetz and Folk, 1984; Guo and Riding, 1998; Jones and Renaut, 2010); mainly shrub facies is an important source of gas bubble production (Chafetz and Folk, 1984). According to Jones and Renaut (2010) bubbles can be produced in hot spring by CO_2 produced by boiling water. Bubbles can have an elongate shape, because gas bubble tries to escape vertically or laterally, and moreover they can form vertically stacked trains of bubbles when the rapid calcification can capture and join some of them in a unique coating (Chafetz and Folk, 1984). The coated gas bubble boundstone is interpreted, in the Tivoli travertines, as deposited in ponds and pools, from stagnant to little agitated water conditions.

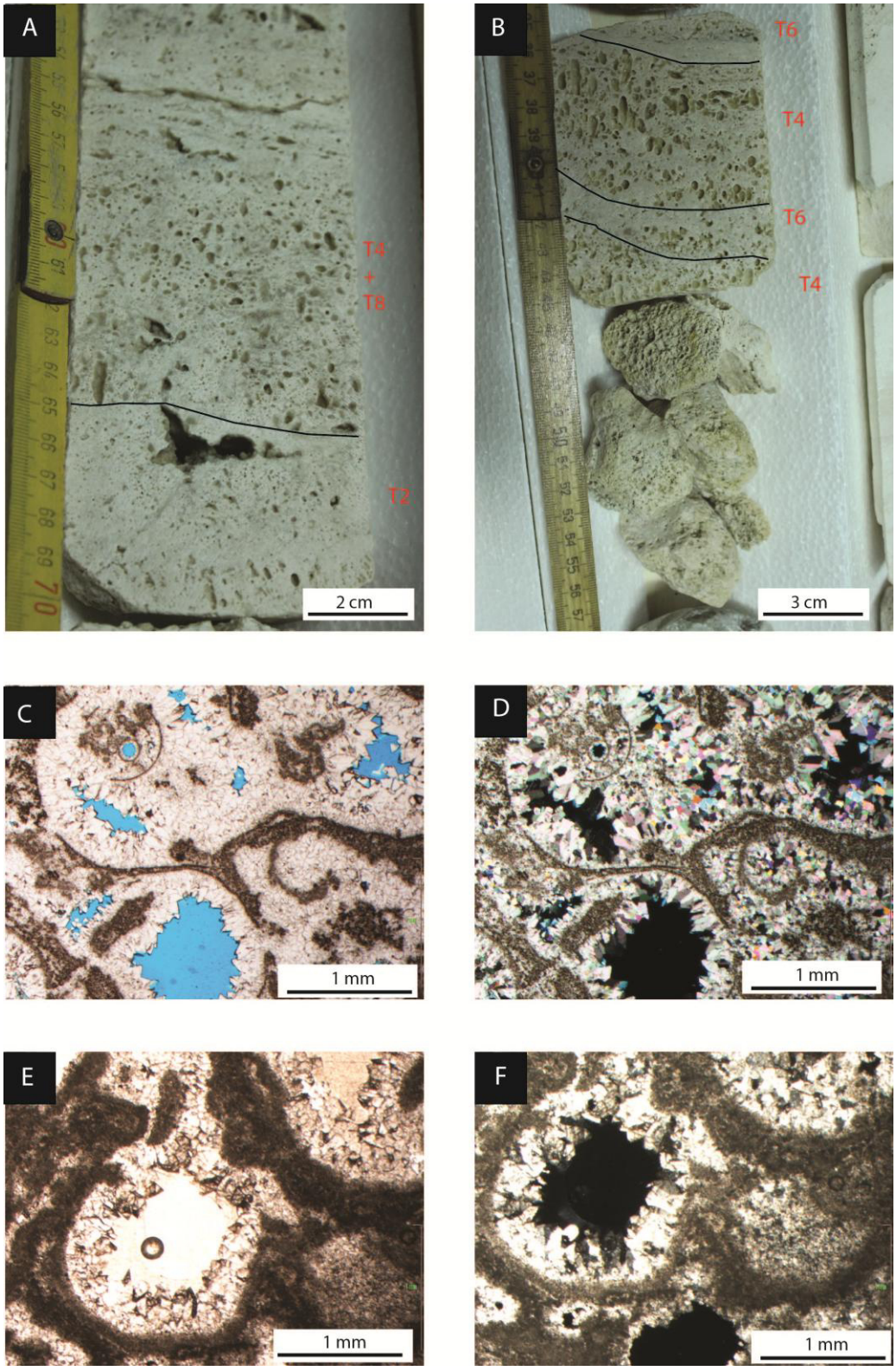

Figure 5.7. A and B) the coated bubble boundstone consists of light cream micrite precipitated around hollows with spherical to elongated vertical shape, varying in size from sub-millimetre to 5 mm in diameter. C) The hollow structures are coated by thin layers of micrite and microsparite forming a concentric layer around what was the gas bubble. D) Isolated ostracods, raft and peloidal clots occur the carbonate precipitate. E and F) Internally the hollow, the micrite coating is lined by cement both equant microsparite/sparite and prismatic cement.

Facies T5: Laminated boundstone

Description

The laminated boundstone consists of dense layers, white in colour of wavy laminae up to 2 mm thick (Fig. 5.8A). These layers are undulated and develop upward convex and concave morphologies, with inclinations that vary from sub-horizontal to sub-vertical (Fig. 5.8B). The thickness of these layers varies between 5 mm and 24 cm (in S4), with average around 5 cm. Facies T4 includes lens-shaped elongated porosity up to 3 cm wide, in between the laminae, that gives a porous appearance to this facies. Sometimes the laminae are densely packed, causing a high decrease of the porosity. The laminated boundstone is vertically alternating with facies T3 and T12 mainly, and T4. Laminated boundstone is often adjacent to T3 crystalline crusts that develop rim morphologies. In S4 core the laminated boundstone facies is infilled by siliciclastic silt, which occludes the inter-laminae pores.

Microscopically the laminae (50 µm to 1-2 mm thick) consist of dense leiolitic micrite and clotted peloidal micrite associated eventually with cloudy microsparite (Fig. 5.8 C, D). Other components which might occur associated are clots of peloidal micrite, rare ostacodes and bivalves.

The cements lining internally the interlaminae porosity and externally the laminated layers are similar to those observed in other facies and consist of limpid equant mosaics of blocky microsparite to sparite (20-100 µm; Fig. 5.8E) and eventually prismatic scalenohedral cement growing perpendicular to the laminae orientation (up to 0.5 mm; Fig. 5.8F).

Interpretation

The laminated boundstone is interpreted as precipitated from thermal water with the influence of microbial mediated processes (Pentecost, 2005; Rainey and Jones, 2009; Gandin and Capezzuoli, 2014). The lamination of this facies is due to periodic changes of flood events, which induce a laminated deposition (Pentecost, 2005). Generally the laminated boundstone precipitates in low-energy environments, such as pools and ponds in terraced slope. Moreover according to Rainey and Jones (2009) the laminated boundstone can precipitate also on steeply inclined slopes, when there are reduced volumes of flowing water from the hydrothermal vents, or there are reduced degassing of CO_2 and energy due to the distance from the vents. In the Tivoli travertines, the laminated boundstone occurs both in sub-horizontal layers, deposited in low-energy environments as ponds, and moreover it can occur in upward concave and convex morphologies, probably in areas where the energy of the flowing water did not permit the degassing of CO_2 and abiotic precipitation, instead favouring the precipitation mediated by microbial activity.

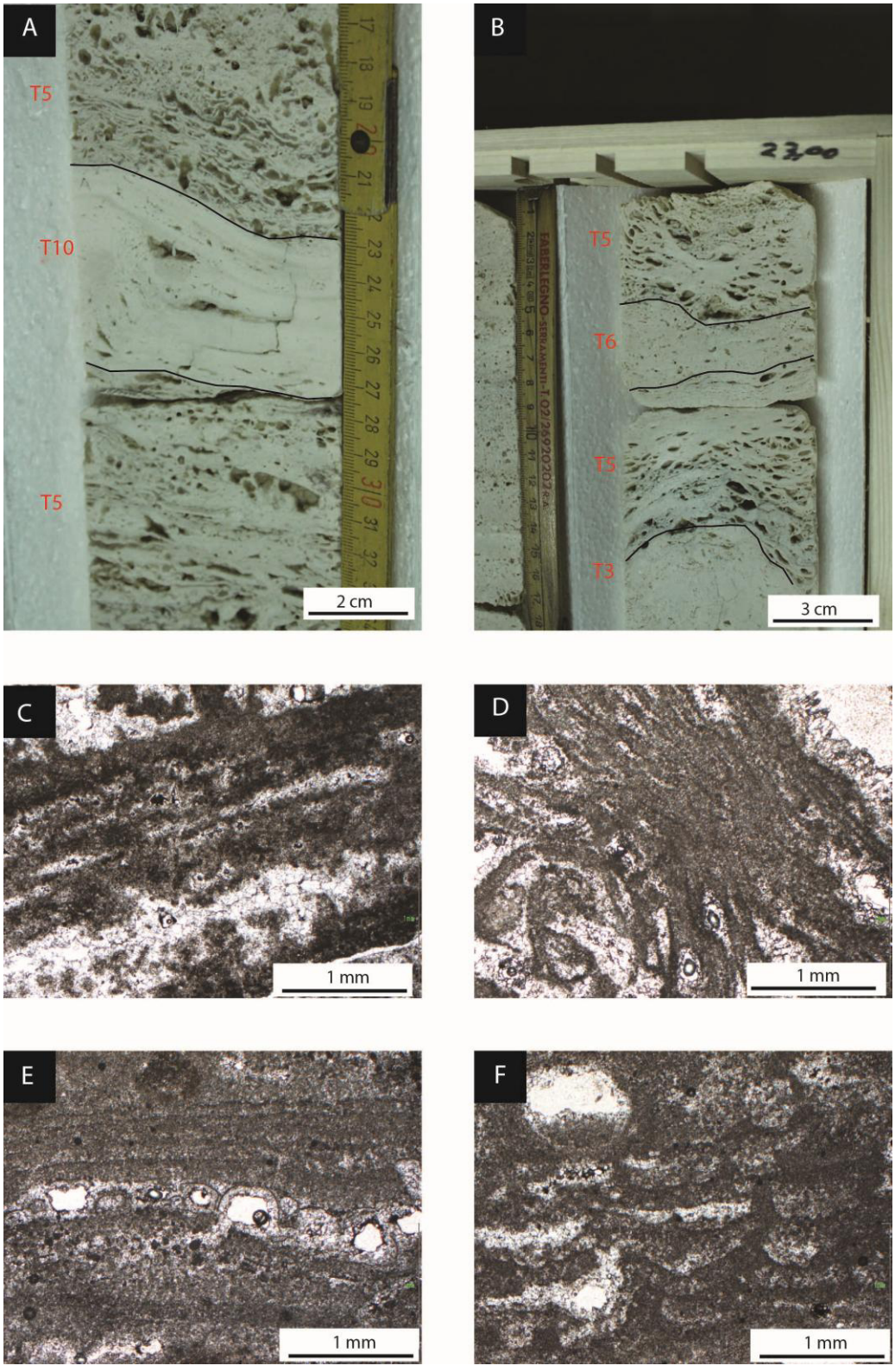

Figure 5.8. A) The laminated boundstone consists of dense white layers, made by 2 mm thick undulated laminae. Laminae can be densely packed, or elongated porosity can occur within them and it can be filled by meteoric cement. B) The laminae of the laminated boundstone facies are often undulated and can develop upward convex or concave morphologies, with inclination that can varies from sub-vertical to sub-horizontal. C-D) The laminae are made by lieolitic micrite and clotted peloidal micrite associated with microsparite. E-F) The cement is mainly equant microsparite and fills both internally and externally the laminated layers.

Facies T6: Sub-rounded coated grain grainstone to boundstone

Description

Facies T6 consists of grainstone (very rarely packstone) to boundstone made of sub-rounded grains with radial to concentric arrangements and often a porous central nucleus, white to cream in colour from 400-700 µm to several millimetres (2-8 mm). These grains form grain-supported layers, often sub-horizontal to low angle dipping beds, varying in thickness between 5 mm to 10 cm and rarely thicker (15 cm in well S2; Fig. 5.9A). These coated grain layers can show no internal structure or display coarsening or fining upward trends (Fig. 5.9B); in some cases they seem to gradually evolve into the T2 dendritic shrub facies. Associated with facies T8 and less frequently with facies T4, this coated grain grainstone/boundstone occurs adjacent to convex-upward rim morphologies, made of the crystalline dendrite T3 facies. Within facies T6, it is possible to find sparse clotted peloidal micrite shrubs and crystalline dendrite both in place and as intraclasts. Layers of the T6 facies are vertically intercalated with all the other travertine facies with the exception of facies T7; facies T6 is mostly associated with facies T2 and T8. These millimetre-size coated grains were addressed as pisoids and radial pisoids by Folk and Chafetz (1984) and Guo and Riding (1998), respectively.

Porosity is mainly interparticle, and intraparticle. Porosity varies from sub-millimetre to 1 cm in size, where it belongs to trapped gas bubbles or irregular fenestral porosity.

Petrographic analysis shows that the coated grains making facies T6 layers have variable fabrics. The most common T6 coated grains are millimetre-size spherical structures made of turbid lozenge-shaped crystals, similar to facies T3 crystalline dendrites, arranged radially around a hollow nucleus or a clots of peloidal micrite (Fig. 5.9C and D). These turbid calcite crystals, range in size from 150 µm nearly 1 mm. The turbidity is, as for the T3 crystals, due to abundance of inclusions and the micrite composition of the calcite crystals. Some of these coated grains have a nucleus mostly made of clotted peloidal micrite with a more irregular shape.

These grains consist of an inner core, made of micrite, peloids and microsparite, and irregular micrite coatings, separated from each other by layers of microsparite equant cement. On the outer coating layer coating layer, it is sometimes possible to observe the growth of crystal dendrites (0.3 mm long) in radial position. Other components of this facies are rare rafts and ostracodes, above which it is common to observe the growth of turbid calcite crystals.

The cement in between and within the coated grains consists of three types: equant blocky mosaics of microsparite (20-30 µm), prismatic crystals with scalenohedral termination (400-500 µm long) (Figure 5.9E); these two cement types can be preceded by pendant microstalactitic cement (100-200 µm irregular rims around the lower side of the grains) (Figure 5.9F).

Interpretation

The sub-rounded coated grains are recognized in many different hydrothermal travertine depositional systems (Chafetz and Folk, 1984, Guo and Riding 1998; Rainey and Jones, 2009). They mainly occur in pools of terraced slopes and in depression horizontally bedded systems on steep slopes, periodically agitated (Chafetz and Folk, 1984; Guo and Riding, 1998). The growth of sub-rounded coated grains, being made of a clotted micrite nucleus and a coat of crystalline calcite, seems

to be influenced both by abiotic and biotic processes; the precipitation starts with a biotic influence in low-energy depositional systems (Guo and Riding, 1994), then some changes in environmental factors, such as an increase of water supply with an increase of energy, can promote abiotic mechanisms of precipitation of calcium carbonate, for instance when the coated grains are transported from a pool to another (Guo and Riding, 1998; Rainey and Jones, 2009). Guo and Riding (1998) observed in Rapolano Terme quarry (Southern Tuscany, Italy) that these grainstones seem to be the result of the reworking of shrubs. Still in Tivoli, travertines of sub-rounded coated grain grainstone to boundstone are interpreted as deposited in depositional systems where there are changes of energy regime, from stagnant to agitated conditions, that are recognizable as pools agitated by turbulent events, or directly as smooth slopes.

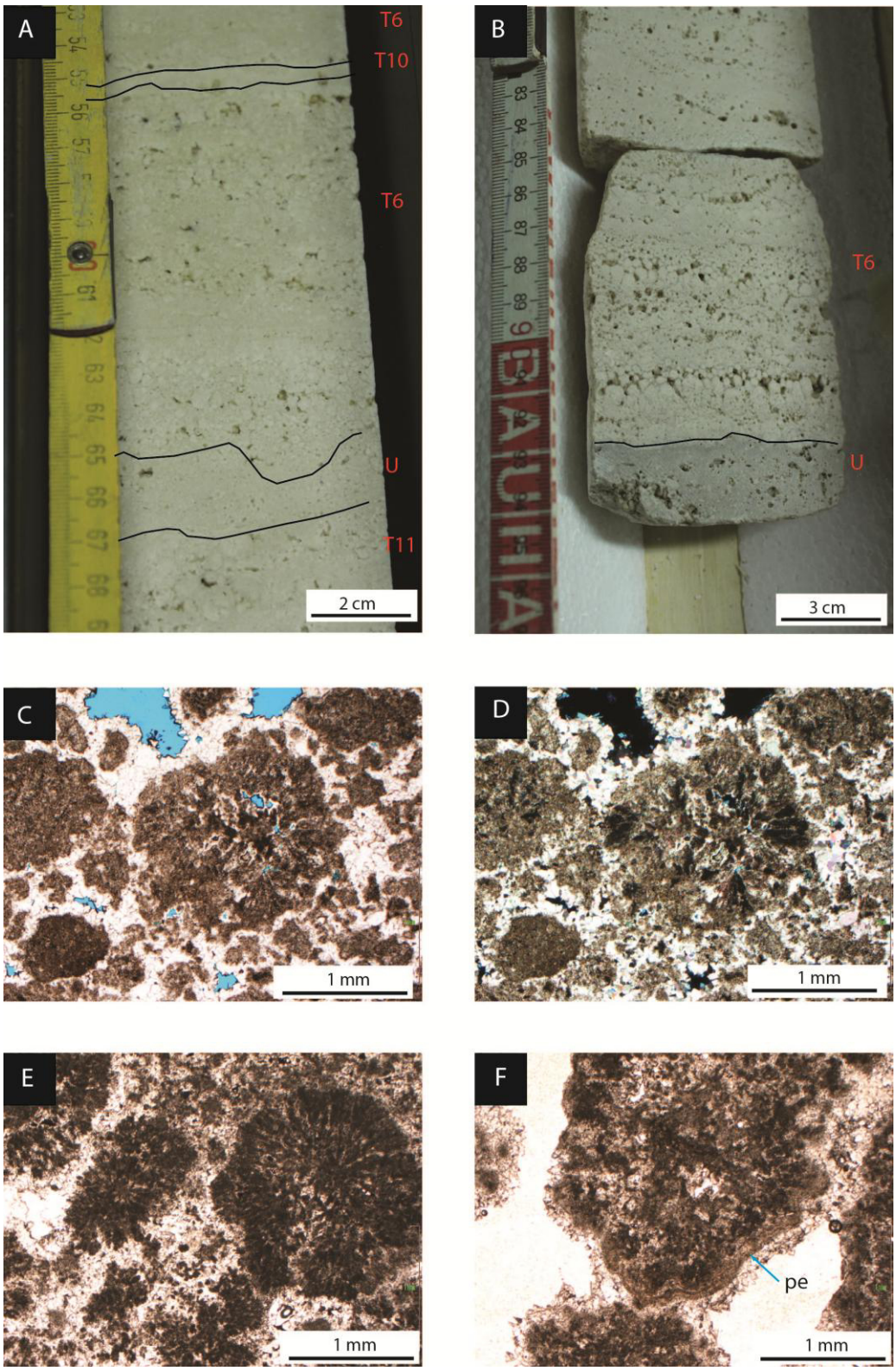

Figure 5.9. A) Sub-rounded coated grain grainstone develops sub-horizontal to low-angle dipping layers, varying in thickness between 5 mm up to 10 cm. The grains consist of radial to concentric arrangements with often a porous central nucleus. B) The grains are from 400-700 µm to 2-8 mm in size and can display coarsening upward trends. C) The most common coated grain is made by a nucleus of clotted micrite surrounded by radial turbid lozenge-shaped crystals, developing spherical structures. D) Crossed polarized thin section shows radial calcite crystals surround the micritic nucleus. E) Between and within the coated grains the cement consists of three type: equant blocky microsparite, prismatic crystals with scalenohedral termination and pendant microstalactitic cement. F) Detail of pendant (pe) microstalactitic cement.

Facies T7: Cream-colour peloidal intraclastic phyto-clastic buondstone to rudstone/floatstone

Description

Macroscopically this facies is a light to dark cream in colour boundstone to rudstone/floatstone including peloids, micritic intraclasts, plants and algae coated fragments (Fig. 5.10A). Grain size varies from sub-millimetre up to 1-4 mm, with plant stems reaching1 cm in height. Also moulds of valves from bivalves and ostracodes are present. Internal sedimentary structures are absent. Locally algae and plant stems have a sub-millimetre white carbonate coating followed by the dark brown carbonates. The colour of the matrix sometimes (in S2 and S3) becomes greenish due to possible silicification (Fig. 5.10B). Thickness of these beds is around 10-20 cm up to 50 cm in S1 well.

Porosity is widespread varying from an irregular framework and interparticle porosity up to 1-2 cm in size, partly filled by grey to brown internal sediment and meteoric cement. Intraparticle and biomouldic porosity within algae and plant stems and ostracod and gastropod shells vary in size from 0.5 mm to 5 mm.

Microscopically (Fig. 5.10 C-D-E-F), the boundstone texture is characterized by an irregular framework of clotted peloidal micrite and microsparite carbonate precipitates around charophytes algae and undetermined tubular plant stems. The grainstone texture consists of peloids, clots of clotted peloidal micrite and fragments of the algae and plant tubes coated by clotted peloidal micrite bound by cement. Other components are ostracodes (both within the clotted peloidal micrite and concentrated within primary framework porosity), gastropods, carbonate intraclasts and rafts. Cement types include: irregular light brown pendant cement, equant microspar to sparite up to 100-200 µm, and scalenohedral prismatic cement 200-800 µm long. Sample S2 27.5 shows charophytes stem overlain by a rim of fibrous crystal fan cement with undulose extinction. Often the cement grows around reed moulds and above small rafts that act as substrate. Clotted peloidal micrite and the early equant sparite cement show evidences of early dissolution.

Interpretation

Brown reed boundstone is interpreted as a typical facies developed distally from source of hot spring water and influenced by influx of rain water, as indicated by the presence of ostracodes (Guo and Riding, 1998). Moreover the presence of the algae in Tivoli deposits, as the charophytes, characterizes better this environment, that must be in a range of water depth up to 10 m (Gierlowski-Kordesch, 2010), in alkaline water, with temperature around 20° C (Pentecost et al., 2006) and little agitated (Murru et al., 2007). Moreover the presence of clotted peloidal micrite is an indicator of microbial activity. This deposit indicates environments comparable to the marsh environment described by Guo and Riding (1998).

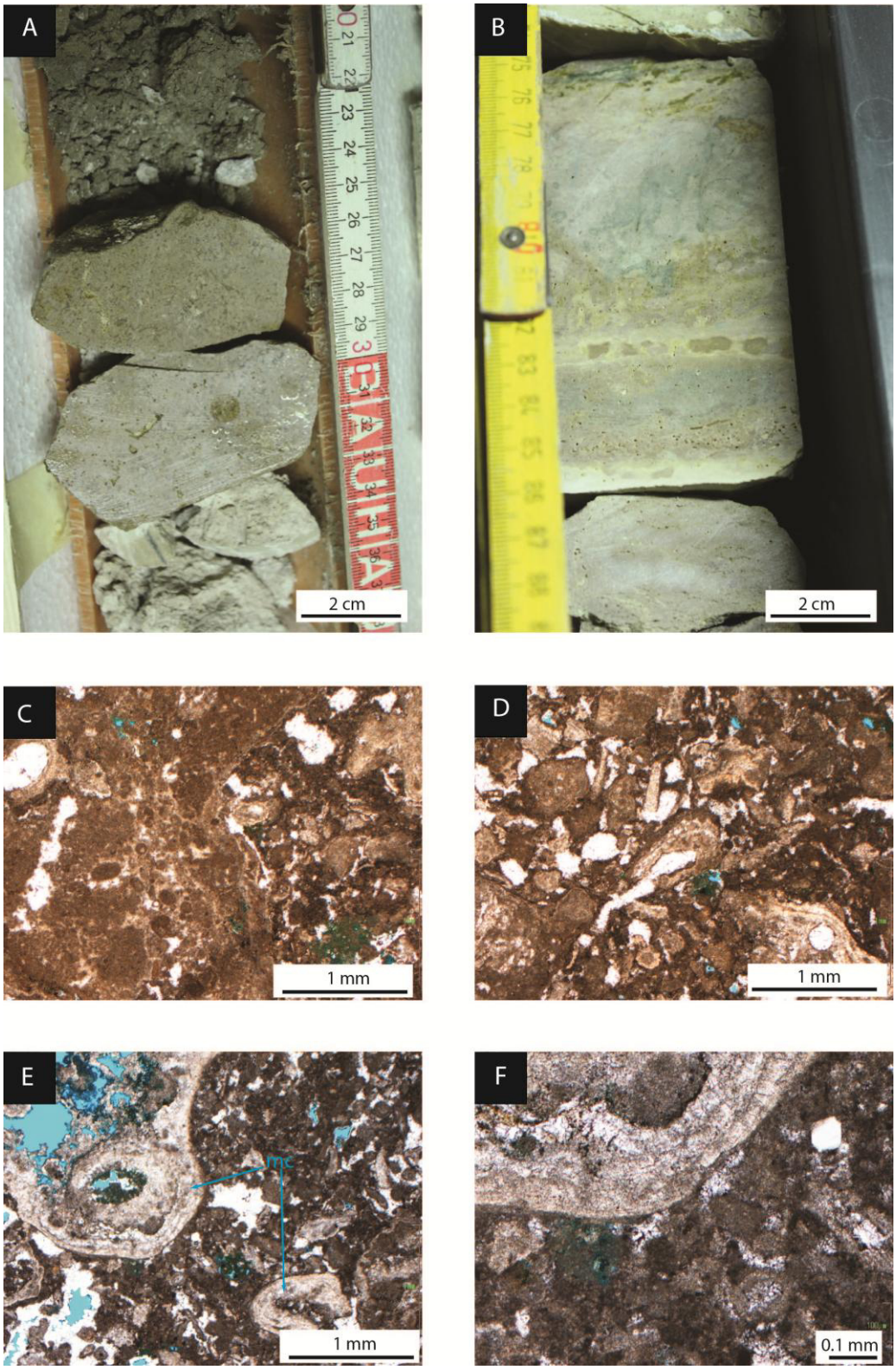

Figure 5.10. A) Facies T7 is a packstone/grainstone including plants and algae, developing layers 5-7 cm thick. B) Possible silicification makes the colour of the matrix from grey/cream to greenish. C) The porosity is both interparticle between the grains, and intraparticle and mouldic, within plant remains. D) Thin section shows that this facies is composed by irregular peloids, micrite clots, plant and algae fragments. Other components are skeletal remains of ostracodes and gastropods. E) Thin section shows that grains are often surrounded by an irregular microsparite coating (mc). F) Detail of grain microsparite coating.

Facies T8: White reed boundstone to grainstone/rudstone

Description

Macroscopically this facies consists of white colour, vertically oriented (Fig. 5.11A), elongated and horizontally prostrated fragmented plant stems with circular cross-section (possibly reeds) with diameters of 0.5-5 mm (Fig. 5.11B) and length up to 10 cm, encrusted by precipitated carbonates to form boundstone to grainstone/rudstone texture. Layers of T8 facies range between 1 cm to 10 cm in thickness. This facies is associated laterally with facies T3 and T2, which develop rim morphologies, and it can be associated with facies T6 or T2 in horizontal layers or making the core of the rim. Vertically this facies is often associated with facies T1 and often overlies facies U or T11.

Facies T8 is characterized by moulds of the plant remains following organic matter degradation, providing characteristic mouldic and intraparticle porosity associated also with interparticle and intra-framework porosity (Fig. 5.11C). Plant stem moulds have different sizes: transversal cross-sections of the stems are circular and range between 0.5 mm to 5 mm in diameter, instead the elongated tubular longitudinal cross-sections reach 5 cm in length (in S2; Fig. 5.11D).

Microscopically this coated plant stem boundstone develops when the organic plant substrate is coated by precipitated carbonates, which range in fabric types. Some reeds are coated by irregular rims of clotted peloidal micrite and microsparite a few hundred microns to 1 mm thick or they are welded together in a continuous clotted peloidal micrite precipitated boundstone (Fig. 5.11E, F); others show a crystalline coating similar to the T3 and T6 turbid crystals (60-150 µm long) arranged radially, eventually followed by clotted micrite and microsparite. Charophytes, both in life position or prostrated, can be associated with the coated reeds. Other components are ostracodes, gastropods and rafts. Ostracodes are both sparse in the clotted peloidal micrite precipitates or concentrated in geopetal position filling primary cavities. Primary framework, interparticle and secondary mouldic porosity can be occluded by equant blocky sparite and by prismatic scalenohedral cement (400-800 µm long). Irregular brown-colour crusts (80-200 µm thick) of pendant cement occur in S2 well around 27-28 m.

Interpretation

Reed boundstone, in a hydrothermal system, as Tivoli, is interpreted as the result due to a first phase in which the plants can colonized the dry surface, or around the edges of the active travertine body, or the entire body when the water supply is stopped; then, when the hydrothermal flow starts again, plants form a barrier to it and they are a substrate for the precipitation of the calcium carbonate (Rainey and Jones, 2009). The reed grainstone to rudstone is interpreted as the result of deposition of the plant remains transported by the water flow and deposited either in low-energy depositional systems as large pools or behind an obstacle as a rim. The presence of clotted peloidal micrite around the stems of the reeds suggests that microbial activity might favour the precipitation of calcium carbonate around vegetation stems.

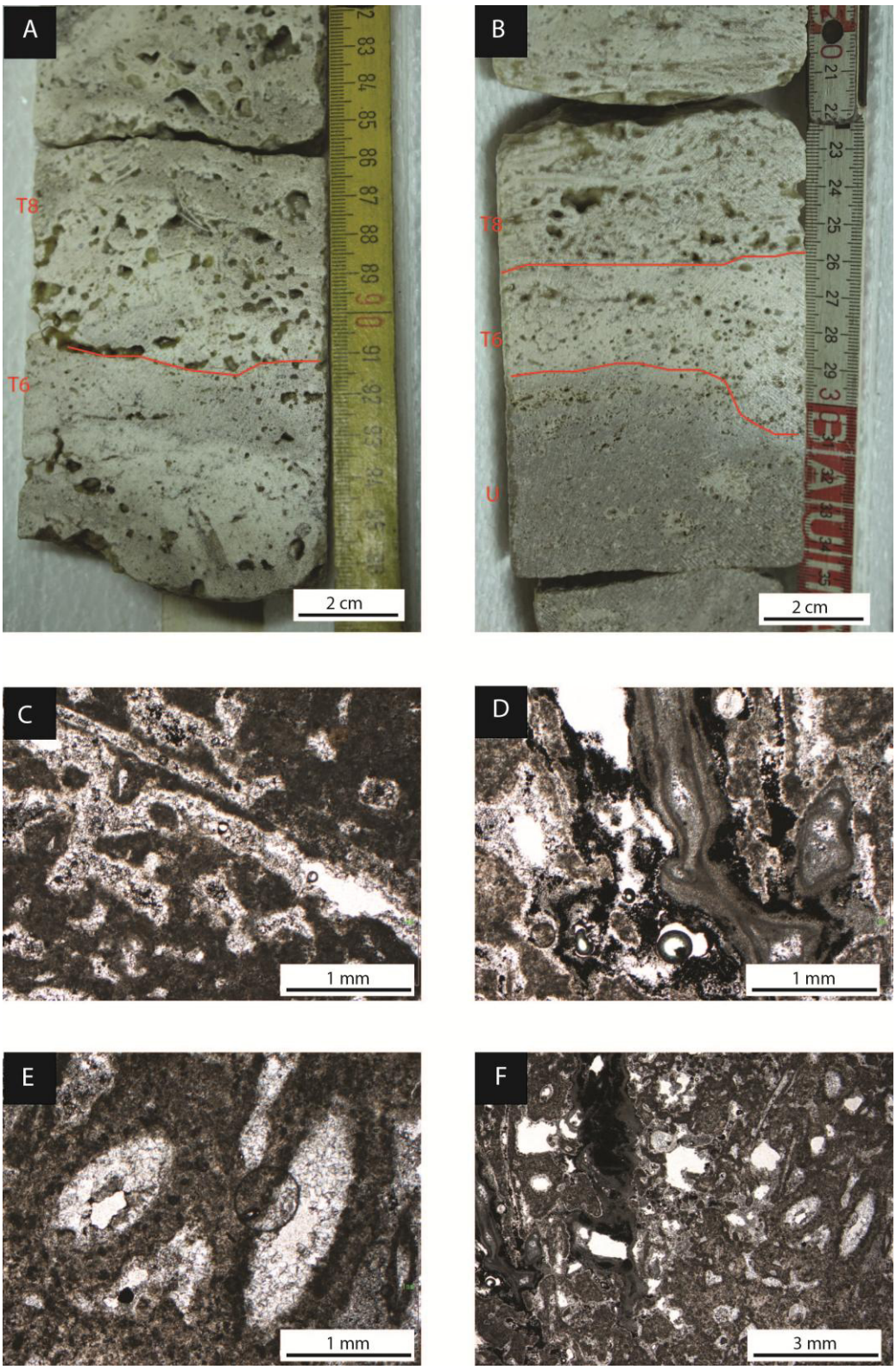

Figure 5.11. A) Hand sample of white reed boundstone consists of vertically oriented elongated plant stems and remains of them, bounded by grey meteoric cement. B) Another hand sample of white reed boundstone/grainstone made of vertically and horizontally oriented remains of plant stems with circular cross-section and diameter up to 5 mm in size. C) The organic matter degradation provides the characteristic mouldic and intraparticle porosity associated with interparticle porosity, developing a widespread porosity, here highlighted by methylene blue. D) Thin section shows an elongate reed remain coated by leiolitic micrite. E-F) Reed moulds are coated by clotted peloidal micrite and microsparite developing a continuous precipitate of carbonate, which bounds the reeds remains. Within the moulds and within the interparticle porosity, equant cement followed by prismatic cement occurs.

Facies T9: Raft grainstone

Description

Macroscopically rafts are sub-millimetre thin and white sheets of sub-horizontal crystalline crusts forming grain-supported grainstone and rudstone (Fig. 5.12A). Frequently rafts appear fragmented, with length of the fragments varying from 1 mm up to 5 cm, cemented by meteoric cement (Fig. 5.12B). Facies T9 layers are rare and thin, 0.5 to 2 cm thick and absent in S4 core. Often raft grainstone/rudstone forms lenses pinching out laterally with a width of a few centimetres. Typical of this facies is the interparticle porosity, which develops between the grain-supported raft sheets; this porosity reaches 1.5 cm in size. Also porosity associated with gas bubbles characterizes this facies. Facies T9 is associated with facies T4, T2, T6 and often overlies facies U and T11.

Microscopically individual rafts are constituted by a micritic and a microsparitic sub-millimetre thick films from which turbid prismatic calcite crystals grow perpendicular to the raft surface. Rafts are cemented by equant microsparite and prismatic crystals with scalenohedral terminations (200 µm long).

Interpretation

Raft developed at the water surface of stagnant pools where surface degassing of CO_2 causes an increases of saturation level that leads to calcite or aragonite precipitation in thin films, which float above the water surface (Folk et al., 1985). Literature reports two main mechanisms that cause the formation of raft grainstone: according to Jones (1989) and Taylor et al. (2004), the rafts can break when the preferential crystal growth under their lower surface increases their density and they sink to the bottom of pool surface. Folk et al. (1985), Guo and Riding (1998) and Gandin and Capezzuoli (2014) reported that the main cause of the raft breakage is due to the agitation of water surface brought by wind and current; moreover Gandin and Capezzuoli (2014) added that also the pressure exerted by gas bubbles under the raft surface is a cause of their breakage. In Tivoli travertine the rare presence of raft grainstone fabric is probably due to the lack of long time stagnant condition of the over-saturated waters, and to the difficult preservation of these deposits in depositional systems characterized by a low-deep sheet of water and often characterized by flowing water.

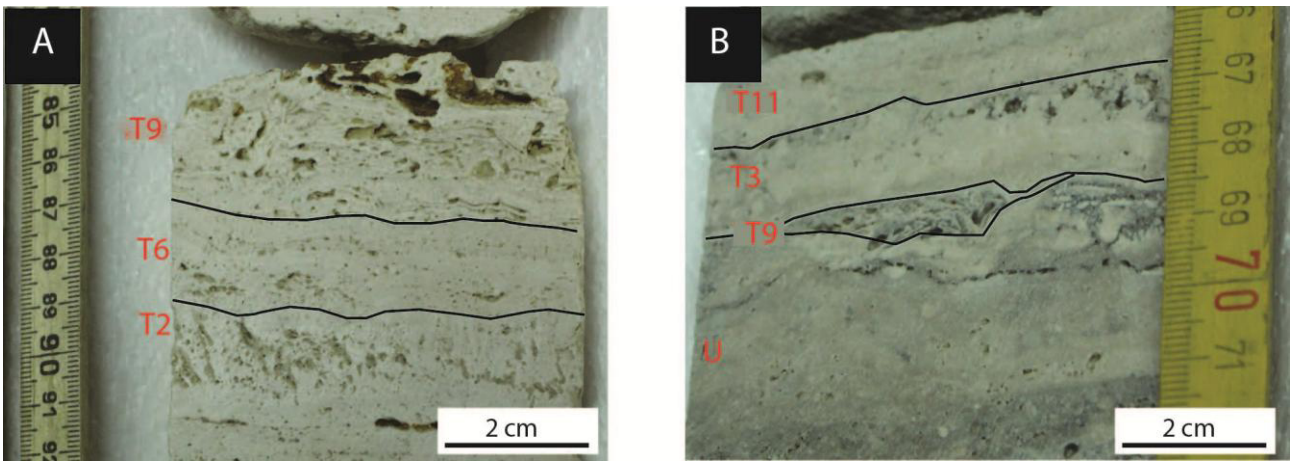

Figure 5.12. A) Rafts are sub-millimetre thin and white sheets of sub-horizontal crystalline crusts, which form grainstone and rudstone. B) Rafts often appear fragmented, with length of the fragments vary from 1 mm up to 5 cm in size and bound by meteoric cement.

T10: Millimetre thick dense laminae

Description

Macroscopically facies T10 (Fig. 5.13A) is characterized by bright white colour laminated layers, with laminae 0.5 mm up to 1.5 mm in thickness, which are usually millimetre thick and rarely form a few centimetres thick layers. Facies T10 layers are often undulated and make millimetre- to centimetre-size stepped terrace morphologies, sub-horizontal or slightly inclined (Fig. 5.13B). Facies T10 often overlies facies T3 and T2 as a draping crust. Facies T10 also occurs alternated within facies T2 layers, and constitutes the millimetre-thick dense substrate on which dendritic fabrics nucleate. This fabric does not show mesoscopic porosity.

Microscopically the laminae are constituted by dense leiolitic micrite (Fig. 5.13C). Moreover the clotted micrite develops small shrub like structures (Fig. 5.13D), with size up to 1.5 mm in length. The macroscopic lamination is probably due to the alternation of micritic layers, dark in colour, and microsparitic layers, which are lighter.

Interpretation

Chafetz and Folk (1984) interpreted the origin of the micritic intervals between shrub layers as caused by the reduced carbonate precipitation in cold seasons. The occurrences of these micritic layers, also not associated with facies T2, indicates that the travertine environment was characterized by thin sheets of water and maybe by cold temperature that inhibited the microbial activity.

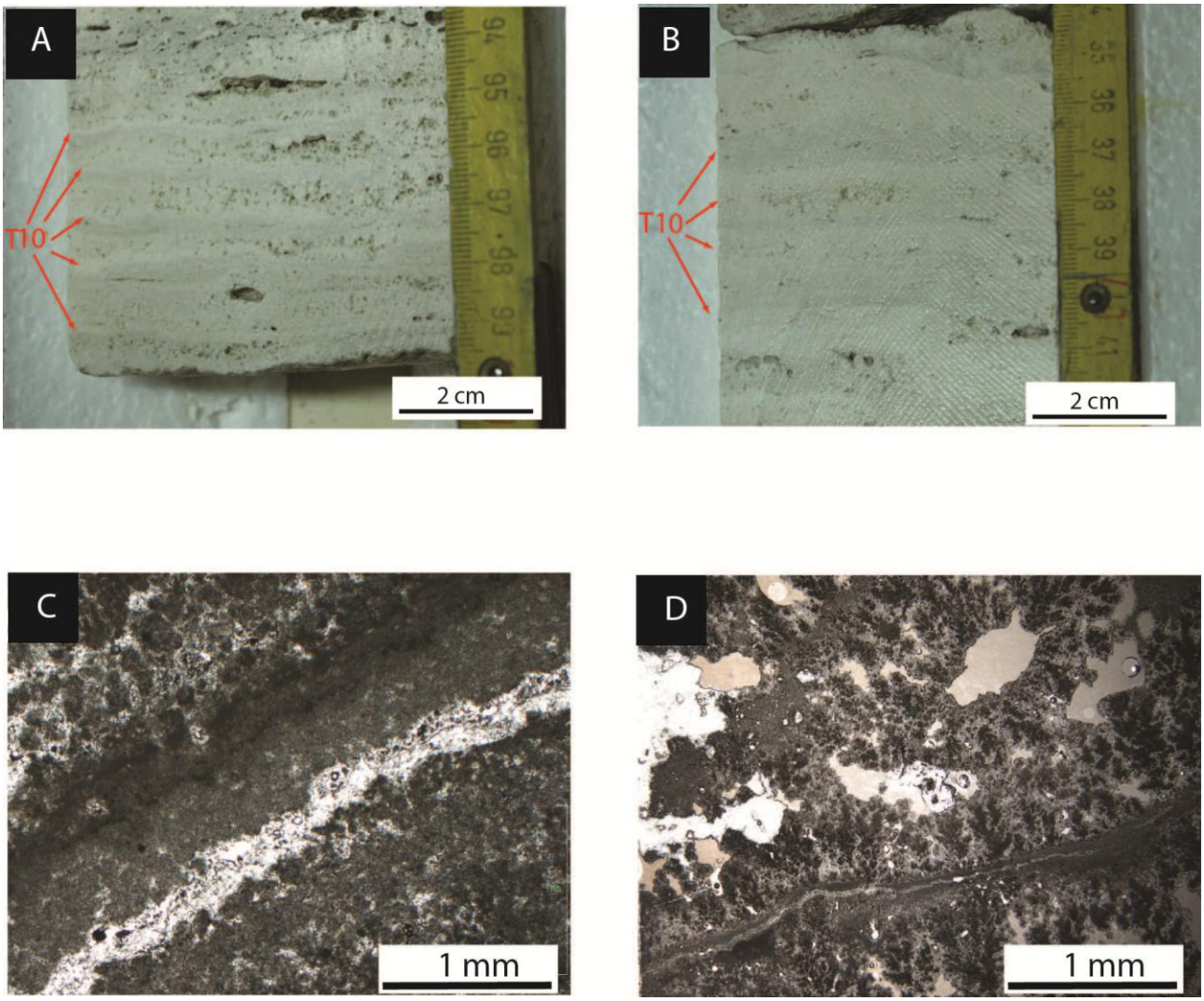

Figure 5.13. A) Facies T10 is made by laminated layers, often undulated. B) The thickness of these layers varies from millimetre size to few centimetre thick. C) Leilotic micrite constitutes this thin laminae. D) The laminae act as substratum for development of micritic dendrites.

T11: Intraclastic grainstone to rudstone

Description

Facies T11 represents the millimetre to centimetre-thick layers of grainstone to rudstone characterized by the presence of travertine intraclasts, mostly constituted by clots of leiolitic or clotted micrite, fragments of coated bubbles, coated plants, rafts, radial pisoids and dendritic shrub facies (Fig. 5.14A), that are bound by cement (Fig. 5.14B). These fragments are maximum 5 cm in size, are mainly sub-rounded or rarely with sub angular edges. Some intraclasts show a micritic to microsparitic carbonate coating. Facies T11 develops beds from 0.5 cm to 10 cm in size (in S3) but mostly is 4-5 mm thick. It lacks internal sedimentary structures. Facies T11 often overlies unconformities with extraclasts and grey matrix and it is covered by facies T6, T2 or T8. Facies T11 is characterized by interparticle porosity that is millimetre-size (1-2 mm), which can be filled by cement and/or micrite matrix; moreover fenestral porosity that can reach 1.5 cm in length is rarely present. Other porosity type is due by plant moulds that reach 5 mm in size.

In addition to various travertine intraclasts (0.1 mm to 5 cm), there are sparse shells of ostracodes, and turbid calcite crystals. The interparticle spaces are filled by equant blocky microsparite and sparite and prismatic scalenohedral cement.

Interpretation

These travertines are interpreted as generated by erosion of lithified carbonate and transported by flowing water towards lower topographic areas and deposited in pools behind the pool rim or in ponds. These deposits could be compared with intraclast facies described by Raney and Jones (2009).

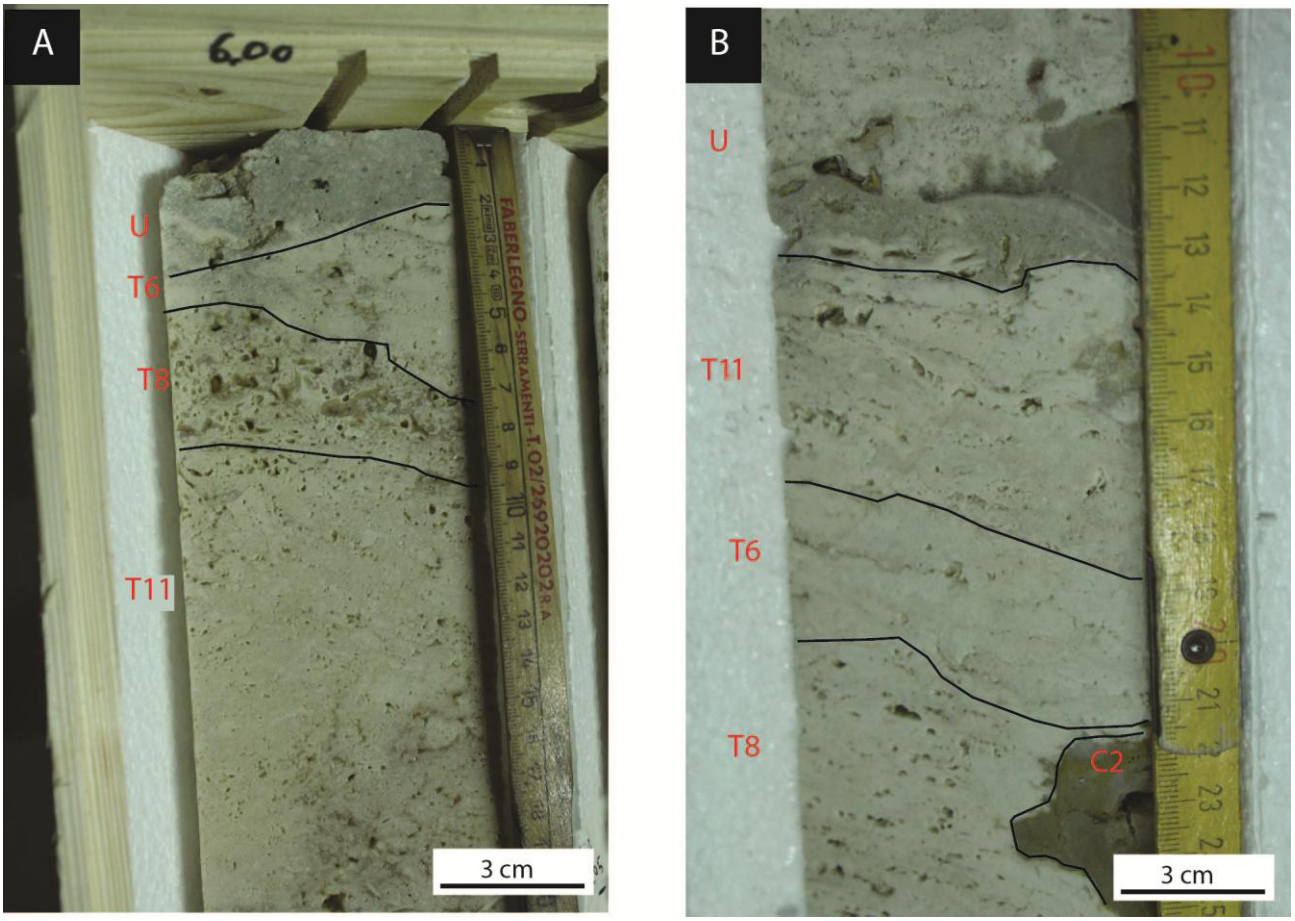

Figure 5.14. A) Facies T11 is grainstone/rudstone in texture and is made by travertine intraclastic remains, mainly clots of leiolitic or clotted micrite, plant remains, dendritic shrubs and radial coated grains remains. B) The intraclasts of this facies are bound by meteoric cement, and the framework is characterized by interparticle porosity 1-2 millimetre in size.

U: Gray lithoclastic/extraclastic wackestone to floatstone/rudstone to lithoclastic marlstone and claystone

Description

Macroscopically this facies includes various non-precipitated travertine detrital textures varying from: claystone and marls with sparse travertine lithoclasts and siliciclastic extraclasts, dark grey calci-mudstone/wackestone to grainstone, packstone, floatstone and rudstone made of previously precipitated travertine intraclasts embedded within a dense micrite matrix, which is mainly grey in colour (Fig. 5.15A), but can vary to greenish (in S7) or intraclasts are cemented by calcite spar (Fig. 5.15B). Grain size of the clasts varies from sub-millimetre to a few decimetres beyond the core width. Travertine intraclasts are angular and made of micrite, clotted peloidal micrite, fragments of facies T2, T3, T1 and T6 with fragments of coated bubbles and plants. Often grain-supported packstone/grainstone and rudstone textures are at the base and top of the U units. The base of this detrital facies is often irregular and erosive truncating the underlying travertine facies. The thickness of these detrital layers varies from 5 mm up to nearly 7 m (in S6). This facies is often vertically followed or preceded by facies T11 and T8.

Porosity (from 1 mm to 2 cm in size) is interparticle and fenestral to vuggy within the grey matrix. Some of the pores have a secondary mouldic origin due to dissolution of the clasts and bioclasts.

Microscopically this detrital facies includes intraclasts of: leiolitic and clotted peloidal micrite, pisoids and shrub fragments of the T6 (Fig. 5.14C) and T2 facies, fragments of coated reeds and bubbles and all the other lithofacies. Extraclasts include quartz, mica and K-feldspar crystals (Fig. 5.15D, E). Wackestone to floatstone facies show a micrite and microsparite matrix, which must include also some clay impurities providing the dark grey colour. Sometimes intraclasts show a clotted peloidal to turbid crystal coating similar to the radial pisoids. Cement types are equant sparite mosaic and scalenohedral prismatic cement. They are dark, have an irregular shape and the edges are undulated. These clasts are often characterized by intraparticle porosity, up to 100 µm in size. Other components are shrubs or coated grains (facies T6) remains. The dimensions of the grains are variable, from 0.1 mm to 2 mm. Sometimes these grains are coated by a layer constituted by turbid calcite crystals, which are up to 500 µm in length (section S2-18). Rarely between this crystalline layer and the clast there is a thin microsparitic crust (60-100 µm), laminated and undulated. The floatstone consists of a micritic matrix, in which there are shrub or turbid calcite crystals remains, reeds moulds, both in rounded and elongated sections, and shells of ostracodes. Also there are detrital minerals such as quartz, feldspar, mica and sanidine (section S1/14-15.20m). The cement is mainly equant and prismatic, average 100 µm in size. The porosity is intraparticle, is abundant, commonly sub-rounded in shape, with size that varies from 0.1 to 2 mm (Fig. 5.15 F).

Interpretation

These deposits are the result of exposure of travertines to subaerial condition altered by rainwater, desiccation, biological activity and soil formation (Guo and Riding, 1998; Ozkül et al., 2002; Gandin and Capezzuoli, 2014). The erosion surface at the base of these deposits constitutes unconformities between travertine facies (Guo and Riding, 1998). This facies corresponds to exposure surfaces described by Faccenna et al. (2008), the main five among them are interpreted as boundaries between the travertine units described by them.

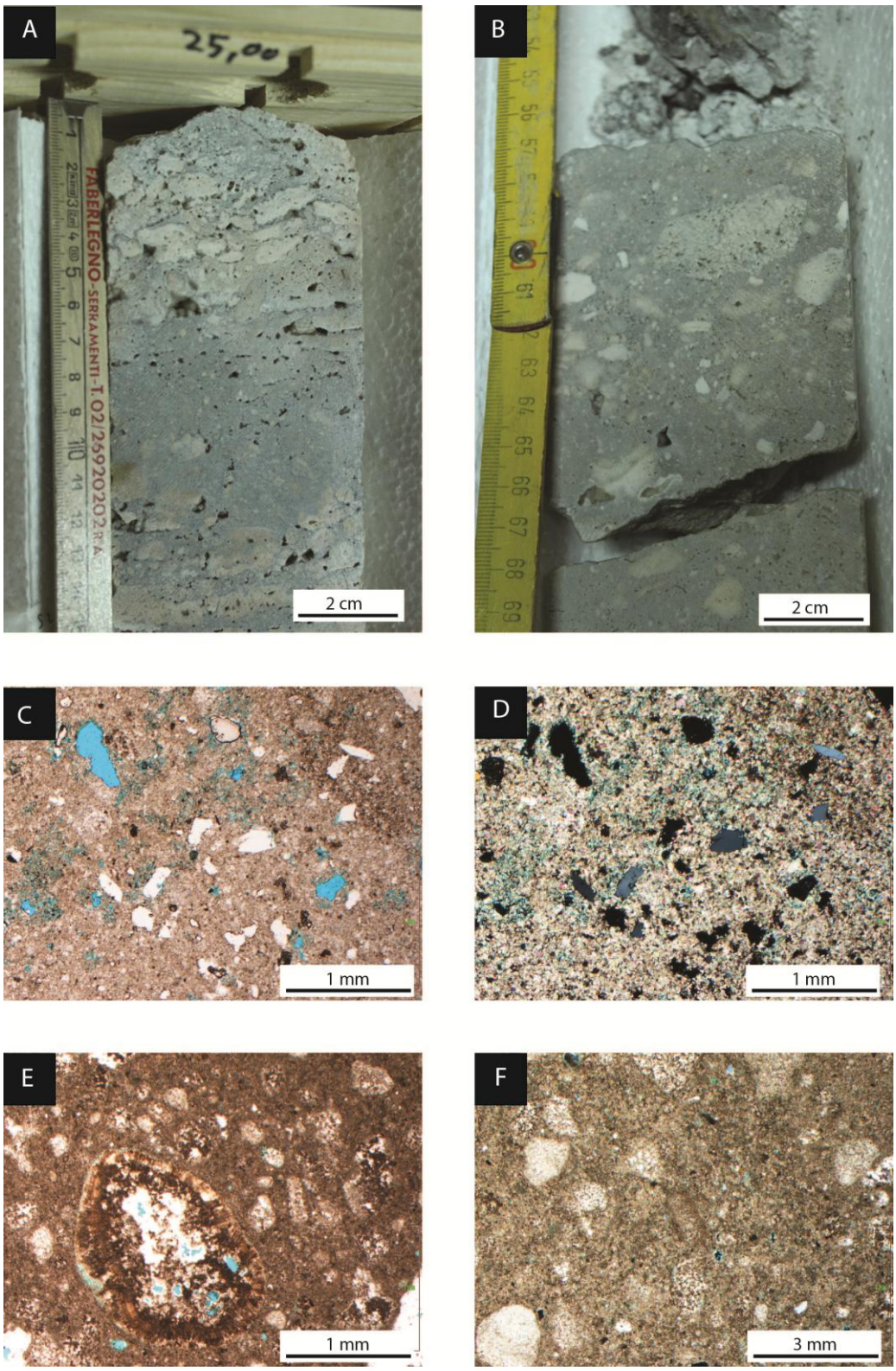

Figure 5.15. A) Grey lithoclastic/extraclastic wackestone to floatstone/rudstone consists of a micrite matrix grey in colour with sparse travertine lithoclasts. Often at the base of this facies rudstone texture occurs and above it the texture becomes a floatstone. B) Sometimes the micrite matrix is substituted by meteoric cement. C) This detrital facies includes leiolitic micrite and clotted peloidal micrite and many kind of travertine intraclast including spherical coated grains of facies T6. D) Extraclasts occur in this deposit, include quartz mica and k-feldspar crystals. Moreover clay minerals occur, giving to the matrix the typical gray colour. E) Same thin section in crossed polarized. F) Thin section shows the presence of sub-millimetre interparticle porosity.

C: cavity facies:

C1:

This facies consists of a matrix, made of crystalline calcite, siltitic and clayey sediments, with the clasts often surrounded by iron oxides. This facies is laminated, planar and undulated, with laminae 1 or 2 mm thick. The deposit varies from sub-horizontal to inclined up to 30°. The deposit fills an irregular dissolution cavity. There is a spare porosity, vuggy or fenestral, with size around 2 mm in diameter for the vuggy porosity and up to 1.5 cm in length for the fenestral porosity. The thickness of these deposits varies from 2 cm up to 20 cm. Vertically this facies often occurs below the unconformities (facies U).

C2

Macroscopically this facies is characterized by a few millimetre-thick (2-3 mm) undulated layers, grey to cream in colour, which are deposited with different geometries: concentric around a micritic (S7, 15.80 m) or conglomeratic (S7, 15.20 m) core (Fig. 5.16A); low-angle inclined (20-30°) with internal structure like prograding rim (S7, 14.00 m), and high-angle crusts dipping from 80 to 90°. Porosity is common and varies from sub-rounded to fenestral (with pores elongated in the same direction of the layers) in shape, with size varying from 1 mm to 1 cm in length. The deposits of this facies are up to 40 cm thick. Often it is associated with the facies C3 and with facies T7.

C3

This facies varies from a floatstone, wackestone to a packstone, rudstone, consisting of a brown matrix and angular clasts (up to 2 cm) of cave filling (facies C3), vadose pisoids (5 mm) and travertine clasts, with size up to 1 cm (Fig. 5.16B-F). The shape of the pisoids varies from rounded, subrounded, to elongated (very rare), with size around 1-2 cm in diameter. The thickness of the laminae around the nuclei is sub-millimetre, but it rarely can reach 2 mm. The matrix within the pisoids is orange in colour. The vuggy porosity is widespread, with single pore size mostly around 2 mm, but it can create elongated pores up to 5-7 mm. This facies is often deposited in centimetre-thick beds (3 to 7 cm); around 13.7 m in core S7 there is a bed 20 cm thick. This facies is often laterally associated with facies C2, and with facies T7.

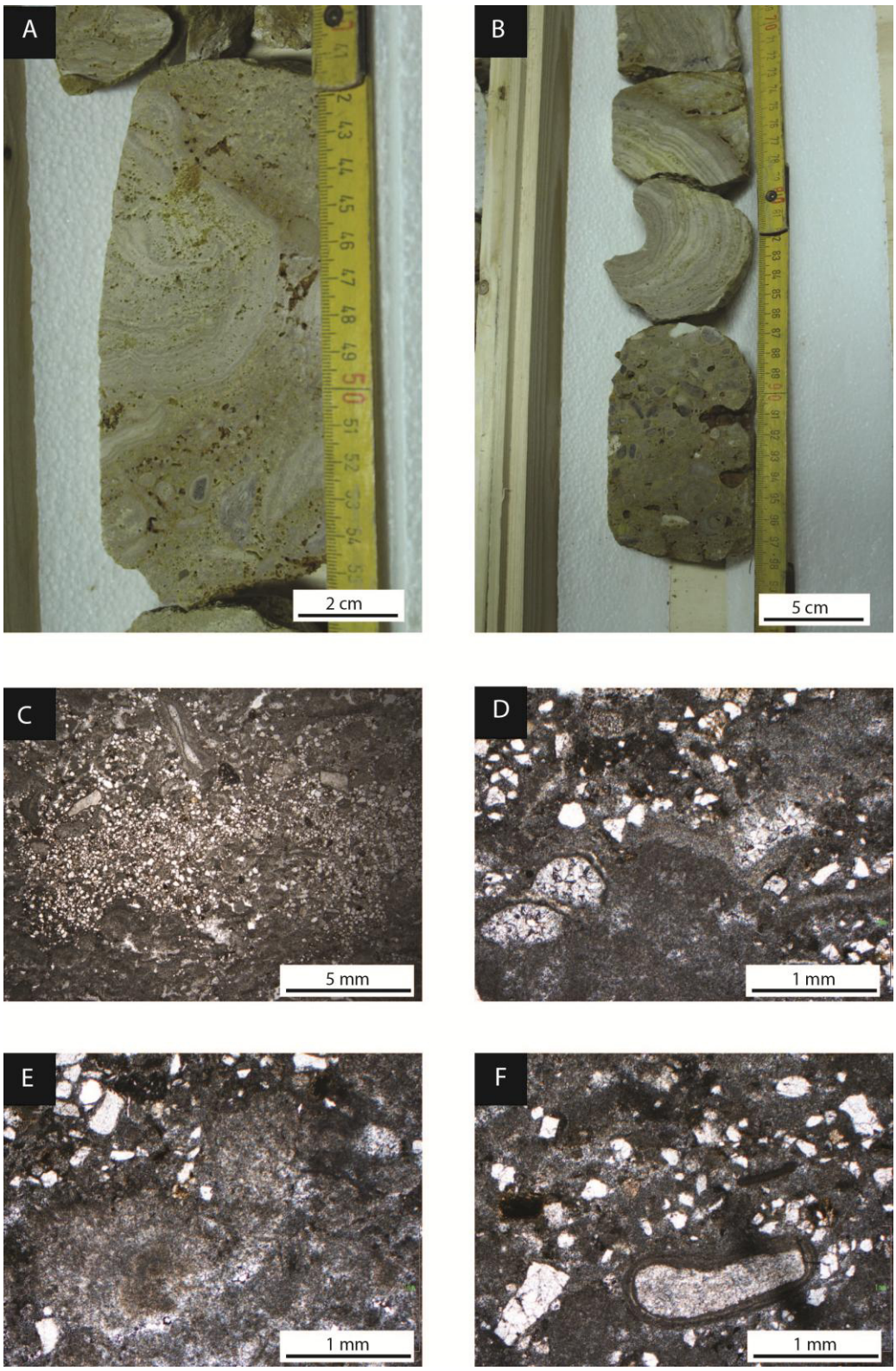

Figure 5.16. A) Hand sample of facies C2 shows the laminated precipitates dark grey in colour 1-2 mm thick, is characterized by the presence of iron oxides that give to the rock an orange colour. B) Hand sample of facies C2 (above) and C3 (below) that consists of vadose pisoids. C-D-E-F) Thin section of facies C3 shows that this facies is a silstone to sandstone.

Facies F1 Black to dark grey mudstone

Facies F1 is a claystone to siltstone black in colour, rich in organic matter. The matrix includes submillimetre- and millimetre-size, up 2 mm, white and grey angular carbonate clasts. The claystone is not characterized by any sedimentary structure. Only in core S2 this facies is characterized by the presence of centimetre and decimetre-size travertine clasts floating in the black claystone matrix. F1 facies occurs at the base of the travertine deposits in S1, S2, S3 and S4 cores where it is overlain by the travertine by a sharp boundary. Usually the first travertine facies is T1 or T8, T13 and U. This facies reaches a maximum thickness of 1.6 m in core S3. The transition between F1 dark claystone and the overlying travertine is sharp (there is a thin alternation with travertine in core S3). Facies F1 represents a stagnant freshwater pool or lake with concentration of organic matter in anoxic conditions.

Facies F2: Green-grey volcanic pyroclastic deposits

Facies F2 is a brown yellow/green mixture of sand, silt and clay with millemetre size angular clasts of black volcanic glass, and detrital green and white minerals possibly belonging to pyroxenes and feldspatoids. Locally also carbonate clasts are present. This facies does not occur in S2 core. In core S6 facies F2 is richer in green clay and are present lignite and coal inside bed 2-3 cm thick. The thickness of these deposits reaches 5 m in the core S4. Facies F2 represents reworking of volcanic pyroclastic deposits.

Facies F3: Grey volcanic pyroclastic deposits with feldspatoids (leucite)

Facies F3 represents a volcanic ash deposit, light to dark grey in colour, with hexagonal leucite crystals. The thickness of this deposit is maximum in core S1 where it reaches 1.8 m.

Facies F4: dark grey to green volcanic ashes

Facies F4 is a green to cream/brown colour claystone to siltstone, which includes millimetre-size black volcanic glass clasts, and eventually vegetation fragments and skeletal shells of ostracodes and gastropods (in S3, 26.15 m). In the core S6 there is a millimetre thick lamination highlighted by the presence of black root moulds, aligned according to the lamination. The maximum thickness of this facies is 1.14 m in core S3. Facies F4 represents probably a lake or alluvial plain where fine sediment, likely sourced by alteration of volcanic deposits, accumulate.

Facies F5: White to light cream/grey marls

Facies F5 is a white to light cream/grey marl, calci-mudstone or calcareous clay, characterized by the absence of internal sedimentary structures. This facies is deposited in beds up to 10 cm in thickness and it is often associated with travertine of facies T7. Facies F5 represents a lacustrine basin where carbonate mud derived from algal and diatoms bloom or settling of micrite precipitated in the water column or detrital from travertine abrasion.

Facies F6: Green/grey to brown unconsolidated fine sand, silt and clays

Facies F6 represents green and cream to light brown fine to medium sand and silt, mostly unconsolidated, with no evidence or reworked volcanic fragments. Carbonate clasts, millimetre to centimetres size, can be present. Facies F6 represents lacustrine to fluvial/alluvial sand deposits.

Facies F7: Green to light brown unconsolidated sand to laminated sandstone

Facies F7 is a light to dark cream siltstone to fine sandstone without evident internal sedimentary structures. This facies is often associated vertically with marls of the facies F5 and must represent a lacustrine deposit with dominant siliciclastic sediment input.

F8: Chaotic mud-supported debris with carbonate clasts in green clay matrix

This facies represents palaeosols at the top of the travertine deposits. The paleosol in core S6 has a red/orange matrix and within there are angular grey clasts, with size from 2 mm to 2 cm. This facies is present only in a bed in the core S6, and is 14 cm thick and at the top of core S3.

Facies F9: Polymictic conglomerate

Facies F9 is a moderately sorted, conglomerate with rounded to sub-angular clasts with size varying between 2 mm and 2 cm. Clasts are sub-spherical in shape, only few clasts have elongated shape and/or angular edges. Clast composition is predominantly white/grey carbonate associated with extraclasts of various lithologies sandstone, siltstone, and mudstone. The silty-sandy matrix is generally green suggesting reworking of clay derived from alteration of volcanic deposits. There is probably also carbonate cement. Porosity is low and interparticle. This conglomeratic facies is present in cores S7 and S6. The thickness of this deposit is around 10 cm on average, only one conglomerate bed is up to 60 cm thick. Facies F9 represents a fluvial conglomerate and it is associated with the cross-bedded and carbonate cemented sandstone of facies F10.

Facies F10: Grey/green medium to coarse cross-laminated sand and sandstone

Facies F10 is a medium to coarse sandstone, cream to grey in colour, well sorted and often cemented by carbonate. This sandstone shows current ripple crossed lamination and it is associated with the fluvial conglomerate deposits of core S7.

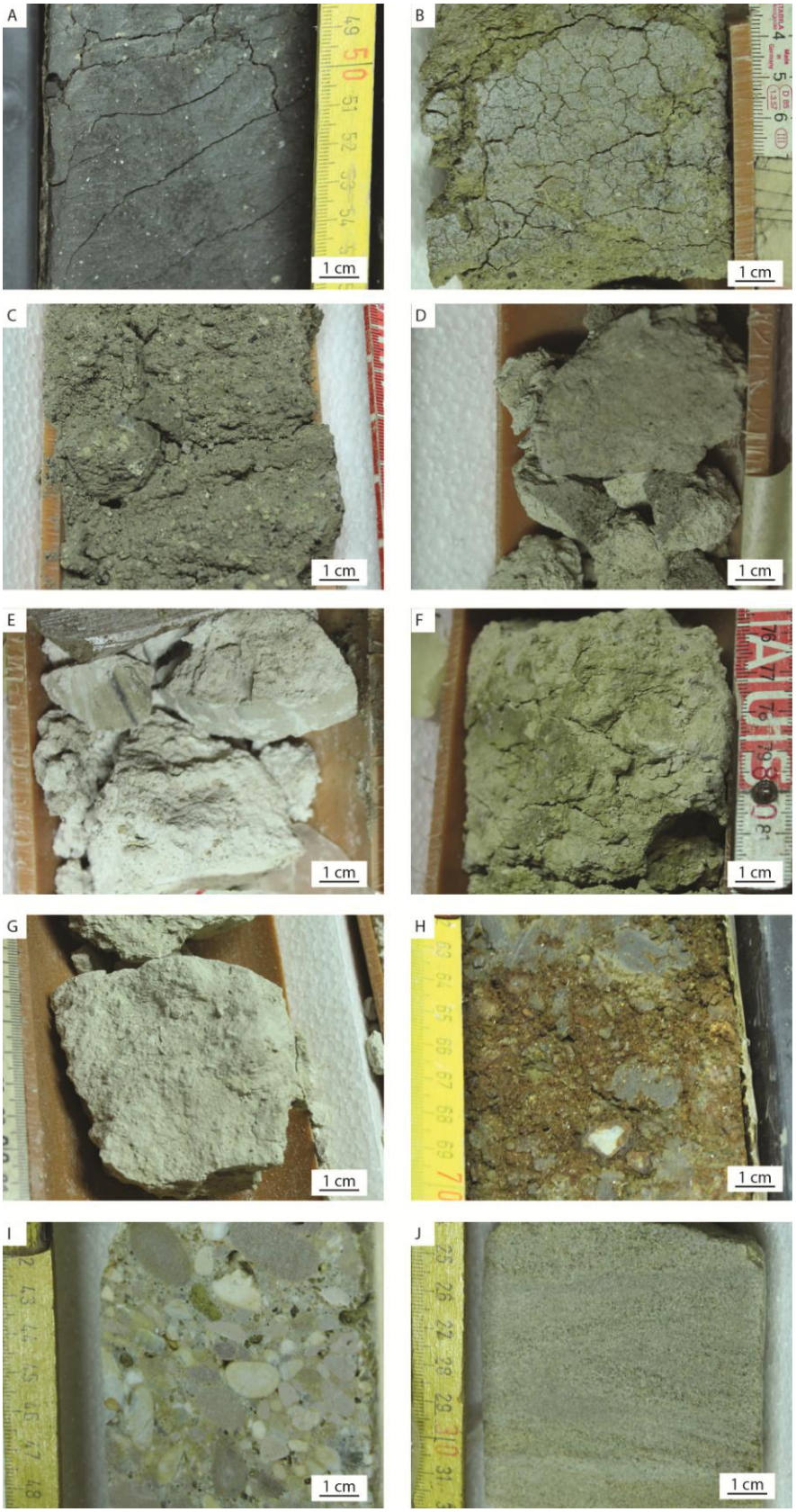
A
1 cm
B
1 cm
C
1 cm
D
1 cm
E
1 cm
F
1 cm
G
1 cm
H
1 cm
I
1 cm
J
1 cm

Figure 5.17. Hand samples of terrigenous facies: A) Facies F1 is a sandstone to siltstone rich in organic matter that gives the black colour to the rock. B) Facies F2 consists of sandstone to siltstone green to brown in colour with black volcanic clast and white minerals such as pyroxenes and feldspatoids, and carbonate clasts. C) Facies F3 consists of ash deposits with leucite crystals. D) Facies F4 represents volcanic deposits rich in roots remains. E) Facies F5 is a calcimudstone characterized by the lack of internal structures. F) Facies F6 consists of green sandstone without volcanic clasts and the occurrence of centimetre thick carbonate clasts. G) Facies F7 consists of gray sandstone without evident internal structures. H) Facies F8 represents palaeosols with an orange matrix and angular clasts. I) Facies F9 is a conglomerate made of rounded to sub-angular clasts of carbonates and extraclasts of varies lithologies. J) Facies F10 consists of laminated coarse to medium laminated sandstone.

Table 1. Description and interpretation of travertine facies recognized in the studied succession.

Facies name and texture	Components	Bedding Thickness and Geometry	Diagenetic Features	Porosity type	Depositional Environment	Distribution and associations
Facies T1: Clotted peloidal micrite grainstone to boundstone with charophytes and ostracodes	aggregates of clotted peloidal micrite (100-300 µm) peloids (10-20 µm) charophytes (5 mm) ostracodes gastropods reed stems	Beds: 5-30 cm, up to 50 cm thick	microsparite (10-20 µm) scalenohedral (200-250 µm) pendant cement	interparticular intraparticular (0.5-2 mm) Bubble porosity fenestral	Shallow lacustrine ponds to palustrine environment	Mostly abundant in S1, S3 and S7
Facies T2: Clotted peloidal micrite dendrite boundstone	peloids (15-30 µm) ostracodes microsparite (5-50 µm) dendritic structures	undulated sub-horizontal 0.2-5 cm convex upward structures 10-20 cm thick	Blocky equant microsparite to sparite (20-150 µm) Scalenohedral (up to 1 mm) Pendant Micrite dissolution	Interdendrite Intrabubbles	Low to moderately energy pools	T2 occurs in all cores. It is associated with T4, T6 and T7
Facies T3: Crystalline dendrite cementstone	Dendritic calcite crystals Laminae of micrite and microsparite	Beds from 5 mm up to 20 cm thick Convex upward structures	Microsparite, cloudy and clear (10-100 µm) Scalenohedral cement	Intercrystalline porosity	Inclined slope and rims of pools	Mostly abundant in S4 and S6 It is associated with T5, T6 and T10
Facies T4 Coated gas bubble boundstone	Micrite and microsparite matrix Raft ostracodes	Beds from 5mm to 5 cm thick	blocky equant microsparite to sparite (20-200 µm) Scalenohedral (100-250 µm)	intra-bubble (0.5-5 mm)	pools of terraced slope system channels	T4 occurs in all cores. It is associated with T2, T6, T8
Facies T5: Laminated boundstone	laminae (clotted peloidal micrite and microsparite)up to 2 mm thick. Rare ostracods Bivalves Gray to green internal sediment	2 mm to 13 cm thick beds	Blocky equant microsparite to sparite (20-100 µm). Scalenohedral cement (500 µm) Pendant cement	Inter-laminae, lens shaped up to 3 cm wide	Inclined surfaces	T5 occurs in all cores except S4. It is associated with T1, T3 and T4
Facies T6: Sub-rounded coated grain grainstone to boundstone	Coated grains consisting of nucleus made of micrite (400 µm to mm in size)	Sub-horizontal to little inclined layers. 5mm to 20 cm thick	Blocky equant microsparite to sparite (50-150 µm) Scalenohedral (up to 500 µm) Pendant (100-200 µm)	Interparticle Intraparticle Fenestral vugs intrabubbles	Shallow ponds and pools of terraced rims	T6 is mostly abundant in S1 and S2. It is associated with T2, T3 and T4
Facies T7: Cream-colour peloidal intraclastic phyto-	Carbonate encrusted algae, reeds and charophytes Ostracodes Gastropods	Beds from 5 to 50 cm thick	Pendant Equant microsparite to sparite (50-200 µm)	Interparticle Intraparticle Secondary mouldic	Shallow lacustrine ponds to	Facies T7 is mostly abundant in S3 and S7. It is associated

clastic buondstone to rudstone/floatstone	Raft intraclast		Scalenohedral (200-800 µm)	porosity	palustrine environments	with T1, T2, T4 and T6
Facies T8: White reed boundstone to grainstone/rudstone	Encrusted reeds (up to 10 cm) Charophytes Ostracodes raft coating of leiolitic micrite and microsparite	Beds 1- 25 cm thick	Pendant cement (80-200 µm) Equant sparite Scalenohedral (up to 800 µm)	Primary intraparticle and interparticle Secondary mouldic porosity	Shallow ponds and pools	Facies T8 is mostly abundant in S2 and S7. It is associated with T6 and T11
Facies T9: Raft grainstone/rudstone	Carbonate plates/raft	Beds 0.5 mm to 2 cm thick. Lens 1-10 cm wide	Blocky equant microsparite Scalenohedral (200 µm)	Interparticle porosity Bubble porosity	Stagnant ponds	Facies T9 is rare in all cores. It is associated with T2, T4 and T6
Facies T10: Millimetre thick dense laminae boundstone	Leiolitic micrite, clotted peloidal micrite and microsparite laminae	1-5 mm thick beds Undulated Terraced morphologies	No cement	No macroscopic porosity	Micro-terraced pools and rims	Facies T10 is mostly abundant in S4. It is associated with T2 and T3
Facies T11: Intraclastic grainstone to rudstone	Travertine intraclasts, micritic coating Coated grains Rare feldspar	0.5 to 20 cm thick beds	Blocky equant microsparite and sparite Scalenohedral pendant	Interparticle Fenestral Mouldic porosity (reed stems)	Accumulation of reworked travertines in pools	Facies T12 is abundant in all cores. It is associated with T2, T6 and T8
Facies U: Gray lithoclastic/extraclastic wackestone to floatstone/rudstone to lithoclastic marlstone and claystone	Intraclasts embedded in a micrite matrix Extraclast: quartz, mica, K-feldspar	Beds from 5 mm up to 10 cm thick Erosive base	Pendant Blocky equant sparite scalenohedral	Interparticle fenestral biomouldic	Detrital deposits due to non-deposition and erosion of travertines during water flow interruption	Facies T11 is abundant in all cores. It is associated with T6
Facies C: Cavity Facies	Cement crust Silt to mud terrigenous to carbonate sediment Ostracodes Vadose pisoids	2-20 cm thick	Scalenohedral cement	Vuggy spare porosity	Filling deposits of primary or secondary vugs	Facies C are abundant in S1-S4 and S7

Lithofacies name	Bedding and structures	Lithofacies thickness	Grain size	Grain composition	Depositional environment
Facies F1: Black to dark grey claystone	Any sedimentary structure	Up to 1.6 m	Claystone to siltstone. Spare clasts 2 mm	Carbonate clasts in a organic rich matrix	Lacustrine pools
Facies F2: Green-grey volcanic pyroclastic deposits	Any sedimentary structure	Up to 5 m	From sand to clay	Volcanic glass Pyroxenes feldspatoids	Reworked volcanic deposits
Facies F3: Grey volcanic pyroclastic deposits with feldspatoids (leucite	Any sedimentary structure	Up to 1.8 m	Clay to silt	Leucite crystals	Volcanic ash deposit
Facies F4: dark gray to green volcanic ashes	Millimetre lamination	Up to 1.14 m	Claystone to siltstone	Volcanic glass Vegetation fragments Skeletal remains	Lake or alluvial plane deposit
Facies F5: White to light cream/grey marls	Any sedimentary structure	Up to 50 cm		Calci mudstone Calcareous clay	Lacustrine pool
Facies F6: Green/grey to brown unconsolidated fine sand, silt and clays	Any sedimentary structure	Up to 5 m	Sandstone and siltstone	Quartz Feldspar Carbonate clast	Lacustrine Fluvial alluvial deposits
Facies F7: Green to light brown unconsolidated sand to laminated sandstone	Millimetre thick lamination	50 cm	Medium sandstone	Vadose pisoids Carbonate clasts Quartz Feldspar Vegetation roots	Fluvial channel in alluvial plane
Facies F8: Palaesols	Any sedimentary structure	Up to14 cm	Siltstone to sandstone	Red orange matrix	palaesol
Facies F9: Polymictic conglomerate	Any sediment structure	Up to 60 cm	conglomerate	Carbonate clasts Volcanic reworked matrix	Fluvial channel deposits
Facies F10: Grey/green medium to coarse cross-laminated sand and sandstone	Current ripples	1 m	Sandstone well sorted	Quartz Carbonate clast Feldspar Volcanic matrix	Fluvial channel deposits

5.4 Architecture of Pleistocene succession of Acque Albule Basin

The Pleistocene Acque Albule succession consists of terrigenous deposits overlain by travertines. The terrigenous succession consists of deposits belonging to three different lithofacies association. These lithofacies associations represent a marsh-lacustrine environment (facies F1, F5, F6, F7, F8), volcaniclastic deposits that are originated from the surrounding volcanic apparatus (facies F2, F3, F4) and, in the southern part of the succession, conglomerates and laminated sandstone represent the deposit of the Aniene river (facies F9, F10). The marsh-lacustrine environment, characterized by organic matter-rich mudstones, covered the study area before the beginning of the precipitation of the studied travertines. The succession is elongated North-South in direction for a total length of 3.1 km. Based on the disposition of the drilled cores and the position of the vents, located mostly in the northern part, according to the published literature (Faccenna et al., 2008), the travertine frame is subdivided in proximal, intermediate and distal part from North to South. Travertine succession is characterized by numerous centimetre to few metres thick intraclastic/extraclastic wackestone to floatstone/rudstone (facies T11 and U) indicative of periods of non deposition and erosion. These periods were due to the temporary interruption of the thermal water out of the springs. Along the whole transect four main unconformities were recognized. These unconformities are characterized by variable thickness from few decimetres up to 8 m. These unconformities separate 4 principal units (Fig. 5.18 and 5.19).

Unit 1, the lower one, is characterized in the northern side of the studied system by a facies association enriched in undulated layers in which sub-rounded coated grains (facies T6) are widespread. In the well S2 this unit is thicker than in the well S1 and S3. Moving to the central part of the travertine body, Unit 1, in the well S4, is characterized by high-energy facies such as crystalline dendrite cementstone (facies T3) deposited on steep inclined layers. Then in the well S6 this unit is characterized by two lithoclastic wackestone/floatstone units (facies T11), which included between them undulated layers of clotted peloidal micrite boundstone (facies T2). The southern part of the travertine system in Unit 1 is represented by reeds and algae facies, intercalated with marls layers.

The northern part of Unit 1 can be interpreted as deposited in a terraced system. The major thickness of Unit 1 in well S2 can be due to the presence of a morphologic depression, also visible in the geological section, fed by an hydrothermal vent, which probably was placed in the western part of well S2 (Faccenna et al., 2008) and that could not feed the higher zones in the first periods of its activity. Moving to the central part of the travertine system, Unit 1 is characterized by the deposition of a smooth slope depositional system, characterized by high energy of the flowing water, favoured by the sloping topography. The well S6 shows a zone little fed by hydrothermal water, testified by the occurrence of lithoclastic floastones (facies T11) and facies enriched by plants (T1, T7, T8) developing a marsh lens. The inclined area that links the wells S4 and S7 presented a terraced lithofacies association that toward the southern part (core S7) of the studied system evolved to a marsh-pool depositional environment.

In the northern part, Unit 2 can be subdivided in two sub-units, which represent two different depositional events: the lower part of Unit 2 is characterized by shrubs and clotted micrite rich facies in the wells S2 and S3, while the well S1 recorded the deposition of facies enriched in plant (facies T7 and T8). The whole upper part of this unit is characterized by the deposition of dark layers rich in plants and algae of facies T7. The central part of the travertine body in the well S4 is still characterized by high-energy facies as in Unit 1. An alternation between facies T1 and T7, with the occurrence of plants remains, charophytes and skeletal remains. Unit 2 in the well S7 is separated from Unit 1 by a marl layer: this part of Unit 2 can be subdivided in three sub-units: the lower and the upper sub-units are characterized by low-energy distal facies, instead the central one is characterized by undulated layers with micrite dendrite (facies T2) and crystalline dendrite facies (facies T3).

The lower sub-unit of the northern part of Unit 2 recorded a terraced system in the well S2 and S3; S3 seems to be in higher topographic position than the well S2, therefore or the two wells were fed by two different vents, or by one placed in the eastern part of the well S3, position of fossil springs already recognized by Faccenna et al. (2008). In well S1 this sub-unit seems to represent the distal part of the slope environment. The upper part of Unit 2, instead, seems to be characterized by the absence of a strong hydrothermal activity along the northern area of the system, with the consequently imposition of a marsh-pool environment. This marsh event is recorded also in the well S6, developing a lens also in this area. The well S4 completely represents a slope system that links the northern and the southern parts of the travertine area. In the end in the southern part of the travertine body, the well S7 is characterized by an alternation of low-energy flats and a low-angle terraced systems that probably was fed by a spring placed in the southern part of the travertine body, as reported by Faccenna et al. (2008).

Unit 3 in the northern part is characterized by an alternation of crystalline dendrite cementstone (facies T3) sub-rounded coated grains grainstone (facies T6) and clotted micrite boundstone (facies T2). The well S1 is also characterized by the occurrence of coated gas bubble boundstone (facies T4). Moving to the well S3 there is the prevalence of facies characterized by charophytes and plants remains (facies T1, T7, T8). In the well S4, Unit 3 is thin, lesser than 1 m. This part is characterized by an alternation of high- and low-energy facies, with the prevalence of the latter. In the well S6, as in the northern part of the body, the occurrence of coated grains grainstones (T6), crystalline dentrite cementstone (T3) and micrite dendrite forms (T2) prevail. Unit 3 in the well S7 is characterized by the presence of a 4 m thick conglomerate deposit beyond it; Unit 3 in this well consists of an alternation of facies T1 andT7.

The northern part of Unit 3 is characterized by a terraced system with an input of hydrothermal water from west, feeding principally the wells S1 and S2. The well S3 still remains on a morphologic high, characterized by stagnant and cooled water that permitted the deposition of facies enriched in plant and algae. Well S3 is characterized also by the occurrence of multiple exposure events at the base of this unit. On the contrary of the intermediate part of Unit 1 and Unit 2, in the Unit 3 the terraced system was developed in the area of well S6, leaving the distal marsh environment in the S4 area. The conglomerates (facies F9) that characterized the base of Unit 3 in the southern part are interpreted as deposited by a river channel, which cut the travertine deposits. Above them Unit 3 is characterized by

a marsh-pool environment that in this area was fed also by freshwater input from the palaeo-Aniene river.

As in Unit 3, the northern part of Unit 4 is characterized by facies T2, T4 and T6 in the wells S1 and S2. The well S3 continues with facies enriched in charophytes stems, but the upper part of the well is characterized by facies similar to those occurred in wells S1 and S2. In the central part the base of this Unit, in well S4 and S6 is characterized by a continuous deposition of lithoclastic floatstone/rudstone, which in S6 is up to 8 m (including the no-cored parts). Above it, mainly facies T1 and T6 occur in the well S4, instead high-energy facies occur in well S6. The base of Unit 4 in well S7 is characterized by 4.5 m thick alternation of C facies. Above it, two sub-units are recognized: the lower one rich in facies T7, the upper one rich in facies T2 and T6.

The northern part of Unit 4 is mainly characterized by terraced system that toward east (to S3) and south (to S4) become a distal pond. In the end of travertine deposition, also in well S3 and S4 a terraced system occurred, probably recording an increase of hydrothermal activity. As in Unit 3, in S6 it seems there is more energy than in well S4, and the deposition of a smooth slope occurs. In well S7, the southern area of the Unit 4 seems characterized by flat systems, enriched in plants developing a marsh environment. Only the upper part, in which there is the deposition of centimetre thick and undulated sub-rounded coated grains layers. These layers testify that the hydrothermal influence had increased reaching the southern travertine area.

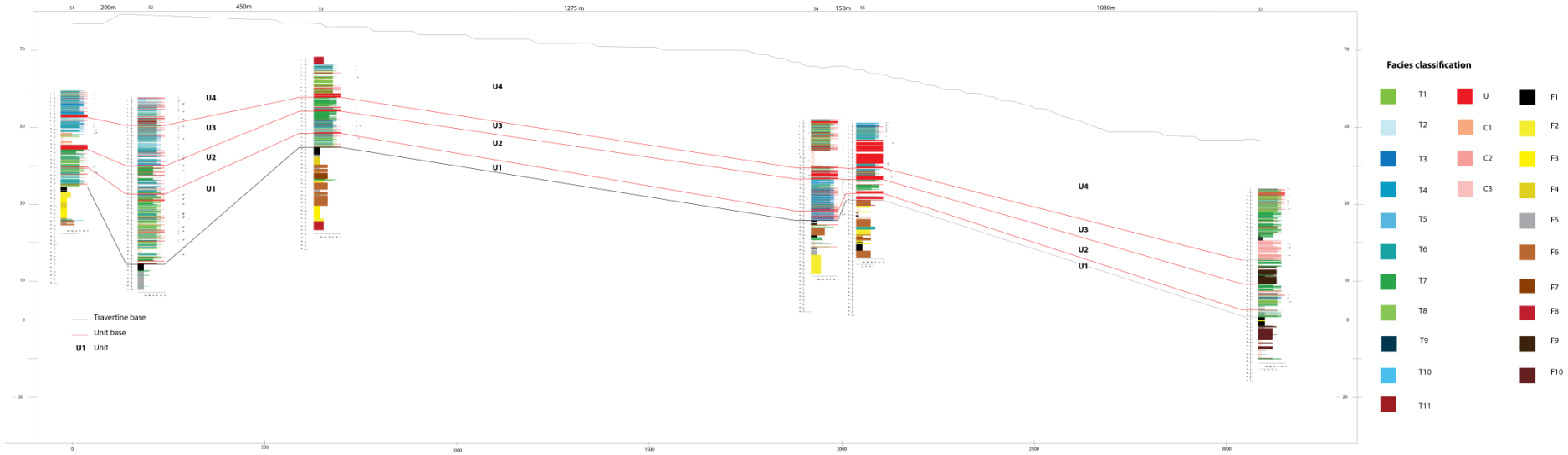

Figure 5.18. Correlation diagram of the cored wells of Tivoli area. Black line divides the terrigenous substratum from the travertine body. Red lines divide the stratigraphic units.

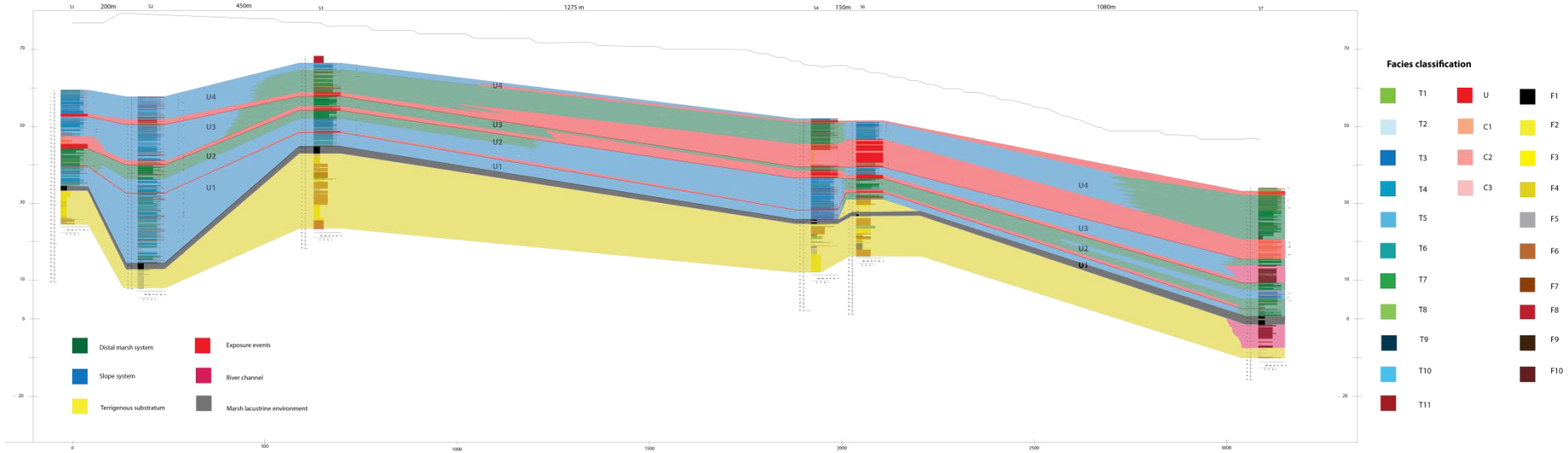

Figure 5.19. Correlation diagram of the cored logs showing the vertical and lateral distribution of the distinguished lithofacies associations

5.5 Conclusions

The Tivoli travertine borehole cores permitted a detailed study of travertine lithofacies and a correlation of different surfaces differentiating four decametre-scale units. Subaerial exposure events (facies U), represented by intraclastic and extraclastic wakestone to floatstone and claystone layers, constitute the travertine sequence boundaries, suggesting the intermittent accretion of the travertine system. Through the description of travertine cores and their correlation, different architectural pattern were recognized, including undulated sub-horizontal, steep inclined layers, and upward convex morphologies belonging to terraced and smooth slope depositional environment and distal marsh sub-horizontal environment. The development of the different lithofacies associations was controlled by the hydrodynamics of the flowing water, the position of the probably large number of active vents and the roughness and gradient of the pre-existing surface and morphology. The slope system includes the following facies: clotted peloidal micrite dendrite boundstone (T2), crystalline dendrite cementstone (T3), coated gas bubble boundstone (T4), laminated boundstone (T5), sub-rounded coated grains grainstone to boundstone (T6), raft grainstone to rudstone (T9) and millimetre-thick dense laminae boundstone (T10). Distal marsh lithofacies association includes the facies: clotted peloidal micrite grainstone to boundstone with charophytes and ostracodes (T1), cream colour peloidal phytoclastic intraclastic boundstone to rudstone/floatstone (T7), white reed boundstone to grainstone/rudstone (T8) and intraclastic grainstone to rudstone (T11). Moreover 3 carbonate facies deposited in karst cavities were recognized (C1, C2 and C3).

The cored substratum of the travertine body consists of 10 different terrigenous lithofacies belonging to a mixed of alluvial plain, volcanic and lacustrine environments. In the southern part of the studied area palaeo-channels intercalated within the travertine body were described. These channels probably belonged to the palaeo Aniene river.

Chapter VI

Lithofacies architecture and evolution through time of travertine depositional systems

Travertine deposits related to out-flowing from vents develop frames with a thickness up to 100 m and extended laterally from a few square metres to a few to hundred square kilometres: for instance the modern and old Neogene-Quaternary travertines of the Denizli Basin in Turkey occupy an area more than 100 km^2 (Ozkul et al., 2002). Mammoth Hot Spring, near the northern boundary of Yellowstone National Park, Wyoming, U.S.A., is one of the world's largest site of active travertine accumulation. These travertines are approximately considered to be 8000 years old (Sturchio et al., 1992), 73 m in thickness, and cover an area more than 4 km^2, laterally extended more than 7 km (Fouke et al., 2000). The Pleistocene Acque Albule travertine deposit covers an area of 35 km^2 circa, 7 km N-S elongated and 90 in thickness (Faccenna et al., 2008), comparable in size to the Yellowstone travertines. The upper Messinian Albegna travertine deposit covers an area of 3.5 km^2 resulting to be definitely less in width than the Acque Albule travertines.

The two studied travertine deposits provided two lithofacies lists, characterized by common and different points. However, following the classification proposed by Della Porta (2015) the classified lithofacies of this research could be grouped in two principal categories: 1) precipitated "boundstone" and "cementstone", that precipitate in place, contribute to the construction of build-ups and consist principally of micrite, clotted peloidal micrite and microsparite that develop irregular frameworks, laminated textures and dendritic forms; and 2) facies made of components not bound at the time of deposition, including different types of grains such as peloids, skeletal and phytoclastic remains, coated grains, intraclasts and extraclasts. The facies that belongs to the first class are: clotted peloidal boundstone (facies F1 and T2), clotted gas bubble boundstone (facie F4 and T4), crystalline dendrite cementstone (facies F5 and T3), laminated boundsone (facies F7a and T8), mudstone to microsparstone (Facies F9) and millimetre thick laminae cemenstone (facies T10). The second class includes raft rudstone to floatstone (facies F2 and T9), sub-rounded coated grains grainstone to packstone (facies F3 and T6), coated rudstone to floatstone (facies F7b, T1 and T7), peloidal and skeletal packstone to grainstone (facies F8) and intraclastic grainstone to rudstone (facies T11).

Discharge rate of the hydrothermal springs, the morphology and the topographic gradient of the substrate and the orientation of the active faults that are necessary for the flowing of thermal waters,

control the geometry of the hydrothermal travertine deposits. Travertines precipitate in basins controlled by faults, developing tabular gently inclined layers on sub-horizontal substrate, or developing wedges, mounds or ridges when the carbonates precipitate on inclined topographic surfaces (Della Porta, 2015). The frames, built up on the inclined surfaces, are commonly smooth or terraced, varying laterally and vertically from one to the other, and characterized by onlap and downlap strata terminations. These different geometries are made of different facies: crystalline dendrite cementstone and laminated boundstone occur on the inclined strata of slopes, precipitating in high-flow environments characterized by high rates of CO_2 degassing. Pools occur too in terraced system, and are made of horizontal layers. These layers consist of clotted peloidal micrite dendrite boundstone, raft rudstone, sub-rounded coated grains grainstone and coated gas bubble boundstone, which precipitate under slow-flowing thermal water and low energy conditions. These facies are widespread in the Albegna Basin where the terraced slope system was well developed. The sub-horizontal layers could form both close to or distally from the vents. In the two cases the tabular travertine precipitates are different and the Acque Albule travertines show both these situations. The travertines that precipitate on a sub-horizontal or little inclined substrate, are characterized by a white colour and also undulated strata. The facies that occur in this setting are similar to the facies of the pools of the terraced system, but in this case they cover a wider area that can reach tens of square metres, forming shrub flat (*sensu* Guo and Riding, 1998). In the distal area from the vent where the thermal water decreases in temperature and is impoverished with respect to Ca^{2+} and HCO_3^-, travertines precipitate in facies characterized by the occurrence of plants, reeds, molluscs and ostracodes. These facies characterize also the last phases of the hydrothermal travertine system. When the hydrothermal activity decreases and mixes with probable freshwater input, the entire travertine area is covered by brownish to grey precipitates rich in phytoclastic and skeletal remains. In both the Albegna Basin and Acque Albule Basin, this terminal stage is recognized in the respectively in the Phase III and in the upper part of the Testina.

According to many authors, the factors that controls the evolution in space and time of travertines are the basin hydrology, tectonics and climate (Minissale, 2004; Faccenna et al., 2008; Capezzuoli et al., 2014). The aquifer should be localized in a limestone formation, where the decarbonatation of carbonate calcium enriches the waters of ions Ca^{2+} and HCO_3^-. This aquifer needs to be linked to a geothermal activity that permits the heating of the waters. The other fundamental prerequisite is tectonics that permit the development of faults acting as fluid conduits feeding the hydrothermal vents, and the formation of accommodation space, required to permit the backlog of the precipitated travertines. Moreover humid climatic phases are needful to recharge the aquifer during time.

Chapter VII

Conclusions and final remarks

This study provides a valid tool to deepen the knowledge about hydrothermal systems and their carbonate deposits but also presents some innovative results. It does not pretend to represent a conclusive answer to the understanding of the complexity of these continental carbonates. This study concerned two case studies: the upper Messinian Albegna Basin travertines (Southern Tuscany, Central Italy) and the upper Pleistocene Acque Albule travertines (Tivoli, Latium, Central Italy), both of them developed in continental extensional and strike-slip basins controlled by faults, in which deposition of terrigenous sediments occurred before and contemporaneously to the travertine precipitation. A description of travertines lithofacies at the macro- and micro-scales is provided, developed using the terminology of the classical classifications of carbonates by Dunham (1962) and Embry and Klovan (1971), combined with previously published travertine fabric nomenclature such as Guo and Riding (1998), Barilaro et al. (2012), Gandin and Capezzuoli (2014) and Della Porta (2015). Concerning the terrigenous deposits, a lithofacies classification is provided. Then the different facies were grouped in lithofacies associations interpreted as typical continental depositional environments. Based on the spatial distribution of the lithofacies associations for both the studied systems, a reconstruction of the architecture of the mixed travertine-terrigenous deposits was provided. Detailed studies of the petrography of the upper Messinian travertines of the Albegna Basin permitted to provide a complex paragenetic history of the succession and moreover to provide a useful comparison for future studies on diagenesis of travertines that are so far quite rare. This study demonstrates the complex paragenetic history existing in a hydrothermal travertine deposit, showing the various possibilities and cases of different hydrothermal, meteoric and burial diagenetic events, characterized by a succession of distinct diagenetic features.

In detail from the study of the two case studies, the follow conclusions can be drawn:

1. **Facies types**. In both travertine systems different travertine fabrics are described: the upper Messinian travertines of the Albegna Basin are classified in nine facies, while the travertines of the Pleistocene Acque Albule Basin include eleven lithofacies. These lithofacies can be synthetically grouped in two families: 1) The precipitated boundstone and cementstone that include clotted peloidal boundstone and microsparstone with an irregular framework, branching dendrite forms cementstone, coated gas bubble boundstone, laminated boundstone and encrusted plants boundstone. The second group includes all the deposits made of grains, such as peloids and faecal pellets, phytoclast and skeletal remains, sub-rounded coated grains, intraclasts and extraclasts, and rafts.

   In addition to the travertine lithofacies, also the associated terrigenous lithofacies are described in both the studied successions: in Southern Tuscany, the studied succession the five terrigenous lithofacies recognized range from claystone to conglomerate and breccia and are interpreted to be deposited in low-energy system such as ponds or overbank areas to high-energy

channel or debris flow fan. In the Acque Albule succession, ten terrigenous lithofacies are described. These lithofacies are principally claystone and sandstone, but also conglomerates are found in the southern part of the succession. These lithofacies are interpreted as deposited in channels, lakes or overbank areas, are associated with pyroclastic volcanic deposits and most of them are characterized by the occurrence of volcanic clasts and minerals such as leucite.

2. Depositional systems. In the studied travertine settings, these continental carbonates precipitate in two main lithofacies associations: 1) the travertine slope system that can be either smooth or terraced. The smooth slope is principally characterized by high-energy and turbulent flow that causes the precipitation of centimetres to decimetres thick crystalline dendrite cemenstone alternated with laminated boundstone and coated gas bubbles boundstone. The terraced slope system consists of a lateral alternation between walls, rims and pools, with the deposition of crystalline dendrite cementstone on rims and walls, and the precipitation, for instance, of micrite dendrite boundstone, sub-rounded coated grains grainstone, and coated gas bubble boundstone. 2) Travertine flat lithofacies association consists of tabular layers that precipitate far away from the hydrothermal vents or the terminal stages of the travertine system, developing pools and ponds characterized by low-energy flow. This environment presents facies enriched in phytoclasts, skeletal remains of ostracodes and molluscs, faecal pellets, micrite mudstone, and intraclast rudstones.

In both the studied areas the travertine lithofacies associations are interlayered or overlie terrigenous lithofacies associations. In the Late Messinian Albegna Basin the travertine deposits are interlayered with colluvial lithofacies association characterized mainly by breccia deposits, and with the alluvial plain lithofacies association with claystones, laminated sandstones and conglomerates. The upper Pleistocene Acque Albule succession is characterized by the deposition of claystones to sandstones interpreted as deposited in an alluvial plane with shallow ponds and lakes, in which also carbonates precipitated, associated with pyroclastic volcanic deposits. This environment preceded the precipitation of the travertine frame. Moreover in the southern part of the studied succession, travertines are intercalated with conglomerates and laminated sandstones representing the palaeo-deposits of the Aniene river.

3. Controlling factors. Hydrology of the basin, tectonics and climate are the external factors that control the evolution in space and time of the studied travertine successions. The aquifers should be localized in carbonate formations that provides Ca^{2+} and HCO_3^- to waters through the decarbonatation of calcium carbonate. The aquifer needs to be linked to geothermal activity that permits the heating of the waters. Tectonics permit the development of faults acting as fluid conduits that connect the aquifer and the vents. Moreover tectonics is fundamental to the creation of accommodation space. A humid climate is required for the recharge of the aquifer.

4. Travertine mineralogy. X-Ray diffraction analyses confirmed that the upper Messinian Albegna Basin travertines were low-Mg!!! calcite in mineralogy. In terms of varieties of calcite the primary precipitate of studied travertine consists of a mixture of clotted peloidal micrite, microsparite and sparite that can form irregular framework, dendrites or can coat grains.

5. Diagenetic processes. Dissolution, micritization, recrystallization and the precipitation of different cement phases are the main processes that can alter the primary fabric appearance. In the upper Messinian Albegna Basin travertine calcite cements precipitated in three different

diagenetic environment: the hydrothermal, the meteoric and the burial environment. These cements are characterized by different responses to cathodoluminescence that is due to the different ratio of content between Mn^{2+} and Fe^{2+}, and to the redox conditions and geochemistry of the pore fluids.

6. **Geochemistry.** Geochemical data of the studied travertine deposits seem to be controlled from chemical and physical processes, for instance CO_2 outgassing, H_2O evaporation, temperature and saturation state of the hydrothermal water. All these factors are dependent on the depositional environments and influence the precipitated fabric types. The negative values of $\delta^{18}O$ appear to be influenced by high temperatures of thermal waters and by the influence of meteoric freshwater. The range of $\delta^{13}C$ values reflects the conditions of precipitation of the travertines, depending mainly on rates of CO_2 degassing linked to the energy of the flowing thermal water and consequently to the fabric precipitated. These geochemical characteristics can be reset by meteoric diagenetic influence.

Acknowledgements

Foremost, I would like to express my sincere gratitude to my tutor Prof. Giovanna Della Porta who expertly guided me through this stimulating experience and for her continuous support, availability and enthusiasm. I'm grateful to her for funding this project.
I would like to express my appreciation to Prof. Elisabetta Erba for guiding the PhD students with effective organisation, understanding and sympathy.
I wish to thank Andrea Niedermayr of Ruhr-Universität of Bochum for the oxygen and carbon stable isotope analysis and Prof. Monica Dapiaggi of University of Milanfor XRD analyses. My appreciation is also directed to the Earth Sciences Department staff: Curzio Malinverno, Andrea Risplendente, Agostino Rizzi and Gabriele Pezzi are thanked for their technical assistance to my project. I also thank the IAS for providing the PGS grant.
I would like to thank Dr Enrico Capezzuoli (Perugia University) for the time shared in the field in Tuscany.
I thank all my "acquario friends" for the fun that we had together, for their sensibility and affection shared with me. I am grateful to Silvia for being a solid support in these years.
My biggest thank is addressed to my beautiful family. From my deep heart my thank to my parents, to Bernardo and Rosanna, to my brother Davide and my aunt Elsa.
My biggest hugs and kisses to Matilde for loving, believing and supporting me during these last three years. Without you I could not finish this.

References

Abilio, S., Inkollu, S.N., 1989. Namibe basin: geology and hydrocarbon potential, Angola. AAPG Search and Discovery Article #91022©1989. AAPG Annual Convention, San Antonio, Texas (April 23-26, 1989).

Acocella, V., Funiciello, R., 2006. Transverse systems along the extensional Tyrrhenian margin of central Italy and their influence on volcanism. Tectonics 25, TC2003.

Alberti, F. Dragone, M. Manfredini, A.G. Segre, 1967. Carta Geologica d'Italia (1967) F. 150 "Roma", Scala 1:100.000

Altunel, E., Hancock, P.L., 1993. Morphology and structural setting of Quaternary travertines at Pamukkale, Turkey. Geological Journal 28 (3-4), 335–346.

Altunel, E., Karabacak, V., 2005. Determination of horizontal extension from fissure-ridge travertines: a case study from the Denizli Basin, southwestern Turkey. Geodinamica Acta 18 (3-4), 333–342.

Armenteros, I., Daley, B., García, E., 1997. Lacustrine and palustrine facies in the Bembridge Limestone (late Eocene, Hampshire Basin) of the Isle of Wight, southern England. Palaeogeography, Palaeoclimatology, Palaeoecology 128 (1), 111–132.

Barchi, M., Minelli, G., Pialli, G., 1998. The CROP 03 profile: a synthesis of results on deep structures of the Northern Apennines. Mem. Soc. Geol. Ital. 52, 383–400.

Barilaro, F., Della Porta, G., Ripamonti, M., Capezzuoli, E., 2011. Petrographic and Facies Analysis of Pleistocene Travertines in Southern Tuscany, Central Italy. AAPG Search and Discovery Article #90124 © 2011 AAPG Annual Convention and Exhibition, April 10-13, 2011, Houston, Texas.

Barilaro, F., Della Porta, G., Cappezuoli, E., 2012. Depositional geometry and fabric types of hydrothermal travertine deposits (Albegna Valley, Tuscany, Italy). Rendiconti. Società Geologica Italiana 21, 1024–1025.

Bartolini A., CeccaF., 1999. 20 My hiatus in the Jurassic of Umbria-Marche Apennines (Italy): carbonate crisis due to eutrophication. Comptes Rendus de l'Academie de Sciences - Serie IIa - Sciences de la Terre et des Planetes **329**(8), 587-595.

Bathurst, R.G.C., 1975. Carbonate sediments and their diagenesis. Elsevier, Amsterdam.

Beglinger, S.E., Doust, H., Cloetingh, S., 2012. Relating petroleum system and play development to basin evolution: West African South Atlantic basins. Marine and Petroleum Geology 30 (1), 1–25.

Bellani, S., Brogi, A., Lazzarotto, A., Liotta, D., Ranalli, G., 2004. Heat flow, deep temperatures and extensional structures in the Larderello geothermal field (Italy): constraints on geothermal fluid flow. J Volcanol Geotherm Res 132:15–29.

Bertini, A., 2006. The Northern Apennines palynological record as a contribute for the reconstruction of the Messinian palaeoenvironments. Sedimentary Geology 188, 235–258.

Bertini, A., Martinetto, E., 2011. Reconstruction of vegetation transects for the Messinian–Piacenzian of Italy by means of comparative analysis of pollen, leaf and carpological records. Palaeogeography, Palaeoclimatology, Palaeoecology 304 (3), 230–246.

Bettelli, G., Bonazzi, U., Fazzini, P., Pellegrini, M., Fontana, D., Gasperi, G.F., 1992. Note alla Carta geologica del bacino del fiume Albegna. Bollettino della Società Geologica 61 (2).

Blair, T.C., 1987. Tectonic and hydrologic controls on cyclic alluvial fan, fluvial, and lacustrine rift-basin sedimentation, Jurassic-lowermost Cretaceous Todos Santos Formation, Chiapas, Mexico. Journal of Sedimentary Research 57 (5), 845–862.

Blikra, L.H., Nemec, W., 1998. Postglacial colluvium in western Norway: depositional processes, faces and paleoclimatic record. Sedimentology 45, 909–959.

Bollati A, Corrado S, Cosentino D, Danese E, Marino M, Mattei M, Parotto M, 2011. Assetto strutturale della catena a pieghe e sovrascorrimenti Umbro-Sabina (Italia Centrale) derivato dal rilevamento dei fogli 366 “Palombara Sabina” e 375 “Tivoli” (Progetto CARG). Rend. Online Soc. Geol. It., 14 , 37-61, 16 figs.; 1 tab. (DOI: 10.3301/ROL.2011.05)

Bollati A, Corrado S, Cosentino D, Danese E, Marino M, Mattei M, Parotto M, 2012. New Structural Scheme of the Umbria-Sabina fold-and-thrust belt (Central Italy) derived from the geological mapping of 366 “Palombara Sabina” and 375 “Tivoli” sheets of the National Carg Project. Rend. Online Soc. Geol. It., 23, 19-21.

Boni, C., Bono, P., Capelli, G., 1986. Schema idrogeologico dell’Italia Centrale [Hydrogeological scheme of Central Italy]. Mem. Soc. Geol. It. 35, 991–1012.

Bosi, C., Messina, P., Rosati, M., Sposato, A., 1996. Età dei travertini della Toscana meridionale e relative implicazioni neotettoniche. Memorie Società Geologica Italiana 51, 293–304.

Bossio, A., Foresi, L.M., Mazzei, R., Salvatorini, G., Sandrelli, F., Bilotti, M., Colli, A., Rossetto, R., 2003–2004. Geology and stratigraphy of the southern sector of the Neogene Albegna River basin (Grosseto, Tuscany, Italy). Geologia Romana 37, 165–173.

Braissant, O., Cailleau, G., Dupraz, C. and Verrecchia, E.P., 2003. Bacterially induced mineralization of calcium carbonate in terrestrial environments: the role of exopolysaccharides and amino acids. J. Sed. Res., 73, 483–488.

Brogi, A., Capezzuoli, E., 2009. Travertine deposition and faulting: the fault-related travertine fissure-ridge at Terme S. Giovanni, Rapolano Terme (Italy). International Journal of Earth Sciences 98 (4), 931–947.

Brogi, A., Capezzuoli, E., Aqué, R., Branca, M., Voltaggio, M., 2010. Studying travertines for neotectonics investigations: Middle–Late Pleistocene syn-tectonic travertine deposition at Serre di Rapolano (Northern Apennines, Italy). International Journal of Earth Sciences 99 (6), 1383–1398.

Brogi, A., Liotta, D., Ruggieri, G., Capezzuoli, E., Meccheri, M., Dini, A., 2015. An overview on the characteristics of geothermal carbonate reservoirs in southern Tuscany. Italian Journal of Geosciences http://dx.doi.org/10.3301/IJG.2014.41.

Brunetti E., Jones J. P., Petitta M., Rudolph D. L., 2013. Assessing the impact of large-scale dewatering on fault-controlled aquifer systems: a case study in the Acque Albule basin (Tivoli, central Italy). Hydrogeology journal 21: 401-423.

Capelli G., Mazza R., Gazzetti C. (Eds.), 2005. Strumenti e strategie per la tutela e l'uso compatibile della risorsa idrica nel Lazio - Gli acquiferi vulcanici. Quaderni di tecniche di protezione ambientale. Protezione delle acque sotterranee, 78. Pitagora Editrice Bologna, 216.

Capezzuoli, E., Gandin, A., Sandrelli, F., 2004. Neogene-Quaternary continental carbonates: the Quaternary deposits of Valdelsa and the Miocene travertines of Pignano (Volterra). In: Morin, D., Bruni, P. (Eds.), The "Regione Toscana" project of geological mappingCase histories and data acquisition. Regione Toscana. Press, Firenze, Italy, 89–96.

Capezzuoli, E., Gandin, A., Pedley, H.M., 2009. Travertine and calcareous tufa in Tuscany (Central Italy). In: Pascucci, V., Andreucci, S. (Eds.), 27th IAS Meeting of Sedimentology, Alghero, Italy. Fieldtrip Guidebook. Press, Alghero, Italy, pp. 129–158. Capezzuoli, E., Gandin, A., Pedley, M., 2014. Decoding tufa and travertine (fresh water carbonates) in the sedimentary record: The state of the art. Sedimentology 61 (1), 1–21.

Carmignani, L., Decandia, F.A., Fantozzi, P.L., Lazzarotto, A., Lotta, D., Meccherini, M., 1994. Tertiary extensional tectonics in Tuscany (Northern Apennines, Italy). Tectonophysics 238, 295–315.

Carucci V., Petitta M., Aravena R., 2012. Interaction between shallow and deep aquifers in the Tivoli Plain (Central Italy) enhanced by groundwater extraction: A multi-isotope approach and geochemical modeling. Applied geochemistry, 27, 266-280.

Casanova, J., 1986. East African rift stromatolites. In: *Sedimentation in the African Rifts* (Ed. by I. E. Frostick, R. W. Renaut, I. Reid and J. J. Tiercelin), *Spec. Publ. geol. Soc.,* **25,** 201-210.

CeccaF., CrestaS., Ferretti A., Pallini G., Santantonio M., Venturi F., 1991. Correlazioni tra zone ad Ammoniti ed unità litostratigrafiche del Giurassico dell'Appennino umbro-marchigiano. In: Giunta Regionale (ed), Regione Marche. L'ambiente fisico delle Marche. Geologia, Geomorfologia, Idrogeologia, 59-66.

Centamore E., Chiocchini M., Deiana G., Micarelli A. & Pieruccini U. (1971) – Contributo alla conoscenza del Giurassico dell'Appennino Umbro-Marchigiano. Studi Geol. Camerti, 1: 7-89, 7 figg., 45 tavv., 2 allegati, Camerino.

Chafetz, H.S., Folk, R.L., 1984. Travertines: depositional morphology and the bacterially constructed constituents. Journal of Sedimentary Research 54 (1), 289–316.

Chafetz, H.S., and Lawrence, J.R., 1994, Stable Isotopic Variability Within Modern Travertines: Géographie physique et Quaternaire, 48, 257-273.

Chafetz, H.S., Rush, P.F., and Utech, M.N., 1991. Microenvironmental controls on mineralogy and habit of $CaCO_3$, precipitates: an example from an active travertine system: Sedimentology, 38, 106-126.

Chafetz, H.S., Guidry, S.A., 1999. Bacterial shrubs, crystal shrubs, and ray-crystal shrubs: bacterial vs. abiotic precipitation. Sedimentary Geology 126 (1), 57–74.

Chiodini, G., Cardellini, C., Amato, A., Boschi, E., Caliro, S., Frondini, F., Ventura, G., 2004. Carbon dioxide Earth degassing and seismogenesis in central and southern Italy. Geophys. Res. Lett. 31, L07615.

Claes, H., Soete, J., Noten, K., El Desouky, H., Marques Erthal, M., Vanhaecke, F., Özkul, M., Swennen, R., 2015. Sedimentology, three- dimensional geobody reconstruction and carbon dioxide origin of Pleistocene travertine deposits in the Ballık area (south- west Turkey). Sedimentology http://dx.doi.org/10.1111/sed.12188 (Accepted Article).

Clarke, J.D.A., Bourke, M.C., 2011. Travertine and tufa from Dalhousie Springs (Australia). Implications for recognizing Martian springs. Geological Society of America Special Papers 483, 231–247.

Cornamusini, G., Foresi, L.M., Massa, G., Bonciani, F., Callegari, I., Da Prato, S., Ielpi, A., 2011. The Miocene successions of the Fiora Hills: considerations about the development of the minor basins of Southern Tuscany. Italian Journal of Geosciences 130 (3), 404–424.

Corrado S., Cosentino D., Crescenzi B., Parotto M., 1992. Geometrie delle deformazioni della Sabina meridionale attraverso la ricostruzione di superfici strutturali (Lazio, Appennino Centrale). In: Tozzi M, Cavinato GP, Parotto M (eds), Studi preliminari all'acquisizione dati del profilo CROP 11 Civitavecchia-Vasto, Studi Geololgici Camerti, Volume Speciale (1991/2), 42-53.

Cosentino D., Montone P., 1990. Geological Map of the Tivoli Area; Lucretil and Tiburtini Mts, Central Apennines, Italy. Scale 1.25000.

Croci, A., Della Porta, G., & Capezzuoli, E., 2016. Depositional architecture of a mixed travertine-terrigenous system in a fault-controlled continental extensional basin (Messinian, Southern Tuscany, Central Italy). *Sedimentary Geology*, *332*, 13-39.

D'Argenio, B., Ferreri, V., 1986. A brief outline of sedimentary models for Pleistocene travertine accumulation in southern Italy. Rendiconti. Società Geologica Italiana 9, 167–170.

Dandurand, J.L., Gout, R., Hoefs, J., Menschel, G., Schott, J. and Usdowski, E., 1982: 'Kinetically control variations of major components and carbon and oxygen isotopes in a calcite-depositing spring', *Chem. Geol.,* 36, 299–315

De Filippis, L., Faccenna, C., Billi, A., Anzalone, E., Brilli, M., Soligo, M., Tuccimei, P., 2013. Plateau versus fissure ridge travertines from Quaternary geothermal springs of Italy and Turkey: Interactions and feedbacks between fluid discharge, paleoclimate, and tectonics. Earth-Science Reviews 123, 35–52.

De Rita, D., Funiciello, R., Parotto, M., 1988. Geological map of the Colli Albani volcanic complex, 1:50,000 scale. SELCA, Florence.

De Rita D., Funiciello, R. Rosa, C. (1992). Volcanic activity and drainage network evolution of the Alban Hills area (Rome, Italy). Acta Vulcanol., Marinelli vol. 2, pp. 185-198.

De Rita, D., Faccenna, C., Funiciello, R., Rosa, C., 1995. Structural and geological evolution of the Colli Albani volcanic district. In: Trigila, R. (Ed.), The Volcano of the Alban Hills. Tipografia SGS, Rome, pp. 33–71.

De Rita, D., Giordano G., Rosa C. and Sheridan M.F., 1995. Volcanic risk at Alban Hills volcano and numerical simulations. In The Volcano of the Alban Hills. Trigila R. (ed.)

Della Porta, G., 2015. Carbonate build-ups in lacustrine, hydrothermal and fluvial settings: comparing depositional geometry, fabric types and geochemical signature. In: Bosence, D.W.J., Gibbons, K.A., Le Heron, D.P., Morgan, W.A., Pritchard, T., Vining, B.A. (Eds.), Microbial Carbonates in Space and Time: Implications for Global Exploration and Production. Geological Society, London, Special Publications 418, 17–68.

Deocampo, D.M., 2010. The geochemistry of continental carbonates. In: Alonso-Zarza, AM, Tanner, L.H. (Eds.), Carbonates in Continental Settings: Geochemistry, Diagenesis and Applications: Developments in Sedimentology 62. Elsevier, Amsterdam, 1–59.

Des Marais, D.J., 1997. Long-term evolution of the biogeochemical carbon cycle. In: Geomicrobiology, Interactions between Microbes and Minerals (Eds J.E. Banfield, and K.H. Nealson), 427–448. Mineral. Soc. Am., Washington, DC.

Di Salvo C., Mazza R. and Capelli, G., 2013. Gli acquiferi in travertino del Lazio: schemi idrogeologici e caratteristiche chimico-fisiche. Rend. Online Soc. Geol. It., 27, 54-76

Decho, A.W., 2000. Exopolymer microdomains as a structuring agent for heterogeneity within microbial biofilms. In: Microbial Sediments (Eds R.E. Riding and S.M. Awramik), pp. 1–9. Springer-Verlag, Berlin.

Dorobek, S., Piccoli, L., Coffey, B., Adams, A., 2012. Carbonate Rock-Forming Processes in the Pre-salt "Sag" Successions of Campos Basin, Offshore Brazil: Evidence for Seasonal, Dominantly Abiotic Carbonate Precipitation, Substrate Controls, and Broader Geologic Implications. AAPG Search and Discovery Article #90153©2012 AAPG Hedberg Conference Microbial Carbonate Reservoir Characterization, Houston, Texas, 3-8 June 2012.

Doveri, M., Mussi, M., 2014. Water Isotopes as Environmental Tracers for Conceptual Understanding of Groundwater Flow: An Application for Fractured Aquifer Systems in the "Scansano-Magliano in Toscana" Area (Southern Tuscany, Italy). Water 6 (8), 2255–2277.

Dupraz, C., Visscher, P.T., 2005. Microbial lithification in marine stromatolites and hypersaline mats: Trends in Microbiology, v. 13, p. 429-438.

Dupraz, C., Visscher, P.T., Baumgartner, L.K., and Reid, R.P., 2004. Microbe–mineral interactions: early carbonate precipitation in a hypersaline lake (Eleuthera Island, Bahamas): Sedimentology, 51, 745-765.

Dupraz, C., Reid, R.P., Braissant, O., Decho, A.W., Norman, R.S., Visscher, P.T., 2009. Processes of carbonate precipitation in modern microbial mats. Earth-Science Reviews 96 (3), 141–162.

Embry, A.F., Klovan, J.E., 1971. A Late Devonian reef tract on northeastern Banks Island, Northwest Territories. Bulletin of Canadian Petroleum Geology 19, 730–781.

Evans, J.E., 1999. Recognition and implications of Eocene tufas and travertines in the Chadron formation, White River Group, Badlands of South Dakota. Sedimentology 46 (5), 771–789.

Faccenna, C., Soligo, M., Billi, A., De Filippis, L., Funiciello, R., Rossetti, C., Tuccimei, P., 2008. Late Pleistocene depositional cycles of the Lapis Tiburtinus travertine (Tivoli, Central Italy): possible influence of climate and fault activity. Global and Planetary Change 63 (4), 299–308.

Farinacci A., Mariotti N., NicosiaU., Pallini G. & Schiavinotto F., 1981. Jurassic sediments in the Umbro-Marchean Apennines: an alternative model. In: Farinacci A. & Elmi S. (eds) Rosso Ammonitico Symposium Proceedings, 335-398. Edizioni Tecnoscienza, Roma.

Farinacci A., 1987. Inquadramento delle facies giurassiche italiane nell'ambito della Tetide. Boll. Soc. Paleont. It., **26**, 295-301.

Fauquette, S., Suc, J.P., Bertini, A., Popescu, S.M., Warny, S., Bachiri Taoufiq, N., Perez Villa, M.J., Chikhi, H., Feddi, N., Subally, D., Clauzon, G., Ferrier, J., 2006. How much did climate force the Messinian salinity crisis? Quantified climatic conditions from pollen records in the Mediterranean region. Palaeogeography, Palaeoclimatology, Palaeoecology 238 (1), 281–301.

Fauquette, S., Bertini, A., Manzi, V., Roveri, M., Argnani, A., Menichetti, E., 2014. Reconstruction of the Northern and Central Apennines (Italy) palaeoaltitudes during the late Neogene from pollen data. Review of Palaeobotany and Palynology 218, 117–126. Flügel, E., 2004. Microfacies of carbonate rocks: analysis, interpretation and application. Springer Science & Business Media, Berlin (976 pp.).

Fischbeck, R. and Müller, G., 1971. 'Monohydrocalcite, hydromagnesite, nesquehonite, dolomite, aragonite and calcite in speleothems of the Frankische Schweiz, Western Germany', *Contr. Min. Petrol.*, 33, 87–92

Folk, R. L., 1993. SEM imaging of bacteria and nannobacteria in carbonate sediments and rocks. *Journal of Sedimentary Research*,*63*(5).

Folk, R.L., 1994. Interaction Between Bacteria, Nannobacteria, And Mineral Precipitation In Hot Springs Of Central Italy: Géographie physique et Quaternaire, 48, 233-246.

Folk, R.L., Chafetz, H.S., 1983. Pisoliths (Pisoids) in Quaternary Travertines of Tivoli, Italy, *in* Peryt, T.M., ed., Coated Grains: Berlin-Heidenberg, Springer-Verlag.

Folk, R.L., Chafetz, H.S., Tiezzi, P.A., 1985. Bizarre forms of depositional and diagenetic calcite in hot-spring travertines, Central Italy. In: Schneidermann, N., Harris, P. (Eds.), Carbonate cements, Society of Economic Paleontologists and Mineralogists Special Publication 36, pp. 349–369.

Ford, T.D., Pedley, H.M., 1996. A review of tufa and travertine deposits of the world. EarthScience Reviews 41 (3), 117–175. Forti, P., Micheli, L., Piccini, L., Pranzini, G., 1990. The karst

aquifers of Tuscany (Italy). Hydrogeological Processes in Karst Terrants (Proceedings of the Antaîya Symposium and Field Seminar, IAHS Publication 207, pp. 341–349.

Fouke, B.W., 2011. Hot- spring Systems Geobiology: abiotic and biotic influences on travertine formation at Mammoth Hot Springs, Yellowstone National Park, USA. Sedimentology 58 (1), 170–219.

Fouke, B.W., Farmer, J.D., Des Marais, D.J., Pratt, L., Sturchio, N.C., Burns, P.C., Discipulo, M.K., 2000. Depositional facies and aqueous-solid geochemistry of travertine depositing hot springs (Angel Terrace, Mammoth Hot Springs, Yellowstone National Park, USA). Journal of Sedimentary Research 70 (3), 565–585.

Freytet, P., Verrecchia, E.P., 2002. Lacustrine and palustrine carbonate petrography: an overview. Journal of Paleolimnology 27 (2), 221–237.

Friedman, I., 1970. Some investigations of the deposition of travertine from hot springs – 1. The isotopic chemistry of a travertine-depositing spring, Geochim. Cosmochim. Acta, 34, 1303–1315.

Galluzzo F., Santantonio M., 2002. The Sabina Plateau: a new element in the Mesozoic palaegeography of Central Apennines. Boll. Soc. Geol. It.,Volume speciale **1**, 561-588.

Gandin, A., Capezzuoli, E., 2008. Travertine versus calcareous tufa: distinctive petrologic features and stable isotopes signatures. Italian Journal of Quaternary Sciences 21, 125–136.

Gandin, A., Capezzuoli, E., 2014. Travertine: Distinctive depositional fabrics of carbonates from thermal spring systems. Sedimentology 61 (1), 264–290.

Gandin, A., Capezzuoli, E., Sandrelli, F., 2002. A Messinian hot-spring travertine system and its system and its modern analogue at Rapolano in Southern Tuscany, Italy. 16th IAS Congress, Johannesburg, Abstract. vol. 110.

Giordano G., De Rita D., Cas R. and Rodani S., 2002. Facies association of rain generated versus crater lake-withdrawal lahar deposits from quaternary volcanoes, Central Italy. J. Volcanol. Geotherm. Res., 118: 145-160.

Gonfiantini, R., Panichi, C. and Tongiorgi, E., 1968. Isotopic disequilibrium in travertine deposition. Earth and Planetary Sc. Lett., 5, 55-58.

Goudie, A.S., Viles, H.A., Pentecost, A., 1993. The late-Holocene tufa decline in Europe. The Holocene 3 (2), 181–186.

Guastaldi, E., Graziano, L., Liali, G., Brogna, F.N.A., Barbagli, A., 2014. Intrinsic vulnerability assessment of Saturnia thermal aquifer by means of three parametric methods: SINTACS, GODS and COP. Environmental Earth Sciences 72, 2861–2878.

Guido, D.M., Campbell, K.A., 2011. Jurassic hot spring deposits of the Deseado Massif (Patagonia, Argentina): characteristics and controls on regional distribution. Journal of Volcanology and Geothermal Research 203 (1), 35–47.

Guo, L., 1993. Fabrics and Facies of Quaternary Travertines, Rapolano Terme, Central Italy. PhD Thesis, University of Wales, Cardiff.

Guo, L., and Riding, R., 1992. Aragonite laminae in hot water travertine crusts, Rapolano Terme, Italy: Sedimentology, 39, 1067-1079.

Guo, L., Riding, R., 1994. Origin and diagenesis of Quaternary travertine shrub fabrics, Rapolano Terme, central Italy. Sedimentology 41 (3), 499–520.

Guo, L., Riding, R., 1998. Hot- spring travertine facies and sequences, Late Pleistocene, Rapolano Terme, Italy. Sedimentology 45 (1), 163–180.

Guo, L., Riding, R., 1999. Rapid facies changes in Holocene fissure ridge hot spring travertines, Rapolano Terme, Italy. Sedimentology 46 (6), 1145–1158.

Guo, L., Andrews, J., Riding, R., Dennis, P. and Dresser, Q., 1996. Possible microbial effects on stable carbon isotopes in hot travertine. J. Sed. Res. 66, 468-473.

Hancock, P.L., Chalmers, R.M.L., Altunel, E., Cakir, Z., 1999. Travitonics: using travertines in active fault studies. Journal of Structural Geology 21 (8), 903–916.

Henchiri, M., 2014. Sedimentology of Quaternary calcareous tufas from Gafsa, southwestern Tunisia. Arabian Journal of Geosciences 7 (5), 2081–2091.

Hernández-Díaz, J.M., Hernández-Enrile, J.L., 2001. Using travertine deformations to characterize paleoseismic activity along an active oblique-slip fault: the Alhama de Murcia fault (Betic Cordillera, Spain). Acta Geologica Hispánica 36 (3), 297–313.

Heward, A.P., 1978. Alluvial fan and lacustrine sediments from the Stephanian A and B (La Magdalena, Cinera Matallana and Sabero) coalfields, Northern Spain. Sedimentology 25 (4), 451–488.

Hofmann, H.J., Grey, A.H., Hickman, A.H., Thorpe, R.I., 1999. Origin of 3.45 Ga coniform stromatolites in Warrawoona Group, Western Australia. Geological Society of America Bulletin 111, 1256–1262.

Holland, H.D., Kirsipu, T.W., Huebner, J.S. and Oxburgh, U.M., 1964. 'On some aspects of the chemical evolution of cave waters', *J. Geol.*, 72, 36–67

Jacobson, R.L. and Usdowski, E., 1975. 'Geochemical controls on a calcite precipitating spring', *Contr. Mineral. Petrol.,* 51, 65–74

Jolivet, L., Faccenna, C., Goffé, B., Mattei, M., Rossetti, F., Brunet, C., Storti, F., Funiciello, R., Cadet, J.P., D'Agostino, N., Parra, T., 1998. Midcrustal shear zones in postorogenic extension: example from the northern Tyrrhenian Sea. J. Geophys. Res. 103, 12,123–12,160.

Jones, B., 1989. Calcite rafts, peloids and micrite in cave deposits from Cayman Brac, British West Indies. Canadian Journal of Earth Sciences 26, 654–664.

Jones, S.J., Arzani, A., 2005. Alluvial fan response times to tectonic and climatic driven processes: example from the Khrud mountain belt, Central Iran. Geophysical Research Abstracts 7.

Jones, B., Peng, X., 2012. Intrinsic versus extrinsic controls on the development of calcite dendrite bushes, Shuzhishi Spring, Rehai geothermal area, Tengchong, Yunnan Province, China. Sedimentary Geology 249, 45–62.

Jones, B., Renaut, R.W., 1995. Noncrystallographic calcite dendrites from hot-spring deposits at Lake Bogoria, Kenya. Journal of Sedimentary Research 65 (1), 154–169.

Jones, B. and Renaut, R.W., 1996: Skeletal crystals of calcite and trona from hot-spring deposits in Kenya and New Zealand. *J. Sed. Res.,* 66, 265–274

Jones, B., Renaut, R.W., 2010. Calcareous spring deposits in continental settings. Developments in Sedimentology 61, 177–224.

Kahle, C. F., 1977. Origin of subaerial Holocene calcareous crusts: role of algae, fungi and sparmicritisation. *Sedimentology*,*24*(3), 413-435.

Kele, S., Demény, A., Siklósy, Z., Németh, T., Tóth, M., Kovács, M.B., 2008. Chemical and stable isotope composition of recent hot-water travertines and associated thermal waters, from Egerszalók, Hungary: Depositional facies and non-equilibrium fractionation. Sedimentary Geology 211 (3), 53–72.

Kele, S., Özkul, M., Fórizs, I., Gökgöz, A., Baykara, M.O., Alçiçek, M.C., Németh, T., 2011. Stable isotope geochemical study of Pamukkale travertines: new evidences of low temperature non-equilibrium calcite-water fractionation. Sedimentary Geology 238 (1), 191–212.

Kitano, Y., 1962. 'A study of polymorphic formation of calcium carbonate in thermal springs with emphasis on temperature', *Bull. Chem. Soc. Japan,* 35, 1980–1985

Kitano, Y., 1963. 'Geochemistry of calcareous deposits found in hot springs.' *J. Earth Sci. Nagoya Univ.*, 11: 68–100

Kligfield, R., 1979. The Northern Apennines as a collisional orogen. American Journal of Science 279 (6), 676–691.

Krumbein, W.E., 1979. Calcification by Bacteria and Algae. Studies in Environmental Science 3, 47–68.

Krumbein, W.E., Paterson, D.M., Zavarzin, G.A., 2003. Fossil and recent biofilms: a natural history of the impact of life on planet Earth. Kluwer Scientific Publishers, Dordrecht, The Netherlands, p. 482.

La Vigna F., Capelli G., Mazza R., 2007. The Acque Albule Plain, results and purposes about hydrogeological monitoring. Geoitalia 2007 – Sessione T42. Rimini.

La Vigna F., Mazza R., Capelli G., 2013. Le risorse idriche nei travertini della piana di Tivoli-Guidonia. La modellazione numerica come strumento di gestione degli acquiferi. Rend. Online Soc.Geol. It., v. 27, pp. 77-85.

Leeder, M.R., 2009. Sedimentology and sedimentary basins: from turbulence to tectonics. John Wiley & Sons, New York, USA, p. 592.

Link, M.H., Osborne, R.H., Awramik, S.M., 1978. Lacustrine stromatolites and associated sediments of the Pliocene ridge Route Formation, Ridge Basin, California. Journal of Sedimentary Research 48 (1), 143–158.

Lippmann, F., 1973. *Sedimentary Carbonate Minerals*, 228 pp, Heidelberg (Springer-Verlag)

Marra F., Freda C., Scarlato P., Taddeucci J., Karner D. B., Renne P. R., Gaeta M., Palladino D. M., Triglia R. and Cavarretta G., 2003. Post-Caldera activity in the Alban Hills volcanic district (Italy): 40Ar/39Ar geochronology and insights into magma evolution. Bull. Volcanol. 65: 227-247.

McCall, J., 2010. Lake Bogoria, Kenya: hot and warm springs, geysers and Holocene stromatolites. Earth-Science Reviews 103 (1), 71–79.

Miall, A.D., 1996. The Geology of Fluvial Deposits. Springer Verlag, Berlín, p. 582. Minissale, A., 1991. Thermal springs in Italy: their relation to recent tectonics. Applied Geochemistry 6 (2), 201–212.

Minissale, A., 2004. Origin, transport and discharge of CO2 in central Italy. Earth-Science Reviews 66 (1), 89–141.

Minissale, A., Kerrick, D.M., Magro, G., Murrell, M.T., Paladini, M., Rihs, S., Sturchio, N.C., Tassi, F., Vaselli, O., 2002a. Geochemistry of Quaternary travertines in the region north of Rome (Italy): structural, hydrologic and paleoclimatic implications. Earth and Planetary Science Letters 203 (2), 709–728.

Minissale, A., Vaselli, O., Tassi, F., Magro, G., Grechi, G.P., 2002b. Fluid mixing in carbonate aquifers near Rapolano (central Italy): chemical and isotopic constraints. Applied Geochemistry 17 (10), 1329–1342.

Nemec, W., Kazanci, N., 1999. Quaternary colluvium in west-central Anatolia: sedimentary facies and palaeoclimatic significance. Sedimentology 46 (1), 139–170.

Neves, M.A., Morales, N., Saad, A.R., 2005. Facies analysis of Tertiary alluvial fan deposits in the Jundiaí region, São Paulo, southeastern Brazil. Journal of South American Earth Sciences 19 (4), 513–524.

Nishikawa, O., Furuhashi, K., Masuyama, M., Ogata, T., Shiraishi, T., Shen, C.C., 2012. Radiocarbon dating of residual organic matter in travertine formed along the Yumoto Fault in Oga Peninsula, northeast Japan: implications for long-term hot spring activity under the influence of earthquakes. Sedimentary Geology 243, 181–190.

Noffke, N., Beukes, N., Gutzmer, J., & Hazen, R., 2006. Spatial and temporal distribution of microbially induced sedimentary structures: a case study from siliciclastic storm deposits of the 2.9 Ga Witwatersrand Supergroup, South Africa. *Precambrian Research*, *146*(1), 35-44.

O'Neil, J.R. and Barnes, I., 1971. C^{13} and O^{18} compositions in some freshwater carbonates associated with ultramafic rocks and serpentinites: western United States', *Geochim. Cosmochim. Acta,* 35, 687–697

Özkul, M., Varol, B., Alçiçek, M.C., 2002. Depositional environments and petrography of Denizli travertines. Bulletin of the Mineral Research and Exploration 125, 13–29.

Özkul, M., Gökgöz, A., Kele, S., Baykara, M.O., Shen, C.C., Chang, Y.W., Kaya, A., Hançer, M., Aratman, C., Akin, T., Örü, Z., 2014. Sedimentological and geochemical characteristics of a fluvial travertine: A case from the eastern Mediterranean region. Sedimentology 61 (1), 291–318.

Palladino D M., Gaeta M. and Marra F., 2001. A large K-foiditic hydromagmatic eruption from the early activity of the Alban Hills Volcanic District, Italy, Bull. Volcanol., 63: 345-359.

Palmer, A.N., 2007. Cave Geology. Dayton, Ohio (454 pp.). Pascucci, V., Martini, I.P., Sagri, M., Sandrelli, F., 2007. Effects of transverse structural lineaments on the Neogene–Quaternary basins of Tuscany (inner Northern Apennines, Italy). In: Nichols, G., Williams, E., Paola, C. (Eds.), Sedimentary Processes. Environments and Basins: A Tribute to Peter Friend, IAS Special Publication 38, pp. 155–182.

Pasquarè, G., Chiesa, S., Vezzoli, L., Zanchi, A., 1983. Evoluzione paleogeografica e strutturale di parte della Toscana meridionale a partire dal Miocene superiore. Memorie Società Geologica Italiana 25, 145–157.

Patacca, E., Sartori, R., Scandone, P., 1990. Tyrrhenian basin and Apenninic arcs: Kinematic relations since Late Tortonian times. Memorie Società Geologica Italiana 45, 425–451.

Pedley, H.M., 1990. Classification and environmental models of cool freshwater tufas. Sedimentary Geology 68 (1), 143–154.

Pedley, M., 2014. The morphology and function of thrombolitic calcite precipitating biofilms: A universal model derived from freshwater mesocosm experiments. Sedimentology 61 (1), 22–40.

Pedley, M., Rogerson, M., Middleton, R., 2009. Freshwater calcite precipitates from in vitro mesocosm flume experiments: a case for biomediation of tufas. Sedimentology 56 (2), 511–527.

Pentecost, A., 1990. The formation of travertine shrubs: Mammoth hot spring, Wyoming. *Geol. Mag.,* **127,** 159- 168.

Pentecost, A., 2005. Travertine. Springer Science & Business Media, Berlin (445 pp.).

Pentecost, A., Tortora, C., 1989. Bagni di Tivoli, Lazio: a modern travertine depositing site and its associated microorganism. Boll. Soc. Geol. Ital. 108, 315–324.

Pentecost, A., Viles, H., 1994. A review and reassessment of travertine classification. Géographie Physique et Quaternaire 48 (3), 305–314. Pertusati. P. C., Musumeci, G., Bonini, L. and Trumpy, E. (2004). Carta Geologica della Toscana, 1:10000, sezione 343050-Manciano.

Petitta, M., Primavera, P., Tuccimei, P., Aravena, R., 2010. Interaction between deep and shallow groundwater systems in areas affected by Quaternary tectonics (Central Italy): a geochemical and isotope approach. Environ. Earth Sci. 63, 11– 30.

Rainey, D.K., Jones, B., 2009. Abiotic versus biotic controls on the development of the Fairmont Hot Springs carbonate deposit, British Columbia, Canada. Sedimentology 56 (6), 1832–1857.

Reitner, D.D.J., 1993. Modern cryptic microbialite/metazoan facies from Lizard Island (Great Barrier Reef, Australia) formation and concepts. Facies 29 (1), 3–39.

Reitner, J., Neuweiler, F., Gautret, P., 1995. Modern and fossil automicrites: implications for mud mound genesis. In: Reitner, J., Neuweiler, F. (Eds.), A Polygenetic Spectrum of Fine-Grained Carbonate Buildups. Facies 32, pp. 4–17.

Riding, R., 2000. Microbial carbonates: the geological record of calcified bacterial-algal mats and biofilms: Sedimentology, 47, 179-214.

Ronchi, P., Cruciani, F., 2015. Continental carbonates as hydrocarbon reservoir, an analogue case study from the travertine of Saturnia, Italy. AAPG Bulletin 99, 711–734.

Sant'Anna, L.G., Riccomini, C., Rodrigues-Francisco, B.H., Sial, A.N., Carvalho, M.D., Moura, C.A.V., 2004. The Paleocene travertine system of the Itaboraí basin, Southeastern Brazil. Journal of South American Earth Sciences 18 (1), 11–25.

Santantonio M., 1993. Facies associations and evolution of pelagic carbonate platform/basin systems:examples from the Italian Jurassic. Sedimentology, **40**, 1039-1067.

Santantonio M., 1994. Pelagic Carbonate Platforms in the Geologic Record: Their Classification, and Sedimentary and Paleotectonic Evolution. American Association of Petroleum Geologists Bulletin, **78**, 122-141.

Schopf, J.W., 2006. Fossil evidence of Archean life. Philosophical Transactions of the Royal Society, B 361, 869–885.

Serri, G., 1997. Neogene-Quaternary magmatic activity and its geodynamic implications in the Central Mediterranean region. Annals of Geophysics 40 (3). Sibson, R.H., 1996. Structural permeability of fluid-driven fault-fracture meshes. Journal of Structural Geology 18 (8), 1031–1042.

Sibson, R.H., 1996. Structural permeability of fluid-driven fault- fracture meshes. Journal of Structural Geology 18, 1031-1042.

Stein, M., 2001. The sedimentary and geochemical record of Neogene-Quaternary water bodies in the Dead Sea Basin-inferences for the regional paleoclimatic history. Journal of Paleolimnology 26 (3), 271–282.

Szulc, J., Gradzinski, M., Lewandowska, A., Heunisch, C., 2006. The Upper Triassic crenogenic limestones in Upper Silesia (southern Poland) and their paleoenvironmental context. In: Alonso-Zarza, A.M., Tanner, L.H. (Eds.), Paleoenvironmental Record and Applications of Calcretes and palustrine Carbonates. Geological Society of America, Special Paper 416, pp. 153–168.

Taylor, M.P., Drysdale, R.N., Carthew, K.D., 2004. The formation and environmental significance of calcite rafts in tropical tufa- depositing rivers of northern Australia. Sedimentology 51 (5), 1089–1101.

Ten Veen, J.H., Woodside, J.M., Zitter, T.A., Dumont, J.F., Mascle, J., Volkonskaia, A., 2004. Neotectonic evolution of the Anaximander Mountains at the junction of the Hellenic and Cyprus arcs. Tectonophysics 391 (1), 35–65.

Tice, M.M., Lowe, D.R., 2006. Hydrogen-based carbon fixation in the earliest known photosynthetic organisms. Geology 34, 37–40.

Török, Á., 2003. Facies analysis and genetic interpretation of travertine, Buda Vár-hegy, Hungary. Acta Geologica Hungarica 46 (2), 177–193.

Trichet, J. and De´farge, C., 1995. Non-biologically supported organomineralization. Bull. Inst. Oceanogr. Monaco Spec. No., 14, 203–236.

Van Gemerden, H., 1993. Microbial mats: a joint venture. Marine Geology 113, 3–25.

Ventriglia U., 2002. Geologia del territorio del Comune di Roma. Amministrazione Provinciale di Roma, Roma.

Viles, H. A., GoudieA.S., 1990. Tufas, travertines and allied carbonate deposits. Progress in Physical Geography, 14, 19.

Viles, H., Pentecost, A., 2007. Tufa and travertine. In: Nash, D., McLaren, S. (Eds.), Geochemical Sediments and Landscapes. Blackwell, Oxford, pp. 173–199.

Watkins S. D., Giordano G., Cas R. A. F. and De Rita D. (2002). Variation in mafic pyroclastic density current deposits caused by pre-eruptive depositional surface characteristic: the Villa Senni eruption unit, Alban Hills Volcano, Rome, Italy. J. Volcanol. Geotherm. Res., 118: 173-204.

Wright, V.P., 1992. A revised classification of limestones. Sedimentary Geology 76, 177–185.
Wright, V.P., 2012. Lacustrine carbonates in rift settings: the interaction of volcanic and microbial processes on carbonate deposition. In: Garland, J., Neilson, J.E., Laubach, S.E., Whidden, K.J. (Eds.), Advances in Carbonate Exploration and Reservoir Analysis. Geological Society, London, Special Publications 370, pp. 39–47.

Wright, V.P., Barnett, A.J., 2015. An abiotic model for the development of textures in some South Atlantic early Cretaceous lacustrine carbonates. In: Bosence, D.W.J., Gibbons, K., Le Heron, D.P., Pritchard, T., Vining, B. (Eds.), Microbial Carbonates in Space and Time: Implications for Global Exploration and Production. Geological Society, London, Special Publications 418, pp. 209–219.

Zanchi, A., Tozzi, M., 1987. Evoluzione paleogeografica e strutturale recente del bacino del fiume Albegna (Toscana meridionale). Geologica Romana 26, 305–325.

Zhang, Dian., Zhang, Y., Zhu, A. and Cheng, X., 2001. ‘Physical mechanisms of river waterfall tufa (travertine) formation’, *J. Sed. Res.,* 71, 205–216

Zembo, I., 2010. Stratigraphic architecture and quaternary evolution of the Val d'Agri intermontane basin (Southern Apennines, Italy). Sedimentary Geology 223 (3), 206–234.

Zentmyer, R., Myrow, P.M., Newell, D.L., 2008. Travertine deposits from along the South Tibetan fault system near Nyalam, Tibet. Geological Magazine 145 (06), 753–765.